

Univerzita Karlova v Praze
Přírodovědecká fakulta

Studijní program: Vývojová a buněčná biologie



Mgr. Tereza Turková

Role řízené tkáňově-specifické produkce ISWI proteinu Smarca5/Snf2h v myší krvetvorbě

Role of tissue-specific expression of the ISWI protein Smarca5/Snf2h in murine
hematopoiesis

Doktorská disertační práce

Školitel:

prof. MUDr. Tomáš Stopka, Ph.D.

Praha, 2024

Prohlášení:

Prohlašuji, že jsem závěrečnou práci zpracovala samostatně a že jsem uvedla všechny použité informační zdroje a literaturu. Tato práce ani její podstatná část nebyla předložena k získání jiného nebo stejného akademického titulu.

V Praze, dne 27. 2. 2024

Podpis:

Poděkování

Na prvním místě bych chtěla poděkovat svému školiteli Tomášovi Stopkovi za veškerou jeho pomoc a podporu počínající už od chvíle, kdy jsem se během svého bakalářského studia stala součástí jeho laboratoře Hematoonkologie a kmenových buněk. Jeho vedení mi umožnilo úspěšně projít všemi dosavadními fázemi mého studia a vědeckého vývoje, byl mi vždy nápomocen a podporoval mě ve všech projektech a aktivitách, jejichž dosavadním vyvrcholením je má prvoautorská publikace, která tvoří základ této disertační práce. Jeho pozitivní přístup a nadšení pro vědu pro mě vždy byly velikou motivací.

Dále bych ráda poděkovala Tomášovi Zikmundovi, který mě naučil většinu vědeckých metod a pravidel práce v laboratoři, za kterých dodnes těžím. Také mu náleží poděkování za jeho přínos při vytvoření SMARCA5 transgenního myšního modelu, který byl využit pro získání výsledků prezentovaných v této práci. Poděkování patří též mému dalšímu kolegovi Juraji Kokavcovi, zejména za jeho podíl na získávání dat a přípravě naší společné publikace a také za všechny jeho znalosti o práci s myšními modely, které mi předal. Chtěla bych poděkovat všem členům naší laboratoře Hematoonkologie a kmenových buněk za veškerou jejich pomoc a podporu, a to zejména Kristýně Pimkové, za její znalosti z oboru proteomiky a naší laborantce Kristině Léblové za její pomoc s péčí o myší linie.

Z našich spolupracovníků bych chtěla zmínit zejména Lukáše Čermáka a Nikol Dibus, kteří se podíleli na přípravě mé prvoautorské publikace a vždy mi ochotně nabídli svou pomoc a radu. V neposlední řadě poděkování patří též Českému centru pro fenogenomiku (CCP) a Radku Sedláčkovi, za jejich podíl na vytvoření SMARCA5 transgenního modelu, ze kterého tato práce těží.

Na závěr bych chtěla poděkovat své matce, která mě vždy podporovala ve všem, co jsem se kdy rozhodla dělat.

Abstrakt

Proces diferenciacie krvetvorných buněk je závislý na chromatin-remodelační aktivitě ISWI ATPázy SMARCA5 (SNF2H) a jejích komplexů. Pro studium funkcí této ATPázy jsme v naší laboratoři vyvinuli řadu myších modelů, počínaje modelem s konstitutivní delecí genu *Smarca5* a na něj navazujícími modely s kondicionální delecí tohoto genu v závislosti na tkáňově specificky exprimované Cre rekombináze (zejména v různých stádiích krvetvorby). Závažnost fenotypových projevů u myších modelů se různí od brzké embryonální letality konstitutivního delečního modelu, přes fetální letalitu spojenou se selháním erytropoézy (Vav1iCre model – delece v definitivním hematopoetickém progenitoru) až po poruchy lymfopoézy neomezující přežití zvířat (hCD2iCre model – delece v T a B lymfocytech) u kondicionálně delečních modelů. Tato práce navazuje na pozorování získaná při studiu delečních modelů genu *Smarca5*, tedy že delece vede k zástavě dělení buněk a jejich vstupu do apoptózy. Defekty byly pozorovány už ve stádiu kmenových buněk a hematopoetických progenitorů, které nebyly schopné vstoupit do procesu diferenciacie v nepřítomnosti SMARCA5 proteinu. V těchto modelech kvůli tomu nebylo možné studovat průběh diferenciacie. Proto jsme se rozhodli vytvořit nový myší model s hypomorfní (exprimující nižší množství proteinu) transgenní alelou SMARCA5 (*S5tg*), exprimovanou na pozadí delece *Smarca5*, který nám umožnil sledovat diferenciaci krvetvorných buněk při různých hladinách exprese proteinu SMARCA5. Zjistili jsme, že transgenní SMARCA5 může v závislosti na množství exprimovaného proteinu zachránit zástavu vývoje lymfocytů v tkáňově specifickém modelu delece *Smarca5* v této linii (hCD2iCre) a také letální fenotyp spojený s konstitutivní delecí nebo kondicionální delecí v krvetvorných kmenových buňkách (Vav1iCre). Model *Vav1iCre S5tg* ukázal, že úroveň exprese proteinu SMARCA5 hraje zásadní roli v krvetvorných kmenových buňkách a progenitorech, v případě snížené (asi 10 %) exprese tohoto proteinu dochází k nahromadění multipotentních progenitorů, které nejsou schopné dále diferencovat. Pozorovaný defekt vzniklý sníženým množstvím proteinu SMARCA5 má největší vliv na diferenciaci lymfocytů a jejich progenitorů a to zejména u B-lymfocytů, které jsou na množství proteinu SMARCA5 nejcitlivější, což vedlo k výraznému snížení jejich počtů v periferní krvi. Počet erytrocytů byl snížen pouze minimálně a myelocyty nebyly hypomorfní expresí SMARCA5 ovlivněny. Transgenní SMARCA5 model dokazuje, že ISWI ATPáza SMARCA5 je nepostradatelná pro správný vývoj krvetvorných buněk a to zejména lymfocytů. Tento výzkum přispívá cennými poznatky k prohloubení znalostí o tomto důležitém epigenetickém regulátoru, které mohou být využity při vývoji léčebných strategií pro poruchy krvetvorby.

Klíčová slova

chromatin, Snf2h, Smarca5, ATPáza, myší model, krvetvorba, kmenové buňky, multipotentní progenitory

Abstract

The process of cell differentiation is dependent on the chromatin-remodeling activity of the ISWI ATPase SMARCA5 (SNF2H) and its complexes. A series of mouse models have been used to study the functions of this ATPase, starting with a model with constitutive deletion of the *Smarca5* gene and followed by models with tissue-specific deletion of *Smarca5* gene (especially at different stages of hematopoiesis). The severity of phenotypic manifestations in mouse models varies from early embryonic lethality in the constitutive deletion model, through fetal lethality associated with erythropoiesis failure (*Vav1iCre* model - deletion in the definitive hematopoietic progenitor) to lymphopoiesis defects that do not limit animal survival (*hCD2iCre* model - deletion in T and B lymphocytes) in conditional deletion models. This work builds on the observations obtained in the study of deletion models of this *Smarca5* gene, i.e. that deletion leads to arrest of cell proliferation and their entry into apoptosis. Defects were observed already at the stem cell and hematopoietic progenitor stages, which were unable to enter the differentiation process in the absence of the SMARCA5 protein. In these models, it was not possible to study the progression of differentiation because of this reason. Therefore, we decided to create a new mouse model with a hypomorphic (expressing lower amounts of the protein) *SMARCA5* transgenic allele (*S5tg*), expressed on a *Smarca5* deletion background, which allowed us to observe hematopoietic cell differentiation at different levels of SMARCA5 protein expression. We observed that transgenic *SMARCA5* can rescue lymphocyte developmental arrest in a tissue-specific model of *Smarca5* deletion in this lineage (*hCD2iCre*), depending on the amount of protein expressed, as well as the lethal phenotype associated with constitutive deletion or conditional deletion in hematopoietic stem cells (*Vav1iCre*). The *Vav1iCre S5tg* model has shown that the expression level of SMARCA5 protein plays a crucial role in hematopoietic stem cells and progenitors; when the expression of this protein is reduced (to about 10 %), it results in the accumulation of multipotent progenitors that are unable to differentiate. The observed defect resulting from reduced SMARCA5 protein levels has the greatest impact on the differentiation of lymphocytes and their progenitors, especially in B-lymphocytes, which are the most sensitive to SMARCA5 protein levels, leading to a significant reduction in their numbers in peripheral blood. Number of erythrocytes was only minimally reduced and myelocytes were not affected by hypomorphic SMARCA5 expression. The transgenic SMARCA5 model demonstrates that the ISWI ATPase SMARCA5 is indispensable for the proper development of hematopoietic cells, especially lymphocytes. This research

contributes valuable insights to deepen the knowledge of this important epigenetic regulator, which can be used in the development of therapeutic strategies for hematopoietic disorders.

Keywords

chromatin, Snf2h, Smarca5, ATPase, mouse model, hematopoiesis, stem cells, multipotent progenitors

Obsah

1	Seznam zkratk	9
2	Úvod	11
2.1	Protein SMARCA5 a jeho komplexy	11
2.1.1	Komplexy ACF a CHRAC	15
2.1.2	Komplex WICH a B-WICH	17
2.1.3	Komplex RSF	17
2.1.4	Komplex NoRC	18
2.1.5	Ostatní komplexy	18
2.2	Deleční myší modely pro gen <i>Smarca5</i>	19
2.3	Protein SMARCA5 a nádorová onemocnění	23
3	Cíle disertační práce	25
4	Seznam publikací	26
4.1	(1. publikace) Differential requirements for <i>Smarca5</i> expression during hematopoietic stem cell commitment	28
4.2	(2. publikace) ISWI ATPase <i>Smarca5</i> Regulates Differentiation of Thymocytes Undergoing β -Selection	74
4.3	(3. publikace) Loss of ISWI ATPase SMARCA5 (SNF2H) in Acute Myeloid Leukemia Cells Inhibits Proliferation and Chromatid Cohesion	90
4.4	(4. publikace) Chromatin Remodeler <i>Smarca5</i> Is Required for Cancer-Related Processes of Primary Cell Fitness and Immortalization	104
5	Diskuse	138
6	Závěr a grantová podpora	146
7	Seznam použité literatury	147

1 Seznam zkratek

ACF	Komplex skládající se z proteinů SMARCA5 a ACF1 (anglicky <u>A</u> TP-utilizing <u>ch</u> romatin assembly and remodeling <u>f</u> actor)
ATP	Adenosin trifosfát (anglicky <u>A</u> denosine <u>t</u> riphosphate)
BAZ	Bromodoména sousedící s doménou zinkového prstu (anglicky <u>B</u> romodomain <u>A</u> djacent to <u>Z</u> inc finger domain)
BCR	B-buněčný receptor (anglicky <u>B</u> -cell <u>r</u> eceptor)
bp	Páry bází DNA (anglicky <u>B</u> ase <u>p</u> airs)
CD	Diferenciační skupina povrchových molekul, které najdeme především na buňkách imunitního systému (anglicky <u>C</u> luster of <u>d</u> ifferentiation)
CERF	Komplex skládající se z proteinů SMARCA5/SMARCA1 a CECR2 (anglicky <u>C</u> ECR2-containing remodeling <u>f</u> actor)
DN	Dvojitě negativní fáze vývoje thymocytů – neexprimují ani CD4 ani CD8 molekulu (anglicky <u>D</u> ouble <u>n</u> egative)
DNA	Deoxyribonukleová kyselina (anglicky <u>D</u> eoxyribo <u>n</u> ucleic <u>a</u> cid)
DP	Dvojitě pozitivní fáze vývoje thymocytů – exprimují CD4 i CD8 molekulu (anglicky <u>D</u> ouble <u>p</u> ositive)
CHRAC	Komplex skládající se z proteinů SMARCA5, ACF1, CHRAC-15 a CHRAC-17 (anglicky <u>C</u> hromatin <u>a</u> ccessibility <u>c</u> omplex)
ISWI	Název jedné z podrodin patřících do proteinové rodiny SWI2/SNF2 (anglicky <u>I</u> mitation mating type <u>s</u> witch)
MPP	<u>M</u> ultipotentní <u>p</u> rogenitor
NHEJ	Nehomologní spojování konců při opravě DNA, může zde docházet k mutacím (anglicky <u>N</u> on- <u>h</u> omologous <u>e</u> nd joining)
NoRC	Komplex skládající se z proteinů SMARCA5 a TIP5 (anglicky <u>N</u> ucleolar remodeling <u>c</u> omplex)
NURF	Komplex skládající se z proteinů SMARCA5/SMARCA1, BPTF, RBBP7, RBBP4 (anglicky <u>N</u> ucleosome remodeling <u>f</u> actor)
RNA	Ribonukleová kyselina (anglicky <u>R</u> ibonucleic <u>a</u> cid)
RSF	Komplex skládající se z proteinů SMARCA5 a RSF-1 (anglicky <u>R</u> emodeling and <u>s</u> pacing <u>f</u> actor)

Smarca5	Faktor remodelující chromatin závislý na ATP, který tvoří katalytickou podjednotku ISWI komplexů, jinak také nazývaný Snf2h (anglicky <u>S</u> WI/SNF related, <u>m</u> atrix associated, <u>a</u> ctin dependent <u>r</u> egulator of <u>c</u> hromatin, subfamily <u>a</u> , member 5)
Snf2h	viz. Smarca5 (anglicky <u>S</u> ucose <u>n</u> onfermenting <u>2</u> <u>h</u> omolog)
Snf21	Faktor remodelující chromatin závislý na ATP, který tvoří katalytickou podjednotku ISWI komplexů, jinak také nazývaný Smarca1 (anglicky <u>S</u> ucose <u>n</u> onfermenting <u>2</u> - <u>l</u> ike protein)
SWI/SNF	Proteinová rodina na ATP závislých faktorů remodelujících chromatin (anglicky Mating type <u>s</u> witch/ <u>S</u> ucose <u>n</u> onfermenting)
TCR	T-buněčný receptor (anglicky <u>T</u> - <u>c</u> ell <u>r</u> eceptor)
Tip5	Protein vyskytující se spolu se Smarca5 v komplexu NoRC (anglicky <u>T</u> ranscription termination factor 1 (Ttf1) – <u>i</u> nteracting protein <u>5</u>)
Vav1	Vav Guanin nukleotidový výměnný faktor 1 (anglicky Vav Guanine Nucleotide Exchange Factor 1)
WICH	Komplex skládající se z proteinů SMARCA5 a WSTF (anglicky <u>W</u> STF- <u>I</u> SWI <u>c</u> hromatin remodeling complex)
WSTF	Protein vyskytující se spolu se Smarca5 v komplexu WICH, gen pro tento transkripční faktor je jedním z deletovaných genů u Williamsova syndromu (anglicky <u>W</u> illiams <u>s</u> ndrome <u>t</u> ranscription <u>f</u> actor)

2 Úvod

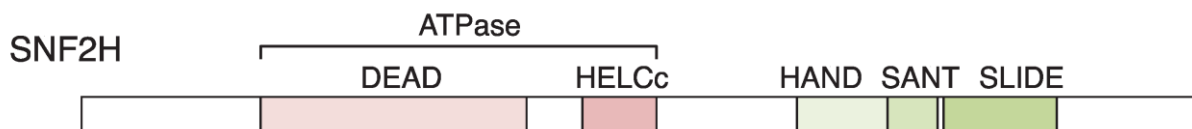
DNA se v jádře buněk organizuje do struktury chromatinu, jež je tvořena zejména dvoušroubovicí deoxyribonukleotidové kyseliny a rozličnými histonovými proteiny, které umožňují velmi dlouhou molekulu DNA uložit a aktivně využívat v prostoru buněčného jádra. Chromatinová struktura nabývá různých stupňů fluidity nebo kondenzace, jež se mění během buněčného cyklu, diferenciaci, poškození či stárnutí buněk. Chromatin je dynamický a jeho struktura hraje roli v procesu regulace genové exprese, především transkripce a elongace RNA, dále též v replikaci a genové opravě tím, že dochází k odhalení či zneprístupnění určitých DNA regulačních sekvencí DNA vazebným faktorům a transkripčním faktorům, kofaktorům a DNA a RNA polymerázám. Změny chromatinové struktury provází změny v epigenetických modifikacích histonů i DNA, které hrají zásadní roli při nastartování diferenciaci buněk ale taktéž v zabránění diferenciaci u kmenových buněk.

Epigenetické modifikace řadíme do dvou druhů – kovalentní modifikace histonových N-konců a nekovalentní modifikace zprostředkované chromatin remodelačními komplexy závislými na ATP. Tato disertační práce shrnuje a dává do kontextu vědeckou práci, jež objasňuje funkci jednoho z klíčových ISWI chromatin remodelačních faktorů, konkrétně proteinu SMARCA5 a jeho komplexů, a to zejména během diferenciaci krvinek, ve kterých je tento protein hojně exprimován. K tomu účelu bylo vytvořeno v naší laboratoři několik myších modelů a také z nich získaných buněčných linií. Tyto modely umožnily provádět vysoce specifický výzkum role SMARCA5, a to především v *in vivo* podmínkách během liniové determinace krvinek kmenové buňky a tím prozkoumat jeho konkrétní zapojení s přirozenými kofaktory v klíčových procesech krvetvorby. Tyto experimenty umožnily studium SMARCA5 posunout na novou úroveň a dosáhnout pochopení funkce tohoto proteinu v diferenciaci krvinek.

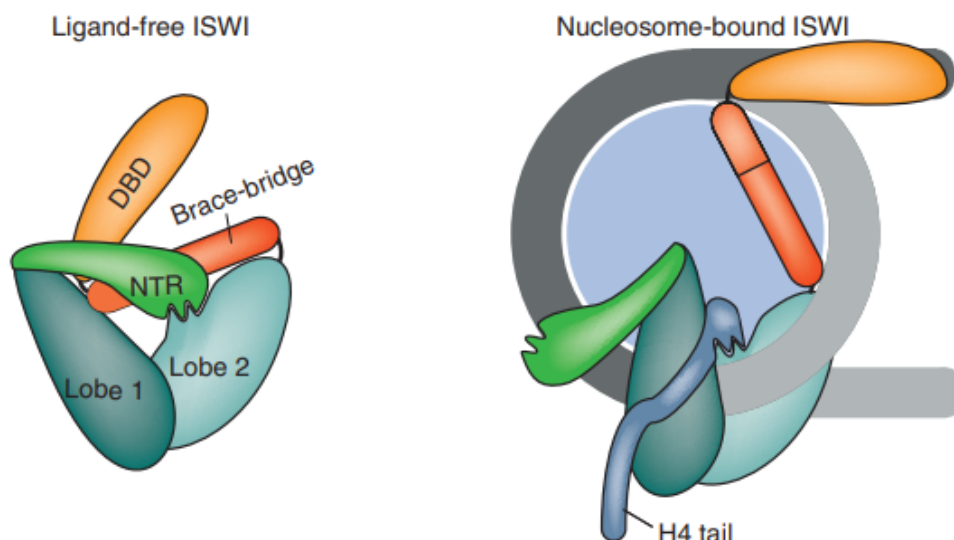
2.1 Protein SMARCA5 a jeho komplexy

Evolučně značně konzervovaný protein SMARCA5 (SWI/SNF Related, Matrix Associated, Actin Dependent Regulator Of Chromatin, Subfamily A, Member 5) patří do rodiny SWI2/SNF2 (Switching defective and Sucrose non fermenting) DNA dependentních helikáz-ATPáz. Tyto enzymy využívají energii vzniklou hydrolýzou ATP pro rozvolnění nekovalentních vazeb mezi DNA a histonovými proteiny a následnou remodelaci struktury chromatinu. To si lze představit jako časově omezené oddálení histonů od vlákna DNA, zpřístupnění úseku DNA enzymům a transkripčním faktorům a následné posunutí či zabalení DNA ve struktuře nukleozómu vůči přilehlým histonovým proteinům (Bowman 2010). Studie

založená na měření pomocí metody FRET (Försterův rezonanční přenos energie) umožnila detailní pohled na to, jak posun vlákna DNA vůči histonovým proteinům probíhá, autoři zde využili kvasinkový ISWI komplex. Celý posun probíhá velmi organizovaným způsobem po krátkých úsecích DNA (napřed 7bp a pak 3bp dlouhých), které jsou po jednom páru bází uvolňovány a opouští strukturu nukleozómu (Deindl, Hwang et al. 2013). ATPázy z rodiny ISWI umožňují posun histonového oktameru po vlákně DNA až o 100 párů bází, čímž může dojít k odhalení a zpřístupnění regulačních oblastí DNA jako jsou například promotory (Becker 2002). Molekula ATP se váže do žlábků mezi RecA-like proteiny helikázové domény, jež je velmi konzervovaná a představuje strukturální podjednotku všech ATPáz ze super-rodiny (či nadrodiny) SWI2/SNF2 (Fairman-Williams, Guenther et al. 2010). Mimo N-koncové helikázové domény dále protein SMARCA5 obsahuje domény HAND, SANT (S*wi*3 A*da*2 N-*Co*R TFIIB, (Boyer, Langer et al. 2002)) a SLIDE (SANT-like ISWI domain), které umožňují specifickou vazbu na strukturu chromatinu (především na N-koncové části histonů H3 a H4) a také interakci se SMARCA5 vazebnými partnery, tzv. BAZ proteiny (Boyer, Latek et al. 2004), (Grune, Brzeski et al. 2003). Umístění jednotlivých domén v rámci proteinu SMARCA5 je znázorněno na obrázku č. 1. Modelové schéma mechanismu posunu nukleozómů po vlákně DNA pomocí ISWI remodelačních faktorů je znázorněno na obrázku č. 2.

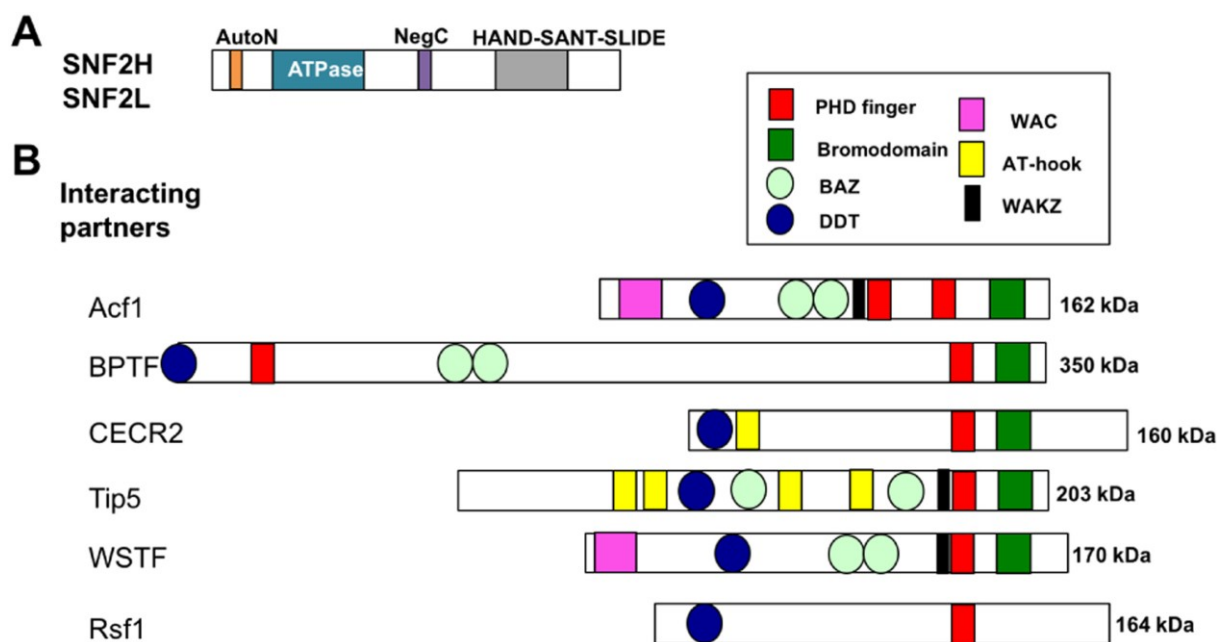


Obrázek č. 1: Schéma struktury proteinu SMARCA5 (SNF2H). Helikázová doména s ATPázovou aktivitou na N-konci proteinu a domény HAND, SANT a SLIDE na C-konci. Převzato z (Kato and Komatsu 2015).



Obrázek č. 2: Model posunu nukleozómů po vlákně DNA pomocí ISWI remodelačních faktorů. Schéma ISWI komplexu bez ligandu (vlevo) a navázaného na nukleozóm (vpravo). Ve stavu bez ligandu je N-terminální oblast proteinu (NTR) v kontaktu s ATPázovou doménou. Tento kontakt zahrnuje motiv AutoN, který je strukturně podobný N-koncové části histonu H4, a spolu s částí proteinu, zde nazvanou „brace-bridge“, stabilizuje ATPázovou doménu ve stavu neslučitelném s hydrolyzou ATP. Vazba ATPázové domény na nukleozóm a N-koncovou část histonu H4 vede k uvolnění vazby NTR. To umožňuje, aby ATPázová doména zaujala konformaci vhodnou pro hydrolyzu ATP. Spolu s tím dochází též k vazbě DNA-vazebné domény (DBD, obsahuje motivy HAND, SANT a SLIDE) na DNA vystupující ze struktury nukleozómu. Takto navázaná ISWI ATPáza pak může katalyzovat posun nukleozómu po vlákně DNA. Tento model byl převzat z (Mueller-Planitz, Klinker et al. 2013).

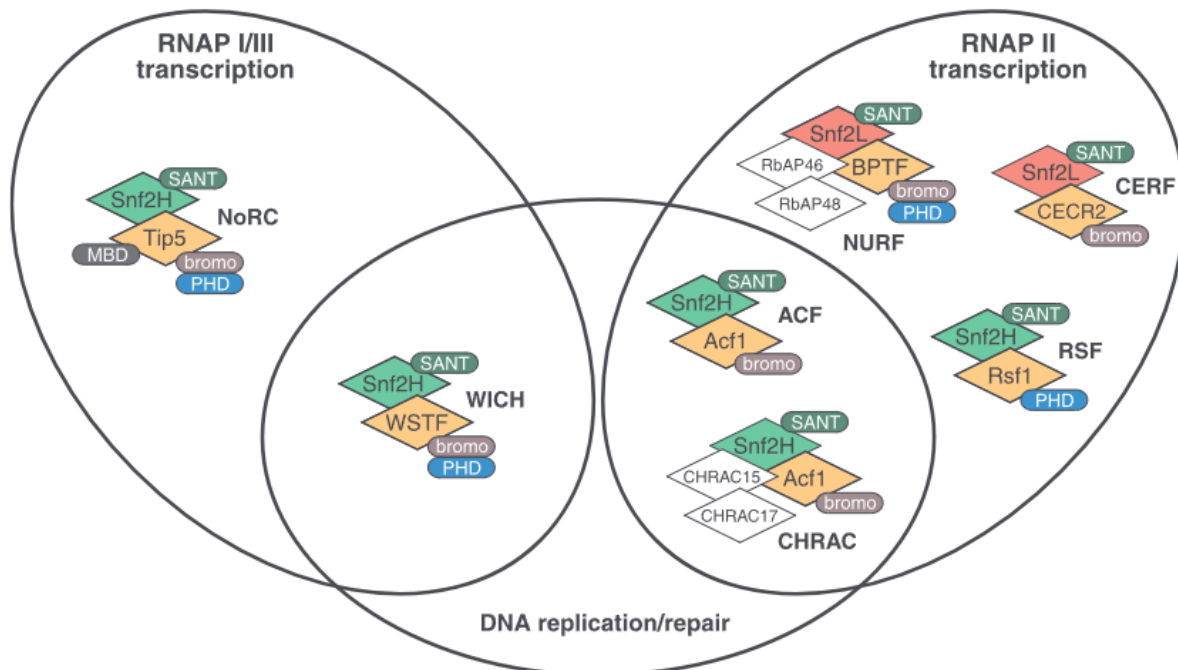
Protein SMARCA5 je v jádru buněk aktivní v komplexech s dalšími proteiny. SMARCA5 zde plní funkci motoru, který díky své ATPázové aktivitě zajišťuje energii potřebnou pro remodelaci, zatímco jeho vazební partneři zajišťují vazbu na strukturu chromatinu, čímž ovlivňují specifické funkce daného komplexu. Protein SMARCA5 může být součástí celkem 7 prozatím objevených komplexů, viz obrázek č. 3. Jedná se o komplexy: ACF (ATP-utilizing chromatin assembly and remodeling factor), CHRAC (chromatin accessibility complex), WICH (Williams syndrome transcription factor-imitation switch), B-WICH, RSF (Remodeling and sparing factor), NoRC (Nucleolar remodeling complex), Smarca5-kohezinový komplex, NURF (Nucleosome remodeling factor) a CERF (CECR2-containing remodeling factor).



Obrázek č. 3.: (A) Schématické znázornění proteinů SMARCA5 (SNF2H) a SMARCA1 (SNF2L). Tyto proteiny jsou z 86 % homologické. (B) Schématické znázornění interakčních partnerů proteinů SMARCA5 a SMARCA1. Všechny tyto proteiny sdílí určité motivy, důležité pro vazbu na strukturu chromatinu, jako je například DDT doména (modře), PHD finger (Plant Homeodomain) doména (červeně), či bromodoména (tmavě zeleně). Převzato z (Goodwin and Picketts 2018).

Komplexy NURF a CERF byly popsány pro druhého člena rodiny ISWI chromatin remodelačních faktorů – protein SMARCA1 (SNF2L), který je s proteinem SMARCA5 z více než 80 % homologický a bylo dokázáno se tyto dva proteiny se mohou nacházet navzájem zaměnitelně ve všech komplexech popsaných pro oba z nich (Oppikofer, Bai et al. 2017). Ukazuje se ale, že proteiny SMARCA1 a SMARCA5 nejsou schopné vzájemně nahradit své funkce, jednak proto, že v delečních modelech pro tyto proteiny nebylo pozorováno, že by homolog nahradil funkce deletovaného proteinu. Dále také bylo pozorováno, že tyto proteiny jsou exprimovány v různých typech buněk, zatímco SMARCA5 je obecný faktor exprimovaný téměř ve všech tkáních, protein SMARCA1 je exprimován hlavně v diferencovaných neuronech, reprodukčních orgánech a placentě (Lazzaro and Picketts 2001). V testes bylo pozorováno, že protein CECR2 vytváří komplex s proteinem SMARCA5 (který je zde více exprimován než SMARCA1) a hraje roli při spermatogenezi, na rozdíl od neurální trubice a vnitřního ucha, kde CECR2 vytváří komplex s proteinem SMARCA1 (Thompson, Norton et

al. 2012). Protein SMARCA5 plní v jádru buněk různé funkce v závislosti na tom, v jakém komplexu se nachází, viz obrázek č. 4, které bych v dalších pár odstavcích chtěla popsat detailněji.



Obrázek č. 4.: ISWI komplexy a jejich funkce. Schématické znázornění komplexů (včetně hlavních proteinových domén), které mohou hrát roli v replikaci, transkripci či opravě DNA. Proteiny SMARCA5 (=SNF2H) a jeho homolog SMARCA1 (=SNF2L) se mohou vyskytovat ve všech zobrazených komplexech. Obrázek převzat z (Erdel and Rippe 2011).

2.1.1 Komplexy ACF a CHRAC

Komplex ACF je tvořen dvěma podjednotkami, proteinem SMARCA5 a dále tzv. BAZ proteinem, konkrétně: ACF1/BAZ1A (Bromodomain adjacent to zinc finger domain 1A) (Ito, Bulger et al. 1997), (Ito, Levenstein et al. 1999). Tento (tzv. ACF, anglicky ATP-utilizing chromatin assembly and remodeling factor) komplex je spojovaný zejména s vysoce kondenzovanou strukturou heterochromatinu, kde může plnit různé funkce. Jednak pomáhá při průchodu polymerázy touto strukturou během procesu replikace DNA v pozdní části S-fáze buněčného cyklu, tím že udržuje chromatin v rozvolněné podobě (Collins, Poot et al. 2002). Komplex ACF také rozvolňuje strukturu heterochromatinu, aby byla přístupná reparačním proteinům, při opravě dvouvláknových zlomů na DNA procesem nehomologní rekombinace (NHEJ) (Klement, Luijsterburg et al. 2014). Roli komplexu ACF v procesech replikace a

opravy DNA potvrdila také studie využívající fluorescenční mikroskopii k lokalizaci tohoto komplexu v jádře, která potvrdila zvýšený výskyt ACF v oblastech, kde tyto procesy aktivně probíhaly (Erdel, Schubert et al. 2010). Tento komplex hraje též roli v rozpoznání poškození DNA během G2/M přechodu během buněčného cyklu, což dále dokazuje jeho význam při opravě DNA (Sanchez-Molina, Mortusewicz et al. 2011). SMARCA5 v komplexech ACF a WICH, skenuje DNA vlákno a hledá místa poškození, jak bylo pozorováno při poškození vyvolaném pomocí UV-zářením. Tyto dva komplexy spolu pravděpodobně interagují a ve chvíli, kdy naleznou místo poškození, tak se váží na chromatinovou strukturu a aktivují nukleotidovou excizní opravu spřaženou s transkripcí (TC-NER) (Aydin, Marteiijn et al. 2014). Komplex ACF dokáže pomocí posunu histonových oktamerů po vláknech DNA vytvořit rovnoměrné rozestupy mezi nukleozómy, což je typické pro kondenzované struktury heterochromatinu. Snížená exprese komplexu ACF vedla též k narušení regulace genové exprese pomocí Polycomb proteinů. Komplex tedy pravděpodobně hraje roli také v procesu umlčování genů (Fyodorov, Blower et al. 2004). Tuto hypotézu podporuje též studie popisující vazbu komplexu ACF na modifikovaný histon macroH2A, který se nachází v inaktivovaném X-chromozomu (Chang, Ferreira et al. 2008). Další studie dokazují roli komplexu ACF v umlčování genů pomocí N-CoR korepresoru (anglicky nuclear receptor corepressor) a histonové deacetylázy 3. N-CoR je korepresor, který blokuje jaderné receptory a tím umlčuje expresi genů, která by jinak byla těmito receptory aktivována. Komplex ACF se váže do promotorových oblastí takto umlčovaných genů a modifikuje zde strukturu chromatinu (Alenghat, Yu et al. 2006), (Ewing, Attner et al. 2007). Deleční myší model (uskutečněný ve všech buňkách myši) pro *Acf1* prokázal esenciální roli ACF komplexu pro spermatogenezi, myší samci s delecí na obou alelách genu jsou sterilní a byl u nich pozorován výrazně snížený počet spermií, které měly navíc sníženou motilitu a defektní morfologii. Změny ve struktuře chromatinu pozorovány nebyly, ale byly naměřeny problémy s regulací genové exprese mnoha genů důležitých pro správný průběh spermatogeneze (Dowdle, Mehta et al. 2013).

Komplex CHRAC se skládá ze stejných proteinů jako komplex ACF, tedy SMARCA5 a ACF1, ale obsahuje navíc ještě proteiny CHRAC-15 a CHRAC-17. Komplex CHRAC má také stejně jako komplex ACF schopnost vytvářet rovnoměrné rozestupy mezi nukleozómy, které jsou charakteristické pro kondenzované části umlčeného chromatinu (Poot, Dellaire et al. 2000). Pozorování získaná z modelového organismu *Drosophila melanogaster* ukazují, že komplex CHRAC je exprimován pouze v časně fázi embryonálního vývoje (Corona, Eberharter et al. 2000).

2.1.2 Komplex WICH a B-WICH

Komplex WICH se skládá z proteinů SMARCA5 a WSTF/BAZ1B (Williams syndrome transcription factor). Gen pro *WSTF* je jedním z genů deletovaných u pacientů s Williamsovým syndromem, což je vývojová porucha postihující mnoho tkání, zejména však kardiovaskulární a nervovou soustavu (Martens 2013). Komplex WSTF se stejně jako komplex ACF podílí na replikaci genů, kdy stejně jako tento komplex remodeluje chromatin do rozvolněné podoby umožňují přístup proteinům replikační vidličky a interaguje s ‚clamp‘ proteiny a topoisomerázou I (Poot, Bozhenok et al. 2004), (Ribeyre, Zellweger et al. 2016). Komplex WICH se pravděpodobně podílí na udržování rozvolněné struktury chromatinu. V experimentech, kdy došlo ke snížení jeho exprese *in vitro*, byl pozorován vyšší podíl heterochromatinového proteinu HP1 a histonových modifikací typických pro kondenzované části chromatinu (Poot, Bozhenok et al. 2004). Komplex WICH může dále vytvářet větší komplex B-WICH hrající roli v procesu transkripce ribozomálních genů polymerázou I a III. Komplex B-WICH obsahuje sliceosomový faktor Sf3b155/SAP155, RNA helikázu II/Gua α , Myb-binding protein 1a, CSB, protoonkogen Dek, nucleární myosin 1 a také RNA (45 S rRNA, 5 S rRNA, 7SL RNA) (Cavellan, Asp et al. 2006), (Percipalle, Fomproix et al. 2006). Stejně jako komplex WICH je i komplex B-WICH spojován s rozvolněnou strukturou chromatinu. Bylo pozorováno, že je schopen rekrutovat histonové acetyl-transferázy (probíhá například acetylace H3K9, která je nezbytná pro transkripci RNA polymerázou III) a tím umožnit počátek transkripce v oblasti genů pro 5S a 7S ribozomální podjednotky (Sadeghifar, Bohm et al. 2015). Dále se ukázalo, že komplex B-WICH také pravděpodobně hraje roli při opravě dvouvláknových zlomů na DNA, kde je schopen díky své vnitřní kinázové aktivitě vytvářet histonové modifikace – fosforylovat tyrozin 142 na histonu H2AX, což je důležitá značka pro započetí opravy zlomů (Xiao, Li et al. 2009).

2.1.3 Komplex RSF

Komplex RSF je tvořen proteiny SMARCA5 a RSF1 (LeRoy, Loyola et al. 2000). Tento komplex se vyznačuje svojí chaperonovou aktivitou, dokáže totiž vázat tetramery histonů H3 a H4 a tyto histony umisťovat na vlákno DNA. Následně s nimi dokáže pohybovat po vlákně DNA, tak aby mezi nimi vznikly rovnoměrné rozestupy a podílet se tímto způsobem na procesu vytváření struktury chromatinu (Loyola, LeRoy et al. 2001). Komplex RSF hraje zásadní roli při formaci centromery, při tomto procesu také využívá svou chaperonovou aktivitu. Mění zde složení nukleozómů, kdy dochází k inkorporaci speciální varianty histonu H3 a to CENP-A do oblasti centromery (Perpelescu, Nozaki et al. 2009). Dále komplex RSF hraje roli v opravě

dvouvláknových zlomů na DNA, do těchto míst inkorporuje proteiny CENP-S a CENP-X, které dále hrají roli pro signalizaci opravy mechanismem NHEJ (Helfricht, Wiegant et al. 2013). Ukázalo se, že navýšení množství RSF1 proteinu v buněčných liniích pomocí transgenního konstruktů vedlo k poškození DNA a navýšení množství dvouvláknových zlomů, což by mohla být jedna z příčin proonkogenních vlastností tohoto proteinu (Sheu, Guan et al. 2010).

2.1.4 Komplex NoRC

Komplex NoRC je tvořen proteiny SMARCA5 a TIP5/BAZ2A (Strohner, Nemeth et al. 2001). Protein TIP5 obsahuje PHD doménu, která přímo interaguje s histonovou deacetylázou 1, jejíž aktivitu pak přináší do promotorových oblastí rDNA, které jsou transkribovány RNA polymerázou I (Zhou, Santoro et al. 2002). Do těchto oblastí je komplex rekrutován díky své interakci s transkripčním faktorem Ttf1, který je nezbytný právě pro transkripci RNA polymerázou I (Strohner, Nemeth et al. 2001). Bylo dokázáno, že komplex NoRC interaguje s histonovou značkou H4K16acetyl a následně deacetyluje okolní lysiny (H4K5, H4K8, H4K12) a interaguje též s DNA methyl-transferázami, které pak dále vytváří modifikace známé pro kondenzovanou strukturu heterochromatinu (Zhou and Grummt 2005). Komplex NoRC může interagovat také s histonovými methyl-transferázami a methylovat například lysin na pozici H3K9 (umlčující značka) a to v oblastech rDNA promotorů (Santoro, Li et al. 2002). K umlčení promotorů může docházet též pomocí již zmiňovaného posunu nukleozómů po vlákně DNA, který ISWI remodelační komplexy katalyzují. Bylo pozorováno, že komplex NoRC posouvá nukleozómy v promotorových oblastech takovým způsobem, že dojde k zneprístupnění oblasti pro transkripční faktory (Li, Langst et al. 2006). Mimo zmíněných funkcí souvisejících s umlčováním transkripce v jádru hraje NoRC také roli ve formaci centromery, byla prokázána přímá interakce s histonovým proteinem CENP-A typickým pro oblast centromery. Po depleci proteinu TIP5 v NIH3T3 buňkách byla pozorována prodloužená doba dělení buněk a narušení struktury mitotického vřeténka, což během anafáze vedlo k problémům s distribucí chromozómů do nově vznikajících buněk (Guertg, Lienemann et al. 2010). Mimo formace centromery komplex NoRC hraje též roli v heterochromatinizaci telomer, čímž napomáhá udržovat stabilitu genomu (Postepska-Igielska, Kronic et al. 2013).

2.1.5 Ostatní komplexy

Protein SMARCA5 dokáže vytvářet komplexy ještě s dalšími typy proteinů, jedním z nich je kohezinový komplex, kde přímo interaguje s proteinem RAD21. Tento komplex je zásadní pro udržení koheze sesterských chromatid (Hakimi, Bochar et al. 2002). Dále, jak již bylo řečeno může protein SMARCA5 vytvářet komplexy se známými vazebnými partnery

proteinu SMARCA1, tedy BPTF a CERF2. Komplex NURF, tvořený proteiny SMARCA5 a BPTF byl popsán jako esenciální pro správný vývoj T-lymfocytů. Ukázalo se, že tento komplex pravděpodobně hraje roli při aktivaci genů při TCR signalizaci během vývoje této buněčné linie (Landry, Sharov et al. 2008). Komplex CECR2 (proteiny SMARCA5 a CERF2) se nachází v embryonálních kmenových buňkách a v testes, kde hraje roli při spermatogenezi, u myších samců s delecí *Cerf2* byla pozorována snížená fertilita, přestože počet spermií ani jejich motilita nebyly výrazně sníženy (Thompson, Norton et al. 2012). Byla též popsána též interakce proteinu SMARCA5 (a také SMARCA1) s vazebným partnerem BAZ2B, funkce tohoto komplexu nejsou zatím známy (Oppikofer, Bai et al. 2017).

2.2 Deleční myší modely pro gen *Smarca5*

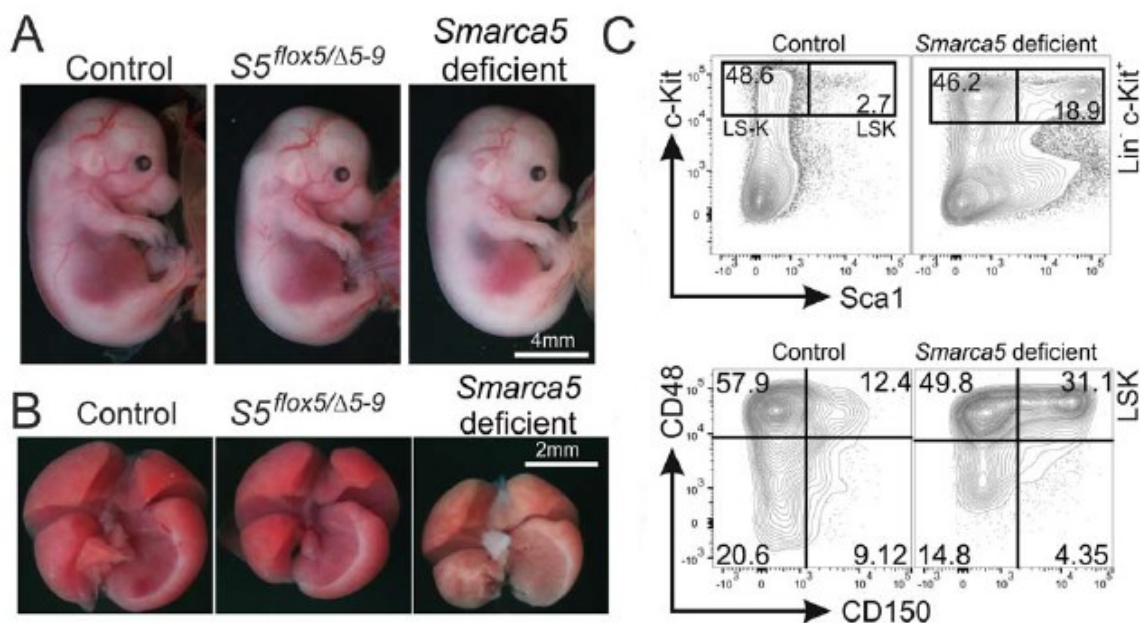
Pro studium chromatin remodelačních komplexů *in vivo* byla vytvořena řada myších modelů, které umožnily rozšířit dosavadní pozorování pocházející hlavně z experimentů provedených *in vitro* nebo na modelech nepocházejících ze třídy savců (*Drosophila melanogaster*, *Xenopus laevis*). *In vitro* modely jsou cenným nástrojem pro výzkum funkcí remodelačních komplexů na molekulární úrovni a jejich rolí v buněčných procesech, neumožňují ale sledovat jejich role při vývoji tkání a orgánů či jednotlivce jako celku. Vzhledem k vysoké expresi proteinu SMARCA5 ve kmenových buňkách a progenitorech, jako jsou například krvetvorné progenitory (Prasad, Lennartsson et al. 2015) bylo možné předpokládat, že tento protein hraje důležitou roli v buněčné diferenciaci, krvetvorbě a vývoji jedince. Za tímto účelem byla v naší laboratoři vytvořena řada myších delečních modelů, prvním z nich byl celotělový knock-out model pro *Smarca5* gen (delece exonů 5-9a kódujících katalytickou doménu ATPázy) (Stopka and Skoultchi 2003). Tento model je letální ve velmi časně fázi embryonálního vývoje a pomocí *ex vivo* kultivace blastocyst s deletovaným genem *Smarca5* na obou alelách bylo zjištěno, že k defektům dochází už 48 hodin po začátku vývoje blastocysty. Buňky vnitřní zárodečné vrstvy (anglicky inner cell mass) nebyly schopné proliferovat a vstupovaly do apoptózy (Stopka and Skoultchi 2003).

Podobný fenotyp byl pozorován také u myší linie MommeD4 (Modifier of murine metastable epiallele dominant, chemicky-vytvořená mutace genu *Smarca5*), které mají nekonzervativní záměnu jedné aminokyseliny v oblasti helikázové domény, která pravděpodobně vede k narušení ATPázové funkce. Existují celkem tři takové linie: výše zmíněná MommeD4 (záměna adeninu za thymin v exonu 12) a dále ještě: MommeD35 (záměna adeninu za guanin v exonu 9) a MommeD37 (záměna thyminu za cystein v exonu 13), u všech

těchto linií dochází k velmi časté embryonální letalitě, pokud nesou mutaci na obou alelách genu pro *Smarca5* (Chong, Vickaryous et al. 2007), (Daxinger, Harten et al. 2013).

Jak už bylo zmíněno protein SMARCA5 je exprimovaný v krvetvorných kmenových buňkách a progenitorech, které v naší laboratoři Hematoonkologie a kmenových buněk studujeme. Celotělový deleční model *Smarca5* prokázal roli SMARCA5 v regulaci délky linkeru, tedy volné DNA, která se nachází mezi jednotlivými nukleozómy. Absence SMARCA5 proteinu vedla ke zvýšení délky linkeru, což je defekt, který změnil dostupnost určitých úseků DNA pro mnoho transkripčních faktorů, včetně vazby vazebného faktoru CTCF (Barisic, Stadler et al. 2019). Hlavní funkcí CTCF je inhibice transkripčních enhancerů, což je jeden z mechanismů řídících expresi transkripčního faktoru PU.1 (SPI1), který je nezbytný pro časnou iniciaci krvetvorby a diferenciaci myelocytárních a lymfocytárních progenitorů (Dluhosova, Curik et al. 2014). Z výše zmíněných důvodů jsme v naší laboratoři chtěli studovat význam proteinu SMARCA5 během procesu myší krvetvorby, za tímto účelem byl vytvořen kondicionální deleční model, ve kterém je možné pomocí Cre rekombinázy deletovat exon 5 *Smarca5* genu, který kóduje helikázovou doménu. Delece je zároveň navržena tak, že dochází k posunu čtecího rámce ve výsledné zkrácené molekule mRNA, která tak nemůže dát vzniknout ani zkrácené verzi proteinu. Tento kondicionální deleční model byl následně křížen s různými Cre expresory, umožňujícími delecí *Smarca5* ve specifické tkáni či buněčné linii (Kokavec, Zikmund et al. 2017), (Zikmund, Kokavec et al. 2019).

Jedním z takto vytvořených modelů je *Vav1Cre Smarca5^{fl/fl}*, ve kterém dochází k delecí v krvetvorné kmenové buňce, *Vav1* je též exprimovaný v téměř celém průběhu krvetvorby (Kokavec, Zikmund et al. 2017). Tento model je také embryonálně letální stejně jako celotělový knock-out, ale embrya umírají až v E18,5 dni jejich vývoje, vlivem selhání erytropoézy. Je pro ně typický anemický fenotyp spojený s defektem ve vývoji jejich hlavního krvetvorného orgánu – fetálních jater. Také u nich dochází k hromadění LSK (Lin⁻Sca1⁺c-Kit⁺) krvetvorných progenitorů, které nejsou schopné další diferenciaci, viz obrázek č. 5 (Kokavec, Zikmund et al. 2017).



Obrázek č. 5: Genotyp *Vav1iCre Smarca5^{f/f}* je embryonálně letální a vykazuje anemický fenotyp. (A) Embrya ve věku E15,5 dne jejich vývoje, zleva první je kontrolní genotyp a vedle něj heterozygotní a homozygotní delece *Smarca5*. (B) Fetální játra vyizolovaná z embryí výše popsaných genotypů. Při homozygotní deleci *Smarca5* dochází k selhání erythropoézy a defektům ve vývoji fetálních jater. (C) Analýza buněčné suspenze vyizolované z E13,5 dne starých fetálních jater pomocí průtokové cytometrie. U *Smarca5* deficientních jedinců můžeme pozorovat akumulaci LSK krvetvorných progenitorů. Tato populace byla dále rozdělena podle exprese CD48 a CD150 markerů, zde můžeme vidět akumulaci CD48⁺CD150⁺ populace, tedy multipotentních progenitorů typu 2. Obrázek převzat z (Kokavec, Zikmund et al. 2017).

Vzhledem k pozorované nezastupitelné funkci proteinu SMARCA5 pro vývoj erytrocytů byl následně vyvinut kondicionálně deleční model *EpoRiCre Smarca5^{f/f}*, kde dochází k deleci v liniově determinovaných erytroidních progenitorech. Účelem tohoto modelu bylo zjistit, zda delece *Smarca5* v pozdějším stádiu krvetvorby (oproti *Vav1iCre* modelu) povede taktéž k zastavení diferenciace. Tento předpoklad se ukázal jako správný, u *EpoRiCre* modelu bylo taktéž pozorováno selhání erythropoézy, tento defekt byl ovšem menší než u *Vav1iCre* modelu a některá embrya přežila vývoj až do dospělého věku. Byla však pozorována menší než očekávaná pravděpodobnost narození jedinců s genotypem *EpoRiCre Smarca5^{f/f}* a u těch co se narodili, byla pozorována snížená hmotnost a anemický fenotyp (Kokavec, Zikmund et al. 2017). Na tento výzkum dále navazoval kondicionální deleční model pro protein SMARCA5

v lymfocytech (*CD2iCre*), pomocí kterého jsme studovali vliv SMARCA5 na tuto linii, v průběhu jejíhož vývoje dochází řízeným dvojláknovým zlomům DNA (během V(D)J rekombinace). Manuskript založený na studiu *CD2iCre Smarca5^{fl/fl}* modelu je součástí této disertační práce (Zikmund, Kokavec et al. 2019).

Mimo výše zmíněných kondicionálních delečních modelů v krvetvorných buňkách byly vytvořeny ještě další, které bych chtěla krátce zmínit. Jedním z nich je model delece v progenitorech granulárních neuronů pomocí Nestin-Cre rekombinázy. U jedinců s delecí na obou alelách byla pozorována výrazně snížená hmotnost a hypoplazie mozečku, dále také jedinci trpěli ataxií a umírali dříve než kontroly (Alvarez-Saavedra, De Repentigny et al. 2014). V této práci dále ještě delemovali *Smarca5* pomocí PCP2-Cre rekombinázy, která je exprimovaná v progenitorech Purkyňových buněk, tyto myši měly normální hmotnost, ale vykazovaly určité defekty v jejich kognitivních schopnostech (Alvarez-Saavedra, De Repentigny et al. 2014). Dalším modelem, je kondicionální delece *Smarca5* v progenitorech oční čočky pomocí Le-Cre rekombinázy. U tohoto modelu byly pozorovány defekty ve vývoji oka, například u buněk oční čočky nedocházelo k denukleaci, což bylo způsobeno defekty v expresi řady genů důležitých pro tento proces (He, Limi et al. 2016). Dalším modelem je kondicionální delece *Smarca5* v retině, která má za následek defekt v jejím vývoji, projevující se defekty laminace a nepřítomností vrstvy fotoreceptorů. Bylo pozorováno, že *Smarca5* deficientní progenitory mohou dát vzniknout všem potřebným buněčným typům, ale byl pozorován výrazný defekt v jejich proliferaci, hlavně v S-fázi buněčného cyklu (Kuzelova, Dupacova et al. 2023).

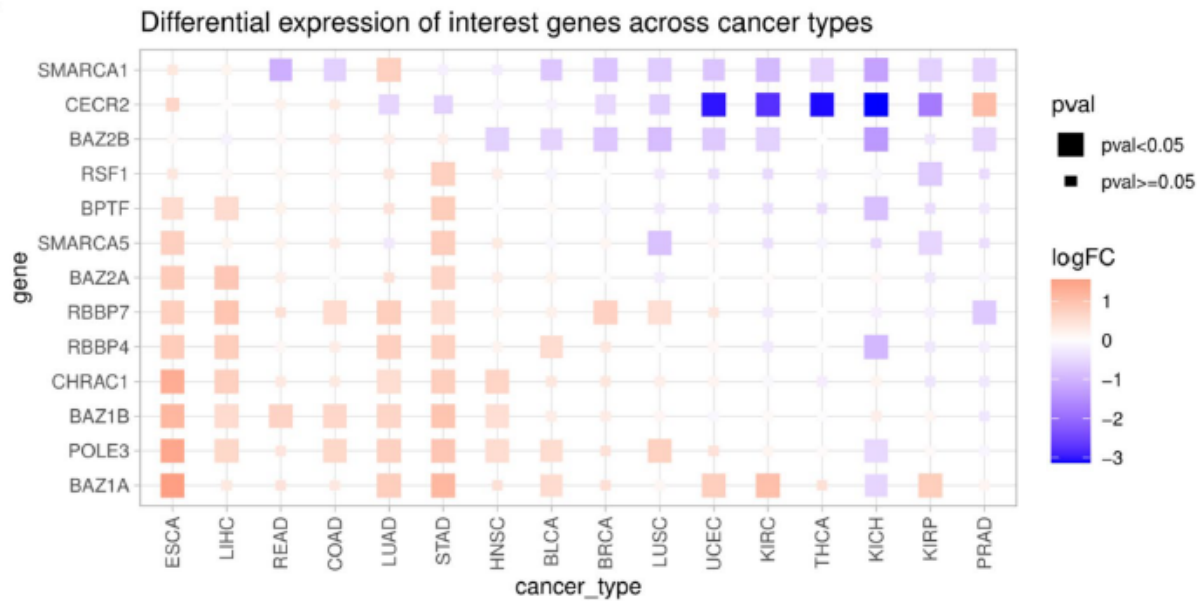
Všechny výše zmíněné deleční myší modely prokázaly, že protein SMARCA5 je nezbytný pro diferencující a dělicí se buňky a jeho delece vede k zastavení buněčného cyklu a vstupu do apoptózy. Abychom mohli studovat funkce tohoto proteinu během procesu diferenciace, vytvořili jsme v naší laboratoři model s transgenní expresí alely genu *Smarca5*, jež je hypomorfní a tedy produkuje nižší množství proteinu oproti normální alele. Po zkřížení s popsányými delečními modely (*Smarca5^{fl/fl}*) jsme tak vytvořili model s odstupňovanými hladinami exprese SMARCA5 proteinu (z jedné či ze dvou alel transgenu), který nám umožnil studovat vliv odstupňované míry exprese tohoto proteinu na viabilitu a funkci různých buněčných podtypů.

2.3 Protein SMARCA5 a nádorová onemocnění

V řadě studií byla pozorována deregulovaná exprese jak *Smarca5* genu, tak jeho paralogu *Smarca1*, tak i jeho vazebných partnerů v různých typech nádorových onemocnění (Li, Gong et al. 2021). Zatímco protein SMARCA1 se jeví spíše jako tumor-supresor a v nádorových buňkách bývá jeho exprese umlčována, jak je tomu např. nádorech trávicího traktu (Takeshima, Niwa et al. 2015), nebo v melanomech (Eckey, Kuphal et al. 2012). Protein SMARCA5 může mít proonkogenní účinky a v nádorových buňkách bývá často nadprodukován, jak tomu je např. u rakoviny prsu (Jin, Mao et al. 2015), hepatocelulárního karcinomu (Wang, Qin et al. 2016), nebo u akutní myeloidní leukémie (Stopka, Zakova et al. 2000).

Co se týče vazebných partnerů pro SMARCA5, v souvislosti s nádorovými onemocněními je nejčastěji zmiňován protein RSF1 (komplex RSF). Zvýšená exprese *Rsf1* byla zjištěna např. u rakoviny plic (Zhang, Fu et al. 2017), gliomu (Zhao, An et al. 2016), karcinomu vaječnicků (Shih Ie, Sheu et al. 2005), (Yang, Ahn et al. 2014). Tato zvýšená exprese je spojována s rychlejší proliferací buněk a špatnou prognózou onemocnění. Ve studii založené na řízené nadprodukci proteinu RSF1 v tumoru pocházejícího z buněk karcinomu vaječnicků u myšího modelu, bylo pozorováno zrychlení proliferace nádorových buněk. SMARCA5 byl v těchto buňkách stabilizován v komplexu s proteinem RSF1 na úkor dalších jeho vazebných partnerů, což pravděpodobně vedlo k narušení rovnováhy buněčných procesů (Sheu, Choi et al. 2008). Výrazné zvýšení (až 10x) exprese *Rsf1* v buňkách karcinomu vaječnicku *in vitro* může vést až k poškození DNA a vstupu buněk do apoptózy (Sheu, Guan et al. 2010).

Dalším vazebným partnerem SMARCA5, který je nadprodukován v nádorových buňkách, je protein WSTF/BAZ1B (komplex WICH). Jeho zvýšená produkce byla popsána např. u rakoviny plic, kde zrychluje proliferaci buněk a agresivitu tumoru (Meng, Zhang et al. 2016). Deregulovaná exprese v nádorových buňkách však byla pozorována i u mnoha dalších SMARCA5 vazebných partnerů viz obrázek č. 6. Význam deregulace exprese BAZ proteinů napovídá, že buňky vnímají změnu exprese SMARCA5 a mají vytvořeny mechanismy její regulace na postranskripční úrovni, zatímco na změnu exprese BAZ proteinů jsou pravděpodobně méně citlivé. Výše zmíněné studie dokazují zásadní roli komplexů obsahujících protein SMARCA5 v různých nádorových onemocněních, jeho konkrétní role při nádorové transformaci však nejsou zatím známy.



Obrázek č. 6.: Analýza genové exprese podjednotek ISWI komplexů u nádorových onemocnění. Červená barva značí upregulaci a modrá downregulaci. Na ose Y jsou názvy jednotlivých genů, na ose X jsou různé typy nádorových onemocnění: ESCA = karcinom jícnu, LIHC = hepatocelulární karcinom jater, READ = adenokarcinom rekta, COAD = adenokarcinom tlustého střeva, LUAD = adenokarcinom plic, STAD = adenokarcinom žaludku, HNSC = spinocelulární karcinom hlavy a krku, BLCA = uroteliální karcinom močového měchýře, BRCA = invazivní karcinom prsu, LUSC = dlaždicobuněčný karcinom plic, UCEC = endometriální karcinom děložního těla, KIRC = světlbuněčný karcinom ledviny, THCA = karcinom štítné žlázy, KICH = chromofobní renální karcinom, KIRP = papilární renální karcinom, PRAD = adenokarcinom prostaty. Převzato z (Li, Gong et al. 2021).

3 Cíle disertační práce

- Studium role ISWI chromatin remodelačního faktoru *Smarca5* v myší krevetvorbě, především lymfopoéze, erytropoéze a kmenových buňkách s využitím několika typů tkáňově specifických Cre expresorů.
- Výzkum vlivu delece *Smarca5* na vývoj lymfocytů a to jak lymfoidních progenitorů, tak i T-buněk v brzlíku a B-buněk ve slezině.
- Vývoj modelu exprimujícího transgenní *SMARCA5* cDNA a studium vlivu snížené hladiny tohoto proteinu na diferenciaci kmenových buněk s využitím všech předchozích Cre-expresorů a v kombinaci s kondicionálním delečním modelem pro *Smarca5*.
- Výzkum SMARCA5 interaktomu ve studovaných systémech a tkáních pomocí proteomiky v transgenních myších modelech pro tento protein.

4 Seznam publikací

Tato práce vychází z níže uvedených publikací:

1. Publikace:

Turkova T, Kokavec J, Zikmund T, Dibus N, Pimkova K, Nemeč D, Holeckova M, Ruskova L, Sedlacek R, Cermak L and Stopka T. Differential requirements for Smarca5 expression during hematopoietic stem cell commitment. *Commun Biol* 2024 Mar, doi: 10.1038/s42003-024-05917-z. Manuskript byl přijat k publikaci 14. 2. 2024.

Autorka se podílela na vytvoření transgenního myšího modelu s hypomorfní alelou *SMARCA5* a studiu defektů v hematopoéze pomocí průtokové cytometrie a *SMARCA5* interaktomu pomocí hmotnostní spektrometrie. Autorka provedla analýzu exprese transgenní *SMARCA5* pomocí metod RT-qPCR a Western blot a podílela se na přípravě vzorků pro analýzu pomocí cílené proteomiky, dále také udržovala myší linie využívané v tomto manuskriptu. Autorka přispěla při vyhodnocení dat a významně se podílela jak na navržení metodického postupu, tak i během analytického procesu vedoucího ke zdárné interpretaci dat. Autorka samostatně komunikovala připomínky oponentů v časopise *Communication Biology* a realizovala požadované experimenty a zodpověděla všechny požadované dotazy. Podíl zastoupení práce autora 70 %.

2. Publikace:

Zikmund T, Kokavec J, **Turkova T**, Savvulidi F, Paszekova H, Vodenkova S, Sedlacek R, Skoultchi AI, Stopka T. ISWI ATPase Smarca5 Regulates Differentiation of Thymocytes Undergoing β -Selection. *J Immunol.* 2019 Jun 15;202(12):3434-3446. doi: 10.4049/jimmunol.1801684. Epub 2019 May 8. PMID: 31068388; PMCID: PMC6548592.

Autorka se věnovala izolaci tkání a následné analýze vzorků pomocí průtokové cytometrie, přípravě vzorků a izolaci a třídění buněčných podtypů průtokovou cytometrií, které byly využity pro sekvenaci RNA, udržováním a genotypováním myších linií využitých v této publikaci. Podíl zastoupení práce autora 20 %.

3. Publikace:

Zikmund T, Paszekova H, Kokavec J, Kerbs P, Thakur S, **Turkova T**, Tauchmanova P, Greif PA, Stopka T. Loss of ISWI ATPase SMARCA5 (SNF2H) in Acute Myeloid Leukemia Cells Inhibits Proliferation and Chromatid Cohesion. *Int J Mol Sci.* 2020 Mar 18;21(6):2073. doi: 10.3390/ijms21062073. PMID: 32197313; PMCID: PMC7139293.

Autorka provedla experimenty na myších embryonálních fibroblastech uvedené v této publikaci včetně izolace této buněčné linie z myších modelů různých genotypů (viz text publikace). Podíl zastoupení práce autora 10 %.

4. Publikace:

Thakur S, Cahais V, **Turkova T**, Zikmund T, Renard C, Stopka T, Korenjak M, Zavadil J. Chromatin Remodeler Smarca5 Is Required for Cancer-Related Processes of Primary Cell Fitness and Immortalization. *Cells.* 2022 Feb 25;11(5):808. doi: 10.3390/cells11050808. PMID: 35269430; PMCID: PMC8909548.

Autorka připravila nezávislé linie myších embryonálních fibroblastů z myších modelů různých genotypů (viz text publikace) na jejichž studiu je tato publikace založena. Také provedla analýzu linií metodou western blot. Dále v rámci této publikace absolvovala čtyřměsíční zahraniční stáž na francouzském pracovišti (IARC). Podíl zastoupení práce autora 15 %.

4.1 (1. publikace) Differential requirements for Smarca5 expression during hematopoietic stem cell commitment.

TITLE: Differential requirements for Smarca5 expression during hematopoietic stem cell commitment.

AUTHORS: Tereza Turkova^{1*} & Juraj Kokavec^{1*}, Tomas Zikmund¹, Nikol Dibus², Kristyna Pimkova¹, Dusan Nemec¹, Marketa Holeckova¹, Livia Ruskova¹, Radislav Sedlacek³, Lukas Cermak^{2†}, and Tomas Stopka^{1†}

AFFILIATIONS: ¹ Hematology Laboratories, BIOCEV; ^{1st} Faculty of Medicine; Charles University; Vestec, Czech Republic

² Laboratory of Cancer Biology, Institute of Molecular Genetics of the Czech Academy of Sciences, Prague, Czech Republic

³ Czech Centre for Phenogenomics; Institute of Molecular Genetics of the Czech Academy of Sciences, Vestec, Czech Republic

Present address: BIOCEV, ^{1st} Faculty of Medicine, Charles University, Prumyslova 595, Vestec, 25242, Czech Republic

AUTHORSHIP: * these authors contributed equally; †corresponding authors

CORRESPONDENCE:

Dr. Tomas Stopka, BIOCEV, ^{1st} Faculty of Medicine, Charles University, Prumyslova 595, Vestec, 25242, Czech Republic; Tel.: +420-325-873-001; e-mail: tstopka@lf1.cuni.cz

Lukas Cermak, Laboratory of Cancer Biology, Institute of Molecular Genetics of the Czech Academy of Sciences, Prague, Czech Republic; e-mail: lukas.cermak@img.cas.cz

ABSTRACT: The formation of hematopoietic cells relies on the chromatin remodeling activities of ISWI ATPase SMARCA5 (SNF2H) and its complexes. The *Smarca5* null and conditional alleles have been used to study its functions in embryonic and organ development in mice. These mouse model phenotypes vary from embryonic lethality of constitutive knockout to less severe phenotypes observed in tissue-specific *Smarca5* deletions, e.g., in the hematopoietic system. Here we show that, in a gene dosage-dependent manner, the hypomorphic allele of SMARCA5 (*S5^{tr}*) can rescue not only the developmental arrest in hematopoiesis in the hCD2iCre model but also the lethal phenotypes associated with constitutive *Smarca5* deletion or Vav1iCre-driven conditional knockout in hematopoietic progenitor cells. Interestingly, the latter model also provided evidence for the role of SMARCA5 expression level in hematopoietic stem cells, as the Vav1iCre *S5^{tr}* animals accumulate stem and progenitor cells. Furthermore, their hematopoietic stem cells exhibited impaired lymphoid lineage entry and differentiation. This observation contrasts with the myeloid lineage which is developing without significant disturbances. Our findings indicate that animals with low expression of SMARCA5 exhibit normal embryonic development with altered lymphoid entry within the hematopoietic stem cell compartment.

INTRODUCTION:

Cellular differentiation begins in the fertilized egg and is characterized by gradual and extensive reprogramming of gene expression, especially during gastrulation, which is dependent on changes in chromatin accessibility and activity. These changes are orchestrated by chromatin remodeling enzymes, which are essential for cell differentiation and organism development¹. Their main role is to mechanically catalyze the process of nucleosome sliding, either in cooperation with transcription factors or independently as a result of their DNA binding activity². Several families of chromatin remodeling complexes differ in the presence of catalytic and regulatory subunits, for example the Imitation Switch Complex (ISWI) family, which contains either SWI/SNF Related, Matrix Associated, Actin Dependent Regulator Of Chromatin, Subfamily A, Member 1 (SMARCA1) or SMARCA5 as a

catalytic subunit³. ISWI complexes play broad and essential roles in nearly all genetic processes, including activation or repression of transcription, DNA repair, and DNA replication. They act either by maintaining evenly spaced nucleosomal arrays or by repositioning nucleosomes near promoters to increase the accessibility of DNA⁴.

Germline deletion of *Smarca5* leads to early embryonic lethality due to the arrest of embryonic stem cell (ESC) differentiation⁵. The knockout of *Smarca5* in ESCs directly demonstrated the role of SMARCA5 in the regulation of nucleosomal distance (linker length). Its absence led to an increased linker length, a defect that changed accessibility for many transcription factors, including the binding of a CCCTC binding factor (CTCF) to the imprinted DNA regions⁶. The main function of CTCF in these regions is the inhibition of transcriptional enhancers, which is one of mechanisms controlling the expression of the transcription factor PU.1 (SPI1). PU.1 is essential for the early initiation of hematopoiesis and its differentiation towards myelopoiesis and lymphopoiesis⁷. In zebrafish, SMARCA5 facilitates the binding of transcription factors that control the expression of hematopoietic regulators such as *bcl11ab*⁸. This process mediates the acquisition of definitive hematopoietic stem and progenitor cell (HSPC) characteristics and facilitates development into definitive fetal HSPCs. In addition, gene expression and chromatin accessibility data from zebrafish HSPCs suggest that SMARCA5 is involved in controlling the activity of genes associated with HSPC expansion and differentiation⁸.

Using conditional inactivation of *Smarca5* in murine hematopoietic progenitors, we followed up on the HSPC study and demonstrated the essential role of SMARCA5 during early HSPC differentiation. Most importantly, in this model, we observed accumulation of hematopoietic progenitors and activation of p53 targets. These changes appear to disrupt normal erythropoiesis and promote premature death of animals during fetal development⁹. To prevent this phenomenon and to study in detail the role of SMARCA5 in early definitive hematopoiesis, we decided to create a transgenic model with a hypomorphic expression (lower expression on protein level) of SMARCA5 in the context of its endogenous gene deletion. This approach allowed us to introduce a model with a graded

SMARCA5 expression. Using cell biology and bone marrow (BM) transplantation techniques, we have shown that SMARCA5 is involved in the very early differentiation of HSPCs, a process with significant consequences for terminal maturation, especially in the lymphoid lineage.

RESULTS

1. Hypomorphic *hCD2-S5^{tg}* allele rescues the developmental thymocyte arrest in *Smarca5* null mutants.

Since heterozygotes carrying a null allele of the *Smarca5* (*S5*) gene have normal hematopoiesis while homozygotes display severe embryonic defects, we created a model using a conditional hypomorphic allele of the *S5* gene (*S5^{tg}*, Fig. 1a) to study how different levels of SMARCA5 affect hematopoietic stem cells and their differentiation potential in adult animals. Our model expresses *tdTomato* under the control of endogenous *Rosa26* promoter (Fig. 1a, S1e), and upon Cre recombinase activation it initiates expression of the transgenic human SMARCA5 protein with FLAG tag on its C-terminus. The reasoning for using hSMARCA5 is that it is functionally indistinguishable from murine protein. As shown in the Supplementary Fig. S1a, the human and murine SMARCA5 proteins are almost identical in amino acid sequence, and most of the differences are conservative and localized to the N-terminal unstructured region. To validate the functional proficiency of *S5^{tg}*, we tested its ability to rescue lymphocyte development which is blocked at progenitor stages in a conditional *hCD2iCre*-induced *Smarca5* knockout¹⁰. First, we confirmed that animals with the genotype *hCD2iCre S5^{tg/tg} S5^{f/f}* are born healthy and in expected Mendelian ratios (Table 1). Analysis of mRNA and protein levels in mouse thymus confirmed the expression of tagged SMARCA5 and revealed complete rescue at the mRNA level even by a single allele of the transgene (Fig. 1b). At the protein level a single *S5^{tg}* allele provided approximately 85% of the protein compared to two endogenous *S5* alleles and two alleles of the transgene can fully rescue SMARCA5 expression (Fig. 1c). We recently reported that the complete loss of *Smarca5* gene in the *hCD2iCre* strain significantly reduces the size of the thymus and its cellularity¹⁰. The introduction of two hypomorphic *S5^{tg}* alleles into the *hCD2iCre S5^{f/f}* background

showed an increase of thymic cellularity to almost 8-times. Despite this positive effect, the rescue was not complete and corresponded to approximately 60% of normal thymic cellularity, a similar effect was observed in splenic cellularity (Fig. 1d, S1f). Analysis of peripheral blood populations revealed almost complete lymphocyte rescue in the presence of two alleles, and one allele of the transgene presented mild lymphopenia (Fig. 1e, S1g). To gain insight into the development of *S5* hypomorphic thymocytes, we analyzed the populations from whole thymic suspension using CD4/CD8 immunostaining by flow cytometry. Results revealed a rescue in numbers of double positive (DP) and CD4⁺/CD8⁺ thymocytes in *S5^{tg}* animals (Fig. 1f). Upon detailed analysis of immature double negative (DN) thymocytes using CD44 and CD25 antibodies, we observed that the severe disruption of differentiation at the DN3/DN4 stage in *Smarca5* knockout (KO) was rescued in the *S5^{tg}* model. This rescue was incomplete for DN1 and DN4 thymocytes, consistent with the reduced cellularity of the *S5^{tg}* thymi (Fig. 1f, 1g).

Our previous work also revealed that SMARCA5 is required for the pro-B/pre-B transition of B cell progenitors. Indeed, the analysis of *hCD2iCre S5^{fl/fl}* mice also revealed a dramatic reduction in spleen cellularity and a defect in the early B cell progenitor population, specifically a complete loss of pre-B cells (CD43⁻CD25⁺)¹⁰. The single *S5^{tg}* allele did not significantly increase the number of pre-B cells, but in the presence of both *S5^{tg}* alleles we observed almost complete rescue (Fig. 1h). Moreover, when we analyzed the pro-B population using CD25/CD117 markers, we observed that the *S5^{tg}* was able to rescue the loss of CD25⁺ cells but not the accumulation of CD117⁺ cells (Fig. 1i). These data confirm that the product of the *S5^{tg}* allele expressed from the ectopic locus is functional and able to almost fully rescue the lymphoid defect caused by the *hCD2iCre Smarca5* KO, which ultimately leads to normalization of peripheral blood lymphocyte numbers in animals with two copies of *S5^{tg}* (Fig. 1e, S1g).

2. Transgenic *Vav1-S5^{tg}* cannot rescue thymocyte development in *Smarca5* null mutants.

To further study the effect of hypomorphic SMARCA5 expression on the development of thymic and splenic progenitors, we simultaneously initiated a deletion of the endogenous *Smarca5*

gene and activation of *S5^{tg}* in early hematopoietic precursors using *Vav1iCre*⁹. Transgenic protein level in the thymus was only ~40 % of the endogenous SMARCA5 level, although their mRNA levels were comparable (Fig. 2a, 2b). In bone marrow, the level of transgenic SMARCA5 was even lower, at only ~18 % (and ~10 % from a single allele) of the level of endogenous protein (Fig. 2a, 2b). Importantly, in thymocytes, the expression of the hypomorphic allele on the background of the endogenous SMARCA5 protein had only an insignificant additive effect on the total protein level, suggesting the existence of a regulatory feedback loop that prevents SMARCA5 overexpression in the cells (Supplementary Fig. 2b). For these experiments, we used mice with a non-conditional variant of the SMARCA5 transgene. The transgene was activated in the parental generation by ActB-Cre recombinase. As a result, the SMARCA5 transgene is constitutively expressed in every cell in the body of the analyzed mice. Although the expression of the *S5^{tg}* allele (initiated by *Vav1iCre*) rescued the embryonic lethality (Table 1), we did not observe complete establishment of definitive hematopoiesis. Specifically, transgenic animals exhibited mild anemia and, consistent with *hCD2iCre* expression model, also severe lymphopenia and reduced cellularity of thymus and spleen (Fig. 2c, 2d, S2c, S2d).

Lymphocyte deficiency was manifested by a decrease in the total white blood cell count (Supplementary Fig. 2d). Furthermore, *S5^{tg}* expression was insufficient to promote the transition of thymocyte progenitors from DN3 to DN4 and simultaneously led to a decrease in the DP and CD4/CD8 fractions of thymocytes (Fig. 2e, 2f). The development of pre-B lymphocytes and pro-B cell fractions (CD117⁺ and CD25⁺) was similarly defective, which corresponded to a decrease in spleen cellularity (Fig. 2c, 2g, 2h, S2e). In addition, we observed the phenotypic changes that were SMARCA5 dose-dependent, as the expression of the transgene from both alleles improved the rescue of definitive hematopoiesis (Fig. 2c-h). While the changes in erythropoiesis were marginal, we found that animals expressing a single copy of the transgene showed mild anemia (lower red blood cell count, hemoglobin and hematocrit levels) and negligible changes in erythropoiesis were also observed in spleen and BM (Supplementary Fig. 2d, 2f-i). Overall, our data confirm the importance of SMARCA5 expression levels during hematopoiesis, with lymphopoiesis and, to some extent, erythropoiesis being dependent on

high expression levels in contrast to other lineages (e.g. myelocytes – Fig. 2d), which were completely rescued even by just a single allele of *S5^{tg}*.

3. Transgenic *Vav1-S5^{tg}* phenotype involves hematopoietic stem and progenitor cell compartments.

The deletion of *Smarca5* at the onset of definitive hematopoiesis (*Vav1iCre*) causes accumulation and blockade of maturation of hematopoietic stem cells (HSCs) and progenitors in the fetal liver, ultimately leading to the death of the developing embryos⁹. Since *Vav1iCre S5^{fl/fl}* individuals expressing the hypomorphic *S5^{tg}* allele overcome this embryonic lethality, we further investigated the potential stem cell defect caused by low levels of SMARCA5 protein. First, we analyzed the composition of hematopoietic stem cells and multipotent progenitor (MPP) populations in *Vav1iCre S5^{fl/del} S5^{tg/tg}* and *Vav1iCre S5^{fl/del} S5^{tg}* animals. Bone marrow isolated from adult (8-10 weeks) mice was analyzed by flow cytometry using stem cell markers (Sca1, c-Kit, CD34, and FLT3), and signal lymphocyte activating molecule (SLAM) antigens CD48 and CD150 (Fig. 3a, 3b). Animals with one copy of *S5^{tg}* exhibited accumulation of the earliest Lin⁻Sca1⁺Kit1⁺ (LSK) population compared to *S5^{tg/tg}* and control (Fig. 3c, S3a).

The largest defect was observed in the MPP populations of LSK cells, which consist of phenotypically distinct and long repopulating HSCs (Fig. 3d-f, S3c). The CD34⁺FLT3⁻ LSK cell population was accumulated in single *S5^{tg}* mice compared to controls, representing up to a ten-fold increase in *Vav1iCre S5^{fl/del} S5^{tg}* mice (Supplementary Fig. 3b, 3f). However, this net increase almost entirely consisted of MPP3 (CD48⁺CD150⁻), which can contribute to both myeloid and lymphoid lineages, and also of myeloid-committed MPP2 (CD48⁺CD150⁺) (Fig. 3e, S3c). Interestingly, lymphoid-committed MPP4 (CD48⁺CD150⁻FLT3⁺) were unaffected, but we observed a significant reduction in the number of IL7Rα⁺ lymphoid progenitors (LP) in animals with one allele of *S5^{tg}* (Fig. 3f, 3h, S3c, S3d). Myeloid progenitors were affected at the level of common myeloid progenitors (CMP), which were reduced in the *S5^{tg}* animals, while the more differentiated MEP and GMP populations were not (Fig. 3g, S3e). We also observed some atypical populations resembling MPP2 and MPP3 but lacking CD34 expression (LSK

CD34⁻FLT3⁻CD48⁺CD150⁻/CD150⁺). These populations were accumulated in single *S5^{tg}* animals (Fig. 3d). The absolute increase in stem and progenitor cells with a marked decrease in mature lymphoid progenitors and a marginal reduction in myeloid progenitors suggests that SMARCA5 depletion leads to severe impairment in the formation of differentiating cells carrying lymphoid programs.

To determine whether the described block in differentiation is related to the amount of SMARCA5 protein, we measured its levels at different stages of progenitor differentiation. The exact levels of SMARCA5 peptides were quantitated by a liquid-chromatography tandem mass spectrometry technique using targeted parallel reaction monitoring (PRM) method. Five selected peptides of human SMARCA5 protein were reliably detected in LSK (Lin⁻Sca1^c-Kit⁺) and LS⁻K (Lin⁻Sca1^c-Kit⁺) cell populations isolated by fluorescence-activated sorting from BM of mice with defined genotypes: control *S5^{fl/fl}*, *Vav1iCreS5^{fl/del}S5^{tg/tg}*, *Vav1iCreS5^{fl/del}S5^{tg}* (Fig. 3i). In the control genotype, we observed a significant (at least twofold) increase in relative SMARCA5 levels during the transition from LSK to LS⁻K stage of differentiation. This trend was again observed in the *Vav1iCreS5^{fl/del}S5^{tg/tg}* genotype although it showed lower relative SMARCA5 levels compared to the control. Interestingly, the *Vav1iCreS5^{fl/del}S5^{tg}* genotype showed comparable levels of SMARCA5 in the LSK population as in the presence of both transgenic alleles, but the LS⁻K population displayed a slight decrease in the amount of the protein. This observation showed that differentiation of cells expressing a single *S5^{tg}* allele is inefficient but still able to produce some LS⁻K cells but with lower levels of SMARCA5 (Fig. 3i).

4. Transgenic *Vav1-S5^{tg}* stem and progenitor cells are defective in repopulating lymphopoiesis.

The accumulation of specific MPPs in *S5^{tg}* animals may reflect their inability to enter the differentiation pathway. To test the extent to which *S5^{tg}* stem cells are functional, we performed a competitive BM cell transplantation assay. To distinguish transgenic and wild-type hematopoietic cells, we employed a system based on the expression of different CD45 isoforms. The transgenic animals were CD45.2⁺ in contrast to CD45.1⁺ wild-type animals. First, wild-type donor BM cells were transplanted to a set of control and transgenic recipients carrying one or two *S5^{tg}* alleles and controls.

Acceptor animals were optionally irradiated (2-6 Gy). Next, we determined short- or long-term repopulating activity by a monthly assessment of lineage antigens in peripheral blood using flow cytometry. The abundance of CD45.1⁺ progeny in *S5^{tg}* (or *S5^{tg/tg}*) mice shows that *S5^{tg}* mice are already highly permissive even without prior irradiation and show 33% engraftment at one month and 80% engraftment four months after transplantation (Fig. 4a, S4a). Next, we analyzed the contribution of individual B/T-lymphoid and myeloid cell lineages of wild-type origin to hematopoietic recovery. Both short- and long-term (1-4 months) repopulating activity of *Vav1iCreS5^{fl/del} S5^{tg}* recipient mice is highly permissive for T- and B-lineage repopulation, compensating for the deficiency in lymphoid cell development in the *S5^{tg/tg}* and *S5^{tg}* recipient mice as well as for myeloid cells in the case of *S5^{tg}* recipients (Fig. 4b, S4b).

In the second part of the experiment, to test the repopulating activity of *S5^{tg}* transgenic stem cells, we isolated *S5^{tg}* BM cells and transplanted them into the control animals. *S5^{tg}* (CD45.2⁺) BM was competitively transplanted together with wild-type (CD45.1⁺) BM cells (3:1 ratio) into lethally (8.5 Gy) irradiated wild-type recipients. Total CD45.2⁺ cell count data showed that *S5^{tg}* HSCs with one copy of the transgene were unable to compete with wild-type HSCs, which gave rise to all repopulated hematopoietic cells (Fig. 4c). Next, we analyzed how different lineages derived from *S5^{tg}* BM cells engraft within the normal recipient mice and observed that donor *S5^{tg}* HSCs were unable to fully repopulate hematopoietic cell lineages as their control counterparts did. While HSCs with both alleles of the *S5^{tg}* were able to repopulate myelocytes their lymphocyte repopulation was severely affected (Fig. 4d, right, S4c). Consistently with our previous observations, the effect of reduced SMARCA5 protein levels was most prominent in the developing lymphocytes.

5. The SMARCA5 transgenic product forms complexes and is essential for lymphopoiesis.

Next, we used the ubiquitously expressed *ActB-Cre* to explore whether it is possible to maintain mouse survival solely on the *S5^{tg}* expression (in the *S5* KO strain). To avoid problems potentially caused by transgene activation and possible delay in *S5* expression, we crossed animals

with already active $S5^{tg}$ (deleted *tdTomato*). Postnatally, we identified only 4 animals ($S5^{del/del}S5^{tg/tg}$) out of ~150 expected. Due to this discrepancy, we analyzed prenatal lethality of this genotype and we observed early mortality at embryonic day E13.5 and further in the fetal period at E18.5 (Table 1). However, even when accounting for the observed prenatal lethality, we did not obtain expected Mendelian-based numbers of animals. This fact indicates a high mortality rate in the early embryonic stages.

Next, to take advantage of the fact that several $S5^{del/del}S5^{tg/tg}$ animals were born, we collected their hematopoietic tissues and analyzed the same populations as in the previous experiments. Again, we observed that the main disturbance was in the lymphoid lineage, while myelopoiesis was more or less preserved, similar to the *Vav1iCre* model (Fig. 5a-f, S5a-m). Thus, the severe anemia in the absence of SMARCA5 that leads to disruption of early development (see previous publication⁵) *de facto* prevented us from finding that of all developmental pathways, it is the earliest stages of lymphopoiesis that are most sensitive to small perturbations of SMARCA5.

These findings led us to investigate functional aspects of the *Smarca5* transgene. As noted above, we used the ubiquitously expressed *ActB-Cre* to activate $S5^{tg}$ expression in the whole body on the *Smarca5^{del/wt}* genotype background. This experimental approach allowed us to study how transgenic SMARCA5 naturally participates in its complexes in tissue-specific manner. The composition of the ISWI chromatin complex in endogenously expressed ATPase-bound regulatory subunits has been described previously¹¹. Analysis of SMARCA5-copurified proteins documented that the following complexes had varying presence in specific tissues: ACF (BAZ1A) was found in all studied tissues at a high abundance, WSTF (BAZ1B) was present in fetal liver, testes, muscle, kidney, and liver at intermediate quantity, while NoRC (BAZ2A) was observed in lower abundance. Finally, SMARCA5-NURF (RBBP4) complex was detected in the brain and spleen. In addition, some ISWI complex members and known interaction partners were detected in the fetal liver (CTCF, POLE3, CHRAC1, NCL) or thymus (STAT3, STAT1, SMARCC1, RUNX1) (Fig. 5g, 5h, S5n, S5o). These data collectively indicate that the

transgenic SMARCA5 participates in formation of all known core ISWI complexes within the transgenic mice.

DISCUSSION:

The SMARCA5/SNF2H ATPase is one of the essential proteins involved in the regulation of DNA replication, gene expression and DNA damage response. SMARCA5 acts as a catalytic subunit of ISWI chromatin remodeling complexes, the molecular function of which depends on their individual composition. Prominent interaction partners belong to the BAZ family³. Our previous studies showed that mouse *Smarca5* is an essential gene for early myelopoiesis and erythropoiesis⁹, and lymphopoiesis¹⁰, an observation consistent with the high expression of *Smarca5* during these stages. In this report, we present a new mouse model of transgenic *SMARCA5* (*S5^{tg}*) expression in the context of the *Smarca5* knockout (KO) strain. *S5^{tg}* not only rescued embryonic lethality of *S5* KO, but also allowed us to study the effect of its graded expression. Overall, these results provided a solid basis for understanding the requirements for *Smarca5* gene expression levels during hematopoiesis.

Knockout in the lymphoid lineage (*hCD2iCre*) revealed that SMARCA5 is necessary for the transition between DN3 and DN4 stages of thymocyte development. At this stage, immature T lymphocytes undergo β -selection, which is accompanied by changes in gene expression. In the *hCD2iCre S5* knockout thymus, the DN3 population accumulates due to a developmental block that is followed by apoptosis. Similarly, B cell development is arrested during the transition from the pro- to the pre-B stage¹⁰. Our hypomorphic transgene rescued both of these situations to some extent, demonstrating that the essential role of SMARCA5 in later lymphoid progenitors depends on its presence but does not require its high expression. Neomorphic alleles of *Pole3*, a SMARCA5 interactor in CHRAC ISWI complex, revealed similar phenotypes showing arrest between DN3 and DN4 stages as well as during B cell differentiation, suggesting that the CHRAC complex is the most important for lymphoid differentiation¹². However, knockouts of other SMARCA5-binding partners did not exhibit any defects associated with lymphopoiesis. In detail, *Acf1* (*Baz1a*) is not essential for hematopoiesis¹³.

Tip5 (Baz2a), *Chrac1* and *Baz2b* KO showed no significant defect in lymphopoiesis, although some of these studies did not include a thorough assessment of hematopoiesis¹⁴. *Rsf1* and *Bptf* KO are embryonic lethal^{14,15}. *Cecr2* KO exhibits a variety of defects (coloboma, microphthalmia, and skeletal, heart, and kidney defects), but none of them were described in hematopoiesis¹⁶. Interestingly, we detected POLE3 in the SMARCA5 interactome in fetal liver, but we did not detect RSF1.

To better understand how *Smarca5* deletion affects early hematopoiesis, we used *Vav1iCre S5* KO mouse model. As shown previously, this model exhibits embryonic lethality at E18, which correlates with severe anemia and accumulation of hematopoietic progenitors⁹. We observed that the *S5^{tg}* rescues this lethality, but transgenic animals exhibit severe lymphopenia and mild anemia. The severity of these defects was inversely related to the copy number of the *S5^{tg}*, indicating a dependence on higher SMARCA5 expression in hematopoiesis. The only population that was fully rescued by the *S5^{tg}* were the myelocytes. The most severe phenotype was associated with an arrest during differentiation of MPP3 to MPP4. This transition is associated with FLT3 activation which is required for lymphopoiesis. *S5^{tg}* can rescue accumulation of MPPs if expressed from both alleles. Expression from a single allele resulted in the accumulation of cells in the MPP3 stage, and to some extent, the MPP2 stage as well. Interestingly, we also observed the accumulation of populations in transgenic animals which have a unique mixture of progenitor markers. Although they resemble the MPP2/3 populations, they are noticeably lacking the CD34 antigen. We hypothesize that these populations likely originate from the accumulated MPP2/3 which are unable to differentiate. Moreover, in this genotype, defects in lymphocyte development continued to the later stages of differentiation (DN3 to DN4 and pro-B to pre-B block), resulting in almost complete loss of lymphocytes in peripheral blood, with B cells being more affected than T cells. These results were consistent with our observations from the *hCD2iCre S5^{tg}* model, but the defect in *Vav1iCre S5^{tg}* model was more pronounced, suggesting that this is a stem cell-level phenotype. The observations from flow cytometry were also supported by measurements of SMARCA5 protein levels in different developmental stages of hematopoietic progenitors. We observed that transition from LSK to the later developmental stage LS⁺K is accompanied by an enhancement of

SMARCA5 protein levels in control mice, whereas in the presence of only one allele of the transgene, there was a slight loss of protein. The reduced levels of SMARCA5 likely result in a decrease in CMP and CLP populations (LSK) in this genotype and an accumulation of MPP3 and MMP2 populations (LSK). These observations imply that *Smarca5* expression undergoes independent regulation from its promoter during hematopoietic progenitor differentiation. Prior research has demonstrated that SMARCA5 can be subjected to degradation through Cullin- and proteasome-dependent pathways¹⁷. Although this represents an interesting and novel concept that is clearly important for hematopoietic differentiation, we currently lack data that unequivocally support it. Interestingly, we observed a discrepancy between SMARCA5 transgene expression at the RNA and protein levels, with the transgene being able to reach endogenous *Smarca5* RNA level but not the protein level suggesting a regulatory mechanism for SMARCA5 at the protein level requiring further investigation.

To support our hypothesis that SMARCA5 expression level has a direct effect on HSCs, we employed competitive transplantation of wild-type HSC into *S5* transgenic acceptors and *vice versa*. Both of these experiments confirmed our hypothesis that high levels of SMARCA5 are important for lymphocyte development, as wild-type HSCs reconstituted lymphopoiesis in animals with a single *S5^{tg}* allele even without pre-transplantation irradiation. *S5^{tg}* BM was only able to reconstitute myelocytes but not lymphocytes in lethally irradiated wild-type acceptors. The effects observed in competitive transplantation were clearly dose-dependent, with the most substantial impact seen when a single *S5^{tg}* allele was expressed. A similar competitive transplantation experiment performed with neomorphic *Pole3* (member of ISWI CHRAC complex) and wild-type BM (1:1) revealed that HSCs with a mutated *Pole3* struggled to repopulate the lymphoid lineage but not the myeloid lineage¹². Deletion of ARID1A in mouse (SWI/SNF complex) resulted in a similar but more severe phenotype with an accumulation of hematopoietic progenitors resulting in defects in lymphopoiesis, myelopoiesis and erythropoiesis. These accumulated progenitors were not able to repopulate host hematopoiesis in a competitive transplantation experiment¹⁸.

The final experiment focused on using a whole-body deletion of *Smarca5* combined with *S5^{tg/tg}* expression to determine whether any other processes during development require higher than transgenic SMARCA5 protein levels. We observed a similar phenotype as in the *Vav1iCre* model with a defect in hematopoiesis combined with very low birth expectancy – less than 1 % (contrasted with the expected value of 25 %). Most of these animals died in the early embryonic stages, suggesting their lower fitness.

As in our experiments, knockouts of SWI/SNF chromatin remodeling factors were found to cause defects in hematopoiesis. For example, in a mouse model with mutant *Baf57* (disruption of DNA binding), CD8⁺ T cell development was blocked even though only one allele was mutated. The same block in differentiation was observed in mice with a heterozygous deletion of *Brg1*¹⁹. In contrast to our findings from *Smarca5* KO, *Brg1* loss results in a block of T cell differentiation at later stages, the DN4 to DP transition²⁰. Another chromatin remodeling factor with a significant role in hematopoiesis is Mi-2 β (Mi-2 family) which is essential for the DN4 to DP transition and especially for CD4⁺ T cell development²¹.

The model of whole-body SMARCA5 expression allowed us to study the composition of its ISWI complexes in a tissue-specific manner. While our results are dominated by canonical complexes with BAZ proteins (as updated in¹¹), it certainly cannot be ruled out that there may be other interactions with DNA at the chromatin level that are not easily detected by the mass spectrometry methodology we used. These non-canonical complexes might be context-dependent and difficult to detect in a mixture of cell populations. Nevertheless, our data also show the involvement of CTCF in the ISWI complex in some tissues, particularly in fetal hematopoiesis as suggested elsewhere⁶.

MATERIALS & METHODS:

Mouse transgenesis

SMARCA5 cDNA fused to a C-terminal *Flag tag* (cleaved from MSCV2.2 vector) was cloned into *NheI* and *SalI* cleavage sites of the p15-6-20 DNA vector containing 5' & 3' homologies of *Rosa26* and the

tdTomato gene surrounded by LoxP sites, allowing excision of *tdTomato* and initiation of *SMARCA5* transgene expression (Fig. 1a)²². The assembled transgenic vector (linearized by *FseI*) was nucleofected (Amaza Nucleofector II instrument, program A-023, Lonza) into R1 ES cells (2×10^6) which were seeded on a layer of irradiated (35 Gy) mouse embryonic fibroblasts in recommended media (details below) supplemented with ESGRO (mLIF 1 kU/ml, cat. no. ESG1107, Merck, Darmstadt, Germany)²³. G418-resistant colonies (200 μ g/ml, cat. no. A1720, Sigma-Aldrich, Saint Louis, MO, USA) expressing *tdTomato* were selected and expanded. A 3.495 kbp PCR band (F: GTGTCTCTTTTCTGTTGGACCCTTACCT; R: AAAAAGAAGAAGGCATGAACATGGTTAG) verified integration of the transgene (Supplementary Fig. 1b). ES cells with a normal karyotype were injected into blastocysts and transferred into the uterus of superovulated *C57BL/6NCrl* females. Mice containing the *Rosa26-S5^{tg}* construct were identified using PCR with the following primers Fwd: ACGAGGACCAAAGCCTTCAACAG, Rev: TGACAGTCGACAACTTCCTGACTAGGGAGTAGAAGT (Supplementary Fig. 1c). Germline transfer and backcrossing was performed into the *C57BL/6NCrl* strain. The progeny was viable, fertile and expressed *tdTomato* in all tissues. Mice expressing *tdTomato* with Cre-inducible *SMARCA5* transgene were then crossed to three Cre expressing strains (*hCD2* which is active from DN3 stage of thymocyte development and pro-B stage of B-cell development and CD2⁺ NK cells^{10, 24}, *Vav1* promoting recombination in c-kit⁺(CD117⁺) definitive hematopoietic progenitors⁹, and constitutively expressed *Gt(ROSA)26Sor^{tm1(ACTB-cre,-EGFP)1cs}*²⁵) containing a conditional knockout allele of *Smarca5* with *loxP1* flanking (fl) exon 5 of the endogenous *Smarca5* gene, resulting in a null allele upon Cre activation^{9,10}.

All mice expressing Cre recombinase were hemizygous for specific Cre transgene. Mice were maintained in a controlled, specific pathogen-free environment. Mice were provided food and water *ad libitum* and kept in the animal facility with a 12-hour light-dark cycle. All experiments met the criteria approved by Czech Ministry of Agriculture and the Committee for Experimental Animals. We have complied with all relevant ethical regulations for animal use. In all experiments, we used mice of both sexes, age is indicated in figure legends.

ES cells culture medium

KnockOut™ DMEM (cat. no. 10829018, Gibco, Thermo Fisher Scientific, Waltham, Massachusetts, United States) supplemented with 15 % KnockOut™ Serum Replacement (cat. no. 10828028, Gibco, Thermo Fisher Scientific, Waltham, Massachusetts, United States), 2 mM L-glutamine (cat. no. G7513, Sigma-Aldrich, St. Luis, MO, USA), 1x Penicillin-Streptomycin (cat. no. P0781, Sigma-Aldrich, St. Luis, MO, USA), 1x MEM Non-Essential Amino Acid Solution (cat. no. M7145, Sigma-Aldrich, St. Luis, MO, USA), 0,1 mM β-mercaptoethanol (cat. no. M3148, Sigma-Aldrich, St. Luis, MO, USA), ESGRO mLIF (1 kU/ml, cat. no. ESG1107, Merck, Darmstadt, Germany).

Tail tip DNA was genotyped with the following primers

S5^{tg}-F: ACGAGGACCAAAGCCTTCAACACAG, R: TGACAGTCGACAACCTCCTGACTAGGGGAGGAGTAGAAGT (852 bp), S5^{fl}-F: ACTGAGGACTCTGATGCAAACAGTCAAG, R: TACACAATAAGGCAGTGGGTTATAGTGC (fl 614 bp, wt 524 bp), S5^{del}-F: GTGCAAAGCCCAGAGACGATGGTATG (471 bp, with S5^{fl}-rev), Cre-F: ACCAGGTTTCGTTCACTCATGG, Cre-R: ACGGGCACTGTGTCCAGACC (449 bp), iCre-F: GATGCTCCTGTCTGTGTGCAG, iCre-R: CCTGCCAATGTGGATCAGC (469 bp).

Cell isolation and analysis

Single cell suspensions from peripheral blood, BM (isolated from 2 femurs and 2 tibias), thymus, and spleen were incubated on ice with specific primary antibodies in PBS + 1 % biotin-free BSA solution for 20 minutes. Biotinylated primary antibodies were then visualized using streptavidin-conjugated fluorescent dyes. Cell suspensions were analyzed on BD LSRFortessa™ SORP (BD Biosciences, San Jose, CA, USA) or CytoFLEX (Beckman Coulter, Brea, CA, USA), and data analysis was performed using FlowJo software.

Antibodies for flow cytometry

Biotin anti-B220 (clone RA3-6B2; cat. no. 103204), FITC anti-B220 (clone RA3-6B2; cat. no. 103206), APC anti-CD4 (clone GK1.5; cat. no. 100412), BV421 anti-CD4 (clone GK1.5; cat. no. 100437), PE/Cy7 anti-CD5 (clone 53-7.3; cat. no. 100621), APC anti-CD8a (clone 53-6.7; cat. no. 100712), Biotin anti-CD11b/Mac-1 (clone M1/70; cat. no. 101204), BV421 anti-CD11b/Mac-1 (clone M1/70; cat. no. 101236), Biotin anti-CD11c (clone N418; cat. no. 117304), BV510 anti-CD16/32 (clone 93; cat. no. 101333), BV605 anti-CD25 (clone PC61; cat. no. 102036), PE anti-CD25 (clone PC61; cat. no. 102008), Biotin anti-CD34 (clone HM34; cat. no. 128604), APC anti-CD43 (clone S11; cat. no. 143208), FITC anti-CD44 (clone IM7; cat. no. 103006), PE/Cy7 anti-CD45 (clone 30-F11; cat. no. 103114), AF700 anti-CD45.1 (clone A20; cat. no. 110724), PE/Cy7 anti-CD45.2 (clone 104; cat. no. 109830), FITC anti-CD48 (clone HM48-1; cat. no. 103404), PE anti-CD71 (clone RI7217; cat. no. 113808), BV421 anti-CD117/c-Kit (clone 2B8; cat. no. 105828), BV786 anti-CD127/IL7Ra (clone A7R34; cat. no. 135037), APC anti-CD135/FLT3 (clone A2F10; cat. no. 135310), BV605 anti-CD150 (clone TC15-12F12.2; cat. no. 115927), Biotin anti-Gr-1 (clone RB6-8C5; cat. no. 108404), BV605 anti-Gr-1 (clone RB6-8C5; cat. no. 108440), Biotin anti-Nk1.1 (clone PK136; cat. no. 108704), PE anti-Nk1.1 (clone PK136; cat. no. 108708), FITC anti-Sca1 (clone D7; cat. no. 108106), PE anti-Sca1 (clone D7; cat. no. 108108), APC anti-Ter119 (clone Ter-119; cat. no. 116212), Biotin anti-Ter119 (clone Ter-119; cat. no. 116204), PerCP anti-Ter119 (clone Ter-119; cat. no. 116226), AF700 anti-mouse Lineage Cocktail with Isotype Ctrl (anti-CD3, clone 17A2; anti-Ly-6G/Ly-6C, clone RB6-8C5; anti-CD11b, clone M1/70; anti-CD45R/B220, clone RA3-6B2; anti-TER-119/Erythroid cells, clone Ter-119; cat. no. 133313), SV-PE/Cy7 (cat. no. 405206), SV-AF700 (cat. no. S21383; Life Technologies Corporation, Eugene, Oregon, USA). All antibodies supplied by BioLegend (San Diego, California, USA) with exception for SV-AF700.

Immunoblotting

Organs from 7–9-week-old mice were homogenized and lysed on ice for 30 min in isotonic lysis buffer (150 mM NaCl, 50 mM Tris-Cl pH 7.5, 0.4 % Triton-X, 2 mM CaCl₂, 2 mM MgCl₂, 1 mM EDTA, 5 mM NaF in dH₂O), supplemented with 1 mM DTT, protease and phosphatase inhibitors and 25 U/μl of non-

specific DNA nuclease (Benzonase; cat. no. SC-391121, Santa Cruz, CA, USA)). Lysates were then mixed with SDS (final 1 %) was heated for 5 min, 95°C. Lysates were cleared by centrifugation (16 000 g, 4°C, 5 min) and protein concentration was determined by bicinchoninic acid assay (cat. No. 23228, Thermo Fisher, Waltham, MA, USA). 20 µg of protein was separated on a 4-20 % SDS gradient of Mini-PROTEAN TGX Precast Protein gels and transferred with the Trans-Blot Turbo Transfer System to a PVDF membrane (all from Bio-Rad, Hercules, CA, USA). Membranes were blocked in 5 % milk in TBS-T and incubated (overnight, 4°C) in primary antibodies diluted in 3 % BSA in TBS-T. After washing, membranes were incubated with horseradish peroxidase-conjugated anti-Rabbit IgG secondary antibody (1:10,000; Jackson ImmunoResearch, Cambridgeshire, UK; cat. no. 711-036-152) or with anti-Mouse IgG secondary antibody (1:10,000; Jackson ImmunoResearch, Cambridgeshire, UK; cat. no. 715-036-150). Primary antibodies: anti-SMARCA5 (1:1,000; Bethyl Laboratories, Montgomery, TX, USA; cat. no. A301-017A), anti-FLAG (1:1,000; Cell Signaling, Danvers, MA, USA; cat. no. 2368), anti-β-ACTIN (1:1,000; Abcam, Cambridgeshire, UK; cat. no. ab6276) and anti-GAPDH (1:1,000; Sigma-Aldrich, Saint Louis, MO, USA; cat. no. HPA040067). The binding efficiency of anti-SMARCA5 antibody with human and murine protein was tested using leukemia cell lines, specifically MEL (murine erythroleukemia) OCI-M2 (adult human acute myeloid leukemia) (Supplementary Fig. 1d). Visualization was performed using Pierce™ ECL Western Blotting Substrate (cat. no. PI32106, Thermo Fisher, Waltham, MA, USA) and detection using ChemiDoc Imaging System (Bio-Rad, Hercules, CA, USA). For densitometry all samples were normalized to their β-ACTIN/GAPDH loading control and the relative amount of protein was calculated compared to wild-type controls. 5. Uncropped and unedited blot images are available in Supplementary Fig. 6.

Hematopoietic reconstitution

For competitive reconstitution experiments 7.5×10^5 BM cells from wild-type adult (12-week-old) *B6 SJL-Ptpr^c Pepc^b/BoyCr1 (Ly5.1/CD45.1)* donors were co-transplanted with 2.25×10^6 BM cells (ratio 1:3, wt:tg) from *C57Bl/6 (Ly5.2/CD45.2) SMARCA5* transgenic donors and their respective controls into

lethally irradiated (8.5 Gy) adult (12-week-old) *Ly5.1* mice. In addition, hematopoiesis was assessed in *SMARCA5* transgenic hosts by transplanting 3×10^6 BM cells collected from wild-type 12-week-old *Ly5.1* mice into non-irradiated or irradiated (2, 3, 4, 5, up to 6 Gy) *Ly5.2 SMARCA5* transgenic hosts and controls. Hematopoietic repopulation was analyzed using flow cytometry analysis of peripheral blood collected at monthly intervals (1 to 4 months) after transplantation.

RT-PCR

RNA from homogenized organs was purified with TRIzol™ (cat. no. 15596026, Thermo Fisher, Waltham, MA, USA), treated with DNA-free™ DNA Removal Kit (cat. no. AM1906, Thermo Fisher, Waltham, MA, USA) and reverse transcribed with High-Capacity cDNA Reverse Transcription Kit (cat. no. 4374966, Thermo Fisher, Waltham, MA, USA). qPCR amplification using LightCycler® 480 SYBR Green I Master (cat. no. 04887352001, Roche, Basel, CH). Primers: *mS5* F: AGAATTTGCTTTCAGTTGGAGATTACCG, *mS5* R: AGATGAGCCAATTCAATCCTCGC, *hS5* F: AGAACTTACTATCCGTTGGCGATTACC; *hS5* R: AAGAAATGAGCCAGTTTAATCCTCGG, *mGapdh* F: ACTTTGTCAAGCTCATTTCTGGTATG-3', *mGapdh* R: TTTCTTACTCCTTGGAGGCCATGTAG, *mHprt* F: GCTGGTGAAAAGGACCTCT, *mHprt* R: CACAGGACTAGAACACCTGC.

Protein immunoprecipitation

Organs from 7–9-week-old mice (*S5^{del/wt} S5^{tg/tg}* and controls) were rapidly frozen using liquid nitrogen, homogenized and lysed in an isotonic lysis buffer (150mM NaCl, 50mM Tris-HCl pH=7.5, 0.4 % Triton X-100, 2mM CaCl₂, 2mM MgCl₂, 1mM EDTA, 5mM NaF in ddH₂O) with Benzonase nuclease (250 U/ml, cat.no. SC-391121B, Santa Cruz Biotechnology, Texas, USA), protease and phosphatase inhibitors and 10mM Na₃VO₄ for 20 min on ice. After sonication, tissue lysates were further cleared by ultracentrifugation (20,000 g, 4 °C, 10 min) and filtration using a 0.45 µm filter. Individual tissue protein concentrations were equilibrated and lysates corresponding to 100-250 mg of tissue were incubated with 50 µl of anti-FLAG M2 Affinity Gel (cat. no. A2220, Sigma-Aldrich, St. Luis, MO, USA) for three

hours. The immunoprecipitated complexes were washed four times with a lysis buffer and eluted with 3xFLAG peptide (cat. no. F4799, Sigma-Aldrich, St. Luis, MO, USA) in a detergent-free lysis buffer. The eluates were then analyzed by mass spectrometry

Mass Spectrometry details

Eluates were acetone precipitated and resuspended in 100mM TEAB containing 1 % SDC. Cysteines were reduced with 5 mM final concentration of TCEP (60°C for 60 min) and blocked with 10 mM final concentration of MMTS (10 min, RT). Samples were cleaved on beads with 1 µg of trypsin at 37°C overnight. After digestion samples were centrifuged and supernatants were collected and acidified with TFA to 1 % final concentration. SDC was removed by extraction to ethyl acetate²⁶. Peptides were desalted using in-house made stage tips packed with C18 disks (Empore) according to²⁷.

Nano Reversed phase column (EASY-Spray column, 50 cm x 75 µm ID, PepMap C18, 2 µm particles, 100 Å pore size) was used for LC/MS analysis. Mobile phase buffer A was composed of water and 0.1 % formic acid. Mobile phase B was composed of acetonitrile and 0.1 % formic acid. Samples were loaded onto the trap column (Acclaim PepMap300, C18, 5 µm, 300 Å Wide Pore, 300 µm x 5 mm, 5 Cartridges) for 4 min at 15 µl/min. Loading buffer was composed of water, 2 % acetonitrile and 0.1 % trifluoroacetic acid. Peptides were eluted with Mobile phase B gradient from 4 % to 35 % B in 60 min. Eluting peptide cations were converted to gas-phase ions by electrospray ionization and analyzed on a Thermo Orbitrap Fusion (Q-OT-qIT, Thermo). Survey scans of peptide precursors from 400 to 1600 m/z were performed at 120 K resolution (at 200 m/z) with a 5×10^5 ion count target. Tandem MS was performed by isolation at 1,5 Th with the quadrupole, HCD fragmentation with normalized collision energy of 30, and rapid scan MS analysis in the ion trap. The MS² ion count target was set to 10^4 and the max injection time was 35 ms. Only those precursors with charge state 2–6 were sampled for MS². The dynamic exclusion duration was set to 45 s with a 10 ppm tolerance around the selected precursor and its isotopes. Monoisotopic precursor selection was turned on. The instrument was run in top speed mode with 2 s cycles²⁸.

All data were analyzed and quantified with the MaxQuant software (version 1.5.3.8) ²⁹. The false discovery rate (FDR) was set to 1 % for both proteins and peptides and we specified a minimum length of seven amino acids. The Andromeda search engine was used for the MS/MS spectra search against the *Caenorhabditis elegans* database (downloaded from Uniprot in April 2015, containing 25 527 entries). Enzyme specificity was set as C-terminal to Arg and Lys, also allowing cleavage at proline bonds and a maximum of two missed cleavages. Dithiomethylation of cysteine was selected as fixed modification and N-terminal protein acetylation, methionine oxidation and serine/threonine/tyrosine phosphorylation as variable modifications. The “match between runs” feature of MaxQuant was used to transfer identifications to other LC-MS/MS runs based on their masses and retention time (maximum deviation 0.7 min) and this was also used in quantification experiments. Quantifications were performed with the label-free algorithms described recently. Data analysis was performed using Perseus 1.5.2.4 software.

Targeted parallel reaction monitoring of SMARCA5 peptides

Sorted cells from LSK (Lin⁻c-Kit⁺Sca⁺) and LS⁻K (Lin⁻c-Kit⁺Sca1⁻) cell populations were washed with PBS and cell pellet was lysed with 0.1% RapiGest (Waters) in 50 mM ammonium bicarbonate (Sigma Aldrich). Protein cysteines were reduced with 5 mM dithiothreitol (Thermo Scientific) for 30 min at 56 °C and alkylated with 10 mM iodoacetamide (Sigma Aldrich) for 30 min at room temperature in the dark. Proteins were digested with sequencing grade modified trypsin (Promega) (enzyme:protein ratio 1:50) at 37 °C O/N. The reaction was stopped by adding trifluoroacetic acid to a final concentration of 1% (v/v), and RapiGest was precipitated by further incubation at 37 °C for 45 min. Supernatant was cleaned up using solid phase extraction stage tips and dried by vacuum centrifugation. Peptide digests were spiked in with equivalent amount of heavy peptides premix normalized to the used cell count (Supplementary Table 2).

Five peptides used for targeted parallel (PRM) reaction monitoring using mass spectrometry were selected according to reliable detection in shotgun analysis fulfilling these criteria (1) unique; (2) no

missed cleavages (3) not containing cysteine; (4) no modifications and using Picky³⁰ (Table 2). Heavy peptides were purchased from JPT Peptide (JPT Technologies, Berlin, Germany). Cell lysates with spiked in heavy standards were first separated using Ultimate 3000 liquid chromatography system (Dionex). Nano reversed phase columns (Aurora Ultimate TS, 25 cm x 75 μ m ID, 1.7 μ m particle size, Ion Opticks) were used for LC/MS analysis. Mobile phase buffer A was composed of water and 0.1% formic acid. Mobile phase B was composed of acetonitrile and 0.1% formic acid. Samples were loaded onto the trap column (C18 PepMap100, 5 μ m particle size, 300 μ m x 5 mm, Thermo Scientific) for 4 min at 18 μ l/min loading buffer was composed of water, 2% acetonitrile and 0.1% trifluoroacetic acid. Peptides were eluted with Mobile phase B gradient from 4% to 35% B in 16 min. Total analysis time was 30 min per sample. Samples were analyzed by PRM on Orbitrap Ascend (Thermo Scientific). Eluting peptide cations were converted to gas-phase ions by electrospray ionization in positive mode with 1600 V spray voltage. MS data were acquired using tMS2 mode. RF lens amplitude was set to 60 %. Peptide precursors were isolated by quadrupole with 1.6 m/z isolation window and fragmented by HCD with collision energy set to 28%. Fragment ions were detected in orbitrap with 30K resolution at 200 m/z. AGC was set to 250% and maximum injection time mode to Auto. Total cycle time was set to 0.8s. All peptides with their corresponding masses and charge states are listed in the Table 2. Data were analyzed using Skyline-daily (64-bit) version 23.1.1.268. Identical heavy and light transitions and retention times confirmed peptide identity. A minimum of four transitions was required for reliable detection. All peaks were manually inspected to confirm correct detection and peak boundaries. Peak integration and calculation of the ratios between light endogenous and the heavy-labeled peptide (L/H) were done in Skyline and result reports exported from the software.

Table 2: List of peptides used for PRM detection of protein SMARCA5. Peptides precursor masses (m/z) and charge states of the precursor ions (z) are indicated. Heavy amino acids are labeled by bold letter.

Compound	m/z	z
EIQEPDPT Y E E EK	739.3383	2
EIQEPDPT Y E E EK	743.3454	2

QNLLSVGDYR	582.804	2
QNLLSVGDYR	587.8082	2
IYVGLSK	390.2367	2
IYVGLSK	394.2438	2
FVFMSTR	500.7679	2
FVFMSTR	505.772	2
IAFTEWIEPPKR	496.2733	3
IAFTEWIEPPKR	499.6094	3

Sequence coverage by selected peptides

>sp|O60264|SMCA5_HUMAN SWI/SNF-related matrix-associated actin-dependent regulator of chromatin subfamily A member 5 OS=Homo sapiens OX=9606 GN=SMARCA5 PE=1 SV=1

MSSAAEPPPPPPESAPSKPAASIASGGSSNSNKGPEGVAAQAVASAASAGPADAEMEEIFDDASPGKQ**KEIQEP**
DPTYEEKMQTDRANRFEYLLKQTELFAHFIQPAAQKTPTSPLKMKPGRPRIKKDEKQNLLSVGDYRHRRTEQEED
ELLTESSKATNVCTRFEDSPSYVKWGKLRDYQVRGLNWLISLYENGINILADEMGLGKTLQTISLLGYMKHYRNIPG
PHMVLVPKSTLHNWMSEFKRWVPTLRVCLIGDKEQRAAFVRDVLPGEWDCVTSYEMLIKEKSVFKFNWRYL
VIDEAHRIKNEKSKLSEIVREFKTTNRLLLTGTPLQNNLHELWSSLNFFLLPDVFNSSADDFDSWFDTNCLGDQKLVER
LHMVLRPFLLRRIKADVEKSLPPKKEVK**IYVGLSK**MQREWYTRILMKDIDILNSAGKMDKMRLLNLMQLRCCNH
PYLFDGAEPGPYTTDMHLVTNSGKMVVDKLLPKLKEQGSRLIFSQMTRVLDILEDYCMWRNYEYCRLDGQTP
HDERQDSINAYNEPNSTK**FVFMSTR**AGGLGINLATADVILYDSDWNPQVDLQAMDRAHRIGQTKTVRVRFIT
DNTVEERIVERAEMKLRDLSIVIQGRLVDQNLNIGKDEMLQMRHGATHVFASKESITDEDIDGILERGAKKTAE
MNEKLSKMGESSLRNFTMDTESSVYNFEGEDYREKQ**IAFTEWIEPPKR**ERKANYAVDAYFREALRVSEPKAPKAP
RPPKQPNVQDFQFFPRLFELLEKEILFYRKTIGYKVPNPPELNAAQAQKEEQLKIDEAESLNDEELEEKEKLLTQGF
TNWNKRDFNQFIKANKEWGRDDIENIAREVEGKTPPEVIEYSVFWERCNELQDIEKIMAQIERGEARIQRRISIKKA
LDTKIGRYKAPFHQLRISYGTNGKKNYTEEDRFLICMLHKLGFDKENVYDELRCIRNSPQFRFDWFLKSRAMEL
QRRCNTLITLIERENMELEEKEKAEEKKRGPKPSTQKRKMDGAPDGRGRKKKLL

Statistics and Reproducibility

All our experiments are reproducible, statistical methods are indicated in figure legends as well as sample sizes.

REFERENCES:

1. de la Serna, I.L., Ohkawa, Y. & Imbalzano, A.N. Chromatin remodelling in mammalian differentiation: lessons from ATP-dependent remodellers. *Nat Rev Genet* **7**, 461-473 (2006).
2. Zhou, C.Y., Johnson, S.L., Gamarra, N.I. & Narlikar, G.J. Mechanisms of ATP-Dependent Chromatin Remodeling Motors. *Annu Rev Biophys* **45**, 153-181 (2016).
3. Erdel, F. & Rippe, K. Chromatin remodelling in mammalian cells by ISWI-type complexes--where, when and why? *FEBS J* **278**, 3608-3618 (2011).
4. Narlikar, G.J., Sundaramoorthy, R. & Owen-Hughes, T. Mechanisms and functions of ATP-dependent chromatin-remodeling enzymes. *Cell* **154**, 490-503 (2013).
5. Stopka, T. & Skoultchi, A.I. The ISWI ATPase Snf2h is required for early mouse development. *Proc Natl Acad Sci U S A* **100**, 14097-14102 (2003).
6. Barisic, D., Stadler, M.B., Iurlaro, M. & Schubeler, D. Mammalian ISWI and SWI/SNF selectively mediate binding of distinct transcription factors. *Nature* **569**, 136-140 (2019).
7. Dluhosova, M. *et al.* Epigenetic control of SPI1 gene by CTCF and ISWI ATPase SMARCA5. *PLoS One* **9**, e87448 (2014).
8. Ding, Y. *et al.* Smarca5-mediated epigenetic programming facilitates fetal HSPC development in vertebrates. *Blood* **137**, 190-202 (2021).
9. Kokavec, J. *et al.* The ISWI ATPase Smarca5 (Snf2h) Is Required for Proliferation and Differentiation of Hematopoietic Stem and Progenitor Cells. *Stem Cells* **35**, 1614-1623 (2017).
10. Zikmund, T. *et al.* ISWI ATPase Smarca5 Regulates Differentiation of Thymocytes Undergoing beta-Selection. *J Immunol* **202**, 3434-3446 (2019).
11. Oppikofer, M. *et al.* Expansion of the ISWI chromatin remodeler family with new active complexes. *EMBO Rep* **18**, 1697-1706 (2017).
12. Siamishi, I. *et al.* Lymphocyte-Specific Function of the DNA Polymerase Epsilon Subunit Pole3 Revealed by Neomorphic Alleles. *Cell Rep* **31**, 107756 (2020).
13. Dowdle, J.A. *et al.* Mouse BAZ1A (ACF1) is dispensable for double-strand break repair but is essential for averting improper gene expression during spermatogenesis. *PLoS Genet* **9**, e1003945 (2013).
14. Koscielny, G. *et al.* The International Mouse Phenotyping Consortium Web Portal, a unified point of access for knockout mice and related phenotyping data. *Nucleic Acids Res* **42**, D802-809 (2014).
15. Landry, J. *et al.* Essential role of chromatin remodeling protein Bptf in early mouse embryos and embryonic stem cells. *PLoS Genet* **4**, e1000241 (2008).
16. Dicipulo, R. *et al.* Ceer2 mutant mice as a model for human cat eye syndrome. *Sci Rep* **11**, 3111 (2021).
17. Emanuele, M.J. *et al.* Global identification of modular cullin-RING ligase substrates. *Cell* **147**, 459-474 (2011).
18. Han, L. *et al.* Chromatin remodeling mediated by ARID1A is indispensable for normal hematopoiesis in mice. *Leukemia* **33**, 2291-2305 (2019).
19. Chi, T.H. *et al.* Reciprocal regulation of CD4/CD8 expression by SWI/SNF-like BAF complexes. *Nature* **418**, 195-199 (2002).
20. Chi, T.H. *et al.* Sequential roles of Brg, the ATPase subunit of BAF chromatin remodeling complexes, in thymocyte development. *Immunity* **19**, 169-182 (2003).
21. Williams, C.J. *et al.* The chromatin remodeler Mi-2beta is required for CD4 expression and T cell development. *Immunity* **20**, 719-733 (2004).

22. Janeckova, L. *et al.* Wnt Signaling Inhibition Deprives Small Intestinal Stem Cells of Clonogenic Capacity. *Genesis* **54**, 101-114 (2016).
23. Nagy, A., Rossant, J., Nagy, R., Abramow-Newerly, W. & Roder, J.C. Derivation of completely cell culture-derived mice from early-passage embryonic stem cells. *Proc Natl Acad Sci U S A* **90**, 8424-8428 (1993).
24. de Boer, J. *et al.* Transgenic mice with hematopoietic and lymphoid specific expression of Cre. *Eur J Immunol* **33**, 314-325 (2003).
25. Birling, M.C., Dierich, A., Jacquot, S., Herault, Y. & Pavlovic, G. Highly-efficient, fluorescent, locus directed cre and FlpO deleter mice on a pure C57BL/6N genetic background. *Genesis* **50**, 482-489 (2012).
26. Masuda, T., Tomita, M. & Ishihama, Y. Phase transfer surfactant-aided trypsin digestion for membrane proteome analysis. *J Proteome Res* **7**, 731-740 (2008).
27. Rappsilber, J., Mann, M. & Ishihama, Y. Protocol for micro-purification, enrichment, pre-fractionation and storage of peptides for proteomics using StageTips. *Nat Protoc* **2**, 1896-1906 (2007).
28. Hebert, A.S. *et al.* The one hour yeast proteome. *Mol Cell Proteomics* **13**, 339-347 (2014).
29. Cox, J. *et al.* Accurate proteome-wide label-free quantification by delayed normalization and maximal peptide ratio extraction, termed MaxLFQ. *Mol Cell Proteomics* **13**, 2513-2526 (2014).
30. Zauber, H., Kirchner, M. & Selbach, M. Picky: a simple online PRM and SRM method designer for targeted proteomics. *Nat Methods* **15**, 156-157 (2018).

Acknowledgements: We thank all members of the laboratory who participated in the discussions, in particular Dr. Lubomir Minarik. We would also like to thank Kristina Leblova for technical assistance. We acknowledge the Imaging Methods Core Facility at BIOCEV for their support with obtaining flow cytometry data presented in this paper, Laboratory of Mass Spectrometry at BIOCEV, where proteomic and mass spectrometric analyses had been done and Czech Centre for Phenogenomics for mouse strain generation. Grant support: Agency of Czech Ministry of Health (NU22-05-00374, NU21-08-00312); Grant Agency of the Czech Republic (24-10435S, 24-10353S), and Charles University (UNCE/MED/016, Cooperatio, SVV260637); Next Generation EU, Programme EXCELES (LX22NPO5102). Czech Center for Phenogenomics was supported by the Czech Academy of Sciences RVO 68378050 and by the projects LM2018126 / LM2023036 Czech Centre for Phenogenomics provided by Ministry of Education, Youth, and Sports of the Czech Republic (MEYS), CZ.02.1.01/0.0/0.0/16_013/0001789, and CZ.02.1.01/0.0/0.0/18_046/0015861 by MEYS & ESIF.

Author Contributions: Conceptualization TS, LC; methodology TZ, LC, JK, RS, TT, KP; investigation TT, JK, LC, KP, DN, ND, MH, LR; validation TT, JK, LC; formal analysis JK, LC, TT, KP; writing-original draft preparation TS, TT, JK; writing-review and editing TS, TT, LC, JK, ND, KP; visualization TT, JK; supervision TS, LC; project administration TS, LC; funding acquisition TS, LC. All authors have read and agreed to the published version of the manuscript.

Competing interests: The authors declare no competing interests.

Data Availability statement: Source data for all figures except for proteomic data are available in the supplementary data file. Uncropped images of all the blots and gels used in the figures are provided in Supplementary Fig. 6. Proteomic data has been uploaded to PanoramaPublic web site as ProteomeXchange dataset PXD048865 (targeted parallel reaction monitoring of SMARCA5 peptides) and to PRIDE (Proteomics Identification Database) with project accession number: PXD049034 (SMARCA5 interactome data).

Materials & Correspondence: For communication in case of interest in the S5 transgenic strain, please contact the senior author Prof. Tomas Stopka, tstopka@lf1.cuni.cz Regarding flow cytometry technology and stem cell transplantation, please communicate with: Dr. Juraj Kokavec, juraj.kokavec@lf1.cuni.cz For further technical information please communicate with Dr. Tereza Turkova, tereza.turkova@volny.cz

TABLES:

Table 1: The table shows the numbers and % of mice born with the respective genotypes from the crosses of the parents described in the left part. Specifically, these are the *hCD2iCre*, *Vav1iCre* and *ActB-Cre* models carrying floxed alleles of the *Smarca5* and *S5* transgene inserted into the *Rosa26* locus.

<i>hCD2iCre S5^{tg}</i>	Progeny genotypes			
Parental genotypes	<i>S5^{fl/fl} S5^{tg}</i>	<i>S5^{fl/fl} S5^{tg/tg}</i>	<i>hCD2iCre S5^{fl/fl} S5^{tg}</i>	<i>hCD2iCre S5^{fl/fl} S5^{tg/tg}</i>
♂ <i>hCD2iCre S5^{fl/fl} S5^{tg}</i> x ♀ <i>S5^{fl/fl} S5^{tg/tg}</i>	141 (24.6 %)	151 (26.3 %)	140 (24.4 %)	142 (24.7 %)

<i>Vav1iCre S5^{tg}</i>	Progeny genotypes			
Parental genotypes	<i>S5^{fl/fl} S5^{tg}</i>	<i>S5^{fl/fl} S5^{tg/tg}</i>	<i>Vav1iCre S5^{fl/fl} S5^{tg}</i>	<i>Vav1iCre S5^{fl/fl} S5^{tg/tg}</i>
♂ <i>Vav1iCre S5^{fl/fl} S5^{tg}</i> x ♀ <i>S5^{fl/fl} S5^{tg/tg}</i>	101 (24.3 %)	104 (25.0 %)	94 (22.6 %)	117 (28.1 %)

<i>ActB-Cre S5^{tg}</i>	Progeny genotypes		
Parental genotypes	<i>S5^{wt/wt} S5^{tg/tg}</i>	<i>S5^{del/wt} S5^{tg/tg}</i>	<i>S5^{del/del} S5^{tg/tg}</i>
Prenatal E13.5			
♂ <i>S5^{del/wt} S5^{tg/tg}</i> x ♀ <i>S5^{del/wt} S5^{tg/tg}</i>	15 (34.9 %)	26 (60.5 %)	2 (4.7 %)
♂ <i>S5^{fl/fl} S5^{tg/tg}</i> x ♀ <i>ActB-Cre S5^{del/wt} S5^{tg}</i>	0	21 (95.5 %)	1 (4.5 %)
Prenatal E18.5			
♂ <i>S5^{del/wt} S5^{tg/tg}</i> x ♀ <i>S5^{del/wt} S5^{tg/tg}</i>	21 (36.2 %)	33 (56.9 %)	4 (6.9 %)
Postnatal			
♂ <i>S5^{del/wt} S5^{tg/tg}</i> x ♀ <i>S5^{del/wt} S5^{tg/tg}</i>	325 (67.6 %)	156 (32.4 %)	0
♂ <i>S5^{fl/fl} S5^{tg}</i> x ♀ <i>ActB-Cre S5^{del/wt} S5^{tg}</i>	0	95 (99.0 %)	1 (1.0 %)
♂ <i>S5^{fl/fl} S5^{tg/tg}</i> x ♀ <i>ActB-Cre S5^{del/wt} S5^{tg}</i>	0	486 (99.4 %)	3 (0.6 %)

FIGURE LEGENDS:

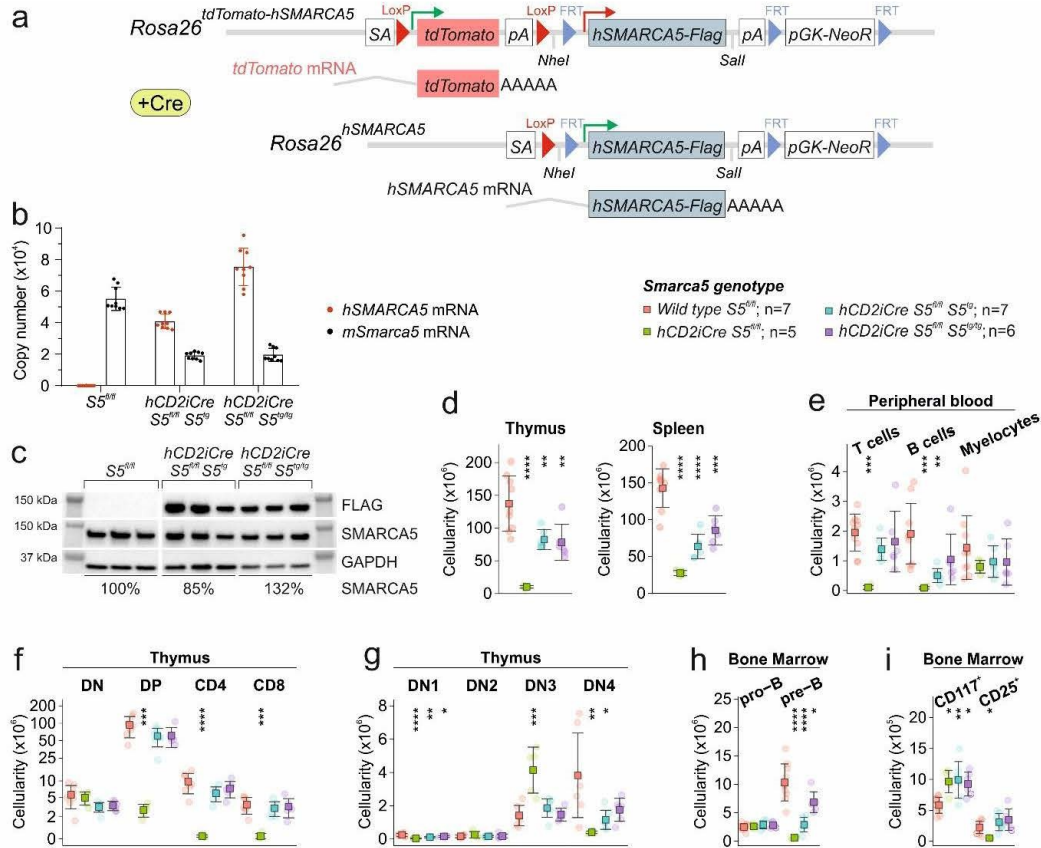


Figure 1. Transgenic *SMARCA5* releases the blockade of T and B cell differentiation after *Smarca5* deletion. (a) Scheme of recombination at the *Rosa26* locus: incorporation of a neomycin resistance construct (*pGK-NeoR*) containing the *tdTomato* gene with polyadenylation signal (*pA*) and *loxP* sites (red triangles) and *SMARCA5-FLAG* cDNA with FRT sites (blue triangles) downstream of the splice acceptor (*SA*) site. The transgene expresses *tdTomato* and, upon activation of Cre recombinase, the *tdTomato* cDNA is removed, leading to the expression of *SMARCA5*. (b) Copy number quantification of mouse and human *Smarca5* mRNA by qRT-PCR (AVG \pm SD, n=3) in thymi of 2-month-old mice of the indicated genotypes after normalization to *Gapdh* and *Hprt* expression. (c) Immunoblot of thymi from 8-week-old mice of the indicated genotypes stained with anti-FLAG or anti-*SMARCA5* antibodies. GAPDH staining was used as a loading control. Signal density is stated in % relative to controls. (d) Thymic and splenic cellularity of 8-week-old mice of the indicated genotypes (analyzed by flow cytometry). (e) Cytometry with anti-CD4/CD8, anti-B220, and anti-Gr-1/CD11b from CD45⁺ peripheral blood cells of the indicated genotypes. (f) Cytometric analysis of thymic populations: DN, DP, and SP of the indicated genotypes. (g) Cytometric analysis of thymocytes (negative for B220, Gr-1, CD11b, CD11c and Nk1.1) of the indicated genotypes using anti-CD25 and anti-CD44 antibodies. (h, i) Cytometric analysis of B cell development of the indicated genotypes using anti-B220 and anti-CD43 staining of BM CD45⁺ cells (h) and anti-CD117 and anti-CD25 staining of pro-B cells (CD43⁺B220⁺) (i). Statistics: One-Way ANOVA with Tukey's Honestly Significant Difference test (p adjusted value: p<0.05=*, p<0.01=**, p<0.001=***, p<0.0001=****, no asterisks = non-significant), the error bars represent standard deviation.

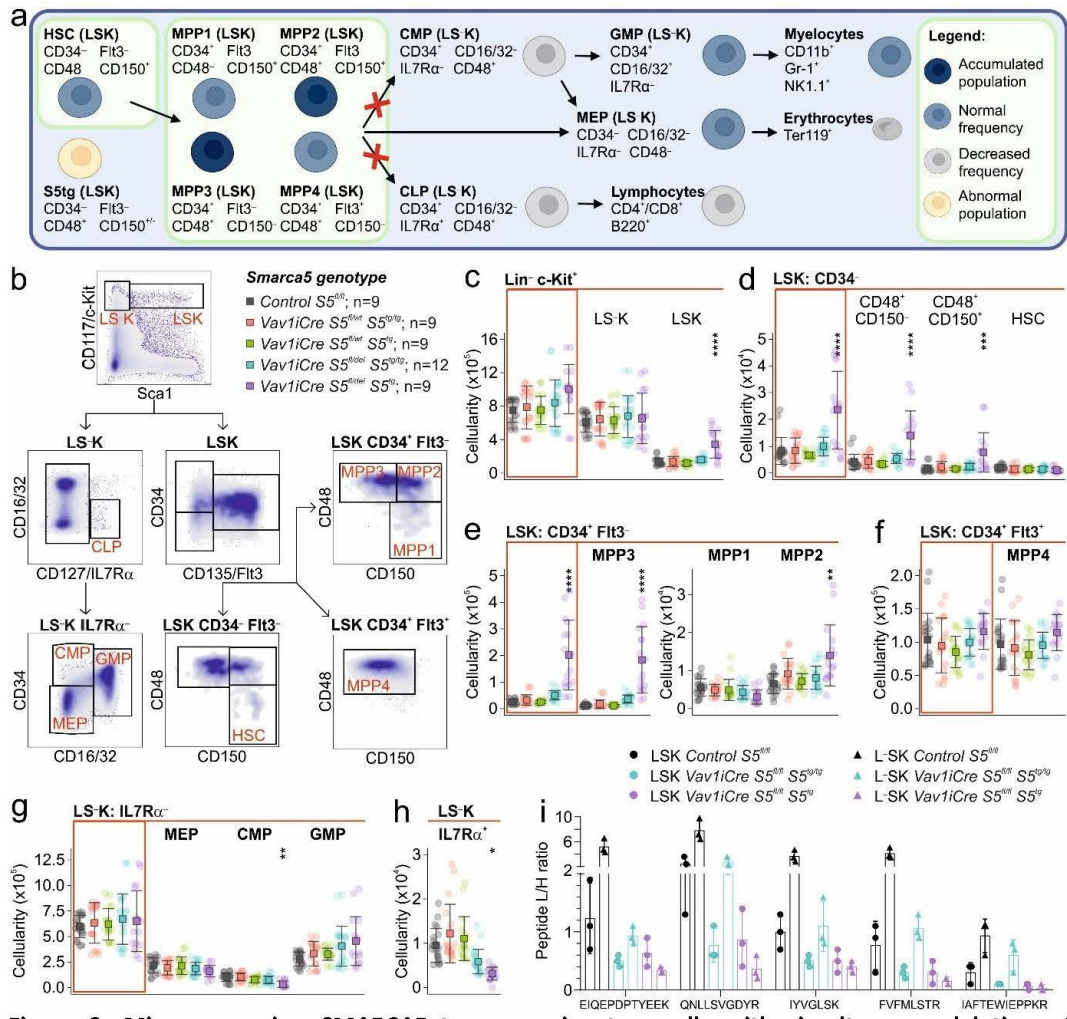


Figure 3. Mice expressing *SMARCA5* transgene in stem cells with simultaneous deletion of endogenous *Smarca5* have impaired early hematopoietic development. (a) Scheme of differentiation of HSC and MPP with their specific antigens in *SMARCA5* transgenic mice. Created with BioRender.com. (b) Gating strategy for flow cytometry analysis of hematopoietic progenitors in bone marrow. (c) Absolute quantification of populations from flow cytometry analysis of BM from 10-week-old mice of the indicated genotypes. Analysis of c-Kit and Sca1 markers excluding lineage antigens (CD3, Ly-6G/Ly-6C, CD11b, B220, Ter-119) yielded isolation of stem (LSK) and early progenitor (LS-K) cells. (d) Absolute quantification of CD34⁺ LSK, total population on the left, CD48⁺CD150⁺ and HSCs on the right. (e) Absolute quantification of CD34⁺ Flt3⁻ LSK subpopulations enriched for MPPs with multi-lineage developmental potential. (f) Absolute quantification of lymphoid-oriented CD34⁺ Flt3⁺ MPP4 population. (g, h) Quantification of lineage-restricted (CD127/IL7Rα⁻) progenitor subpopulations (g) and early IL7Rα⁺ lymphoid progenitors (h) in LSK BM cells using myeloid marker CD16/32 and CD34. MEP = megakaryocytic-erythroid progenitor, CMP = common myeloid progenitor, GMP = granulocyte-monocyte progenitor. (i) Bar chart depicts ratio of intensities of light over heavy peptides from protein *SMARCA5* detected by targeted parallel reaction monitoring in sorted mouse LSK and LS-K cell populations of indicated genotypes. For n numbers and cell counts see Supplementary Table 2. Statistics: One-Way ANOVA with Tukey's Honestly Significant Difference test (p adjusted value: p<0.05=*, p<0.01=**, p<0.001=***, p<0.0001=****, no asterisks = non-significant), the error bars represent standard deviation.

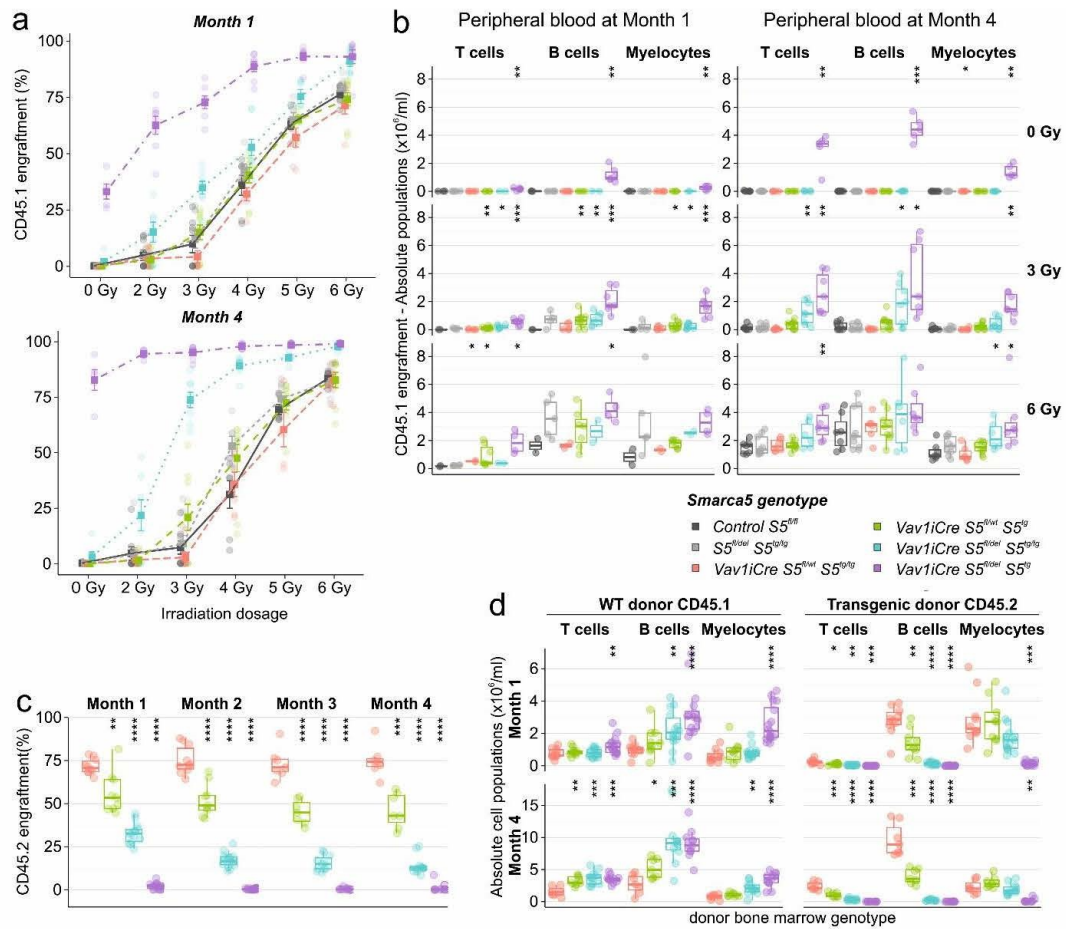


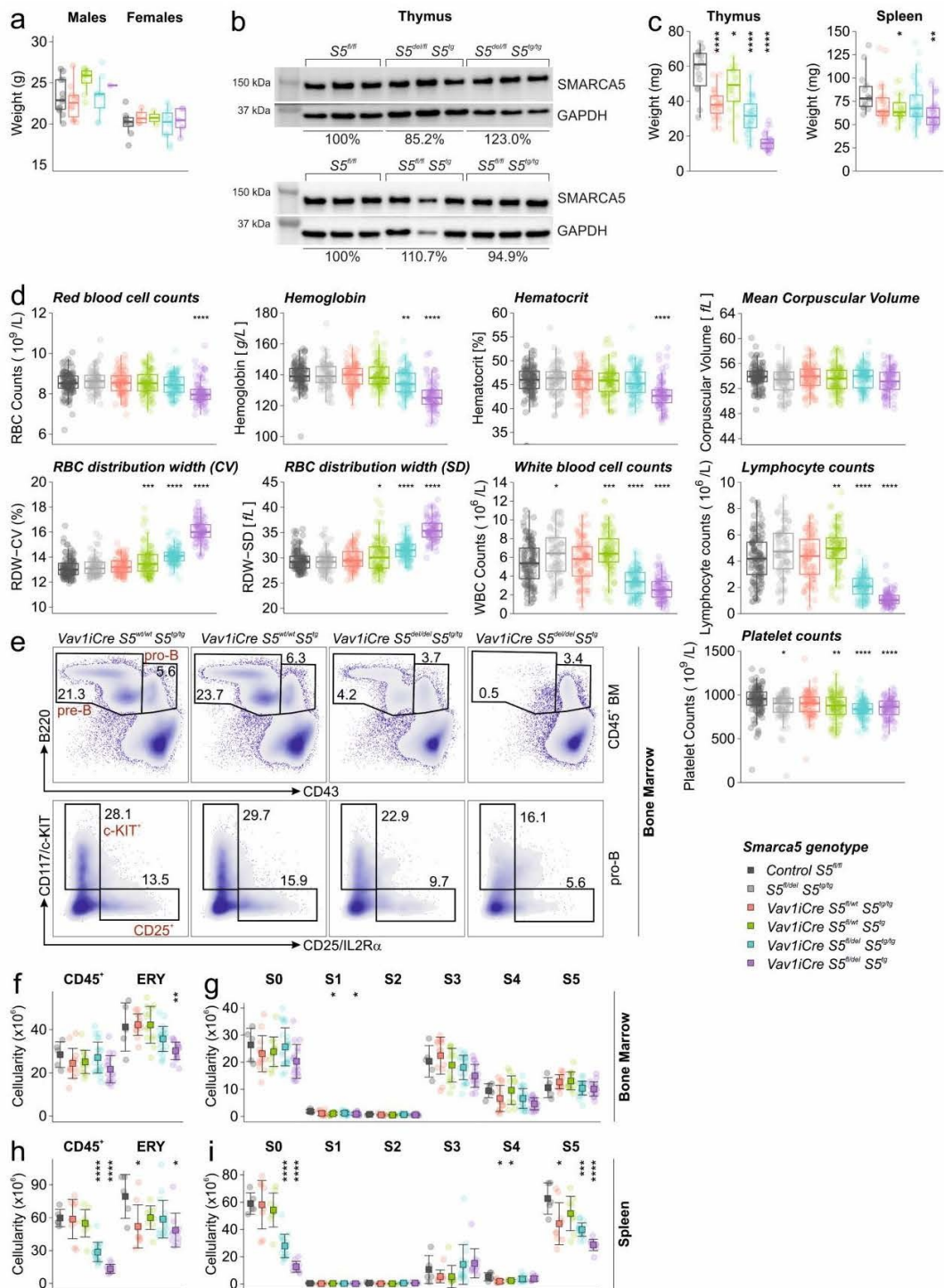
Figure 4. Transplantation of stem cells with only transgenic *SMARCA5* expression reveals defects in T and B cell repopulation. (a) Dose dependence of *SMARCA5* expression levels (indicated genotypes) on graft repopulation (X-axis). Cytometry (%) of reconstitution of control CD45.1 donor BM cells in *S5^{tg}* recipient mice on CD45.2 background at 1 (short-term repopulation) and 4 months (long-term) after transplantation depending on irradiation dosage. (b) Absolute quantification (Y-axis) of engraftment of wild-type hematopoietic cells in BM niches of the indicated genotypes. Quantification of hematopoietic lineage progeny (T, B, and myeloid cells, X-axis) after reconstitution of CD45.1 BM donor cells from peripheral blood by flow cytometry at 1 and 4 months after transplantation depending on irradiation dosage. (c) Relative quantification of competitive transplantation (3:1 ratio) of BM from indicated *SMARCA5* transgenic mice (CD45.2, indicated genotypes) along with wild-type CD45.1 into lethally (8.5 Gy) irradiated wild-type CD45.1 recipients at 1-4 months. (d) Absolute quantification of competitive hematopoietic BM engraftment of the indicated genotypes. Peripheral blood progeny (T, B, and myeloid cells, X-axis) after reconstitution at 1 and 4 months (see C for details). Statistics: T-test relative to controls ($p < 0.05 = *$, $p < 0.01 = **$, $p < 0.001 = ***$, $p < 0.0001 = ****$, no asterisks = non-significant), the error bars represent standard deviation, for n numbers see Supplementary Table 3.

Supplementary figures:

a



Supplementary Figure 1. Transgenic *SMARCA5* releases the blockade of T and B cell differentiation after *Smarca5* deletion. (a) Alignment of human and murine *SMARCA5* amino acid sequence. (b) Electrophoretic gel (0.8 % agarose) with PCR analysis of mouse embryonic stem cells (ESC) with *S5^{tg}* construct integrated in *Rosa26* locus. Positive band is 3.495 kbp long with fwd primer in *Rosa26* sequence and rev primer in *tdTomato* sequence. (c) Electrophoretic gel (1.5 % agarose) with PCR analysis of genomic DNA from chimeric mice with *S5^{tg}* genotype. Positive band is 852bp long. (d) Western blot analysis of two leukemic cell lines MEL (murine erythroleukemia) and OCI-M2 (human adult acute myeloid leukemia) using antibody against *SMARCA5*. Numbers indicate total amount of protein loaded to the gel in micrograms. Staining with GAPDH were used as loading control. (e) Thymi of 8-week-old mice of indicated genotypes. Merge of visible light and fluorescence. The *S5^{tg}* mouse (without Cre recombinase activation) expresses *tdTomato* (red), upon *hCD2iCre* activation, *tdTomato* is deleted and *S5^{tg}* is expressed. (f) Thymus and spleen weight and bone marrow cellularity of indicated genotypes. Statistics: t-test relative to controls (g) Hematological measurements of peripheral blood from 2-month-old experimental animals of indicated genotypes. Statistics: One-Way ANOVA with Tukey's Honestly Significant Difference test (p adjusted value: p<0.05=*, p<0.01=**, p<0.001=***, p<0.0001=****, no asterisks = non-significant), the error bars represent standard deviation.



Supplementary Figure 2. Mice expressing *SMARCA5* transgene in stem cells with simultaneous deletion of endogenous *Smarca5* have defects in T and B differentiation. (a) Weight of 2-month-old mice of the indicated genotypes and sex. (b) Immunoblot of thymi of 2-month-old mice of the indicated genotypes with anti-*SMARCA5*, antibody. For these experiments, we used mice with a non-conditional variant of the *SMARCA5* transgene; the transgene was activated in the previous generation by ActB-Cre recombinase. As a result, the *SMARCA5* transgene is non-conditionally expressed in every cell in the body of the analyzed mice. GAPDH staining was used as a loading control. Signal density is stated in % relative to controls. (c) Thymus and spleen weight of indicated genotypes. (d) Hematological measurements of peripheral blood from 2-month-old experimental animals of indicated genotypes. (e) Flow cytometry analysis of B-cell development in 2-month-old bone marrow (BM) of indicated genotypes. Upper panels: using B220 and CD43 staining of CD45⁺ cells in BM. Lower panels: using CD117 and CD25 staining of pro-B cells (CD43⁺B220⁺). (f, h) Flow cytometry analysis of erythroid development in 2-month-old animals of indicated genotypes. Estimated size of CD45⁺ and ERY (Ter119⁺) populations in BM (f) and spleen (h). (g, i) Estimated size of stage 0 to 5 (S0-S5) populations of erythroid development in 2-month-old animals distinguished using anti-Ter119 and anti-CD117/c-kit antibodies in BM (g) and spleen (i). Statistics: One-Way ANOVA with Tukey's Honestly Significant Difference test (p adjusted value: p<0.05=*, p<0.01=**, p<0.001=***, p<0.0001=****, no asterisks = non-significant), the error bars represent standard deviation, for n numbers see Supplementary Table 1.

Supplementary Table 1.

Table of animals used in experiments in Figure 2 and Supplementary Figure 2:

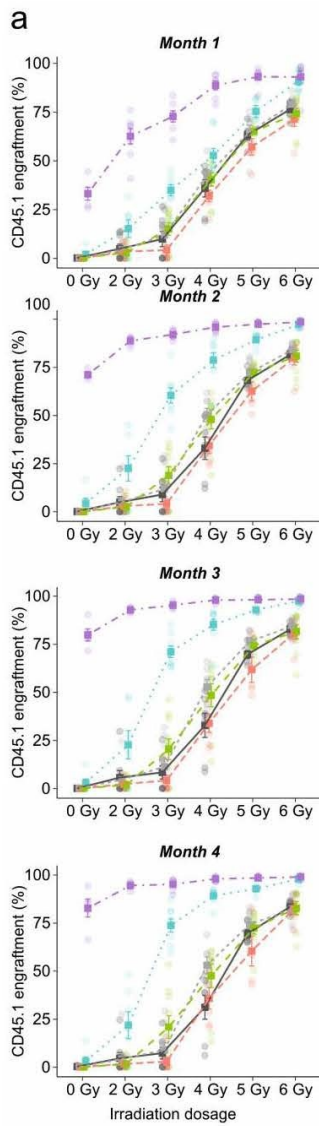
	<i>Ctrl S5^{fl/fl}</i>	<i>S5^{fl/wt} S5^{tg/tg}</i>	<i>Vav1iCre S5^{fl/wt} S5^{tg/tg}</i>	<i>Vav1iCre S5^{fl/wt} S5^{tg}</i>	<i>Vav1iCre S5^{fl/del} S5^{tg/tg}</i>	<i>Vav1iCre S5^{fl/del} S5^{tg}</i>
Fig. 2c, S2c, S2a Thymus	9		20	13	33	18
Fig. 2c, S2c Spleen	9		20	18	38	24
Fig. 2c, S2c Bone Marrow	9		27	26	47	31
Fig. 2d	45	13	21	22	30	25
Fig. 2e, 2f	9		10	2	21	6
Fig. 2g, 2h	9		9	13	23	16
Fig. S2d	117	68	78	96	107	84
Fig. S2f, S2g	9		13	13	23	17
Fig. S2h, S2i	9		9	9	17	10

Supplementary Figure 3: Mice expressing *SMARCA5* transgene in stem cells with simultaneous deletion of endogenous *Smarca5* have impaired early hematopoietic development. (a) Flow cytometry of 10-week-old bone marrow from mice of the indicated genotypes. Analysis of c-Kit and Sca1 markers to exclude lineage antigens (CD3, Ly-6G/Ly-6C, CD11b, B220, Ter-119) yielded isolation of stem (LSK) and early progenitor (LS-K) cells. (b) Flow cytometry of stem-cell marker CD34 and lymphoid/myeloid marker FLT3/CD135 in LS-K (upper panels) and LSK (lower panels) cells. (c) Cytometry of LSK CD34⁺ (upper panels, long-term HSC) and LSK CD34⁺ enriched multipotent progenitor (MPP) stem-cell populations (lower panels) differentiated by expression of SLAM markers CD48 and CD150. MPP1 – short-term HSCs, MPP2 – myeloid-oriented, MPP3 – lineage-balanced MPP. (d) Flow cytometry of lineage progenitor enriched LS-K cells in bone marrow using myeloid CD16/32 and lymphoid IL7R α markers. (e) Flow cytometry of lineage-restricted (CD127/IL7R α) progenitor subpopulations in LSK bone marrow cells using myeloid marker CD16/32 and CD34, MEP = megakaryocytic-erythroid progenitor, CMP = common myeloid progenitor, GMP = granulocyte-monocyte progenitor. (f) Absolute quantification of CD34⁺ and Flt3/CD135⁺ LSK cells. Statistics: One-Way ANOVA with Tukey's Honestly Significant Difference test (p adjusted value: p<0.05=*, p<0.01=**, p<0.001=***, p<0.0001=****, no asterisks = non-significant), the error bars represent standard deviation.

Supplementary Table 2.

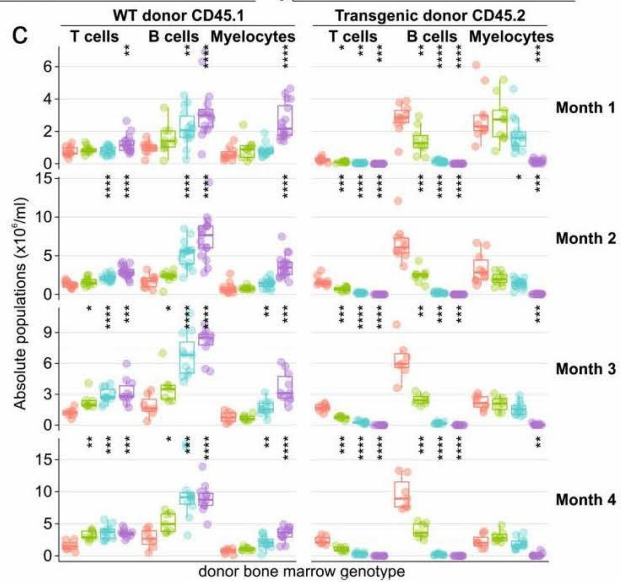
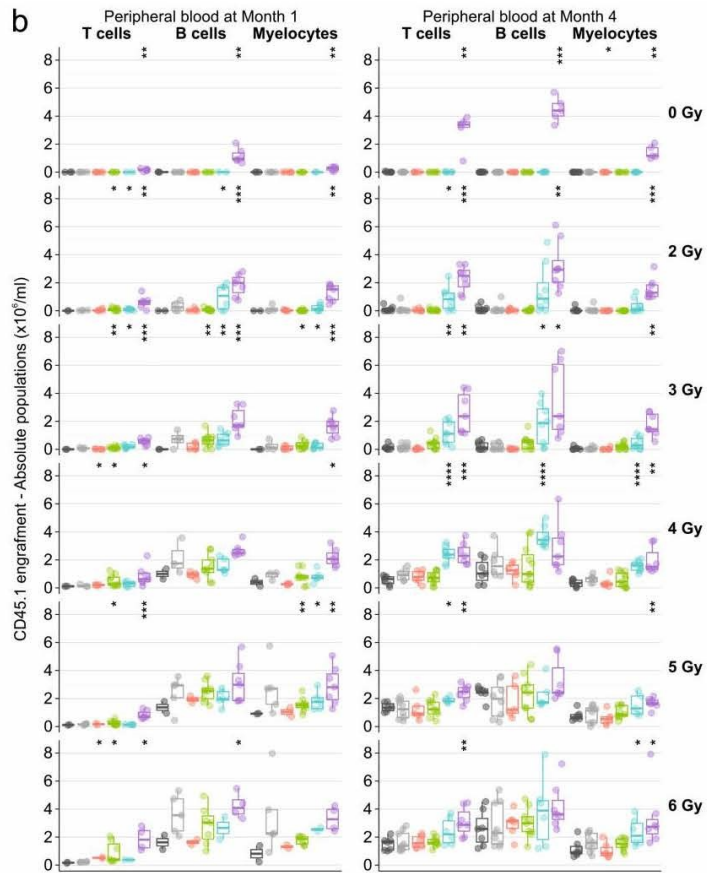
Table of animals used in experiments in Figure 3i including total cell counts sorted from bone marrow of indicated genotypes:

Replicate number	Sex	Genotype	Sorted LSK	LSK count per replicate	Sorted LS-K	LS-K count per replicate
Rep1	F	<i>Ctrl S5^{fl/fl}</i>	87687	130836	195736	390719
	M	<i>Ctrl S5^{wt/wt}</i>	43149		194983	
Rep2	M	<i>Ctrl S5^{wt/wt}</i>	77272	142357	261607	449603
	F	<i>Ctrl S5^{wt/wt}</i>	65085		187996	
Rep3	F	<i>Ctrl S5^{fl/fl}</i>	43244	124261	149213	368872
	M	<i>Ctrl S5^{wt/wt}</i>	81017		219659	
Rep1	F	<i>Vav1iCre S5^{fl/fl} S5^{tg/tg}</i>	69210	161481	131633	282849
	F	<i>Vav1iCre S5^{fl/fl} S5^{tg/tg}</i>	92271		151216	
Rep2	F	<i>Vav1iCre S5^{fl/fl} S5^{tg/tg}</i>	143015	143015	174271	174271
Rep3	M	<i>Vav1iCre S5^{fl/fl} S5^{tg/tg}</i>	134538	134538	249369	249369
Rep1	F	<i>Vav1iCre S5^{fl/fl} S5^{tg}</i>	79803	181431	71670	174403
	M	<i>Vav1iCre S5^{fl/fl} S5^{tg}</i>	49073		75996	
	F	<i>Vav1iCre S5^{fl/fl} S5^{tg}</i>	52555		26737	
Rep2	M	<i>Vav1iCre S5^{fl/fl} S5^{tg}</i>	119203	175354	123538	149361
	F	<i>Vav1iCre S5^{fl/fl} S5^{tg}</i>	56151		25823	
Rep3	F	<i>Vav1iCre S5^{fl/fl} S5^{tg}</i>	76484	169753	85785	187391
	M	<i>Vav1iCre S5^{fl/fl} S5^{tg}</i>	49324		73652	
	F	<i>Vav1iCre S5^{fl/fl} S5^{tg}</i>	43945		27954	



Smarca5 genotype

- Control $S5^{fl/fl}$
- $S5^{tdel} S5^{tg/tg}$
- $Vav1Cre S5^{fl/wt} S5^{tg/tg}$
- $Vav1Cre S5^{fl/wt} S5^{fl}$
- $Vav1Cre S5^{tdel} S5^{tg/tg}$
- $Vav1Cre S5^{tdel} S5^{fl}$



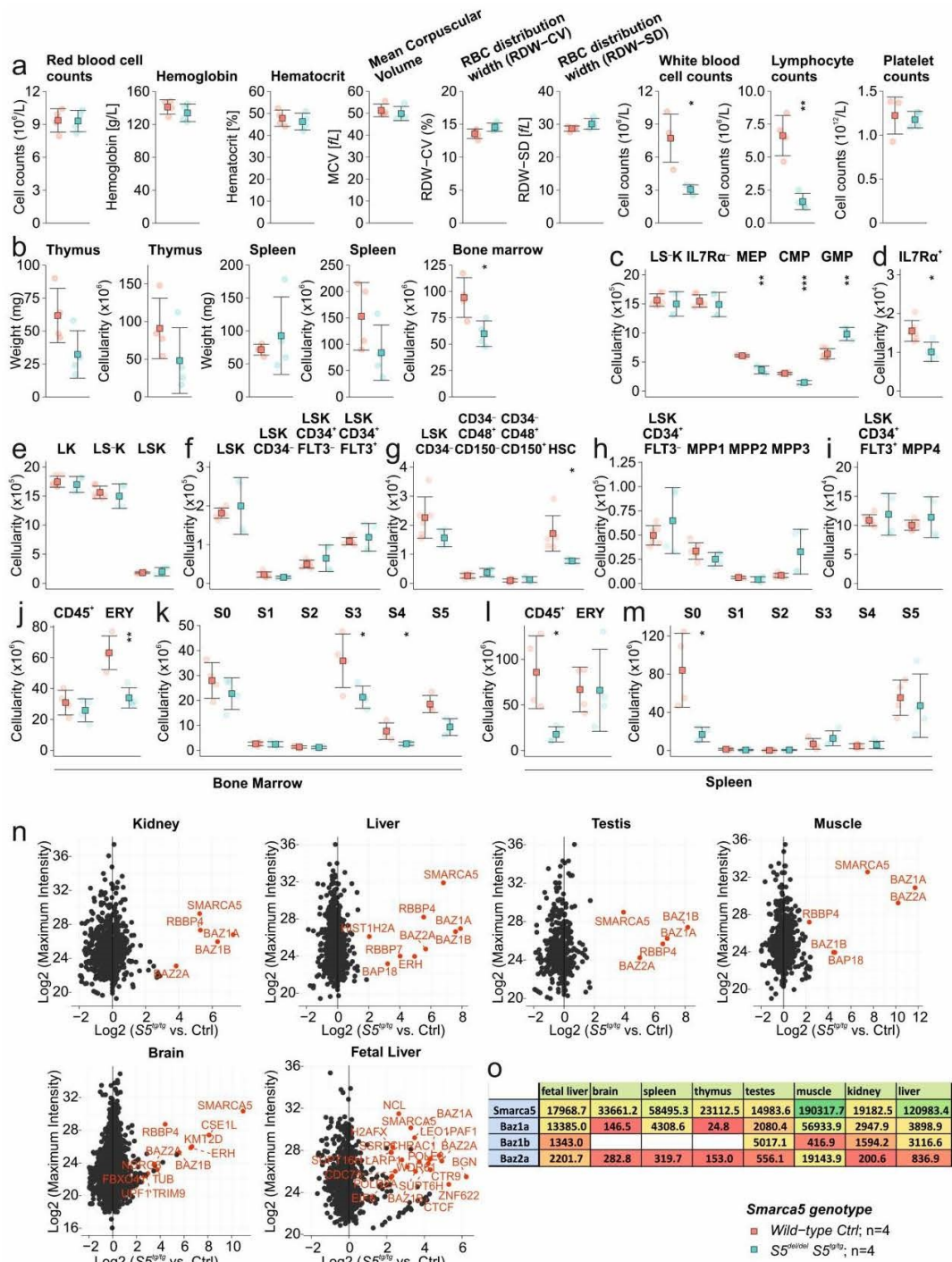
Supplementary Figure 4: Transplantation of stem cells with only transgenic *SMARCA5* expression reveals defects in T and B cell repopulation. (a) Dose dependence of *SMARCA5* expression levels (indicated genotypes) on graft repopulation (X-axis). Cytometry (%) of reconstitution of control CD45.1 donor bone marrow cells (BMCs) in *S5^{tg}* recipient mice on CD45.2 background at 1 (short-term repopulation) to 4 months (long-term) after transplantation depending on irradiation dosage. (b) Absolute quantification (Y-axis) of engraftment of wild-type hematopoietic cells in bone marrow niches of the indicated genotypes. Quantification of hematopoietic lineage progeny (T, B, and myeloid cells, X-axis) after reconstitution of CD45.1 bone marrow (BM) donor cells from peripheral blood by flow cytometry at 1 to 4 months after transplantation depending on irradiation dosage. (c) Absolute quantification of competitive hematopoietic BM engraftment of the indicated genotypes. Peripheral blood progeny (T, B, and myeloid cells, X-axis) after reconstitution at 1 to 4 months. Statistics: t-test relative to controls ($p < 0.05 = *$, $p < 0.01 = **$, $p < 0.001 = ***$, $p < 0.0001 = ****$, no asterisks = non-significant), the error bars represent standard deviation, for n numbers see Supplementary Table 3.

Supplementary Table 3.

Table of animals used in transplantation experiments in Figure 4 and Supplementary Figure 4:

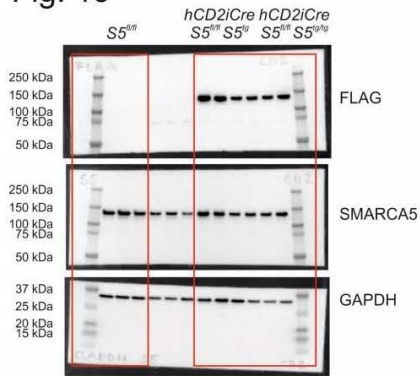
Fig. 4a, 4b, S4a, S4b	Ctrl <i>S5^{fl/fl}</i>	<i>S5^{fl/wt} S5^{tg/tg}</i>	<i>Vav1iCre S5^{fl/wt} S5^{tg/tg}</i>	<i>Vav1iCre S5^{fl/wt} S5^{tg}</i>	<i>Vav1iCre S5^{fl/del} S5^{tg/tg}</i>	<i>Vav1iCre S5^{fl/del} S5^{tg}</i>
0 Gy	8	9	5	6	6	5
2 Gy	8	9	7	11	7	8
3 Gy	8	9	7	10	8	7
4 Gy	7	7	6	9	9	7
5 Gy	6	8	5	9	6	7
6 Gy	7	9	6	10	6	7

Fig. 4c, 4d, S4c	<i>Vav1iCre S5^{fl/wt} S5^{tg/tg}</i>	<i>Vav1iCre S5^{fl/wt} S5^{tg}</i>	<i>Vav1iCre S5^{fl/del} S5^{tg/tg}</i>	<i>Vav1iCre S5^{fl/del} S5^{tg}</i>
Month 1	10	9	14	17
Month 2	10	9	15	17
Month 3	10	9	15	17
Month 4	7	7	11	11



Supplementary Figure 5. The SMARCA5 transgenic product forms complexes and is essential for lymphopoiesis. **(a)** Hematological measurements of peripheral blood from 1-year-old experimental animals of indicated genotypes. **(b)** Thymus and spleen weight and thymus, spleen, and bone marrow cellularity of 1-year-old animals of indicated genotypes. **(c)** Flow cytometry analysis of the 1-year-old bone marrow of indicated genotypes. The expression of stem cell and progenitor markers c-Kit and Sca1 was used to identify bone marrow populations enriched for stem (LSK) and early progenitor cell populations (LS^cK). Lineage-positive (CD3, Ly-6G/Ly-6C, CD11b, B220, Ter-119) cells were excluded from all measurements. **(d)** Flow cytometry of stem cell marker CD34 and lymphoid/myeloid marker Flt3/CD135 in LS^cK and LSK cells. **(e)** Flow cytometry of stem cell enriched LSK CD34⁻ (HSC = long term-repopulating HSCs) and multipotent progenitor (MPP) enriched LSK CD34⁺ populations distinguished by expression of SLAM markers CD48 and CD150. **(f)** Estimated sizes of CD34⁺ LSK subpopulations enriched for hematopoietic progenitors with multi-lineage developmental potential (MPPs). MPP1 – short-term HSCs, MPP2 – myeloid-oriented, MPP3 – lineage-balanced MPP. **(g)** Estimated size of lymphoid-biased MPP4 population. **(h, i)** Quantification of lineage-restricted (CD127/IL7R α ⁻) progenitor subpopulations **(h)** and early IL7R α ⁺ lymphoid progenitors **(i)** in LSK bone marrow cells using myeloid marker CD16/32 and CD34. MEP = megakaryocytic-erythroid progenitor, CMP = common myeloid progenitor, GMP = granulocyte-monocyte progenitor. **(j, k)** Flow cytometry analysis of erythroid development in 1-year-old animals of indicated genotypes. Estimated size of CD45⁺ and ERY (Ter119⁺) populations in bone marrow **(j)** and spleen **(k)**. **(l, m)** Estimated size of stage 0 to 5 (S0-S5) populations of erythroid development in 1-year-old animals distinguished using anti-Ter119 and anti-CD117/c-kit antibodies in bone marrow **(l)** and spleen **(m)**. Statistics: t-test relative to controls (p<0.05=*, p<0.01=**, p<0.001=***, p<0.0001=****, no asterisks = non-significant), the error bars represent standard deviation. **(n)** Mass spectrometry (MS) analysis of SMARCA5 complexes in represented organs. Tissues from 2-month-old wild-type (negative control) and transgenic animals were lysed and tagged SMARCA5 was immunoprecipitated using FLAG-M2 agarose beads. **(o)** Table showing the intensity of MS data of SMARCA5 co-purified proteins from the depicted tissues. Only proteins with significantly higher intensities compared to control animals are shown in the table.

Fig. 1c



Suppl. Fig. 1c

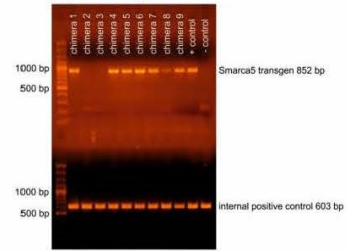
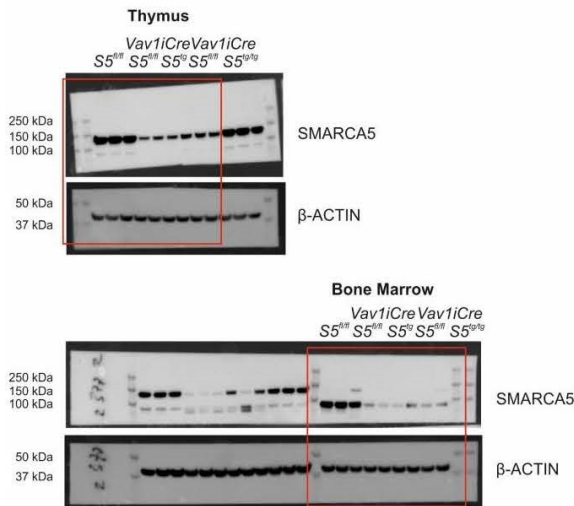
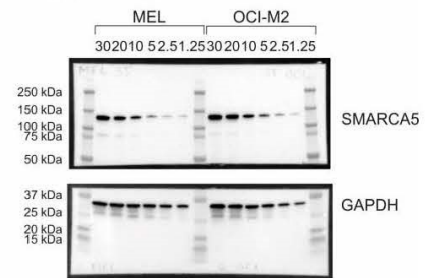


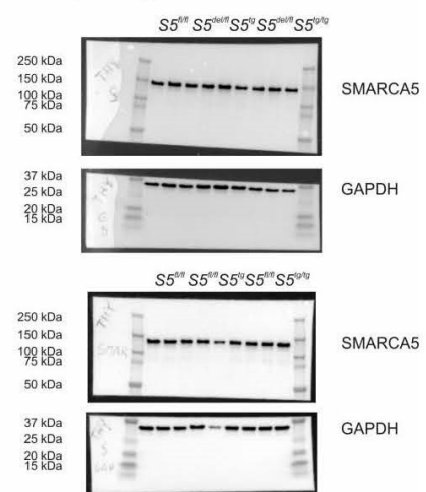
Fig. 2b



Suppl. Fig. 1d



Suppl. Fig. 2b



Supplementary Figure 6. Uncropped blots and gels.

4.2 (2. publikace) ISWI ATPase Smarca5 Regulates Differentiation of Thymocytes Undergoing β -Selection.

Is your inflammatory disease model falling short?

See how you can model complex human immune response and drug efficacy.



WATCH NOW

The Journal of Immunology

RESEARCH ARTICLE | JUNE 15 2019

ISWI ATPase Smarca5 Regulates Differentiation of Thymocytes Undergoing β -Selection **FREE**

Tomas Zikmund; ... et. al

J Immunol (2019) 202 (12): 3434–3446.

<https://doi.org/10.4049/jimmunol.1801684>

Related Content

Antigen specificity of tuberculosis-specific CD4⁺ T cells in IKEPLUS immunized mice (P3122)

J Immunol (May,2013)

Gads^{-/-} Mice Reveal Functionally Distinct Subsets of TCR β ⁺ CD4⁻ CD8⁻ Double-Negative Thymocytes

J Immunol (July,2007)

ISWI ATPase Smarca5 Regulates Differentiation of Thymocytes Undergoing β -Selection

Tomas Zikmund,* Juraj Kokavec,* Tereza Turkova,* Filipp Savvulidi,[†] Helena Paszekova,* Sona Vodenkova,^{‡,§} Radislav Sedlacek,[¶] Arthur I. Skoultchi,^{||} and Tomas Stopka*

Development of lymphoid progenitors requires a coordinated regulation of gene expression, DNA replication, and gene rearrangement. Chromatin-remodeling activities directed by SWI/SNF2 superfamily complexes play important roles in these processes. In this study, we used a conditional knockout mouse model to investigate the role of Smarca5, a member of the ISWI subfamily of such complexes, in early lymphocyte development. *Smarca5* deficiency results in a developmental block at the DN3 stage of $\alpha\beta$ thymocytes and pro-B stage of early B cells at which the rearrangement of Ag receptor loci occurs. It also disturbs the development of committed (CD73⁺) $\gamma\delta$ thymocytes. The $\alpha\beta$ thymocyte block is accompanied by massive apoptotic depletion of β -selected double-negative DN3 cells and premitotic arrest of CD4/CD8 double-positive cells. Although *Smarca5*-deficient $\alpha\beta$ T cell precursors that survived apoptosis were able to undergo a successful TCR β rearrangement, they exhibited a highly abnormal mRNA profile, including the persistent expression of CD44 and CD25 markers characteristic of immature cells. We also observed that the p53 pathway became activated in these cells and that a deficiency of p53 partially rescued the defect in thymus cellularity (in contrast to early B cells) of *Smarca5*-deficient mice. However, the activation of p53 was not primarily responsible for the thymocyte developmental defects observed in the *Smarca5* mutants. Our results indicate that Smarca5 plays a key role in the development of thymocytes undergoing β -selection, $\gamma\delta$ thymocytes, and also B cell progenitors by regulating the transcription of early differentiation programs. *The Journal of Immunology*, 2019, 202: 3434–3446.

The production of mature T and B cells is a multistep process of differentiation from a multipotent progenitor that requires a coordinated regulation of gene expression,

*BIOCEV, First Faculty of Medicine, Charles University, Vestec 25250, Czech Republic; [†]Institute of Pathological Physiology, First Faculty of Medicine, Charles University, Prague 12853, Czech Republic; [‡]Institute of Experimental Medicine, Czech Academy of Sciences, Prague 14220, Czech Republic; [§]Third Faculty of Medicine, Charles University, Prague 10000, Czech Republic; [¶]Czech Centre for Phenogenomics, Institute of Molecular Genetics, Czech Academy of Sciences, Vestec 25250, Czech Republic; and ^{||}Department of Cell Biology, Albert Einstein College of Medicine, Bronx 10461, NY

ORCID: 0000-0003-2452-3749 (T.Z.); 0000-0003-0267-4570 (J.K.); 0000-0002-5329-1812 (T.T.); 0000-0002-6479-6592 (H.P.); 0000-0003-0315-5668 (S.V.); 0000-0001-7236-6894 (T.S.).

Received for publication January 2, 2019. Accepted for publication April 15, 2019.

The Stopka Laboratory at the BIOCEV was supported by Charles University Grant Agency GAUK 534212, Czech Science Foundation GACR 18-01687S and 19-03586S, Czech Health Research Council AZV 16-27790A, Charles University UNCE/MED/016, KONTAKT LH15170, Czech Ministry of Education, Youth and Sport (MEYS) LM2015040 and NPU II LQ1604, Operational Programmes of MEYS OP RDI CZ.1.05/2.1.00/19.0395 and CZ.1.05/1.1.00/02.0109, and institutional programs funded by Charles University PROGRES Q26 and SVV 260374/2017. S.V. support: GACR 19-10543S and AZV 17-30920A. A.I.S. support: National Institutes of Health GM116143 and DK096266.

The sequences presented in this article have been submitted to ArrayExpress (<https://www.ebi.ac.uk/arrayexpress/experiments/E-MTAB-7758/>) under accession number E-MTAB-7758.

Address correspondence and reprint requests to Dr. Tomas Stopka, BIOCEV, First Faculty of Medicine of the Charles University, Prumyslova 595, Vestec 25250, Czech Republic. E-mail address: tstopka@ifi.cuni.cz

The online version of this article contains supplemental material.

Abbreviations used in this article: BM, bone marrow; DN, double-negative; DP, double-positive; DSB, double-strand break; FDR, false discovery rate; GSEA, gene set enrichment analysis; iCre, codon-improved Cre recombinase; log₂FC, log₂ fold change value; LSK, Lin[−]Scal⁺Kit⁺; RNA-seq, RNA sequencing; Smarca5, SWI/SNF-related matrix-associated actin-dependent regulator of chromatin subfamily A member 5; SP, single-positive; wt, wild-type.

Copyright © 2019 by The American Association of Immunologists, Inc. 0022-1767/19/37.50

www.jimmunol.org/cgi/doi/10.4049/jimmunol.1801684

replication, DNA rearrangement, and repair. Progenitors of T cells migrate from the bone marrow (BM) into the thymus where they respond to a new environment by initiating a transcriptional program of T cell specification while proliferating extensively (1). During this process, CD4[−]CD8[−] double-negative (DN) CD44⁺ positive early T lineage precursors (immature DN1) permanently silence the group of progenitor-related regulatory genes leading to the gradual upregulation of CD25 and the downregulation of c-Kit surface markers and resulting in the commitment completion at the end of the DN2 stage (CD44⁺CD25⁺c-Kit^{int}) (2). Thymocytes at the subsequent DN3 stage (CD44[−]CD25⁺) cease from cycling and, importantly, undergo a random rearrangement of gene segments at the *TCRb* locus and commence the expression of components related to the β -selection program. Upon the successful rearrangement that yields functional pre-TCR complexes, thymocytes proliferate rapidly, become rescued from the p53-regulated cell cycle arrest and apoptosis (3), and then are allowed to progress into the DN4 stage (CD44[−]CD25[−]). This transient population hence upregulates the expression of CD4 and CD8 to become double-positive (DP) cells and initiates *TCRa* locus rearrangement. DP cells with productive TCR $\alpha\beta$ are positively and negatively selected so that only those with “proven” TCR can undergo differentiation into CD4 or CD8 single-positive (SP) cells (4).

Eukaryotic cells evolved numerous epigenetic regulatory mechanisms of gene expression, DNA replication, and repair to accomplish the T cell development. During early T cell differentiation, NURD and SWI/SNF chromatin-remodeling complexes were shown to play important roles in both activating as well as silencing the gene transcription (5, 6). The SWI/SNF-related matrix-associated actin-dependent regulator of chromatin subfamily A member 5 (*Smarca5*) represents a widely expressed and conserved chromatin-remodeling factor required for the early development in mouse and lower organisms (7). *Smarca5* is an

ATPase from the ISWI subfamily that functions as a molecular motor for nuclear complexes that assemble and slide basic chromatin subunits, nucleosomes. Smarca5-containing complexes have diverse nuclear functions: guiding the transcription of ribosomal (in NoRC and B-WICH complexes) and some coding genes (within the ACF or RSF complexes), participating in regularly spacing the nucleosomal array before and after DNA replication, facilitating the recruitment of DNA repair machinery (CHRAC and WICH complexes), and finally, orchestrating higher-order chromatin structure formation of centromeres and chromosomes (RSF) (8). Although several members of SWI/SNF and CHD family have had their roles established in T cell development through studies involving gene inactivation mouse models, such a role for the ISWI subfamily has not been determined yet.

Currently, there is only a limited knowledge of how Smarca5, which is highly expressed in lymphocytes (9), participates in lymphopoiesis. We previously showed that deletion of the *Smarca5* gene resulted not only in the depletion of myeloerythroid precursors but also affected the earliest development of lymphoid progenitors in the mouse fetal liver (10). Additionally, Smarca5 was implicated in the V(D)J cleavage of the polynucleosomal substrate in a cell-free system (11). Another report implicated that Smarca5 in the ACF complex represses the IL2- α gene (CD25) via chromatin organizer Satb1 (12). Lastly, Smarca5 regulates the expression of key ILs (IL-2, IL-3, and IL-5) in murine EL4 T cell lymphoma (13). Although the role of Smarca5 in lymphopoiesis was previously suggested, the knockout models of Smarca5-interacting partners revealed no alterations in lymphoid development, including the deletion of *Acf1/Baz1a* (ACF and CHRAC complexes) (14, 15) or *Tip5/Baz2a* (NoRC) (15) genes in mice. Interestingly, it has been shown in vitro that Smarca5 can also remodel nucleosomes alone without being part of the complexes (16). As several of Smarca5-interacting partners are dispensable, studying the requirement of a catalytic subunit of the ISWI complexes by targeting experimentally Smarca5 during lymphoid development may represent a successful strategy to reveal its function in lymphopoiesis.

We, in this study, focused on deciphering the role of Smarca5 in thymocyte development and studied the molecular consequences of conditional Smarca5 deficiency in mice. Our work suggests that Smarca5 controls early T cell development by guiding early differentiation-coupled transcriptional programs at the DN3 stage and its deficiency results in thymocyte proliferation and survival defects through the activation of the DNA damage response.

Materials and Methods

Mice

Smarca5^{lox} conditional knockout mice contain loxP1 sites flanking the exon 5 of the *Smarca5* gene (17), deletion of which produced a frameshift mutation (*Smarca5^{del}*) that disrupts the expression of the Smarca5 protein. The murine strain expressing a codon-improved Cre recombinase (iCre) under hCD2 promoter [B6.Cg-Tg(CD2-cre)4Kio/J] was purchased from The Jackson Laboratory. The OT-II strain [B6.Cg-Tg(TcrTcrb)425Cbn/J] was kindly provided by Dr. T. Brdička (Institute of Molecular Genetics, Czech Academy of Sciences). *Rag1* knockout (B6.129S7-Rag1tm1Mom/J) strain was kindly provided by Dr. T. Brabec (Institute of Molecular Genetics, Czech Academy of Sciences). *Trp53* knockout strain (B6.129S2-Trp53tm1Tyj/J) was kindly provided by Dr. W. Edelmann (Albert Einstein College of Medicine).

Flow cytometry

A single cell suspension from thymi and spleens of 4–6-wk-old mice was obtained using a Dounce homogenizer. Cells were first preincubated for 10 min on ice with Fc receptor-blocking anti-CD16/32 (clone 93) Ab in PBS-1% bovine serum albumin solution and then stained for 20 min with specific

primary Abs. Biotinylated primary Abs were revealed with streptavidin-conjugated fluorescent dyes (SAV-PE/Cy7, SAV-APC, and SAV-APC/Cy7). Labeled cells were analyzed on BD FACSCanto II (BD Biosciences) or CytoFLEX (Beckman Coulter) flow cytometers, and data analysis was performed using FlowJo software. The clones of mAbs were as follows: anti-CCR6 (29-2L17), anti-CD3 ϵ (145-2C11), anti-CD4 (GK1.5), anti-CD5 (53-7.3), anti-CD8 (53-6.7), anti-CD11c (N418), anti-CD24 (M1/69), anti-CD25 (PC61), anti-CD27 (LG.3A10), anti-CD28 (E18), anti-CD44 (IM7), anti-CD45.1 (A20), anti-CD45.2 (104), anti-CD71 (RI7217), anti-CD73 (TY/11.8), anti-CD117 (c-Kit, 2B8), anti-B220 (RA3-6B2), anti-CD11b (Mac1, M1/70), anti- γ 8 T cell (GL3), hamster IgG-PE/Cy7 (HTK888), anti-Ly6G/Ly6C (GR1, RB6-8C5), anti-Nk1.1 (PK136), anti-TCR β (H57-597), anti-TCR β (V α 2) (B20.1), and Ter119 (all from BioLegend). Splenocytes were analyzed as previously described (18).

BM transplantation

For BM reconstitution experiments, 1×10^7 BM cells from adult (8-wk-old) control C57BL/6J Ly5.1 (CD45.1) mice and *S5^{fl/fl}*hCD2iCre Ly5.2 (CD45.2) donors were reciprocally transplanted into lethally irradiated (7.5Gy) adult (8 wk) *S5^{fl/fl}*hCD2iCre Ly5.2 and C57BL/6J Ly5.1 control recipients, respectively. After 1 mo posttransplantation, thymi were tested for the presence of donor-derived cells using flow cytometric analysis. The Ab panel included CD45.1, CD45.2, CD44, CD25, CD4, lineage mixture (CD8, B220, Mac-1, Gr-1, Nk1.1, CD11c, and Ter119) and CD45.1, CD45.2, CD4, CD5, CD8, and lineage mixture (B220, Mac-1, Gr-1, Nk1.1, CD11c, and Ter119) for thymus.

BrdU labeling

Smarca5 conditional knockout mice and their age- and gender-matched respective controls were i.p. injected with 1 mg of BrdU in 100 μ l PBS. After 3 h, the thymocytes were isolated and Ab-stained for flow cytometry analysis or cell sorting. BrdU Ag recovery and its detection by fluorescently labeled Ab were performed using the APC BrdU Flow Kit (BD Biosciences).

OP9/N-DLL1 stromal cell cultures

FACS-sorted DN3 thymocytes (small CD4⁺CD8⁺CD25⁺) and Lin⁻Sca1⁺Kit⁺ (L.SK) BM cells were cocultured with OP9 stromal cells expressing the Delta-like ligand (OP9/N-DLL1) in the presence of 1 ng/ml mIL-7 (407-ML-005) and 5 ng/ml hrFLT3 ligand (308-FK-005; PeproTech) as previously described (19). In BM cell cocultures, the concentration of IL-7 was lowered to 0.1 ng/ml from day 12 to allow differentiation. For CFSE labeling, 3×10^4 DN3 cells were stained with 2.5 μ M CFSE following the manufacturer's guidelines (CellTrace CFSE Cell Proliferation Kit; Invitrogen) and plated onto OP9 stromal cultures. Their proliferation and survival were analyzed by flow cytometry at 2, 4, 6, and 8 d of cocultures. OP9/N-DLL1 cells were kindly provided by Hiroshi Kawamoto (Kyoto University).

Histopathology and the detection of apoptotic cells in thymic sections

Thymi and spleens were fixed in 4% buffered formaldehyde for 48 h, transferred in 70% ethanol, and paraffin embedded. Sections were obtained at 3 μ m thickness and stained in H&E and Giemsa. Cleaved Caspase-3 was detected by immunohistochemistry using a 1:1000 dilution of Ab (ab52293; Abcam) and visualized on a Zeiss Axio Scan.Z1. Casp3-positive cells were quantified using the Zen Blue Edition software (ZEISS).

RNA sequencing analysis

CD4⁺CD8⁺(B220⁻Gr-1⁻Nk1.1⁻CD11c⁻CD11b⁻) thymocytes were sorted by FACS, and the total RNA was isolated using TRIzol Reagent (Invitrogen). DP cells pooled from 25 to 37 *S5^{fl/fl}*hCD2iCre thymi (each pool of 3×10^6 DP cells), 6 *S5^{fl/fl}*hCD2iCre *Trp53^{-/-}* thymi ($\sim 2.5 \times 10^6$ DP cells/pool), and single nonpooled control thymi provided sufficient amounts of RNA for RNA sequencing analysis. Strand-specific cDNA libraries were prepared from a minimum of 1.7 μ g of each DNase-treated (AM1906; Ambion DNA-Free Kit) RNA sample using the TruSeq Stranded mRNA LT Kit (Illumina). The RNA libraries were sequenced on an Illumina HiSeq 2500 instrument in Rapid Run mode with paired-end 100-bp sequencing length. Reads were mapped and aligned to mouse reference genome assembly GRCm38.p6, and transcripts were annotated and counted with Ensembl Release 94 (October 2018) using a HISAT2 aligner (20). The two RNA-seq technical replicates for each sample were combined. Differential expression analysis of RNA-seq

data were performed in R Studio (21) using package DESeq2, which uses a median of ratios normalization method that accounts for sequencing depth as well as RNA composition (22). Volcano plots were drawn using the ggplot2 (23) package in R suite. Expression levels (transcripts per kb million) for Ensembl 94 genes were calculated in R using gene lengths retrieved by EDASeq package (24) and in-house scripts. The shrinkage of \log_2 fold change values (\log_2FC) was estimated using DESeq2 lfcShrink function using the adaptive t prior shrinkage estimator "apeglm" (25). The RNA-seq data are publicly available at the ArrayExpress database under accession number E-MTAB-7758 (<https://www.ebi.ac.uk/arrayexpress/experiments/E-MTAB-7758/>).

Quantitative PCR

Quantitative measurements of *TCR β* rearrangement were done on genomic DNA (DNeasy; QIAGEN) isolated from the FACS-sorted DN subpopulations. Quantitative PCR was run on 7900HT using Power SYBR Green PCR Master Mix (no. 4367659, Applied Biosystems) with the following primers: *D β 1* fwd: 5'-GTGGTTTCTCCAGCCCTCAAG-3', *D β 1* rev: 5'-GGCTTCCCATAGAATTGAATCACC-3' and *D β 2* fwd: 5'-CAGGC-TCTGGGTAGGCAC-3', *D β 2* rev: 5'-CCTCTCCAGTTGAATCATT-GTGG-3'. Primers for the control region were as follows: *Apob* ex29 fwd: 5'-CTGCCGTGGCCAAAATAAT-3' and *Apob* ex29 rev: 5'-AATCCTGCAGATTGGAGTGG-3'. Cycle threshold (c_t) values of *D β 1* and *D β 2* regions were normalized to c_t from *Apob* control region.

Immunoblotting

Freshly isolated thymocytes were collected by centrifugation and resuspended in PBS with inhibitors of phosphatases (PhosSTOP; Roche) and proteases (cComplete ULTRA; Roche). The cell suspension was then diluted 1:1 by adding a solution of 50 mM Tris-Cl (pH = 8) and 2% NaDodSO₄ (SDS) and incubated for 30 min at 97°C. Protein concentration was determined by bicinchoninic acid assay (no. 23228; Pierce Biotechnology). Proteins were then resolved on SDS gradient 4–15% polyacrylamide gels (Mini-PROTEAN TGX Stain-Free Gels; Bio-Rad Laboratories) and wet blotted (1 h at 100 V) onto PVDF membranes (no. 162-0177; Bio-Rad Laboratories). PVDF membranes were blocked for 1 h in 5% nonfat milk in TBS/0.1% Tween-20 (TBST) and incubated overnight at 4°C in 3% BSA/TBST 0.1% sodium azide with the following Abs: Smarca5 (1:1000, no. A301-017A-1; Bethyl Laboratories) and histone H3 (1:1000, no. ab791; Abcam). Membranes were 3 × 5 min washed in TBST buffer and incubated with peroxidase-conjugated F(ab')₂ Ab fragment, either donkey anti-rabbit or donkey anti-mouse (1:10,000; Jackson ImmunoResearch), in 5% nonfat milk in TBST for 1 h. Membranes were 3 × 5 min washed in TBST, and the protein signal was visualized by Pierce SuperSignal West Femto Maximum Sensitivity Substrate (Thermo Fisher Scientific) and detected with the ChemiDoc Imaging System (Bio-Rad Laboratories).

Results

Smarca5 deficiency disrupts thymocyte development

To delineate specific roles of Smarca5 *in vivo*, we previously created the *Smarca5^{fl}* allele containing two loxP1 sites surrounding exon5, the deletion of which results in removing the portion of evolutionarily conserved helicase domain and introducing a frame-shift mutation (10, 17) (Fig. 1A). To execute the T cell-specific deletion of the *Smarca5* gene, we crossed *Smarca5^{fl/fl}* mice with hCD2iCre transgenic mice, in which the hCD2 promoter and locus control region drive the expression of the iCre recombinase (26). Use of the hCD2-iCre transgene to study thymocyte development was chosen as this model alone caused no defect in thymus development (27) as well as the cellularity and subset composition of the major lymphoid organs (including thymus, spleen, and lymph nodes) did not differ between hCD2-iCre-expressing mice and wild-type (wt) (28). We initially evaluated the onset of the *Smarca5^{fl}* gene deletion by PCR. Genomic DNA was prepared from FACS-sorted CD4/CD8 DN thymocyte subpopulations of *Smarca5^{+/fl}*hCD2iCre mice and three primer sets amplifying wt, *Smarca5*-floxed (*S^{fl}*), and recombined-floxed (*S^{del}*) allele were used. Consistent with previous reports that used the hCD2iCre transgene (26), we observed Cre-mediated recombination of loxP1 sites as early as the DN1 stage in which the recombined *S^{del}* allele was detectable

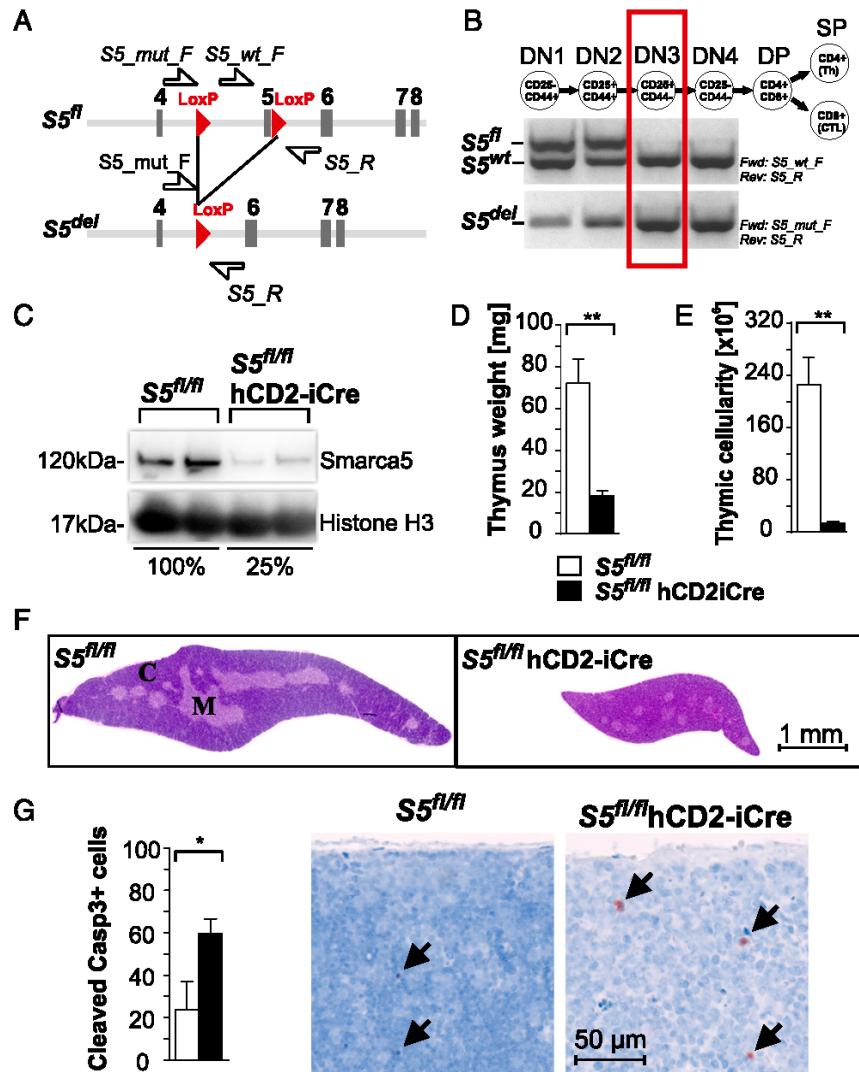
(Fig. 1B). However, the deletion of the *S^{fl}* allele at DN1 was only partial, whereas its complete deletion was observed at the DN3 stage. Western blot analysis of the whole thymic cellular extracts from *S^{fl/fl}*hCD2iCre mice confirmed a high efficiency of recombination as we observed a marked reduction of Smarca5 protein levels (Fig. 1C).

*S^{fl/fl}*hCD2iCre pups were born healthy and at normal Mendelian ratios. Following the third month of age, the *Smarca5* mutants, however, displayed rectal prolapses, suggesting the disturbance of immune functions. Gross dissection of the *Smarca5* mutant animals revealed severe thymic defects. Thymi from the mutant mice were dramatically reduced in size and weight (Fig. 1D), which was reflected by a 17-fold reduction in cellularity (Fig. 1E). Histological evaluation revealed an alteration of thymic corticomedullary architecture (Fig. 1F) and a higher number of cleaved Caspase-3-positive apoptotic death events in the cortex (Fig. 1G). The quantification of multiple cortical sections from different animals showed there was a 3-fold increase of apoptotic cells in the cortex of *S^{fl/fl}*hCD2iCre thymi. These observations indicated a developmental defect in thymocytes, accompanied by an increased cell death within the thymi of *S^{fl/fl}*hCD2iCre animals.

To gain insight into the developmental defects of thymocytes, we used flow cytometry of thymic cell suspensions of 4–6-wk-old *S^{fl/fl}*hCD2iCre mice. CD4/CD8 immunostaining revealed a marked reduction of DP and CD4-SP cell populations with a corresponding relative increase in DN thymocytes in the mutant thymi (Fig. 2A). In absolute counts, the DP cells were depleted by 60-fold, CD4-SP 90-fold, and CD8-SP cells 12-fold, whereas the DN thymocyte population was similar to controls (Fig. 2B). Because the *Smarca5* allele deletion is completed by the DN3 stage (Fig. 1B), we analyzed each subpopulation of DN thymocytes to more precisely determine a stage in which the block of development occurs. CD44/CD25 Ag expression profiles of lineage-negative DN thymocytes revealed a relative increase in DN3 cells to the detriment of DN4 thymocytes (Fig. 2C). Translated into absolute counts, it was an almost complete absence of DN4 thymocytes in mutants, whereas the DN3 population was present in comparable numbers to controls (Fig. 2D).

We also examined the impact of Smarca5 deficiency on $\gamma\delta$ T cell development. Using flow cytometry, we observed that Smarca5-deficient animals contain twice as many TCR δ^+ thymocytes (CD4⁻CD8⁻TCR δ^+) compared with controls (Fig. 2E, 2F). However, out of these TCR δ^+ thymocytes, only 18.4% (compared with 42% in controls) were able to adopt the $\gamma\delta$ fate (Fig. 2E) as indicated by the CD73 surface marker that discriminates TCR δ^+ thymocytes committed to the $\gamma\delta$ lineage (29). Additionally, the expression of surface CD24, which is normally enriched on immature $\gamma\delta$ thymocytes and downregulated upon maturation into effector cells (30), was reduced in Smarca5 mutants (Fig. 2E). In contrast to controls, the lower expression of CD24 surface marker observed in the mutants compromised a clear separation of the CD73⁺ population into immature and mature subsets. The mature $\gamma\delta$ thymocytes (CD24^{low}CD73⁺) were further distinguished along the expression of the mutually exclusive CD27 and CCR6 surface markers into IFN- γ (CD27⁺)-producing or IL-17a(CCR6⁺)-producing $\gamma\delta$ subsets (31, 32). The IFN- γ - and IL-17a-producing $\gamma\delta$ subsets display a subtle imbalance in favor of an IL-17a-producing subset in the Smarca5 mutants (Fig. 2E). We conclude that the commitment to $\gamma\delta$ lineage and CD24 expression by TCR δ^+ thymocytes and the development of mature $\gamma\delta$ subsets are impaired in the *S^{fl/fl}*hCD2iCre mice. Although Smarca5 plays important roles in thymocyte development during the DN3 to DN4

FIGURE 1. *Smarca5* is required for thymocyte development and survival. **(A)** Scheme of Cre-mediated deletion in the *Smarca5* gene. Indicated are exons 4–8 (boxes), positions of loxP1 sites (red triangles), and positions of genotyping primers (white arrows). **(B)** PCR detection of the floxed ($S5^{fl}$), wt ($S5^{wt}$), and deleted ($S5^{del}$) *Smarca5* allele in the $S5^{fl/wt}$ hCD2iCre thymus. **(C)** Immunoblot showing *Smarca5* protein expression in thymi of control (one animal per sample) versus $S5^{fl/wt}$ hCD2iCre (a pool of four animals per sample) mice. Histone H3 served as a loading control. **(D and E)** Weight and cellularity of thymi of indicated genotypes. Bars depict the mean \pm SD from four controls and four $S5^{fl/wt}$ hCD2iCre mice. **(F)** Histology (H&E staining) of thymi from 6-wk-old mice of indicated genotypes showing medulla (M) and cortex (C). **(G)** Immunohistochemistry of cleaved Caspase-3 in Mayer hematoxylin-stained thymic sections. y-axis: mean number/square millimeter \pm SD of cleaved Casp3-positive cells in the cortex ($n = 3$ /genotype). Significance in two-tailed t test. * $p < 0.05$, ** $p < 0.01$.



transition of $\alpha\beta$ subsets, it also guides the development of the $\gamma\delta$ compartment.

Developmental blockade in Smarca5-deficient thymocytes is cell autonomous

As hCD2-iCre transgene initiates deletion also in other murine hematopoietic cell subtypes (18), we tested whether the DN3 to DN4 transition defect is cell autonomous to thymocytes or a result of the impaired thymic microenvironment in which they develop. Using syngeneic transplantation, we assessed the ability of control BM (marked by CD45.1 isoform) to repopulate thymocytes in lethally irradiated $S5^{fl/wt}$ hCD2iCre mice (marked by CD45.2 isoform) and vice versa. At day 35 after transplantation, we observed that engrafted thymocytes from controls (CD45.1) developed normally to produce CD4/CD8 double and SP cells in the thymic microenvironment of $S5^{fl/wt}$ hCD2iCre (CD45.2) animals (Fig. 3A, 3B). In turn, the engrafted donor $S5^{fl/wt}$ hCD2iCre BM-derived thymocytes (CD45.2) recapitulated the developmental defect at DN3 to DN4 transition within the control acceptor animals (CD45.1). These results suggested that the DN3 to DN4 transition became defective independently of the thymic

stromal components (of $S5^{fl/wt}$ hCD2iCre mice) but rather intrinsically to the thymocytes lacking *Smarca5*. To further settle the point of whether the developmental defect of thymocytes observed in vivo is cell autonomous, we used ex vivo cocultures with a BM-derived stromal OP9/N-DLL1 cell line (19). Sorted pre-selection early DN3e cells (small CD4⁻CD8⁻CD25⁺ thymocytes) were added on the OP9/N-DLL1 cells to evaluate the formation of DN4 and DP thymocytes in a time course of 8 d (Fig. 3C). Although control DN3e cells apparently proliferated and progressed into more mature developmental stages under ex vivo conditions, the majority of *Smarca5*-depleted cells were held at the DN3 stage till day 8, and their absolute numbers remained similar to the starting cocultures (Fig. 3C, 3D). Thus, the outcome of the ex vivo experiment was highly reminiscent of the phenotype of $S5^{fl/wt}$ hCD2iCre mice. We used yet another approach to test whether the defect of DN3 to DN4 transition could have emerged from a secondary effect, mainly because the DN3e thymocytes in the OP9/N-DLL1 cocultures were sorted from $S5^{fl/wt}$ hCD2iCre mice with the potentially impaired thymic microenvironment. We isolated LSK BM hematopoietic progenitors from $S5^{fl/wt}$ hCD2iCre or control mice

Downloaded from http://jimmunol.org/immunol/article-pdf/201/12/3437/1444343/1501684.pdf by guest on 10 January 2024

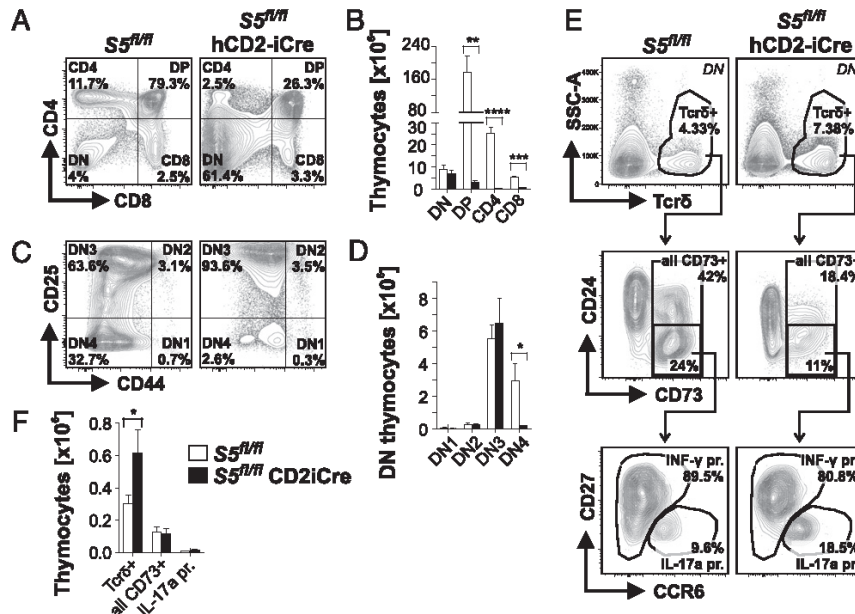


FIGURE 2. Smarca5 is required for thymocyte development at DN3 to DN4 stage. (A and B) Flow cytometry analysis of CD4 and CD8 DN, DP, and SP cell populations in thymi of 4–6-wk-old control ($n = 4$) and $S5^{fl/fl}$ hCD2iCre ($n = 4$) mice. Relative (A) and absolute (B) quantitation of thymic fraction sizes are shown. (C and D) Flow cytometry analysis of thymic DN ($CD4^{-}CD8^{-}$) cells of indicated genotypes using anti-CD25 and CD44 staining shown as relative (C) or absolute (D) values. Bar graphs depict the mean \pm SD from four controls and four $S5^{fl/fl}$ hCD2iCre mice [same animals as in (A) and (B)]. Lineage-positive (B220, Gr-1, CD11b, CD11c, and Nk1.1) cells were excluded from all measurements. (E and F) Flow cytometry analysis of $\gamma\delta$ T cells in DN ($CD4^{-}CD8^{-}$) thymic fraction. (E) Expression profiles of surface markers are shown as a contour plot, and the proportions of cells within each gate are given. (F) Bar graphs depict the mean \pm SD of absolute numbers. Data are representative of three control and three $S5^{fl/fl}$ hCD2iCre animals. Significance in two-tailed t test; * $p < 0.05$, ** $p < 0.01$, *** $p < 0.001$, **** $p < 0.0001$.

and kept them differentiating ex vivo on the OP9/N-DLL1 cells. Again, both the control as well as $S5^{fl/fl}$ hCD2iCre-derived hematopoietic progenitor cells developed normally into the DN2 stage (day 9); however, from the 16th day of culture, the $S5^{fl/fl}$ hCD2iCre thymocytes were progressively underrepresented, and by day 22, the DN3 to DN4 transition defect was revealed (Fig. 3E, 3F). Thus, the loss of Smarca5 in developing T cells caused a defect intrinsic to the thymocytes undergoing DN3 to DN4 transition, as evidenced by the cocultures using the OP9 cells, and was not a result of a secondary effect due to impaired thymic stromal components or thymic microenvironment.

Smarca5-deficient thymocytes undergo marked apoptosis and proliferation impairment

We next investigated whether reduced cell numbers in $S5^{fl/fl}$ hCD2iCre thymi and ex vivo OP9/N-DLL1 cocultures (Figs. 1E, 3D) may be attributed to premature cell death and/or impaired proliferation. As determined by flow cytometry, the ex vivo cultivation of purified DN3e thymocytes eventually resulted in a gradual increase of Annexin V positivity up to 71% by day 8 that did not exceed 15% in controls (Fig. 4A), indicating that the loss of Smarca5 induced apoptosis in developing T cell precursors. Similarly, we examined the effect of Smarca5 loss on the proliferation by labeling purified DN3e thymocytes with the intracellular fluorescent dye (CFSE) immediately before plating them on OP9/N-DLL1 cells. As seen in Fig. 4B, the analysis of the CFSE signal dilution indicated that the DN control thymocytes proliferated rapidly ex vivo. Conversely, those DN cells that did survive the ex vivo conditions exhibited a decreased division rate, confirming an impaired proliferation of $S5^{fl/fl}$ hCD2iCre thymocytes. We then used the BrdU incorporation assay to analyze the ability

of Smarca5-depleted cells to progress through the various stages of the cell cycle. After a 3 h pulse of BrdU in vivo, we observed that the percentage of proliferating BrdU⁺ DN3 cells (after exclusion of postreplicative BrdU⁺ events) was almost the same in mutants as in controls (14.8% versus 15.8%), and thus, the G1-to-S progression was not altered after the Smarca5 loss at DN3 stage (Fig. 4C). However, the portion of postreplicative cells at this stage, which is defined as strictly diploid BrdU⁺ events (33), was 2.5-fold decreased in mutant DN3 cells. These data indicate that Smarca5-depleted DN3 cells normally enter S phase and begin to replicate their DNA; however, they are limited in completing the cell cycle to re-emerge as G1 cells. Mutant DP cells were also impaired because a substantial fraction of the DP cells became arrested at the G2/M phase (Fig. 4D). Thus, the developmental defects observed upon the loss of Smarca5 are likely the consequence of cell death and impaired cell cycle progression at late S through G2/M phase. This is in contrast to defects in G1/S checkpoint mechanisms as previously observed in human cancer cell lines upon *SMARCA5* knockdown (34).

Smarca5 mutants undergo pre-TCR signaling and the TCR rearrangement

The accumulation of Smarca5-depleted DN3 cells resembles the phenotype of mice that have a defect in pre-TCR signaling or *TCRb* locus rearrangement (35). To test whether the induction of pre-TCR signaling was affected by a loss of Smarca5, we performed i.p. injections of anti-CD3e Ab into $S5^{fl/fl}$ hCD2iCre and into RAG1 (*Rag1*^{-/-})-deficient mice. Anti-CD3e Ab can mimic pre-TCR signaling in vivo and stimulates preselection DN3 thymocytes to proliferate and differentiate into the DN4 cells even in the *Rag1*^{-/-} mice lacking the TCR β -chain expression

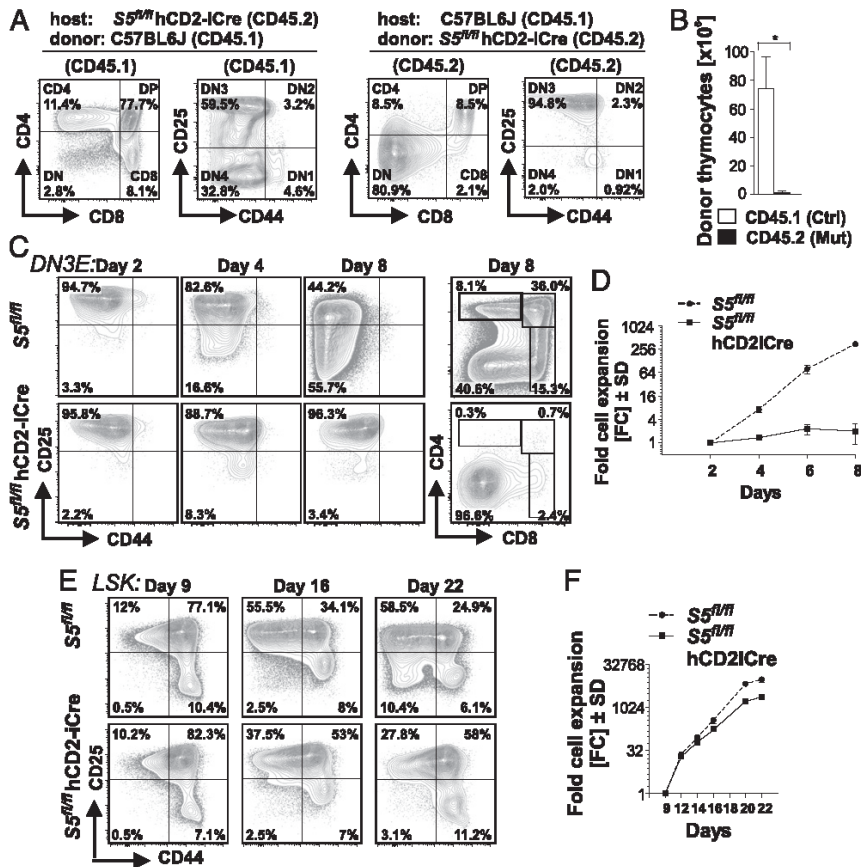
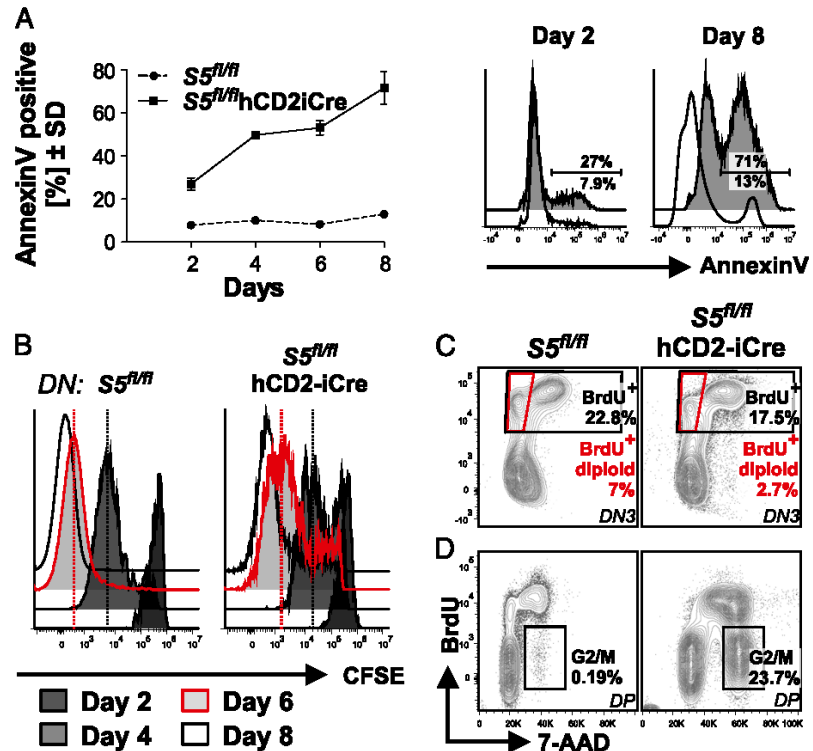


FIGURE 3. Developmental blockade in *Smarca5*-deficient thymocytes is cell autonomous. **(A)** Flow cytometric evaluation of donor-derived thymic populations regenerated after 1 mo following the transplantation of donor BM cells (BMT) into lethally irradiated (7.5Gy) hosts. Donor and host-derived thymocytes were distinguished by the surface expression of distinct variants of marker CD45. Control mice were CD45.1⁺ (Ly5.1), and *S5^{fl/fl}*hCD2iCre were CD45.2⁺ (Ly5.2). Data are representative of three BMT experiments. **(B)** Bar diagram shows mean number \pm SD of donor (CD45.1 = wt; CD45.2 = *S5^{fl/fl}*hCD2iCre) thymocytes 1 mo after BMT. Data are representative of three experiments. Significance in two-tailed *t* test; **p* < 0.05. **(C)** FACS-sorted DN3e (small CD4⁺CD8⁺CD25⁺) thymocytes from control and *S5^{fl/fl}*hCD2iCre mice were cocultured with OP9/N-DLL1 stromal cell line. Cells were harvested on days 2, 4, and 8, and expression profiles of CD44/CD25 or CD4/CD8 markers were analyzed by flow cytometry. Data are representative of two experiments. **(D)** Cumulative growth curve (represented as fold change) of all live CD45⁺ cells isolated from OP9/N-DLL1 cocultures on days 2, 4, 6, and 8. Cells were the same as in (C). **(E)** Flow cytometry of purified Lin⁻Sca1⁺c-Kit⁺ (LSK) BM progenitors after 9, 16, and 22 d of cultivation with OP9/N-DLL1 cells. Data are representative of four control and four *S5^{fl/fl}*hCD2iCre animals. **(F)** Cumulative growth curve (represented as fold change) of cells analyzed in (E).

(36). We observed that the anti-CD3e Ab stimulated the downregulation of surface CD25 molecules on *Rag1*^{-/-} as well as on *Smarca5*-deficient DN3 thymocytes (Fig. 5A), which suggested that pre-TCR signaling pathway was not disrupted after *Smarca5* loss. However, we noted that compared with highly proliferating *Rag1*^{-/-} DN cells, the *S5^{fl/fl}*hCD2iCre DN cells were almost completely absent at day 2 of treatment (Fig. 5B), further confirming the poor survival of differentiating and proliferating *Smarca5*-deficient DN cells. We next examined the expression of CD2 and CD5 on the DN and DP cells to assess their upregulation upon pre-TCR signaling (37, 38). Data from flow cytometry show that β -selected DN cells that survived *Smarca5* loss are still capable of upregulating the expression of CD2 and CD5 molecules (Supplemental Fig. 1A). Additionally, at the DP stage, the expression of these molecules was almost identical compared with controls (Supplemental Fig. 1B). In summary, the ability of *S5^{fl/fl}*hCD2iCre DN cells to upregulate CD2 and CD5 indicated that *Smarca5* deficiency in thymocytes does not perturb the pre-TCR signaling.

Next, we analyzed the intracellular expression and rearrangement of the TCR β -chain, another prerequisite for the DN3 to DN4 transition. Analysis of intracellular (i)TCR β expression together with membrane-bound CD28 has been shown as a tool to distinguish between preselection and β -selected DN3 cells that have successfully rearranged their *TCRb* locus (39). Using this approach, we observed that mutant DN3 thymocytes contain a significantly reduced fraction of iTCR β ⁺/CD28⁺ β -selected cells compared with controls (Fig. 5C). Conversely, the genomic DNA analysis of the *Smarca5* mutant DN thymocytes by quantitative PCR showed that the recombination rate of D β 1-J β 1 and D β 2-J β 2 gene segments was not altered (Supplemental Fig. 1C). As determined by RNA-seq analysis of DP cells (see further), the expression pattern of the constant (*Trbc*) and variable (*Trbv*) gene segments was similar to controls (Supplemental Fig. 1D), indicating that *Smarca5* deficiency did not abolish the *TCRb* locus rearrangement. To test whether the defective formation of the β -selected DN3 cells was a result of impaired TCR β rearrangement, we crossed *S5^{fl/fl}*hCD2iCre mice

FIGURE 4. Smarca5-deficient thymocytes induce apoptosis and block proliferation. **(A)** Purified preselection DN3e thymocytes (from two animals of each genotype) were cocultured with OP9/N-DLL1 cells, and the mean fraction \pm SD of CD45⁺ cells that became Annexin V positive was assessed by flow cytometry following 2, 4, 6, and 8 d. Histograms (blank = control mice; gray, filled histogram = $S^{fl/fl}$ hCD2iCre mice) show results of the experiments at day 2 and 8. **(B)** Histograms of control and $S^{fl/fl}$ hCD2iCre DN thymocytes stained with CFSE and cocultured with OP9/N-DLL1 cells. CFSE signal dilution was analyzed by flow cytometry on days 2, 4, 6, and 8. Data are representative of four control and three $S^{fl/fl}$ hCD2iCre animals. **(C)** Flow cytometry analysis of control and $S^{fl/fl}$ hCD2iCre DN3 population cell cycle progression using BrdU/7-aminoactinomycin D (7AAD) double staining. Black rectangles depict all gated BrdU⁺ cells. Red trapezoid indicates BrdU⁺ diploid postreplicative cells that accomplished the mitosis. **(D)** Flow cytometry for BrdU and 7-AAD in DP cells. Rectangles show the proportion of G2/M fraction. Data are representative of at least three individual animals of each genotype.



with *TCRb/a* transgenic mice (OT-II). Expression of the fully rearranged *TCRb/a* construct in OT-II background is able to suppress V(D)J recombination at endogenous loci and also “rescue” thymocyte development in mice lacking essential factors for the *TCRb/a* rearrangement (40, 41). Analysis of $S^{fl/fl}$ hCD2iCre OT-II animals revealed that expression of the transgenic *TCRb/a*-chains failed to rescue the *Smarca5* knockout phenotype. The absolute and relative counts of DN and DP subpopulations remained similar to the $S^{fl/fl}$ hCD2iCre mice (Fig. 5D–F). Particular exceptions were mature SP thymocytes, where the CD4 SP cells whose 3-fold increase to the detriment of the CD8 SP cells likely reflected the positive selection of thymocytes toward CD4 lineage that normally occurs in the OT-II strain (Fig. 5D). Thus, rather than the poor survival of β -selected DN cells than defects in pre-TCR signaling or *TCRb* locus rearrangement could best explain the phenotype of $S^{fl/fl}$ hCD2iCre mice.

As the surface expression of *TCRb* in DP thymocytes is essential for the production of SP subpopulations, we focused on stages beyond DN3 to decipher how *Smarca5* deficiency influenced the *TCRb* expression. Normally, the surface expression of *TCRb* is low or none in the DN3 stage, becomes induced at the DN4 stage, and further upregulated in SP thymocytes. We examined the level of surface *TCRb* expression on individual developmental stages of thymocytes and mature peripheral T cells in the spleen. We observed that surface *TCRb* expression was detectable in all developmental stages from a subfraction of DN3 (low expression) to mature SP populations (high expression) in both *Smarca5*-deficient as well as control thymocytes (Fig. 5G, Supplemental Fig. 1E). However, the fraction of cells with upregulated *TCRb* expression was reduced within each analyzed *Smarca5*-deficient thymic subpopulation compared with controls. Taken together, *Smarca5*-deficient thymocytes are able to express

and upregulate the surface *TCRb* expression during their development with an exception at the DN4 stage that almost lacks fraction of *TCRb*-positive cells.

Smarca5 deficiency altered the developmental program of post β -selection stages

It has been shown that during differentiation from DN to DP stage, the ACF complex containing *Smarca5* and *Acf1* represses, in cooperation with *Satb1*, the *Il2ra* (*CD25*) gene (12, 42). Indeed, flow cytometry indicated that DP cells of $S^{fl/fl}$ hCD2iCre mice inappropriately express both *CD44* and *CD25*, the markers of earlier developmental stages. Whereas the *CD25* molecule becomes partially downregulated, the *CD44* remains upregulated in DP cells, implicating the dysregulation of early expression programs (Fig. 6A). Our previous studies suggested that *Smarca5* participates in the regulation of gene expression programs associated with survival and differentiation of lens, cerebellum, and hematopoietic progenitor cells (10, 17, 43). To gain a global view on the gene expression programs dysregulated by *Smarca5* loss in β -selected thymocytes, we purified DP cells from $S^{fl/fl}$ hCD2iCre mice and used RNA-seq to compare the gene expression profiles with those from control DP cells. Of >21,500 expressed genes, a total of 3,318 transcripts were differentially expressed with false discovery rate (FDR) <0.05 and BaseMean value >10. From these, 1,503 mRNAs were (<2-fold) downregulated and 1,815 mRNAs were (>2-fold) upregulated. Gene ontology analysis of the differential expression using gene set enrichment analysis (GSEA) (44) showed the enrichment of mRNAs involved in expected categories such as apoptosis and the p53 pathway; however, most of them were either immunologic or lymphocyte associated (Fig. 6B). By dividing the differentially expressed genes into previously published mRNA clusters with similar behaviors during thymocyte differentiation (45), we observed

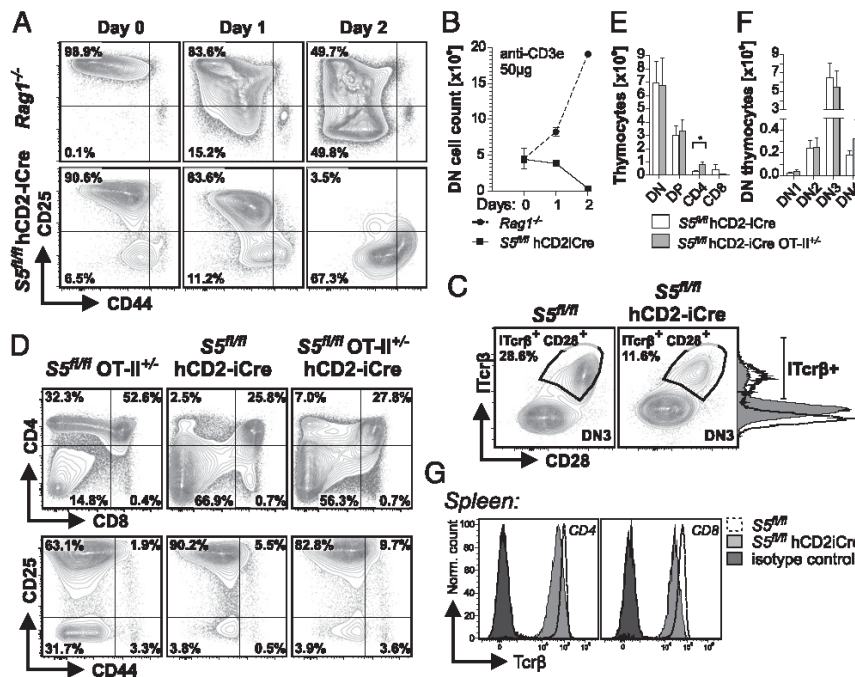


FIGURE 5. Smarca5 is not required for pre-TCR signaling and the TCR rearrangement. **(A)** Flow cytometry analysis of differentiation markers on thymocytes isolated 1 and 2 d after i.p. injection of *Rag1*^{-/-} and *S5*^{fl/fl};hCD2iCre mice with anti-CD3 (50 μg/mice). Contour plots showing DN (CD4⁺CD8⁻) cells. Data are representative of five (day 0), two (day 1), and three (day 2) *Rag1*^{-/-} or *S5*^{fl/fl};hCD2iCre animals. **(B)** Mean of absolute numbers ± SD of cells isolated from the thymus of mice used in (A). **(C)** Contour plots showing the expression of CD28 and intracellular TCRβ (iTCRβ) in DN3 thymocytes of indicated genotypes. Data are representative of three experiments. **(D)** Flow cytometry of DN, DP, and SP fractions using CD4 and CD8 markers in thymic suspensions from 4- to 6-wk-old *S5*^{fl/fl}; OT-II^{+/+} control, *S5*^{fl/fl};hCD2iCre, and *S5*^{fl/fl};hCD2iCre; OT-II^{+/+} mice. The relative population sizes are indicated. DN thymocytes were analyzed for CD25 and CD44 marker expressions. All B220-, Gr-1-, Mac-1-, CD11c-, and Nk1.1 lineage-positive cells were excluded from the analysis. Data are representative of more than three experiments. **(E and F)** Mean of absolute numbers ± SD of thymic subpopulations as in (D). Two-tailed *t* test; **p* < 0.05. **(G)** Surface expression of TCRβ protein on CD4 and CD8 T cells of control and *S5*^{fl/fl};hCD2iCre animals analyzed by flow cytometry. As an isotype control to H57-597 clone (anti-TCRβ), fluorescently labeled Armenian Hamster IgG was used (dark histograms). Data are representative of three experiments.

that the group of upregulated genes in the mutant DP cells overlapped to those mRNAs that peaked in expression at the early (DN1–DN2) or pre-β-selection DN3a stage (Fig. 6C). Such genes were, for example, receptors (*Il7r*, *Ctla4*, *Ptcr*, *Ly6a* and also *Il2ra*/Cd25 and *Cd44*), signaling molecules (*Dtx1*, *Hes1*, *Notch1*, *Lfng*, *Rab44*), and transcription factors (*Irf7*, *Tcf7l2*, *Spib*) (Fig. 6D). Accordingly, the group of downregulated genes (total 97) fall into the category of genes that are gradually expressed by β-selected cells during the transition into DP, such as transcription factors (*Klf7*, *Ets2*, *Irf3*, *Bcl6*), surface molecules (*Plxnd1*, *Slamf1*, *Cd81*), signaling (*Themis*), and others (*Tdrd5*, *Cacna1e*). To evaluate whether the mutant DP cells more closely resembled pre- or post-β-selected cells, we used a previously published transcriptome analysis of microarray data of wt C57BL/6J DN3a and DP stage cells (45) and created two sets of the 200 most upregulated and downregulated genes in wt DN3a compared with wt DP stage (Supplemental Fig. 2A). Hence, the GSEA analysis of mRNAs dysregulated upon Smarca5 deficiency revealed a strong enrichment of upregulated (normalized enrichment score = 2.37, FDR < 0.001) and downregulated (normalized enrichment score = -2.53, FDR < 0.001) mRNAs of the wt DN3a stage (Fig. 6E). This finding indicates that although Smarca5-deficient cells express post-β-selection surface markers (e.g., CD4, CD8, CD5, CD2) as normal DP cells, RNA-seq data reveals that they retain a transcriptional program of pre-β-selection DN cells. Thus, *Smarca5* ablation

greatly disorders the developmental programming of T cell progenitors.

Smarca5 is required for pro-B/pre-B transition of B cell progenitors

Additional analysis of *S5*^{fl/fl};hCD2iCre mice revealed also a dramatic reduction of the spleen cellularity (Fig. 7A). Besides the reduction of splenic T cells and NKT cells, which both developed in the thymus from the CD4⁺CD8⁺ DP precursors (46), we also observed a marked depletion of B lymphocytes, whereas the numbers of myeloid cells were not significantly altered (Fig. 7B, 7C). Indeed, immunohistochemistry of mutant spleens showed a prominent follicular hypoplasia affecting both T cell as well as B cell zones (Fig. 7D), suggesting also a defect in the B cell development of *S5*^{fl/fl};hCD2iCre mice. To investigate a stage at which the developmental defect occurred, the early B cell progenitor populations from BM were analyzed. Flow cytometry analysis revealed an almost complete loss of pre-B cells (B220⁺CD43⁻) in mutants, whereas the proportion of pro-B cells (B220⁺CD43⁺) was virtually unperturbed (Fig. 7E). Closer examination of the pro-B population showed a developmental arrest between early preselected pre-B-I cells (CD117⁺) and pre-B-II (CD25⁺) cells that underwent productive IgH gene loci rearrangement (47). Taken together, *Smarca5* deficiency affects development of early B220⁺CD43⁺ pro-B cells in BM, implicating the requirement of Smarca5 for both early T as well as B lymphocyte development.

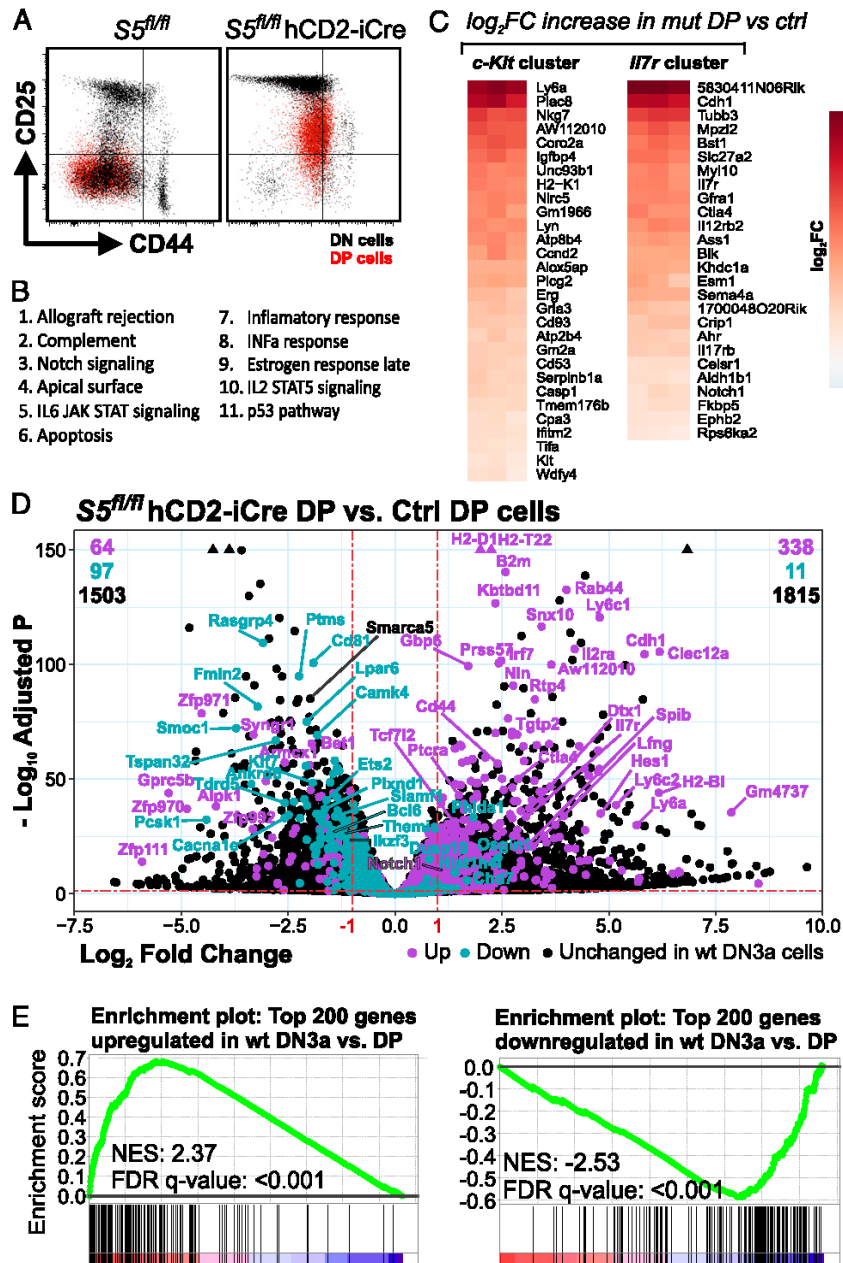
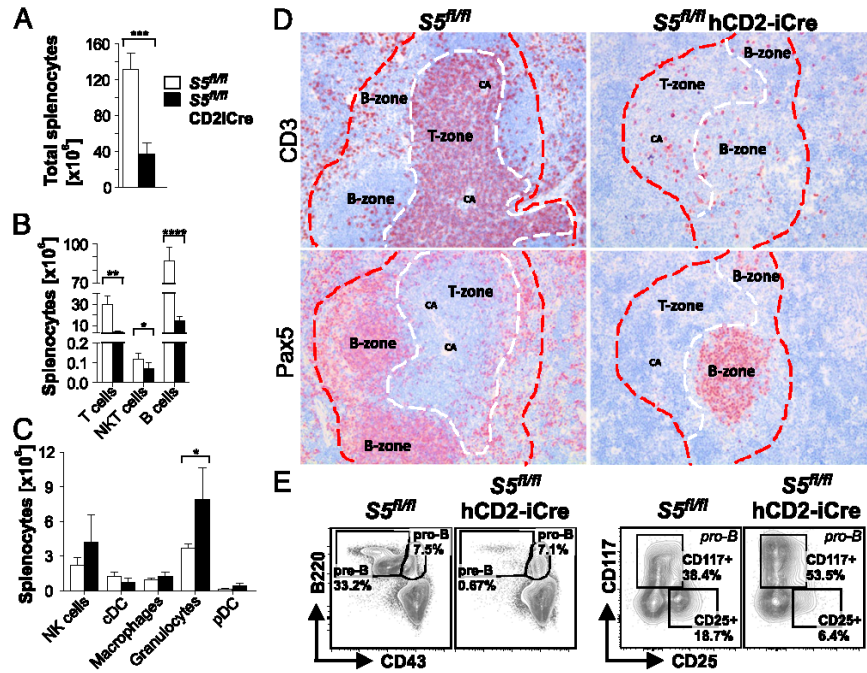


FIGURE 6. Smarca5 deficiency altered the developmental program of post- β -selection stages. **(A)** Flow cytometry of thymus. Dot plot shows the analysis of CD25 and CD44 marker expressions on the surface of CD4/CD8 DN (black dots) and overlapping DP (red dots) thymocytes. **(B)** The list of 11 most significantly enriched Hallmark gene sets in Molecular Signatures Database v6.2 by GSEA. **(C)** Heat maps of upregulated genes (\log_2FC scale) in $S5^{fl/fl}$ hCD2iCre mutant DP cells versus control $S5^{fl/fl}$ DP thymocytes. The *c-Kit* and *Il7r* gene clusters were defined previously using microarray analysis of thymocyte development (45). Gene expression profile heatmaps represent three individual experiments from sorted DP cells, each pooled from 25 to 37 $S5^{fl/fl}$ hCD2iCre animals and normalized to controls ($n = 3$). **(D)** Data from RNA-seq presented as Volcano plot. The x-axis represents \log_2 fold change in the expression of mutant DP cells as compared with the control ($S5^{fl/fl}$) DP cells. The y-axis represents adjusted p value (p_{adj}). The horizontal dashed line is equal to $p_{adj} = 0.05$. Genes (as green dots) are those that are normally downregulated in DN3a cells and become upregulated in DP cells during development and vice versa; the violet gene dots are upregulated in DN3a and, during development, become downregulated [based on microarray analysis of thymocytes (45)]. Numbers in upper corners indicate the numbers of differentially expressed genes between mutant and control of each gene set within \log_2FC of < -1 or > 1 . **(E)** Enrichment analysis of differentially expressed genes in $S5^{fl/fl}$ hCD2iCre DP thymocytes versus control DP cells [same as in (D)] was performed on the two gene sets containing 200 most upregulated (left plot) and downregulated (right plot) transcripts in wt DN3a compared with wt DP stage thymocytes [according to (45)]. For the complete list of genes pertaining to each of the gene sets, see Supplemental Fig. 2A. Positive (left plot) GSEA enrichment score curve indicates that the genes comprising the leading edge of the GSEA plot (mostly DN3a abundant transcripts) are positively correlated with mutant $S5^{fl/fl}$ hCD2iCre DP cells. Similarly, for downregulated genes, the GSEA indicated a correlation between $S5^{fl/fl}$ hCD2iCre DP cells and normal DN3a cells (lower plot). NES, normalized enrichment score.

FIGURE 7. Smarca5-deficient B cell progenitors are arrested at pro-B/pre-B transition. **(A)** Bar diagrams show the mean number \pm SD of CD45⁺ cells or **(B)** peripheral lymphocytes or **(C)** myeloid cells in spleens of control ($n = 5$) and $S5^{fl/fl}$ hCD2iCre ($n = 5$) mice. Two-tailed t test; * $p < 0.05$, ** $p < 0.01$, *** $p < 0.001$, **** $p < 0.0001$. **(D)** Immunohistochemistry for CD3 (T cell marker) and Pax5 (B cell marker) in the spleen of 6-wk-old control or $S5^{fl/fl}$ hCD2iCre mice. Data are representative of three experiments. CA, central arterioles. **(E)** Flow cytometry analysis of early B cell subpopulation in the BM of control or $S5^{fl/fl}$ hCD2iCre mice. Left plots show B220 and CD43 staining of all Ter119-negative cells in BM. Right plots show CD117 and CD25 staining of CD43⁺B220⁺ (pro-B) cells gated in upper plots. Data are representative of six control and nine $S5^{fl/fl}$ hCD2iCre animals.



p53 guides survival in the Smarca5-depleted thymocytes undergoing β -selection

It has been previously noted that deletion of *Smarca5* gene in hematopoietic progenitors induces the expression of p53 transcriptional targets (10). Our current RNA-seq data suggested that increased cell death and impaired cell cycle progression of thymocytes coincide with the activation of the p53 program (Fig. 8A). To test the biological significance and requirement of the *Trp53* gene for the *Smarca5* mutant phenotype in developing lymphocytes, we used an additional mouse strain homozygous for the *Trp53* null allele (48) to create the $S5^{fl/fl}$ hCD2iCre *Trp53*^{-/-} mice. Interestingly, the *Smarca5* deletion slightly prolonged the survival of the *Trp53* knockout mice (Fig. 8B). We observed that the introduction of the *Trp53* knockout allele improved thymic cellularity of the *Smarca5*-deficient mice (Fig. 8C). Flow cytometry analysis revealed a proportional increase (from 26.3 to 55.1%) as well as absolute cell number expansion (4-fold) of the double knockout DP population (Fig. 8D, 8E), whereas the absolute numbers of DN cells were unchanged, indicating a DN to DP transition rescue (Fig. 8E, 8F). We performed RNA-seq of samples derived from the double knockout DP cells and compared gene expression profiles with previous data. Expression analysis confirmed that the p53 targets, especially those that are associated with the induction of apoptosis in response to DNA damage such as *p21/Cdkn1a*, *Noxa/Pmaip1*, and *Bax*, were upregulated specifically in the *Smarca5*-deficient DP cells, whereas upon the introduction of the *Trp53*^{-/-} allele, their expression became normalized (Fig. 8G). Although the thymic cellularity in double knockouts was partially recovered, we still observed markedly dysregulated expression of the mRNAs connected to normal thymocyte development (Supplemental Fig. 2B). Thus, the activation of p53 targets was rather a modifier of the severity of the phenotype and not contributory to differentiation defects observed in $S5^{fl/fl}$ hCD2iCre mice. Indeed, flow cytometry analysis showed that *Smarca5* and *Trp53* double knockout DP cells contained up to a 3.5-fold excess

of H3S10^{phos} positive (mitotic) cells as compared with single *Smarca5* knockout (Fig. 8H). However, the G2/M blockade in the DPs of the *Smarca5* and *Trp53* double knockout mice persisted (Supplemental Fig. 2C).

To test whether the p53 loss could also recover the development of early B cell progenitors, BM cells from $S5^{fl/fl}$ hCD2iCre mice with or without *Trp53*^{-/-} loci were analyzed for the expression of B220 and CD43 molecules. However, unlike the partial rescue observed in the thymocyte compartment, the data from flow cytometry show that the p53 loss failed to rescue the survival and/or maturation at pro-B (B220⁺CD43⁺) to pre-B stage (B220⁺CD43⁻) transition (Fig. 8I). To conclude this part, the introduction of the *Trp53* knockout allele into the *Smarca5*-deficient strain significantly improved the proliferation and/or survival of thymocytes but not of early B cells. Importantly, the rescue experiment was unable to restore the dysregulated differentiation pathways in both B and T lineages.

Discussion

Although the SWI/SNF and CHD chromatin-remodeling factors have been implicated in the regulation of lymphocyte progenitor-specific transcription and differentiation (6, 49), the role of ISWI proteins in the development of early T and B cells has not been addressed. This study brings yet unknown evidence that the ISWI ATPase Smarca5 regulates early lymphocyte development by promoting stage-specific gene expression and, secondarily, cell survival and proliferation. Interestingly, the role of Smarca5-containing remodeling complexes was previously implicated in the DNA double-strand break (DSB) repair in human immortalized cell lines (50, 51). These reports showed that SMARCA5 is rapidly recruited to DSBs, and the knockdown of SMARCA5 sensitizes cells to DNA damage. SMARCA5 protein was shown recruited to the sites of DSB by histone deacetylase Sirtuin 6 (SIRT6) (51). Additional pathways and interaction partners of Smarca5 participating at the sites of DNA damage were also established (52, 53). Thus, Smarca5 seemed to be a suitable candidate for testing its in vivo role in lymphocytes, in

Downloaded from http://jimmunol.org/immunol/article-pdf/201/2/3434/1444343/1501684.pdf by guest on 10 January 2024

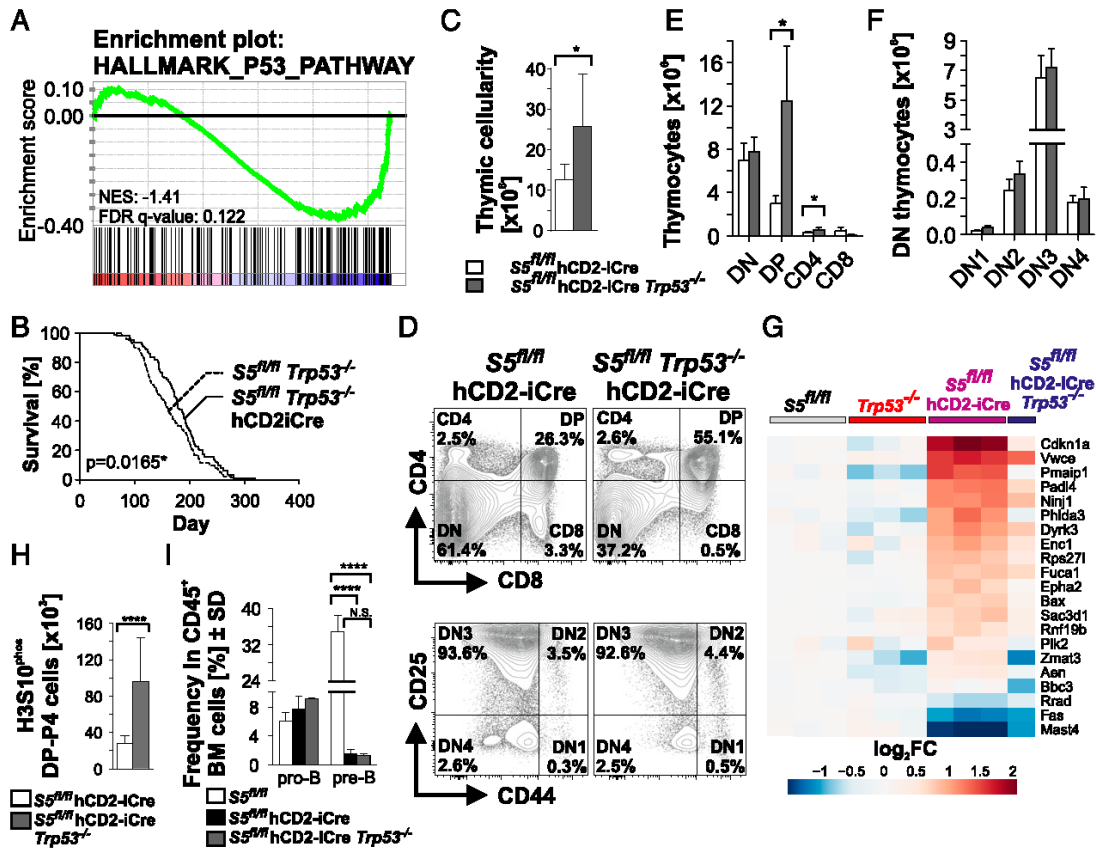


FIGURE 8. *Trp53* codeletion rescues survival but not differentiation of *Smarca5*-deficient thymocytes. **(A)** GSEA showing a representative enrichment plot of genes involved in p53 pathways and networks comparing DP thymocytes sorted from *S5^{fl/fl}hCD2iCre* (three individual pools, see Fig. 6C) mice versus DP thymocytes isolated from *S5^{fl/fl}* controls ($n = 3$). The negative GSEA enrichment score curve indicates that the genes comprising the leading edge of the GSEA plot are positively correlated with mutant *S5^{fl/fl}hCD2iCre* DP cells. **(B)** Kaplan–Meier survival curve of controls (dashed line, $n = 125$) and *Smarca5/Trp53* double mutants ($n = 115$). Log-rank (Mantel–Cox) test used; $*p < 0.05$. **(C)** Bars depict the mean of absolute numbers \pm SD of thymocytes from *S5^{fl/fl}hCD2iCre* ($n = 4$) and *S5^{fl/fl}hCD2iCre Trp53^{-/-}* ($n = 5$) mice. **(D)** Flow cytometric plots showing distributions of thymic CD4/CD8 positive and negative developmental stages of indicated genotypes. The CD4/CD8 DN cells were further distinguished using CD25 and CD44 surface markers (lower graphs). Lineage-positive (B220, Gr-1, Mac-1, NK1.1, CD11c, Ter119) cells were excluded from all measurements. Data are representative of four *S5^{fl/fl}hCD2iCre* and five *S5^{fl/fl}hCD2iCre Trp53^{-/-}* animals. **(E and F)** Mean of absolute numbers \pm SD of thymic subpopulations as in (D). Two-tailed *t* test; $*p < 0.05$. **(G)** Heat map showing the expression of genes that were differentially regulated in *S5^{fl/fl}hCD2iCre* mice but normally expressed in *S5^{fl/fl}hCD2iCre Trp53^{-/-}* animals compared with controls and *Trp53^{-/-}* mice. The expression is normalized to controls; log₂ scale. The last column represents gene expression profiles of pooled DP cells sorted from six *S5^{fl/fl}hCD2iCre Trp53^{-/-}* animals. **(H)** Absolute counts of mitotic phospho-histone H3 (Ser10) positive DP cells in *S5^{fl/fl}hCD2iCre* and *S5^{fl/fl}hCD2iCre Trp53^{-/-}* double knockouts. Two-tailed *t* test; $****p < 0.0001$. **(I)** Relative numbers of early B cell subpopulations in BM of indicated genotypes. Data are normalized to all CD45⁺ cells and represent the mean of at least three animals. Two-tailed *t* test; $*p < 0.05$, $****p < 0.0001$.

which the developmentally programmed DSBs occur. Indeed, our data showed that *S5^{fl/fl}hCD2iCre* mice initially exhibited a marked reduction of those early progenitors that productively rearranged Ag receptor loci, the TCR β expressing DN3 thymocytes (Fig. 5C) and B220⁺CD43⁺CD25⁺ early B cells (Fig. 7E). Coincidentally, the upregulation of p53 target genes (Fig. 8G) and the partial recovery of thymus cellularity in the *S5^{fl/fl}hCD2iCre Trp53^{-/-}* mice (Fig. 8C) could also be interpreted as *Smarca5* being involved in the DSB repair during the Ag receptor gene rearrangement. However, further experiments challenged this view. The developmental defect, at least in thymocytes, could not be attributed mainly to the DSBs repair aberration, as the OT-II transgene was unable to rescue the DN3 to DN4 transition defect of *Smarca5*-deficient cells (Fig. 5D). Notably, the data from RNA-seq showed that the expression pattern of the constant (*Trbc*) and variable (*Trbv*) gene segments was similar compared with the

control DP cells (Supplemental Fig. 1D), indicating that the relative use of the different gene segments during TCR β rearrangement was not affected in the mutants. In addition, the *S5^{fl/fl}hCD2iCre Trp53^{-/-}* mice displayed a comparable life span as *S5^{fl/fl} Trp53^{-/-}* mice (Fig. 8B), which is contrasting to the mouse knockout models of genes employed directly in the NHEJ that upon codeleting with the *Trp53*, accelerated tumorigenesis with shortened animal survival (54). Thus, the *Smarca5* deletion-mediated maturation defect is not primarily mediated via the disrupted repair of developmentally programmed DSBs.

Generally, except in the SP CD8 and CD4 T cells that expressed a lower level of surface TCR β (Fig. 5G, Supplemental Fig. 1E), the iTCR β expression and proximal pre-TCR signaling seem to be preserved in the *Smarca5*-deficient mice as *S5^{fl/fl}hCD2iCre* DN3 cells gave rise (albeit with a very low rate) to some DP-like cells and could be normally stimulated by anti-CD3 Ab. The DN3 stage

and all the following developmental stages were considerably altered in the *S5^{fl/fl}hCD2iCre* mice. Once *Smarca5* was inactivated, β -selected DN3, DN4, DP, and also pre-B cells lost their ability to accumulate and became depleted. *Smarca5* loss leads to a marked increase in the number of cells undergoing apoptosis (Fig. 1G). Our data indicate that this was not caused by the induction of a generalized apoptotic response as resting DN3e cells displayed very low level (up to 5%) of cell deaths even after 6 d of ex vivo cultivation (data not shown). This result, together with the observation that *Smarca5*-deficient DN3 stage lacks post-replicative cells (Fig. 4C), rather suggested that the disruption of *Smarca5* function triggers apoptosis of highly proliferating cells and especially those that have already entered the S phase. Others reported that depletion of *Smarca5* in murine lens (using Le-Cre system) results in a reduction of BrdU and Ki67 positive presumptive lens epithelial cells, leading to the lens developmental defect (43). Also, the early deletion of *Smarca5* in cerebellar progenitors (using the Nestin-Cre system) resulted in a lower number of BrdU-positive Purkinje cells and of granule neuron progenitors at E17.5, possibly because of massive cell death (17). Moreover, the defective S phase progression in the DN3 stage could also explain the formation of G2/M-arrested *S5^{fl/fl}hCD2iCre* DP cells (Fig. 4D). In the erythroid cell compartment, the *Smarca5* loss caused the emergence of tetraploid cells permanently exiting the cell cycle in populations of highly proliferating proerythroblasts-to-basophilic erythroblasts (10). This, along with a substantial number of apoptotic events, was interpreted mainly as a consequence of the activation of the DNA damage-associated p53 program. Indeed, stressed replicating cells activate their replication checkpoint to delay S phase progression and G2/M transition (55). The p53 and its downstream molecules are then required to maintain a G2 or tetraploid G1 arrest, which afterward promotes cell senescence (56–58). However, although *S5^{fl/fl}hCD2iCre* DP cells also upregulated some proapoptotic (*Noxa*, *Bax*, *Puma*) and cell cycle regulating (*Cdkn1a/p21*) p53 target genes, the rescue of phenotype was incomplete, and the tetraploid events were still present in the *Smarca5* and *Trp53* double knockouts (Supplemental Fig. 2C), indicating that the cell cycle arrest and induction of apoptosis were predominantly p53 independent.

We hypothesize that the dysregulated expression of the stage-specific mRNAs (including the surface markers) in *Smarca5*-depleted β -selected cells stay behind the thymocyte defects observed in the *S5^{fl/fl}hCD2iCre* mice. Indeed, the ablation of chromatin remodelers Brg1 or Chd4/Mi-2 β leads to differentiation defects, cell cycle arrest, or apoptosis in β -selected thymocytes partially because of dysregulated gene expression (reviewed in 59). Unlike the Brg1 or Chd4 chromatin remodelers that regulate differentiation from DN4 to DP stages (60, 61), the *Smarca5* knockout phenotype appears early and is relatively unique as the pre- β -selected DN3 cells lacking *Smarca5* are unable to down-regulate marker molecules (CD25, CD44). Among the mechanisms behind inappropriate CD25 molecule expression might be the previously reported participation of *Smarca5* in the Satb1-directed repression of *Il2ra/Cd25* loci (12, 42). Genome-wide characterizations of binding into chromatin by chromatin immunoprecipitation sequencing revealed that *Smarca5* is enriched mostly at the gene promoters and the regulatory regions (62, 63). Transcriptome analysis by RNA-seq confirmed a considerable number of ectopically expressed transcripts associated with β -selection and also genes that were not activated and remained downregulated during the transition into the DP stage (Fig. 6D), suggesting that the absence of *Smarca5* disables a crucial component of the β -selection transcription machinery. The function of

Smarca5 as a transcriptional activator and repressor was shown in studies using murine EL4 T lymphoma cell line upon small interfering RNA-mediated depletion. Although *Smarca5* participates in repression of IL genes, including *Il2*, *Il5*, *Il13*, *Il17a*, and in activation of *Il3* after stimulation with PMA and ionomycin (13), we have not observed this during the transition into the DP stage as those ILs are expressed mainly by mature T cells. Perturbation of *Smarca5* functions may have also affected other profiles during the transition from pre- to post- β -selected DN3 thymocytes by dysregulating genes related to proliferation, metabolism, and β -selection (45). To conclude, *Smarca5* represents an important transcriptional regulator that participates indispensably during early T cell development. To further address the role of *Smarca5* in regulating T cell promoters, we are currently preparing a transgenic mouse line with tagged *Smarca5* protein.

Acknowledgments

We thank Christian Lanctôt and Vladimír Divoký for helpful discussion, Ivan Kanchev for histopathology reports, Emanuel Nečas and Martin Molík for CD45.1 mice and assistance with the BM transplantations, Dana Mikulenková and Ilona Jirasková for cytospin preparations, Luděk Šefc for help with flow cytometry analysis, Jan Kubovciak for help with RNA-seq analysis, and Martin Drobis for style and writing.

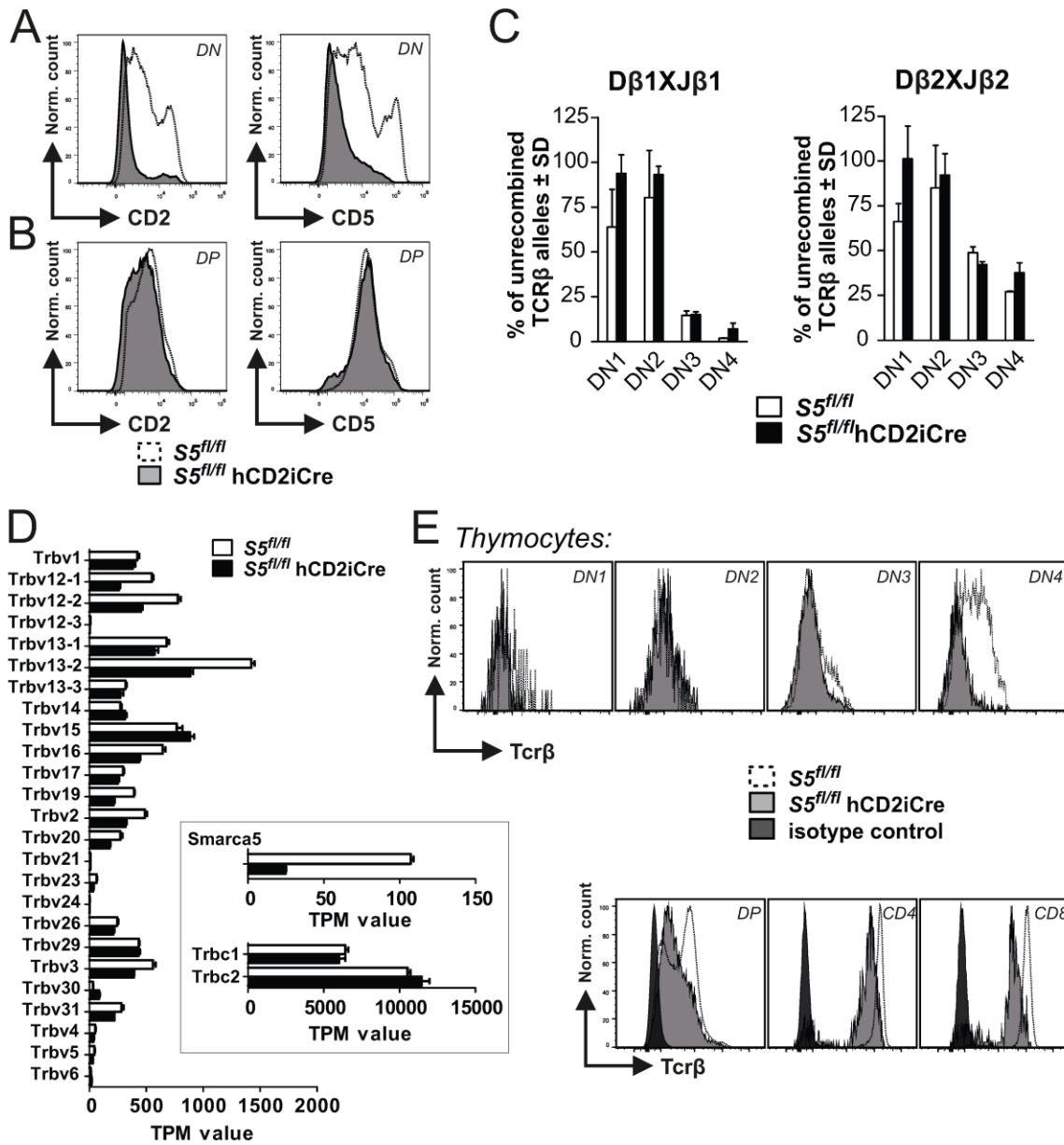
Disclosures

The authors have no financial conflicts of interest.

References

1. Rothenberg, E. V., J. E. Moore, and M. A. Yui. 2008. Launching the T-cell-lineage developmental programme. *Nat. Rev. Immunol.* 8: 9–21.
2. Zhang, J. A., A. Mortazavi, B. A. Williams, B. J. Wold, and E. V. Rothenberg. 2012. Dynamic transformations of genome-wide epigenetic marking and transcriptional control establish T cell identity. *Cell* 149: 467–482.
3. Haks, M. C., P. Krimpenfort, J. H. van den Brakel, and A. M. Kruisbeek. 1999. Pre-TCR signaling and inactivation of p53 induces crucial cell survival pathways in pre-T cells. *Immunity* 11: 91–101.
4. Shah, D. K., and J. C. Zúñiga-Pflücker. 2014. An overview of the intrathymic intricacies of T cell development. *J. Immunol.* 192: 4017–4023.
5. Winandy, S. 2005. Regulation of chromatin structure during thymic T cell development. *J. Cell. Biochem.* 95: 466–477.
6. Dege, C., and J. Hagman. 2014. Mi-2/NuRD chromatin remodeling complexes regulate B and T-lymphocyte development and function. *Immunol. Rev.* 261: 126–140.
7. Tsukiyama, T., J. Palmer, C. C. Landel, J. Shiloach, and C. Wu. 1999. Characterization of the imitation switch subfamily of ATP-dependent chromatin-remodeling factors in *Saccharomyces cerevisiae*. *Genes Dev.* 13: 686–697.
8. Erdel, F., and K. Rippe. 2011. Chromatin remodelling in mammalian cells by ISWI-type complexes—where, when and why? *FEBS J.* 278: 3608–3618.
9. Wurster, A. L., and M. J. Pazin. 2008. BRG1-mediated chromatin remodeling regulates differentiation and gene expression of T helper cells. *Mol. Cell. Biol.* 28: 7274–7285.
10. Kokavec, J., T. Zikmund, F. Savvulidi, V. Kulvait, W. Edelmann, A. I. Skoultschi, and T. Stopka. 2017. The ISWI ATPase *Smarca5* (*Snf2h*) is required for proliferation and differentiation of hematopoietic stem and progenitor cells. *Stem Cells* 35: 1614–1623.
11. Patenge, N., S. K. Elkin, and M. A. Oettinger. 2004. ATP-dependent remodeling by SWI/SNF and ISWI proteins stimulates V(D)J cleavage of 5 S arrays. *J. Biol. Chem.* 279: 35360–35367.
12. Yasui, D., M. Miyano, S. Cai, P. Varga-Weisz, and T. Kohwi-Shigematsu. 2002. SATB1 targets chromatin remodelling to regulate genes over long distances. *Nature* 419: 641–645.
13. Precht, P., A. L. Wurster, and M. J. Pazin. 2010. The SNF2H chromatin remodeling enzyme has opposing effects on cytokine gene expression. *Mol. Immunol.* 47: 2038–2046.
14. Dowdle, J. A., M. Mehta, E. M. Kass, B. Q. Vuong, A. Inagaki, D. Egli, M. Jasin, and S. Keeney. 2013. Mouse BAZ1A (ACF1) is dispensable for double-strand break repair but is essential for averting improper gene expression during spermatogenesis. *PLoS Genet.* 9: e1003945.
15. Koscielny, G., G. Yaikhom, V. Iyer, T. F. Meehan, H. Morgan, J. Atienza-Herrero, A. Blake, C. K. Chen, R. Easty, A. Di Fenza, et al. 2014. The International Mouse Phenotyping Consortium Web Portal, a unified point of access for knockout mice and related phenotyping data. *Nucleic Acids Res.* 42(Database issue): D802–D809.

Supplemental Fig. 1



Supplemental Figure 1

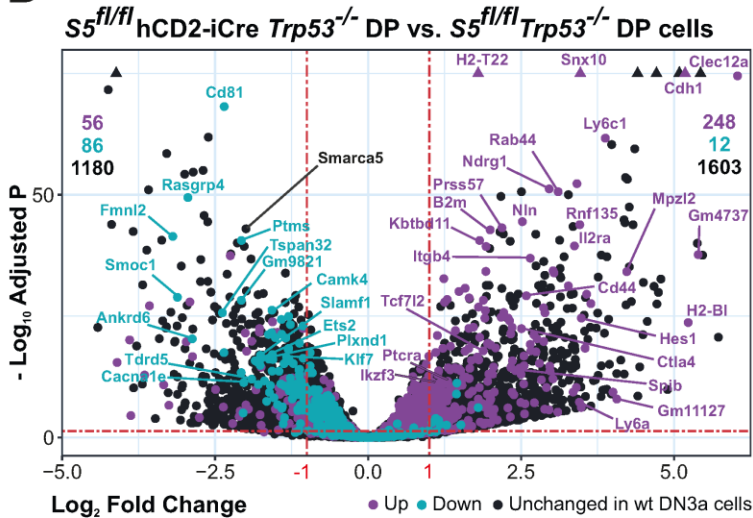
Flow cytometry analysis of CD2 (A) and CD5 (B) molecules on CD4 and CD8 double negative (DN) and double positive (DP) cell populations in thymi of control and $S5^{fl/fl}$ hCD2iCre mice. Similar results were obtained in at least 3 repeat experiments. (C) Quantitative detection of the D-J recombination of the *Tcrb* gene. qPCR determines relative loss of the intact allele after the TCR recombination. Graphs show relative proportion \pm SD of non-recombined *Tcrb* gene (measured here as presence of intact Dβ1-Jβ1 and Dβ2-Jβ2 segments, respectively) in individual DN populations. Data are representative at least of three control and three $S5^{fl/fl}$ hCD2iCre animals. (D) RNA-seq analysis of *Tcrb* gene rearrangement associated transcripts expressed in control (white bars) and $S5^{fl/fl}$ hCD2iCre (black bars) DP stage thymocytes. The transcript abundance of *Smarca5*, *Tcrb* constant regions (both shown in rectangle) and all expressed *Tcrb* variable regions with BaseMean value higher than 10 were quantified as transcripts per kilobase million (TPM). (E) Surface expression of Tcrβ on individual thymic subpopulations of control and $S5^{fl/fl}$ hCD2iCre animals analyzed by flow cytometry. As an isotype control to H57-597 clone (anti-Tcrβ) was used fluorescently labeled Armenian Hamster IgG (dark histograms). Data are representative of three experiments.

Supplemental Fig. 2

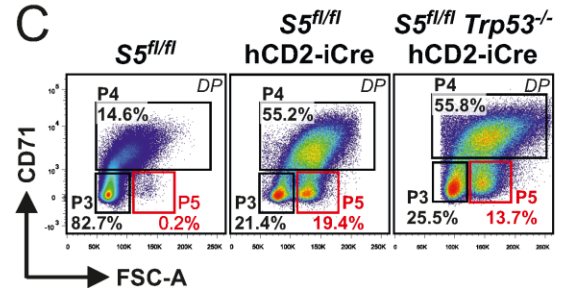
A

Genes downregulated in wt DN3a compared to DP	A130050007Rik, Abca1, Adam12, Adgre5, Akap12, Als2cl, Ankrd44, Ankrd50, Anxa5, Arap2, Arhgef11, Arntl, Arsi, Aspm, At12, Atp10a, Atp2b1, B230359F08Rik, Bcl2l1, Bcl6, Bub1, C920008G01Rik, Cacna1e, Camk4, Casc5, Ccna2, Ccr4, Ccr9, Cd2, Cd28, Cd4, Cd5, Cd52, Cd6, Cd81, Cd8a, Cd8b1, Cdh24, Cdkn1b, Cenpe, Cenpf, Chd1, Ckap2l, Cnr2, Colq, Csgalnact2, Dek, Depdc1a, Dgkd, Dnajb4, Dusp6, E2f2, E2f8, Ect2, Egr1, Ephb6, Erc1, Esco2, Esrp2, Ets2, F13a1, Fas, Flna, Fmn12, Gimap8, Glcci1, Gm10210, Gm10459, Gm10644, Gm10785, Gm16489, Gm4884, Gpr162, Gramd3, Gsn, H2-Q2, Hist1h1a, Hist1h2ba, Hist1h2bb, Hist1h2bc, Hist1h2be, Hist1h2bf, Hist1h2bg, Hist1h2bh, Hist1h2bj, Hist1h2bk, Hist1h2bl, Hist1h2bm, Hist1h2bn, Hist1h2bp, Hist1h2ba, Hist1h2br, Hist1h4f, Hist1h4h, Hmnr, Id3, Ikzf3, Il21r, Il4ra, Itgb2, Jup, Kif11, Kif14, Kif15, Kif5b, Klf7, Ldlrad3, Lipa, Lmnb1, Lrig1, Lyst, Macf1, Map4, Map4k5, Medag, Mef2a, Mfhas1, Mki67, Mns1, Mr1, Nav2, Ncagp, Ndc80, Neto2, Nfatc3, Nfkbia, Nhsl1, Nipbl, Nsg2, Olfr1537, P3h4, Phlda1, Phxr2, Pik3cb, Plcl1, Plcl2, Plekhf1, Plxnd1, Polg, Pptc7, Prc1, Pvr, Rasa2, Rasgrp1, Rb1, Rcbtb2, Rdm1, Rgs14, Rmnd5a, Rnu2-10, Rock1, Rorc, Rrm2, Sgol2a, Skil, Sla, Slamf1, Slc37a3, Slc6a19, Slc7a11, Slco3a1, Smoc1, Snord15a, Snord15b, Snord16a, Spc25, Sqrdl, St6gal1, Tcra-V22.1, Tdrd5, Tdrp, Tnk2, Top2a, Top2b, Trav12-1, Trav12-2, Trav12n-1, Trav12n-2, Trav14-1, Trav14d-3-dv8, Trav14n-2, Trav16d-dv11, Trav3-3, Trav3n-3, Trav4d-4, Trav7-4, Trav7d-4, Trav9d-3, Trav9d-4, Trib2, Trio, Tspan32, Tube1, Txk, Ube2v1, Ublcp1, Umad1, Usp33, Wapl, Wisp3, Xrra1, Zfp36
Genes upregulated in wt DN3a compared to DP	1700048O20Rik, 4930427A07Rik, 4930567H12Rik, 5430410E06Rik, 5830411N06Rik, Adams17, Adgrg1, Ahr, Akr1c13, Aldh2, Ankrd27, Apex1, Arhgap26, Arhgef10l, Ass1, Atp2b4, Atp8b4, AW112010, B2m, Bri3bp, Bst1, Bst2, Camkv, Capn5, Cblb, Ccnd2, Ccnd3, Ccnd5, Cdh1, Cdk6, Cdkn1a, Clpb, Coro2a, Cpa3, Cpe2, Cpt1a, Crip1, Ctla4, Cyth4, D8Ert82e, Dtx1, Eef2k, Epcam, Ephx3, Ern1, Etv6, Fads2, Fam169b, Fkbp5, Frmd4a, Gas5, Gfra1, Gid4, Gm12191, Gm2a, Gm32211, Gm4759, Gm5111, Gm5424, Gm5481, Gm6525, Gm6756, Gm7120, Gm8995, Gnl3, Gpx1, Gria3, Grn, Gsto1, Gstp1, Gstz1, Gzma, H2-D1, H2-K1, H2-L, Hdac4, Hes1, Hmgcs2, I730030J21Rik, Idi1, Ifitm2, Igbp1, Il17rb, Il2ra, Il7r, Irgm1, Itgam, Kcnk5, Kdelc1, Khdc1a, Khdc1b, Khdc1c, Kit, Ldlr, Lfng, Lgals3bp, Lph, LOC547349, Ly6a, Ly6c1, Ly6c2, Ly6d, Lyz2, Mcoln2, Mif, Mir1, Mir675, Mpzl2, Mrps18b, Msmo1, Mybbp1a, Myc, Myl10, ND3, Ndrgr1, Nkg7, Nlrc5, Notch1, Notch3, Npm1, Nsdhl, Odc1, Park7, Parp8, Pdgfrb, Pebp1, Phgdh, Pik3cd, Plac8, Pld4, Plekha7, Polr1b, Ppt1, Pqlc3, Prdx3, Prss57, Psme1, Ptcra, Rabl2, Repin1, Rny3, Rpl12, Rpl13a, Rpl30, Rpl31, Rpl31-ps12, Rpl35, Rpl36a, Rpl38, Rpl39, Rpl41, Rpl5, Rpl9, Rps18, Rpsa, Rras2, Rrp1b, Rsu1, Rtp4, Scin, Scn4b, Sema4a, Sigmar1, Smim5, Smyd2, Snord1b, Snord1c, Snord32a, Snord47, Snrpg, Snx30, Spats2, Spib, Srgn, Srm, Sstr2, St6galnac4, Suclg2, Supt6, Susd1, Syt1, Tbc1d5, Tcrg-V1, Tcrg-V4, Tcrg-V6, Tgtp1, Tgtp2, Tifa, Tmem173, Tmem176b, Tmem180, Tmem50b, Tnfrsf1b, Tpi1, Trgv2, Tspan31, Tuba4a, Unc93b1, Usmg5, Wdfy4, Ybx3, Zfp36l2, Zfp991

B



C



Supplemental Figure 2

(A) The top 200 upregulated and top 200 downregulated transcripts identified in microarrays comparing adult wild-type DN3a and DP thymocytes (45). (B) Data from RNA-seq presented as Volcano plot. The X-axis represents \log_2 fold change of the expression in *S5^{fl/fl} hCD2iCre Trp53^{-/-} vs Trp53^{-/-} DP cells*. The Y-axis represents *adjusted p-value* (horizontal dashed line is equal to $p_{adj} = 0.05$). Colored dots indicate genes normally downregulated (green) or upregulated (violet) in wild-type DN3a cells as compared to wild-type DP stage thymocytes (from a microarray analysis of thymocytes by Mingueneau *et al.* 2013). Numbers in corners indicate differentially expressed genes between *Smarca5* mutants and controls of each gene set within \log_2FC of <-1 or >1 . (C) Flow cytometric plots showing expression of CD71 and forward scatter (FSC-A) of DP-gated thymic suspension. Genotypes are indicated on the top. DP fractions designated as P3-P5 are shown. P5 fraction corresponds to the G2/M arrested cells population. Data are representative at least of three experiments.

4.3 (3. publikace) Loss of ISWI ATPase SMARCA5 (SNF2H) in Acute Myeloid Leukemia Cells Inhibits Proliferation and Chromatid Cohesion.



Article

Loss of ISWI ATPase SMARCA5 (SNF2H) in Acute Myeloid Leukemia Cells Inhibits Proliferation and Chromatid Cohesion

Tomas Zikmund ^{1,†}, Helena Paszekova ^{1,†}, Juraj Kokavec ¹, Paul Kerbs ^{2,3,4}, Shefali Thakur ¹, Tereza Turkova ¹, Petra Tauchmanova ¹, Philipp A. Greif ^{2,3,4} and Tomas Stopka ^{1,*}

¹ Biocev, 1st Medical Faculty, Charles University, 25250 Vestec, Czech Republic;

tomzikmund@gmail.com (T.Z.); paszekova.helena@gmail.com (H.P.); juraj.kokavec@gmail.com (J.K.); shefalithakur.st@gmail.com (S.T.); tereza.turkova@volny.cz (T.T.); petra-tauchmanova@seznam.cz (P.T.)

² Department of Medicine III, University Hospital, LMU Munich, D-80539 Munich, Germany;

paul.kerbs@med.uni-muenchen.de (P.K.); pgreif@med.uni-muenchen.de (P.A.G.)

³ German Cancer Consortium (DKTK), partner site Munich, D-80336 Munich, Germany

⁴ German Cancer Research Center (DKFZ), D-69120 Heidelberg, Germany

* Correspondence: tstopka@lf1.cuni.cz; Tel.: +420-32587-3001

† These authors contributed equally.

Received: 26 February 2020; Accepted: 16 March 2020; Published: 18 March 2020



Abstract: ISWI chromatin remodeling ATPase SMARCA5 (SNF2H) is a well-known factor for its role in regulation of DNA access via nucleosome sliding and assembly. SMARCA5 transcriptionally inhibits the myeloid master regulator PU.1. Upregulation of SMARCA5 was previously observed in CD34+ hematopoietic progenitors of acute myeloid leukemia (AML) patients. Since high levels of SMARCA5 are necessary for intensive cell proliferation and cell cycle progression of developing hematopoietic stem and progenitor cells in mice, we reasoned that removal of SMARCA5 enzymatic activity could affect the cycling or undifferentiated state of leukemic progenitor-like clones. Indeed, we observed that CRISPR/cas9-mediated *SMARCA5* knockout in AML cell lines (S5KO) inhibited the cell cycle progression. We also observed that the *SMARCA5* deletion induced karyorrhexis and nuclear budding as well as increased the ploidy, indicating its role in mitotic division of AML cells. The cytogenetic analysis of S5KO cells revealed the premature chromatid separation. We conclude that deleting *SMARCA5* in AML blocks leukemic proliferation and chromatid cohesion.

Keywords: SMARCA5; SNF2H; AML; leukemia; CRISPR; therapeutic target

1. Introduction

Acute myeloid leukemia (AML) is a malignant hematopoietic disease derived from myeloid-primed stem cells resulting in accumulation of myeloid blasts. AML patients have a poor prognosis and the only known efficient therapy is bone marrow transplantation combined with chemotherapy. Next-generation sequencing revealed that despite similar cytology and cellular features, the mutational profile of AML clones can be very heterogeneous. Leukemogenesis involves multiple types of genomic alterations from single nucleotide variants to large chromosomal abnormalities (involving deletions, translocations, or chromosomal gains and losses). Targets of mutagenesis are often genes encoding regulators of gene transcription (e.g., *RUNX1*, *CEBPA*, *GATA2*), DNA methylation (e.g., *DNMT3A*, *IDH1*, *IDH2*), and genome organization (e.g., *CTCF*, *RAD21*, *SMC3*).

Immature cells during tissue development require ATP-dependent chromatin remodeling activities to ensure accession of regulatory proteins to DNA in order to control replication, transcription, or DNA repair. Activities that facilitate nucleosome spacing and assembly during tissue development are

provided mainly by evolutionary conserved Swi2/Snf2 family helicases. Smarca5 (also known as Snf2h) belongs to important enzymes of the Swi2/Snf2 family with remodeling activity that is required for successful hematopoietic development in mammals [1–3]. In mouse, Smarca5 represents the catalytic subunit of ISWI remodeling complexes that is indispensable for developing embryo and later for fetal hematopoiesis [1,2]. Interestingly, Smarca5 loss was accompanied by upregulation of p53 and of its transcriptional targets that are usually linked to the induction of apoptosis in response to DNA damage (e.g., p21/Cdkn1a, Noxa/Pmaip1, and Bax) [1]. Our work and the work of others suggested that Smarca5 not only facilitates proliferation-associated events but also helps to activate transcriptional programs of particular developmental stages to set proper expression identity of immature cells [4,5]. Additional evidence implicated that Smarca5 regulates global gene expression programs and function of many human gene regulatory elements by cooperating with CTCF [6–8].

Smarca5 represents an integral part of heterodimeric ISWI complexes that contain usually a bromodomain-containing protein (BAZ1A, BAZ1B, BAZ2A, BAZ2B). ISWI complexes were originally identified in *Drosophila* but later they were discovered also in humans, namely, NURF (ATPase motor of the nucleosome remodeling factor), ACF (ATP-utilizing chromatin assembly and remodeling factor), and CHRAC (chromatin assembly complex). Later, additional human complexes were found, such as RSF, NoRC, WICH, CERF, and finally, SNF2H-cohesin [9]. Most ISWI complexes are involved in regulating cell cycle progression albeit via different mechanisms. While many ISWI complexes regulate transcription by nucleosome sliding mechanism utilizing either RNA-Polymerase 1 (RNAP1) (NoRC, B-WICH) or RNAP2 (ACF, NURF, CERF, WINAC), other complexes are linked to replication/repair (CHRAC, WICH) or chromatid cohesion (SNF2H-cohesin) [10]. It appears that SMARCA5 plays an indispensable part in the ISWI complexes (albeit it can remodel chromatin alone in acellular systems); however, in certain situations, it may be replaced within ISWI complexes by its close homologue SMARCA1 (SNF2L) as shown in rather differentiated cells of the cerebellum [4].

Currently, over 20% of all malignancies carry mutations in one of the subunits of chromatin remodeling complexes of the SWI/SNF family (see [11,12]). These mutations often decrease protein stability and cause loss of the particular subunit, which leads to the assembly of incomplete remodeling complexes with different functions in vivo and altered capability to precisely regulate gene expression [13]. In the case of the ISWI subfamily, the mutations of various ISWI subunits identified in oncologic diseases have still yet unknown impact on tumorigenesis. In solid tumors the overexpression of SMARCA5 [14–18] has been associated with disease aggressiveness, chemoresistance and proliferation activity [7]. SMARCA5 expression was found dysregulated in many human malignant tumors, such as aggressive gastric cancer, breast cancer, or prostate cancer. In addition, the SMARCA5 gene is a target of cancer-associating miRNA regulation [14–18]. SMARCA5 overexpression has been also observed in AML CD34+ progenitors [7,19]. SMARCA5, through the interaction with CTCF in leukemic cells, actively inhibits expression of the *SPI1/PU.1* gene [7] that represents key hematopoietic transcription factor and dose-dependent leukemia suppressor [20]. Additional work utilizing the CRISPR/Cas9 genome editing in vitro revealed that among hematopoietic cancer cell lines, those derived from AML patients were the most SMARCA5 dependent [21]. We herein studied the consequences of SMARCA5 deletion in AML cells and showed that SMARCA5 targeting affected proliferation and resulted in chromosomal aberrations and polyploidy pointing to the role of SMARCA5 in mitotic division. We believe that delineating the effects of SMARCA5 targeting might pave the way for new approaches in the therapy of AML.

2. Results

2.1. SMARCA5 Overexpression Marks the Hyperproliferation and Cytogenetically Abnormal AML Patients

Based on previous evidence documenting SMARCA5 overexpression in small AML patient subset [19], we examined RNAseq data of bone marrow samples from AML patients with recorded overall survival (OS). We confirmed our previous observation [19] that SMARCA5 levels are significantly

elevated at the time of diagnosis and decreased after the patients achieved complete hematologic remission (Figure 1A). We next associated SMARCA5 expression and clinical parameters and (due to genetic AML heterogeneity) followed separately cytogenetically normal (CN) and abnormal (CX) AML patients. Hence, we could observe a trend for decreased OS in the AML patient population with higher SMARCA5 expression and carrying cytogenetic abnormalities (Figure 1B). We also observed that higher SMARCA5 levels correlated with mRNA expression of proliferation biomarkers such as AURKA, PLK1, CCNA2, CENPF (Figure 1C).

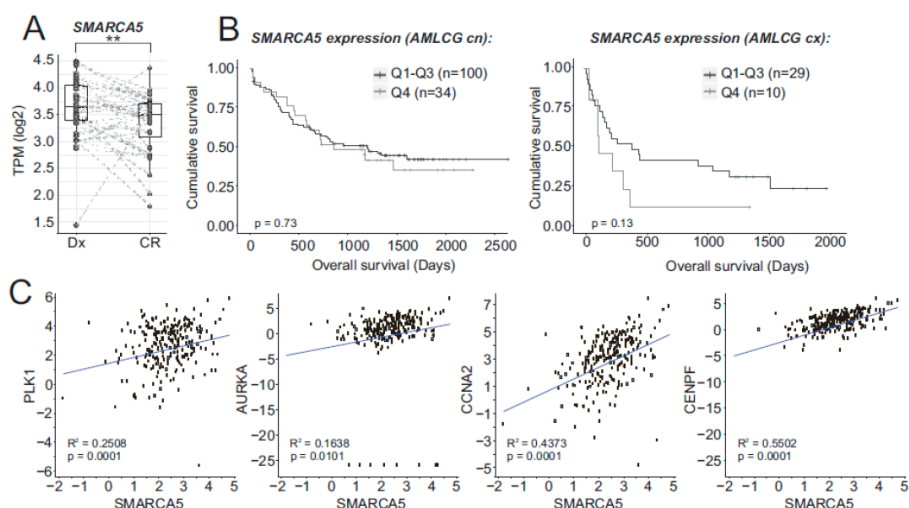


Figure 1. (A) SMARCA5 expression of matched AML samples at the time of diagnosis (Dx) and complete remission (CR). Dots represent individual samples; dashed lines connect matched patient samples. Boxes: distribution of the Dx and CR groups; intermediate line = median. Significance was estimated using a paired Wilcoxon test. (B) Survival analysis of AML patients divided into quartiles (from low Q1 to high Q4; Q1: 0–25% + Q2: 25–50% + Q3: 50–75% vs. Q4: 75–100%) based on SMARCA5 mRNA levels (cn: cytogenetically normal, cx: cytogenetic abnormalities). (C) Correlation of mRNA levels of PLK1, AURKA, CCNA2, CENPF, and SMARCA5 (R² and p-value indicated).

2.2. SMARCA5 Deletion Inhibits AML Cell Proliferation

To test requirement of SMARCA5 for AML cell growth, we produced a null allele using CRISPR/Cas9 genome editing technology (Figure 2A). Targeted was exon5, which codes a portion of evolutionarily conserved ATPase domain and that was previously shown to be a targetable region using the Cre-loxP1 system. Deletion of exon5 results in a frame shift mutation disabling expression of Smarca5 protein in mouse [1]. For the experiments, human K562 cells (AML M6 subtype) were initially utilized as they were previously used for antisense oligonucleotide-mediated transient knockdown of SMARCA5 [2]. K562 cells were transfected by a pair of pX330-mVenus vectors containing sgRNAs complementary to a sequence in the SMARCA5 introns 4 & 5 and the effect of CRISPR/Cas9-mediated deletion of exon5 was tested by PCR. Analysis of fragments amplified from genomic DNA of FACS-sorted mVenus-positive clonal populations identified 5 clones (#H10, D7, H4, E7, H7) with a single shortened PCR product (~632bp compared to 1175bp in controls) that were homozygously mutated (Figure 2B). Sanger sequencing of PCR products confirmed that clones H10, D7, E7, and H5 contained the same deletion (543bp) and clone H4 an even larger deletion (582bp) within SMARCA5 exon5 (Figure 2C). In addition, quantitative PCR and Western blot analyses of the cellular extracts confirmed that the Cas9-mediated deletion of the SMARCA5 gene resulted in loss of SMARCA5 expression (Figure 2D,E). The resulting subclones had no expression of vector-coded & episomally expressed Cas9 nuclease. In addition, eight predicted off-target candidates (SRGAP2, RNF17, PRG4,

GYPA, POLQ, CYB5R4, BCKDHB, NAV2) had no alteration of their sequences. Thus, we managed to effectively delete SMARCA5 in the K562 subclones to create a cellular model for studying how SMARCA5 loss affected AML cell growth.

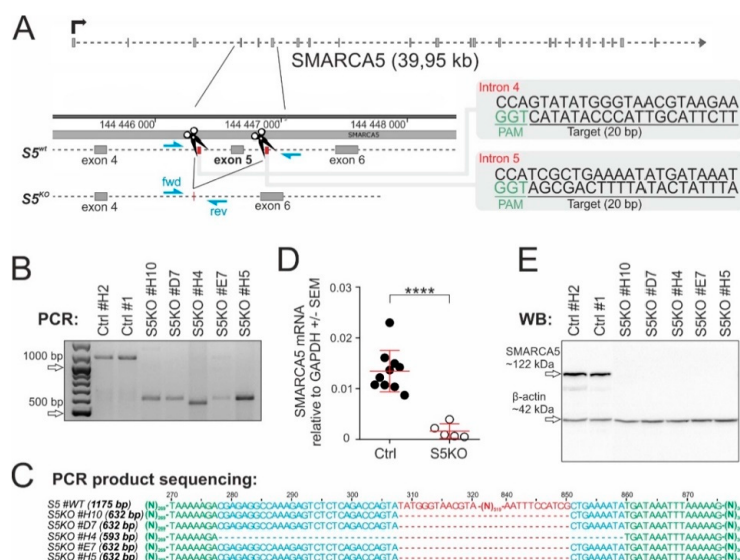


Figure 2. Inactivation of *SMARCA5* gene expression (S5KO) in AML cells. **(A)** Scheme of generating the S5KO using CRISPR/Cas9 technology. The Cas9 nuclease was targeted into two intronic sites (scissors) surrounding exon 5 of the *SMARCA5* gene. The sequences of guide RNAs are depicted in gray boxes on the right. Indicated are exons 4–6 (small rectangles) and genotyping primers (blue arrowheads). **(B)** PCR verification of the exon 5 deletion in the indicated S5KO clones. **(C)** Analysis of *SMARCA5* gene region following the Cas9 nuclease deletion. PCR products (same as in B) were Sanger-sequenced and aligned with the wt sequence using the Kalign web tool. After sequencing, the precise length of the resultant PCR amplified region was determined (on the left in brackets). **(D)** Quantitative PCR analysis of *SMARCA5* mRNA expression in the S5KO clones ($n = 5$) compared to controls ($n = 10$). Data normalized to the GAPDH mRNA. Student's t -test, $p < 0.00001$ ****. **(E)** Immunoblotting of *SMARCA5* expression in CRISPR/Cas9-treated K562 or controls. β -actin controlled the load.

2.3. *Smarca5* Deletion Inhibits Proliferation of Myeloblasts and Affects Function of Normal Stem Cells

To characterize the effect of *SMARCA5* deletion in the AML-S5KO subclones, we monitored their growth in culture by the WST-1 assay correlating the number of metabolically active cells in the 72-hr culture within a 96-well plate. We quantitated the data with a scanning multiwell spectrophotometer (ELISA reader) (Figure 3A, upper panel) and also in parallel counted the viable cells with an automated cell counter (Figure 3A, lower panel). We observed that starting day 1, the S5KO subclones produced less formazan product/s compared to AML 'control' cells, indicating that loss of *SMARCA5* impaired proliferation of leukemic cells. We also attempted to create S5KO clones from additional AML cell lines. We repeatedly used OCI-M2, NB4, SKM1, MOLM-13, however, despite the fact that these AML cell lines grew normally in tissue culture conditions, the recombined cells by pX330-mVenus vectors followed by the single cell sorting could not produce clones with exon 5 deletion. We therefore used the method of serial dilution of transfected cells. This approach, in contrast to the previous approach, produced populations of OCI-M2 and SKM1 cell lines with detectable Cas9-edited *SMARCA5* loci. However, the signals of mutated alleles markedly decreased during long-term cultivation, suggesting that the S5KO cells were overgrown by cells containing at least one intact *SMARCA5* allele. Thus, the deletion of the *SMARCA5* gene completely impaired leukemic cell proliferation in most of the AML cell lines,

while in K562 cells it was tolerated albeit under markedly lower proliferation activity, which allowed us to study it in more detail.

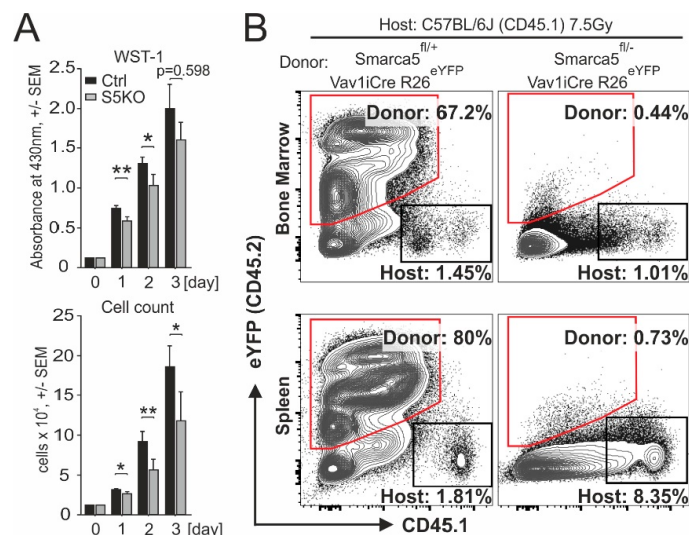


Figure 3. Proliferation of AML and progenitor cells upon *Smarca5* gene deletion. **(A)** Proliferation of S5KO clone #D7 and control cells analyzed by WST-1 assay. Mean \pm SEM of formazan absorbance (top) and cell count (bottom) (pentaplicates). Student's *t*-test, $p < 0.05$ *, $p < 0.01$ **. **(B)** Flow cytometry analysis of donor (CD45.2) and host (CD45.1) derived hematopoietic cells at 14 days following the transplantation of donor fetal liver cells into lethally (7.5 Gy) irradiated host animals. Donor (red trapezoid) and host-derived (black rectangles) bone marrow cells (upper dot plots) and splenocytes (lower dot plots) were distinguished by the expression of yellow fluorescent protein (eYFP) or surface variant of CD45. Control mice: *Smarca5*^{fl/+} Vav1iCre R26^{eYFP}; *Smarca5* mutant mice: *Smarca5*^{fl/fl} Vav1iCre R26^{eYFP}. Data are representative of repeated experiments.

AML cell population resembles early hematopoietic progenitors. Thus, as controls to AML cells, we studied early murine blood progenitors. Previously it was shown that *Smarca5* loss in mouse partially inhibits differentiation of early Lin⁻Sca-1⁺c-Kit⁺ hematopoietic progenitors [1]. To test whether *Smarca5* deletion affects reconstitution of early blood progenitors after transplanting them into normal murine recipients, we utilized the hematopoietic reconstitution assay. We transferred E13.5 mouse fetal liver cells (C57Bl/6J Ly5.2 background) isolated either from control *Smarca5*^{fllox/+} Rosa26^{eYFP/+} Vav1-iCRE or *Smarca5*-deficient (*Smarca5*^{fllox/-} Rosa26^{eYFP/+} Vav1-iCRE) embryos into lethally irradiated adult C57Bl/6J Ly5.1 recipients. Flow cytometric analyses of bone marrow and spleen at several weeks after transplantation revealed that repopulation was detected only in animals transplanted with cells in which the *Smarca5* gene was preserved. Thus, homeostatic expression of *Smarca5* is very important for hematopoietic reconstitution (Figure 3B), implicating a possibility that the *Smarca5* role in AML cells might also involve a very early leukemia-initiating compartment.

2.4. Inactivation of *Smarca5* Causes Nuclear Abnormalities and Polyploidy

To gain insight into the subcellular structures of the AML S5KO cells, we utilized hematology staining using a standardized May–Grunwald and Giemsa–Romanowski stain procedure. As indicated within Figure 4A, the control AML cells were represented by a uniform layer of myeloblasts with large round nuclei, fine chromatin structure, and prominent nucleoli. Significantly more frequent nuclear abnormalities were observed in the S5KO cells compared to controls. These included nuclear budding, internuclear bridging, karyorrhexis, and multinuclearity seen in 10% to 65% of all analyzed cells (Figure 4B). To study effect/s of S5 depletion in nonhematopoietic cells, we derived mouse embryonic

fibroblast (MEF) with Tamoxifen-regulated Cre-recombinase activity (Cre-Esr1) from *Smarca5^{fl/fl} Trp53^{-/-}* animals. *Trp53*-mutated MEFs were chosen because of their lower propensity to enter proliferation senescence and because most AML cell lines including K562 have *TP53* gene inactivation [22]. After 6 h incubation with 100 nM 4-hydroxy-tamoxifen (4OHT) and additional 90 h of culture, the MEF cells were depleted of Smarca5 protein (Figure 4C). Decrease of Smarca5 protein level negatively influenced the cell growth and the proliferation defect had already occurred within 40 h from the start of the 4OHT treatment while 4OHT untreated and control Cre-Esr1 lacking cells proliferated normally (Figure 4D). This proliferative defect resembled one observed in AML S5KO clones. The flow cytometry analysis revealed that aberrant proliferation was accompanied by lower proportion of S-progressing and mitotic (pH3S10⁺) cells. In addition, we noted a higher number of cells with polyploid nuclei (Figure 4E) that was concomitant to a decreased proportion of diploid cells upon S5 deficiency in MEFs. Taken together, inactivation of SMARCA5 triggers a cell proliferation blockade and results in nuclear abnormalities of exceedingly cycling leukemic as well as normal hematopoietic cells.

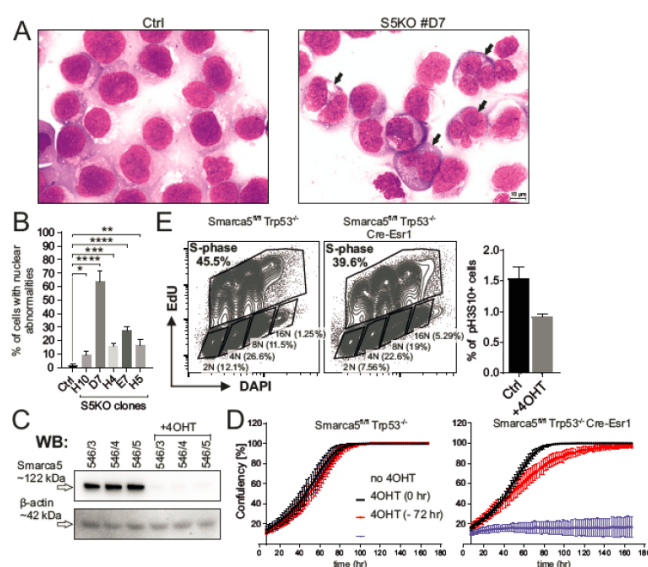


Figure 4. Nuclear abnormalities in S5KO cells. (A) Cytology of control (left) and S5KO clone #D7 (right), nuclear abnormalities indicated and shown (B) as mean % \pm Stdev of control, 400 cells/subclone analyzed. Student's *t*-test, $p < 0.05$ *, $p < 0.01$ **, $p < 0.0001$ ***. (C) Immunoblotting of Smarca5: MEF cell lines (*Smarca5^{fl/fl} Cre-Esr1*: untreated, 4OHT-treated (100 nM, 6 h exposure, 4 days of culture). β -actin = loading control. (D) IncuCyte cell proliferation analysis; control *Smarca5^{fl/fl}* (upper panel) vs. *Smarca5^{fl/fl} Cre-Esr1* (lower panel) MEFs in absence/presence of 4OHT (100 nM, 6 h exposure), or alternatively, 4OHT was added 72 h prior to IncuCyte monitoring (4OHT—72 h). Y-axis: mean confluency (%) and \pm Stdev of at least 16 different regions of the cultivation plate, X-axis: time (h). (E) Flow cytometry analysis of control and *Smarca5^{fl/fl} Cre-Esr1* MEF population cell cycle progression using EdU/DAPI double staining (upper dot plots). Black rectangles depict all S-phase and non-S-phase cells with different ploidy (2N–16N). Histograms show percentage of phospho-histone H3 (Ser10) positive mitotic events in experimental cell lines. (D) and (E) represent biological triplicates.

2.5. Cytogenetic Abnormalities and Gene Expression Dysregulation in the S5KO AML Cells

As pointed out in the Introduction section, SMARCA5 protein was previously shown to load cohesin complex onto human chromosomes [23]. As the canonical role of cohesin is the sister chromatid cohesion, we next analyzed the structures of mitotic chromosomes in the AML S5KO cells on metaphase spreads. The analysis of the S5KO subclone D7 consistently showed (Figure 5A) that among other chromosomal abnormalities, the cohesion defects were by far the most frequent involving premature

chromatid separation and loss of cohesion. Compared to the controls that contained only 12%, the S5KO mitotic cells displayed defects in chromatin cohesion in 70% of all cases. Similarly, the defects of chromatid cohesion were seen also in MEF cell-derived mitotic chromosome spreads (Figure 5B,C). These data suggest that SMARCA5 inhibition affects cohesin function in general.

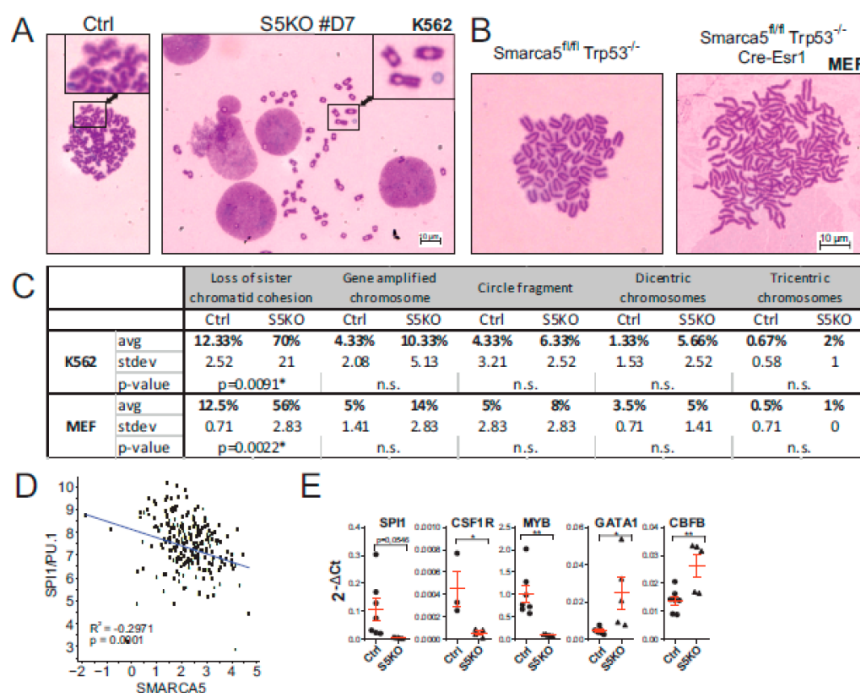


Figure 5. SMARCA5 loss causes karyotypic changes in K562 cells. (A,B) Mitotic chromosome analysis of S5KO cells vs control K562 cells (clone #D7, (A)) or MEF cells (B). 1000X magnification. (C) Table summarizes all chromosomal aberrations; data from technical triplicates, for each replicate a total of 100 mitotic nuclei were counted. Mean percentage of chromosomal abnormalities with Stdev, Student's *t*-test, $p < 0.05$ *. (D) Computational analysis of correlations between expression of SPI1/PU.1 and SMARCA5 in samples of adult AML patient samples; for details, see Materials and Methods section. (E) Quantitative PCR analysis of SPI1, CSF1R, MYB, GATA1, and CBF β mRNAs expression in the S5KO clones ($n = 5$) compared to controls ($n = 7$). Data were normalized to the GAPDH mRNA. Student's *t*-test, $p < 0.05$ *, $p < 0.001$ **.

In order to better understand the cooperative nature of SMARCA5 and its interacting partners in AML, we correlated their expression using RNAseq data in AML patients. Hence, significant association exists between the expression pattern of SMARCA5 and BAZ proteins (BAZ1A, BAZ1B, BAZ2A, BAZ2B) as well as the members of the CTCF/cohesin complex across human AML samples. This implicates, albeit indirectly, a role of SMARCA5 in CTCF/cohesin function in AML that also coincides with karyotype abnormalities imposed by a SMARCA5 loss.

We recently showed that SMARCA5 (together with the CTCF/cohesin complex) represses PU.1-mediated myeloid differentiation [7] and similarly, we noted that SMARCA5 regulates GATA1-mediated erythropoiesis [1]. We therefore next decided to analyze the levels of SPI1/PU.1 and GATA-1 transcripts with respect to SMARCA5. As expected, transcriptomic data from AML Cooperative Group München (Figure 5D) showed an inverse correlation between SPI1/PU.1 and SMARCA5 expression in AML patient samples. To further assess the role of SMARCA5 in regulation of the hematopoietic transcription program, we determined the expression of a set of selected mRNAs upon the genetic ablation of the SMARCA5 gene in K562 cells. Compared with previously published

data documenting an inverse relationship between SMARCA5 and hematopoietic transcription factors PU.1 or GATA-1, we observed that upon SMARCA5 deletion in K562 cells the level of SPI1/PU.1 and some of its targets (CSF1R) became downregulated while other transcription factors (GATA1, CBFβ) were upregulated. The dysregulation of mRNA pattern of SMARCA5 targets upon SMARCA5 deletion can be attributed to the heterogeneity of the AML cell lines and also possibly to multiple genetic/cytogenetic abnormalities imposed by the SMARCA5 loss.

3. Discussion

We herein studied how ISWI ATPase SMARCA5/SNF2H controls in AML the proliferation and gene expression of myeloblasts as SMARCA5 appeared to be an interesting target for anti-AML therapy. Our previous work demonstrated a pattern of SMARCA5 upregulation at AML diagnosis followed by its normalization upon achieving the hematologic remission. Importantly, additional work has not identified recurrent mutations of SMARCA5 in AML or any malignant disease (so far analyzed by next-generation sequencing-based techniques). For example, for the SMARCA5 gene, only 186 variants with an amino acid residue substitution exist in nearly ~20 thousand oncologic patients (<1%). There also exist infrequently the variants in ISWI-interacting BAZ proteins detected in cancer, however, the significance of these variants remains also unknown. Importantly, among the AML-associated variants, only the SMARCA5-interacting proteins, CTCF and members of the cohesin complex, were shown consistently mutated in AML [24]. Based on this, we expected SMARCA5 indispensability for AML proliferation and its levels possibly reflecting the proliferative nature of AML cells. Indeed, the RNAseq analysis of a large set of AML patients confirmed that AML cells overexpressed SMARCA5 and its levels correlated with many ISWI-complex members including also cohesin complex, and finally, that the proliferative nature of AML cells marked by upregulation of SMARCA5 was supported by a trend in shorter OS albeit only in those AML patients that were marked by cytogenetic aberrations (see Figure 1).

Upon targeting of the SMARCA5 gene in AML cell lines with a CRISPR/Cas9-mediated deletion strategy, we could observe that AML cells lacking SMARCA5 markedly slowed the proliferation rate and became dysplastic with multiple karyotypic abnormalities. Inhibiting SMARCA5 to achieve suppression of AML growth may be thus a very efficient strategy as AML cells that are likely addicted to SMARCA5 in order to overcome various chromatin obstacles such as complex karyotype or also polyploidy often seen during progression of AML. Other data further implicated that SMARCA5 is very important also at the stem cell level to regulate their innate function: to repopulate the progeny. Indeed (as shown by Figure 3), repopulation activities were greatly reduced in normal hematopoietic stem cells in which the *Smarca5* gene was genetically deleted. Our observation, however, does not rule out the possibility of SMARCA5 being an AML target as i) the AML cells are highly proliferating compared to their normal counterparts, and ii) SMARCA5 being expressed in stem cells implicates that antiSMARCA5 therapy would preferentially target the leukemia stem and progenitor cells.

While SMARCA5 expression represents a potential target for AML therapy, it may also serve as a factor of therapeutic resistance in AML. It is likely that additional factors will be involved in modulating therapy efficacy using SMARCA5 inhibitors in the future. As the *Smarca5* loss was sensed in a mouse model by a) increased p53 levels and b) associated with DNA damage response (DDR), and c) activation of the p53 targets [1], very likely the tumor cells with DDR sensing defect would have a higher propensity to tolerate SMARCA5 level downregulation. This notion is supported by our other study demonstrating that proliferation defect imposed by *Smarca5* deficiency can be partly restored with concomitant *Trp53* deletion in murine thymocytes [3].

Our herein presented data indicate that AML growth is dependent on the expression of chromatin remodeling protein SMARCA5 that is a known partner of AML-associated targets: cohesin complex and CTCF [23]. Data presented in Figures 4 and 5 implicate that proliferation inhibition upon SMARCA5 targeting is at least in part caused by karyotype abnormalities, especially cohesion defects, and possibly also by a putative replication defect due to defective chromatin compaction as well as

dysregulation of gene expression pattern of the key hematopoietic lineage restricted transcription factors. Interestingly, the nuclear changes after S5 deletion such as polyploidy were also described in other cell lines of hematologic origin [1,3] but not as a result of *Smarca5* deletion of developing brain or eye lens [4,5]. Similar evidence was noted upon experimental manipulation with cohesin complex members; for example, the nonsense mutations in STAG2 (generated in the THP1 AML cell line) led to defects in sister chromatid cohesion and induced anaphase defects, which resulted in proliferation blockade [25]. Important connections between replication and cohesion have been established in the HeLa tumor cells, in which the interfering with replication affected chromatid cohesion and caused a defect in mitotic progression [26]. Others suggested that cohesion defects depend on a functional mitotic spindle checkpoint in regulating mitotic progression [27]. It seems that the strategy of inhibiting SMARCA5 in AML to block leukemogenesis becomes even more vital as shown recently using inhibitors of SMARCA5 (ED2-AD101) that target the HELICc-DExx domain to release the terminal AML cells into differentiation while sparing normal hematopoiesis in preclinical animal models [28]. Our work also suggests that upon inhibiting SMARCA5-mediated proliferation of AML cells, we also can face the problem of inhibiting proliferation of normal cells. Further work in this respect on experimental animals is under way. An additional strategy to inhibit AML cell growth specifically could be to target the *SMARCA5* exon5 in AML cells by CRISPR/Cas9 as evidenced by the herein presented data. Data from global CRISPR/Cas9 screen identified that SMARCA5 targeting was very efficient and caused cell growth inhibition in several additional AML cell lines (OCI-AML2, OCI-AML3) and also in lymphoma and carcinoma cell lines [21]. Together, our as well as others' data demonstrate that SMARCA5 is a valuable epigenetic target suitable for inhibitor discovery projects and subsequent validation in MDS/AML and potentially also in other types of cancer.

4. Materials and Methods

4.1. CRISPR Vector Design

pX330-Venus (kindly provided by Dr. Bjoern Schuster) produces CRISPR/Cas9 enzyme that cleaves at a specific location based on sequence guide sgRNA defined target sequences in SMARCA5 intron4 (5'-TTCTTACGTTACCCATATACTGG-3') and SMARCA5 intron5 (5'-ATTTATCATATTTTCAGCGATGG-3'). CRISPR/Cas9 enzyme is also fused with fluorescent protein mVenus, that enables selection of successfully transfected clones by FACS sorting. The DNA sequences for the sgRNA SMARCA5 intron4 and sgRNA SMARCA5 intron5 were synthesized by Sigma-Aldrich as four oligonucleotides with modifications at position 1 (to encode a Guanine due to the transcription initiation requirement of the human U6 promoter). These two pairs of complementary oligos were mixed together, boiled at 95 °C for 10 min, and allowed to cool down to RT to hybridize. Double-stranded oligos also designed with complementary BbsI overhangs on 3' and 5' ends were ligated into BbsI linearized pX330-Venus vector using T4 Ligase enzyme (Thermo Fisher Scientific, Waltham, MA, USA). Ligation mixtures were transformed into Subcloning Efficiency DH5 α Competent Cells (Invitrogen, Carlsbad, CA, USA) following the manufacturer's protocol. pX330-Venus sgRNA hSMARCA5 intron4 and pX330-Venus sgRNA hSMARCA5 intron5 were isolated and purified by GenElute HP Plasmid Midiprep kit (Sigma-Aldrich, St. Louis, MO, USA) and correct oligo insertion verified by Sanger sequencing.

4.2. Cell Lines

K562 cells (ATCC, Manassas, Virginia, USA) were cultured in 90% Iscove's Modified Dulbecco's Medium supplemented with 10% fetal bovine serum and 1% penicillin/streptomycin. NB4, SKM-1, and MOLM-13 were cultured in 90% RPMI-1640 medium (Sigma-Aldrich), OCI-M2 in 80% Iscove's Modified Dulbecco's medium (Biosera, Kansas City, MO, USA) at 37 °C and 5% CO₂. The media were supplemented with 10-20% fetal bovine serum (Biosera) and 1% penicillin/streptomycin (Biosera). Cell lines were purchased from DSMZ. Both pX330-Venus sgRNA SMARCA5 intron4 (1 μ g) and

px330-Venus sgRNA SMARCA5 intron5 (1 µg) were transfected into 2.5×10^6 K562 cells using Amaxa Cell Line Nucleofector kit (Lonza, Basel, Switzerland) and 1×10^6 K562 cells using Neon Transfection System 10 µL Kit (Invitrogen). Cells were cultivated for 48 h, Venus-positive cells sorted on BD FACS Aria Fusion and divided to form single cell clones on 96-well plates. DNA from growing clones was used as a template for PCR with the following primers: forward 5'-GAGATGGAGGGCTACACTGTG-3' and reverse 5'-GACATTCCCAAAGTCATCTAGCAG-3'. The resulting amplification produced 1175 bp fragment from wild-type and approximately 632 bp long fragment from CRISPR/Cas9 edited allele of the SMARCA5 gene. Cell smears ($0.5\text{--}1 \times 10^5$ cells) were fixed with methanol and stained with May-Grünwald solution (mixed 1:1 with distilled water, Penta, Limassol, Cyprus) for 5 min and Giemsa-Romanowski solution (mixed 1:13 with distilled water, Penta) for 12 min. Cell Proliferation Reagent WST-1 (Roche, Basel, Switzerland) was used following manufacturer's protocol starting from day 0 with seeding 0.5×10^4 cell/100 µL/well in triplicates and continued by daily measurement of absorbance at 430 nm on microplate reader Infinite 200 PRO (Tecan, Männedorf, Switzerland). Cells were simultaneously counted by Luna Automated Cell Counter (Logos Biosystems, Dongan, South Korea).

4.3. AML Patients and Statistics

RNA-Seq data sets from AML patient samples were previously described including the informed consent and ethical issues [29–31]. Reads were mapped with STAR aligner version 2.7.2d using GRCh37 reference and annotation version 32 from GENCODE (www.genencodegenes.org). Reads were counted using FeatureCounts version 1.6.5, normalized to transcripts per million (TPM) and log2 transformed. Log-rank test was performed in survival analysis, Wilcoxon test was used to assess differences in gene expression.

4.4. Real-Time qPCR

Total RNA from wild-type ($n = 10$) and knockout ($n = 5$) K562 clones was isolated by TRIzol Reagent (Invitrogen) and reverse-transcribed by High Capacity cDNA Reverse Transcription kit (Thermo Fisher Scientific). Quantitative PCR was run in triplicates on LightCycler 480 (Roche) using LightCycler 480 SYBR Green I Master (Roche) and specific primers for human SMARCA5 (forward primer 5'-AACTTACTATCCGTTGGCGATT-3', reverse primer 5'-GGTTGCTTTGGAGCTTTCTG-3') and GAPDH (forward 5'-AGCCACATCGCTCAGACAC-3', reverse primer 5'-GCCCAATACGACCAAATCC-3') gene. Ct values served for fold-change calculation using $2^{-\Delta\Delta C_t}$ equation. Student's *t*-test was used for statistical analysis.

4.5. Western Blot

Wild-type and S5KO K562 clones (1×10^7) were lysed in RIPA Buffer (Sigma-Aldrich) supplemented with protease and phosphatase inhibitors (Roche). Denatured cell lysates were run on 1 mm thick 10% SDS-PAGE gel (40 µg/lane) in Mini-Protean Electrophoresis system (Bio-Rad, Hercules, CA, USA) and semi-dry-blotted onto PVDF membrane (Bio-Rad) using Trans-Blot Turbo transfer system (Bio-Rad). PVDF membrane was blocked for 1 h in 5% nonfat milk in 1x TBS/0.1% Tween-20 and incubated with primary antibodies: Snf2h/ISWI (Bethyl Laboratories Inc., #A301-017A-1, Montgomery, TX, USA) and β-actin (Santa Cruz Biotechnology, #sc-1616-R, Dallas, Texas, USA) overnight at 4 °C. Horseradish peroxidase-conjugated secondary antibodies (anti-rabbit, anti-goat) visualized bands using Pierce ECL Western Blotting substrate (Thermo Fisher Scientific).

4.6. Cytogenetics

Standard cytogenetic methods published previously [10,11] were used for preparation of slides, with few modifications. Briefly, the K562 cells were synchronized with colcemid (10 µl/mL) at 37 °C and hypotonized in 0.075 M KCl for 20 min. The cells were then fixed in three changes of cold Carnoy's fixative (ethanol: glacial acetic acid, 3:1) and dropped onto a slide inclined at an angle of 45 degrees

from a height. The chromosomal preparations were air-dried overnight and stained using 5% Giemsa blue solution (Sigma-Aldrich) prepared in standard Sorenson buffer. Preparations were inspected under a light microscope BX43 (Olympus, Sony, Shinjuku, Japan) with microscope camera Infinity 2-2 (Lumenera, Ottawa, ON, Canada). Selected plates were photographed under a 100x immersion oil objective using software QuickPHOTO CAMERA 3.1 (Olympus).

4.7. Hematopoietic Reconstitution

For hematopoietic reconstitution experiments, 2.5×10^6 fetal liver cells isolated from E13.5 control (Smarca5^{fl/+} Rosa26^{eYFP/+} Vav1-iCRE) and Smarca5-deficient (Smarca5^{fl/-} Rosa26^{eYFP/+} Vav1-iCRE) with C57Bl/6J Ly5.2 background were transplanted into lethally irradiated (7.5 Gy) adult (8 weeks) C57Bl/6J Ly5.1 recipients. After 12 days, the recipients were euthanized, and their bone marrow and spleen were tested for the presence of donor-derived eYFP+ hematopoietic cells using flow cytometry. The antibody panel included CD45.1, CD45.2, c-Kit, Sca1, and lineage cocktail (CD3, B220, Mac-1, Gr-1, Ter119).

4.8. Analysis of S5KO MEF Cells

S5KO MEF cells ($n = 3$) were isolated from E14.5 embryos, in which the *Smarca5* gene contained the LoxP1 sites upstream and downstream of exon5 and also expressed Cre Recombinase-Estrogen receptor fusion protein that translocated into the nucleus upon addition of 4OHT into the cultures for 6 h. Deletion of *Smarca5*-exon5 represents a null allele [2]. Production of stable MEF cells was enabled by concurrent deletion of *Tp53* gene [32]. Gene targeting of the Smarca5^{fllox/fllox} Cre-Esr1 cells upon 4OHT addition was confirmed by previously published detection methods [2]. Analysis of cell proliferation of MEFs was determined by IncuCyte (Sartorius, Göttingen, Germany) that enables analysis in 96 wells under real-time continuous visualization and monitoring.

Author Contributions: CRISPR design and mouse transgenics and writing: T.Z., clone preparation and functional analysis: H.P., MEF cells: T.T., cytogenetics: S.T., IncuCyte: P.T., AML patient data and statistics: P.K. and P.A.G., hematopoietic reconstitution: J.K., supervision and writing: T.S. All authors have read and agree to the published version of the manuscript.

Funding: Specific grants: 18-01687S, 19-03586S, NV19-08-00144, Student grants: GAUK 228316 & SVV 260374/2017, Institutional: UNCE/MED/016, Progres Q26, LM2015040, NPU II LQ1604 (MEYS), OP RDI CZ.1.05/2.1.00/19.0395, CZ.1.05/1.1.00/02.0109 (ERDF, MEYS).

Acknowledgments: We are thankful to Kristina Leblova for technical support.

Conflicts of Interest: The authors declare no conflict of interest

Abbreviations

SMARCA5	SWI/SNF-Related, Matrix-Associated, Actin-Dependent Regulator of Chromatin, Subfamily A, Member 5
SNF2H	Sucrose Nonfermenting Protein 2 Homolog
AML	Acute Myeloid Leukemia
CRISPR	Clustered Regularly Interspaced Short Palindromic Repeats

References

1. Kokavec, J.; Zikmund, T.; Savvulidi, F.; Kulvait, V.; Edelmann, W.; Skoultchi, A.I.; Stopka, T. The ISWI ATPase Smarca5 (Snf2h) Is Required for Proliferation and Differentiation of Hematopoietic Stem and Progenitor Cells. *Stem Cells* **2017**, *35*, 1614–1623. [[CrossRef](#)]
2. Stopka, T.; Skoultchi, A.I. The ISWI ATPase Snf2h is required for early mouse development. *Proc. Natl. Acad. Sci. USA* **2003**, *100*, 14097–14102. [[CrossRef](#)]
3. Zikmund, T.; Kokavec, J.; Turkova, T.; Savvulidi, F.; Paszekova, H.; Vodenkova, S.; Sedlacek, R.; Skoultchi, A.I.; Stopka, T. ISWI ATPase Smarca5 Regulates Differentiation of Thymocytes Undergoing beta-Selection. *J. Immunol.* **2019**, *202*, 3434–3446. [[CrossRef](#)]

4. Alvarez-Saavedra, M.; De Repentigny, Y.; Lagali, P.S.; Raghu Ram, E.V.; Yan, K.; Hashem, E.; Ivanochko, D.; Huh, M.S.; Yang, D.; Mears, A.J.; et al. Snf2h-mediated chromatin organization and histone H1 dynamics govern cerebellar morphogenesis and neural maturation. *Nat. Commun.* **2014**, *5*, 4181. [[CrossRef](#)]
5. He, S.; Limi, S.; McGreal, R.S.; Xie, Q.; Brennan, L.A.; Kantorow, W.L.; Kokavec, J.; Majumdar, R.; Hou, H., Jr.; Edlmann, W.; et al. Chromatin remodeling enzyme Snf2h regulates embryonic lens differentiation and denucleation. *Development* **2016**, *143*, 1937–1947. [[CrossRef](#)]
6. Barisic, D.; Stadler, M.B.; Iurlaro, M.; Schubeler, D. Mammalian ISWI and SWI/SNF selectively mediate binding of distinct transcription factors. *Nature* **2019**, *569*, 136–140. [[CrossRef](#)]
7. Dluhosova, M.; Curik, N.; Vargova, J.; Jonasova, A.; Zikmund, T.; Stopka, T. Epigenetic control of SPI1 gene by CTCF and ISWI ATPase SMARCA5. *PLoS ONE* **2014**, *9*, e87448. [[CrossRef](#)]
8. Morris, S.A.; Baek, S.; Sung, M.H.; John, S.; Wiench, M.; Johnson, T.A.; Schiltz, R.L.; Hager, G.L. Overlapping chromatin-remodeling systems collaborate genome wide at dynamic chromatin transitions. *Nat. Struct. Mol. Biol.* **2014**, *21*, 73–81. [[CrossRef](#)]
9. Goodwin, L.R.; Picketts, D.J. The role of ISWI chromatin remodeling complexes in brain development and neurodevelopmental disorders. *Mol. Cell Neurosci.* **2018**, *87*, 55–64. [[CrossRef](#)]
10. Erdel, F.; Rippe, K. Chromatin remodelling in mammalian cells by ISWI-type complexes—Where, when and why? *FEBS J.* **2011**, *278*, 3608–3618. [[CrossRef](#)]
11. Kadoch, C.; Crabtree, G.R. Mammalian SWI/SNF chromatin remodeling complexes and cancer: Mechanistic insights gained from human genomics. *Sci. Adv.* **2015**, *1*, e1500447. [[CrossRef](#)]
12. Garraway, L.A.; Lander, E.S. Lessons from the cancer genome. *Cell* **2013**, *153*, 17–37. [[CrossRef](#)]
13. Dutta, A.; Sardi, M.; Gogol, M.; Gilmore, J.; Zhang, D.; Florens, L.; Abmayr, S.M.; Washburn, M.P.; Workman, J.L. Composition and Function of Mutant Swi/Snf Complexes. *Cell Rep.* **2017**, *18*, 2124–2134. [[CrossRef](#)]
14. Gigeck, C.O.; Lisboa, L.C.; Leal, M.F.; Silva, P.N.; Lima, E.M.; Khayat, A.S.; Assumpcao, P.P.; Burbano, R.R.; Smith Mde, A. SMARCA5 methylation and expression in gastric cancer. *Cancer Investig.* **2011**, *29*, 162–166. [[CrossRef](#)]
15. Reis, S.T.; Timoszczuk, L.S.; Pontes-Junior, J.; Viana, N.; Silva, I.A.; Dip, N.; Srougi, M.; Leite, K.R. The role of micro RNAs let7c, 100 and 218 expression and their target RAS, C-MYC, BUB1, RB, SMARCA5, LAMB3 and Ki-67 in prostate cancer. *Clinics* **2013**, *68*, 652–657. [[CrossRef](#)]
16. Sheu, J.J.; Choi, J.H.; Yildiz, I.; Tsai, F.J.; Shaul, Y.; Wang, T.L.; Shih Ie, M. The roles of human sucrose nonfermenting protein 2 homologue in the tumor-promoting functions of Rsf-1. *Cancer Res.* **2008**, *68*, 4050–4057. [[CrossRef](#)]
17. Jin, Q.; Mao, X.; Li, B.; Guan, S.; Yao, F.; Jin, F. Overexpression of SMARCA5 correlates with cell proliferation and migration in breast cancer. *Tumour. Biol.* **2015**, *36*, 1895–1902. [[CrossRef](#)]
18. Zhao, X.C.; An, P.; Wu, X.Y.; Zhang, L.M.; Long, B.; Tian, Y.; Chi, X.Y.; Tong, D.Y. Overexpression of hSNF2H in glioma promotes cell proliferation, invasion, and chemoresistance through its interaction with Rsf-1. *Tumour. Biol.* **2016**, *37*, 7203–7212. [[CrossRef](#)]
19. Stopka, T.; Zakova, D.; Fuchs, O.; Kubrova, O.; Blafkova, J.; Jelinek, J.; Necas, E.; Zivny, J. Chromatin remodeling gene SMARCA5 is dysregulated in primitive hematopoietic cells of acute leukemia. *Leukemia* **2000**, *14*, 1247–1252. [[CrossRef](#)]
20. Rosenbauer, F.; Wagner, K.; Kutok, J.L.; Iwasaki, H.; Le Beau, M.M.; Okuno, Y.; Akashi, K.; Fiering, S.; Tenen, D.G. Acute myeloid leukemia induced by graded reduction of a lineage-specific transcription factor, PU.1. *Nat. Genet.* **2004**, *36*, 624–630. [[CrossRef](#)]
21. Behan, F.M.; Iorio, F.; Picco, G.; Goncalves, E.; Beaver, C.M.; Migliardi, G.; Santos, R.; Rao, Y.; Sassi, F.; Pinnelli, M.; et al. Prioritization of cancer therapeutic targets using CRISPR-Cas9 screens. *Nature* **2019**, *568*, 511. [[CrossRef](#)]
22. Law, J.C.; Ritke, M.K.; Yalowich, J.C.; Leder, G.H.; Ferrell, R.E. Mutational inactivation of the p53 gene in the human erythroid leukemic K562 cell line. *Leuk. Res.* **1993**, *17*, 1045–1050. [[CrossRef](#)]
23. Hakimi, M.A.; Bochar, D.A.; Schmiesing, J.A.; Dong, Y.; Barak, O.G.; Speicher, D.W.; Yokomori, K.; Shiekhattar, R. A chromatin remodelling complex that loads cohesin onto human chromosomes. *Nature* **2002**, *418*, 994–998. [[CrossRef](#)]

24. Welch, J.S.; Ley, T.J.; Link, D.C.; Miller, C.A.; Larson, D.E.; Koboldt, D.C.; Wartman, L.D.; Lamprecht, T.L.; Liu, F.; Xia, J.; et al. The origin and evolution of mutations in acute myeloid leukemia. *Cell* **2012**, *150*, 264–278. [[CrossRef](#)]
25. Kim, J.-S.; He, X.; Orr, B.; Wutz, G.; Hill, V.; Peters, J.-M.; Compton, D.A.; Waldman, T. Intact Cohesion, Anaphase, and Chromosome Segregation in Human Cells Harboring Tumor-Derived Mutations in STAG2. *PLoS Genet.* **2016**, *12*, e1005865. [[CrossRef](#)]
26. Leman, A.R.; Noguchi, C.; Lee, C.Y.; Noguchi, E. Human Timeless and Tipin stabilize replication forks and facilitate sister-chromatid cohesion. *J. Cell Sci.* **2010**, *123*, 660–670. [[CrossRef](#)]
27. De Lange, J.; Faramarz, A.; Oostra, A.B.; de Menezes, R.X.; van der Meulen, I.H.; Rooimans, M.A.; Rockx, D.A.; Brakenhoff, R.H.; van Beusechem, V.W.; King, R.W.; et al. Defective sister chromatid cohesion is synthetically lethal with impaired APC/C function. *Nat. Commun.* **2015**, *6*, 8399. [[CrossRef](#)]
28. Kishtagari, A.N.; Jarman, C.; Tiwari, A.D.; Phillips, J.G.; Schuerger, C.; Jha, B.K.; Sauntharajah, Y. A First-in-Class Inhibitor of ISWI-Mediated (ATP-Dependent) Transcription Repression Releases Terminal-Differentiation in AML Cells While Sparing Normal Hematopoiesis. *Blood* **2018**, *132*, 216. [[CrossRef](#)]
29. Herold, T.; Jurinovic, V.; Batcha, A.M.N.; Bamopoulos, S.A.; Rothenberg-Thurley, M.; Ksienzyk, B.; Hartmann, L.; Greif, P.A.; Philippou-Massier, J.; Krebs, S.; et al. A 29-gene and cytogenetic score for the prediction of resistance to induction treatment in acute myeloid leukemia. *Haematologica* **2018**, *103*, 456–465. [[CrossRef](#)]
30. Stief, S.M.; Hanneforth, A.L.; Weser, S.; Mattes, R.; Carlet, M.; Liu, W.H.; Bartoschek, M.D.; Dominguez Moreno, H.; Oettle, M.; Kempf, J.; et al. Loss of KDM6A confers drug resistance in acute myeloid leukemia. *Leukemia* **2020**, *34*, 50–62. [[CrossRef](#)]
31. Batcha, A.M.N.; Bamopoulos, S.A.; Kerbs, P.; Kumar, A.; Jurinovic, V.; Rothenberg-Thurley, M.; Ksienzyk, B.; Philippou-Massier, J.; Krebs, S.; Blum, H.; et al. Allelic Imbalance of Recurrently Mutated Genes in Acute Myeloid Leukaemia. *Sci. Rep.* **2019**, *9*, 11796. [[CrossRef](#)] [[PubMed](#)]
32. Jacks, T.; Remington, L.; Williams, B.O.; Schmitt, E.M.; Halachmi, S.; Bronson, R.T.; Weinberg, R.A. Tumor spectrum analysis in p53-mutant mice. *Curr. Biol.* **1994**, *4*, 1–7. [[CrossRef](#)]







© 2020 by the authors. Licensee MDPI, Basel, Switzerland. This article is an open access article distributed under the terms and conditions of the Creative Commons Attribution (CC BY) license (<http://creativecommons.org/licenses/by/4.0/>).

4.4 (4. publikace) Chromatin Remodeler Smarca5 Is Required for Cancer-Related Processes of Primary Cell Fitness and Immortalization.

Article

Chromatin Remodeler Smarca5 Is Required for Cancer-Related Processes of Primary Cell Fitness and Immortalization

Shefali Thakur ^{1,2,3} , Vincent Cahais ¹, Tereza Turkova ³, Tomas Zikmund ^{3,4} , Claire Renard ¹, Tomáš Stopka ³ , Michael Korenjak ^{1,*} and Jiri Zavadil ^{1,*} 

- ¹ Epigenomics and Mechanisms Branch, International Agency for Research on Cancer, World Health Organization, 69008 Lyon, France; thakurs@iarc.fr (S.T.); cahaisv@iarc.fr (V.C.); renardc@iarc.fr (C.R.)
- ² Faculty of Science, Charles University, 128 43 Prague, Czech Republic; thakurs@iarc.fr (S.T.)
- ³ Biocev, First Faculty of Medicine, Charles University, 252 50 Vestec, Czech Republic; tereza.turkova@lf1.cuni.cz (T.T.); tomas.zikmund@helmholtz-muenchen.de (T.Z.); tomas.stopka@lf1.cuni.cz (T.S.)
- ⁴ Institute of Epigenetics and Stem Cells (IES), Helmholtz Zentrum, D-81377 München, Germany; tomas.zikmund@helmholtz-muenchen.de (T.Z.)
- * Correspondence: korenjakm@iarc.fr (M.K.); zavadilj@iarc.fr (J.Z.)



Citation: Thakur, S.; Cahais, V.; Turkova, T.; Zikmund, T.; Renard, C.; Stopka, T.; Korenjak, M.; Zavadil, J. Chromatin Remodeler Smarca5 Is Required for Cancer-Related Processes of Primary Cell Fitness and Immortalization. *Cells* **2022**, *11*, 808. <https://doi.org/10.3390/cells11050808>

Academic Editor: Alexandra Lusser

Received: 17 December 2021

Accepted: 22 February 2022

Published: 25 February 2022

Publisher's Note: MDPI stays neutral with regard to jurisdictional claims in published maps and institutional affiliations.



Copyright: © 2022 by the authors. Licensee MDPI, Basel, Switzerland. This article is an open access article distributed under the terms and conditions of the Creative Commons Attribution (CC BY) license (<https://creativecommons.org/licenses/by/4.0/>).

Abstract: Smarca5, an ATPase of the ISWI class of chromatin remodelers, is a key regulator of chromatin structure, cell cycle and DNA repair. Smarca5 is deregulated in leukemia and breast, lung and gastric cancers. However, its role in oncogenesis is not well understood. Chromatin remodelers often play dosage-dependent roles in cancer. We therefore investigated the epigenomic and phenotypic impact of controlled stepwise attenuation of Smarca5 function in the context of primary cell transformation, a process relevant to tumor formation. Upon conditional single- or double-allele *Smarca5* deletion, the cells underwent both accelerated growth arrest and senescence entry and displayed gradually increased sensitivity to genotoxic insults. These phenotypic characteristics were explained by specific remodeling of the chromatin structure and the transcriptome in primary cells prior to the immortalization onset. These molecular programs implicated Smarca5 requirement in DNA damage repair, telomere maintenance, cell cycle progression and in restricting apoptosis and cellular senescence. Consistent with the molecular programs, we demonstrate for the first time that Smarca5-deficient primary cells exhibit dramatically decreased capacity to bypass senescence and immortalize, an indispensable step during cell transformation and cancer development. Thus, Smarca5 plays a crucial role in key homeostatic processes and sustains cancer-promoting molecular programs and cellular phenotypes.

Keywords: Smarca5; Snf2h; cell immortalization; cell cycle; homologous recombination; non-homologous end-joining; senescence; ATAC-seq; RNA-seq; MEF

1. Introduction

Chromatin remodeling is a quintessential step for all DNA-associated core cellular processes, many of which determine key cell fate decisions, including those implicated in cancer onset and evolution [1]. The role of chromatin remodeling in cell transformation and cancer development has been of increasing interest over the last decade [2–5], and various chromatin remodelers have been intimately linked to carcinogenesis [6–12]. Findings from large-scale epigenomics and transcriptomics studies highlight the frequent mutation or deregulation of chromatin remodelers in cancer [8,13], suggesting that aberrant chromatin remodeling plays an important role in cancer development. Four major classes of chromatin remodelers are described [14], each containing a conserved core Snf2 helicase [15] that uses the energy from ATP hydrolysis to disrupt the contacts between histones and DNA [16,17]. One such ATPase, belonging to the highly conserved ISWI family of chromatin remodelers, is Smarca5 [18]. It plays an important role in nucleosome assembly and spacing and

contributes to processes involved in cell fate decisions, including DNA replication [19], repair [20–22] and transcription via all three classes of RNA polymerase [23].

Smarca5 is frequently overexpressed in different cancer types, including glioma [24], leukemia [25], breast [26,27] and gastric [28] cancer. In contrast, *Smarca5* loss in cancer cell lines (by depletion using siRNA) [29] and in murine hematopoietic, progenitor cells [30] as well as murine oocytes [31] using complete knockout has been shown to negatively impact cell proliferation [29,30]. *Smarca5* deletion is embryonically lethal in mice and the derived embryonic cells [32]. Loss of *Smarca5* also impacts sensitivity to radiation exposure [33] and gene expression of DNA repair genes [24,30]. It also causes chromosomal aberrations [34], indicative of genomic instability [35]. Hence, *Smarca5* has a major impact on pathways involved in cell transformation, cancer development and evolution. However, these changes have not been investigated and reported in terms of *Smarca5* dosage variation and may provide important insights into its function. This is particularly relevant because chromatin remodelers often have a dosage-sensitive role in the genesis of human cancer [8]. To address this, we assessed for the first time the effects of gradual *Smarca5* decrease in a model of primary cell immortalization based on primary mouse embryonic fibroblasts (MEFs) using single and double allele knockout. The rationale for using this model is two-tiered. Firstly, the consequences of *Smarca5* knockout or knockdown are frequently studied in transformed cell lines [29,36], which are not ideal for studying the early stages of cell transformation. In addition, available knowledge on *Smarca5* molecular targets and functions in primary cells comes from embryonic stem cells [37,38] in the context of development and not oncogenic cell transformation. Primary MEFs are a validated model for investigating early steps of cell immortalization and transformation via cellular senescence bypass, during which they closely recapitulate molecular programs and events observed in human cancers [39–43]. Secondly, due to the pronounced effects of complete *Smarca5* loss on phenotype, it is challenging to dissect phenotypic and molecular alterations caused by *Smarca5* loss from changes observed due to compromised cellular fitness in the double-knockout cells. Thus, focusing only on the molecular and phenotypic changes common to both single and double allele knockout cells can overcome this issue. Using massively parallel sequencing, we studied the effects of gradual loss of *Smarca5* on global chromatin accessibility and gene expression programs, two key processes controlled by *Smarca5* [23,44,45]. *Smarca5* loss in the primary cells affected gene regulation programs involving DNA damage repair, DNA replication, telomere maintenance, chromosomal segregation, apoptosis and cell aging. Complementing the gene regulation analyses, functional studies of the cell phenotype outcomes upon *Smarca5* loss revealed increased susceptibility of the primary cells to chemical mutagens and severely decreased cell immortalization potential. By integrating comprehensive analyses at the molecular as well as phenotypic levels, our study delineates the critical role of *Smarca5* in primary cell fitness and the early stages of the cancer-like process of primary cell immortalization, characteristics relevant to cancer onset and evolution.

2. Materials and Methods

2.1. Genetically Modified Mice

Smarca5^{fl} allele contains two loxP1 sites flanking the exon 5 of the *Smarca5* gene. Cre mediated recombination of *Smarca5*^{fl} allele causes removal of the region critical for enzymatic activity of *Smarca5* as well as produces a frameshift mutation resulting in disruption of *Smarca5* protein expression. *Smarca5*^{fl} was produced in our laboratory as previously described [30]. The murine strain expressing a tamoxifen-inducible Cre Recombinase-Estrogen receptor (Cre-Esr1) fusion protein [B6.Cg-Tg(CAG-cre/Esr1*)5Amc/J, Stock No: 004682] was purchased from The Jackson Laboratory (Bar Harbor, ME, USA) [46]. The reporter R26-stop-EYFP strain [B6.129X1-Gt(ROSA)26Sortm1(EYFP)Cos/J, Stock No: 006148] was kindly provided by Dr. Vladimir Korinek. Mice were maintained in individually ventilated cages with unlimited supply of water and food as well as regular bedding exchange. All experiments met criteria approved by Czech ministry of agricul-

ture and committee for experimental animals. For the genotyping of mice, we isolated genomic DNA from tail tips and performed PCR using Sapphire Amp Fast PCR Master Mix (RR350A, Takara Bio, Kusatsu, Shiga, Japan) with following primers: S5fl-fwd: 5'-ACTGAGGACTCTGATGCAAACAGTCAAG-3', S5fl-rev: 5'-TACACAACAAAGGCAGTGGTTATAGTGC-3', S5del-fwd: 5'-GTGCAAAGCCCAGAGACGATGGTATG-3' (with S5fl-rev, for identification Cre recombined S5fl allele), Cre-fwd: 5'-ACCAGGTTTCGTTCACTCATGG-3', Cre-rev: 5'-ACGGGCACTGTGTCCAGACC-3', EYFP-fwd: 5'-AAGACCGCGAAGAGTTTGTC-3', EYFP-rev: 5'-AAAGTCGCTCTGAGTTGTTAT-3'.

2.2. Mouse Embryonic Fibroblast Isolation and Maintenance

Smarca5^{fl} mice were crossed with Cre-Esr1 and R26-stop-EYFP strains to obtain parental lineages with suitable genotypes for following breeding and MEF isolation. Pregnant female mice at 14th day post-coitum were sacrificed, washed with 70% ethanol and transferred into flow box. From each mouse, both uterine horns were isolated, quickly washed with 70% ethanol and placed into Petri dish with PBS. Embryos were separated from placenta and extra-embryonic tissues and then transferred into 12-well plate. Head and organs of each embryo were carefully removed and used for genomic DNA isolation and genotyping. The rest of the body was washed in PBS, finely minced using razor blade and incubated with 1 mL 0.05% trypsin/0.02%EDTA/DNase I (100U) solution for 15–20 min at RT in 35 mm sterile dishes. After the embryonic tissue was dissociated, the resulting cell suspension was resuspended in MEF culture medium (DMEM containing 4.5 g/L glucose without phenol red supplemented with 10% FBS, 1% Penicillin-Streptomycin, 1% non-essential amino acids, 2 mM L-glutamine). The suspension from each embryo was individually plated to the 0.2% gelatin-coated 10-centimeter petri dish and incubated at 37 °C, 5% CO₂. After the fibroblasts were attached to the surface of the culture dish (within approximately 30–60 min), they were washed twice with warm PBS and cultured in MEF medium in incubator until they reached 80% confluence. All fibroblast cultures were then frozen in MEF medium containing 20% FBS and 10% DMSO and kept in liquid nitrogen until the genotyping results were known. Since Cre-Esr1 fusion construct is activated by presence of phenol red in culture media, the MEF cells were strictly maintained in media without this dye.

2.3. Cell Culture

MEFs were grown in DMEM culture medium without phenol red (Sigma-Aldrich, St. Louis, MO, USA). Cell count and viability were measured using trypan blue staining and Bio-Rad TC20 automated cell counter. For conditional deletion of *Smarca5^{fl}* allele, 4-Hydroxytamoxifen (4-OHT) (100 nM final, H6278, Sigma-Aldrich) was added for 6 h into the medium. Successful activation of the Cre-Esr1 fusion protein was verified by comparing EYFP positivity of 4-OHT treated and untreated cells using a CytoFLEX flow cytometer (Beckman Coulter, Brea, CA, USA). *Smarca5^{fl}* allele deletion in the Cre-Esr1 activated cells was analyzed by PCR from genomic DNA using S5del-fwd and S5fl-rev primers.

2.4. Immunoblotting

MEFs were collected, washed with PBS and lysed 30 min in lysis buffer (150 mM NaCl, 50 mM Tris-Cl pH 7.5, 0.4% Triton-X, 2 mM CaCl₂, 2 mM MgCl₂, 1 mM EDTA, 5 mM NaF in dH₂O) supplemented with 1 mM DTT, protease (TPCK, TLCK, PMSF) and phosphatase inhibitors (Na₃VO₄) and 25U/μL non-specific DNA nuclease (Benzonase; SC-391121, Santa Cruz Biotechnology; Dallas, TX, USA) on ice. After 30 min, 2% SDS solution was added into each lysate in 1:1 ratio (final conc. of SDS 1%) and tubes containing protein lysates were heated for 5 min at 95 °C. Protein lysates were then cleared by centrifugation at 16,000 × g, 10 min, 4 °C and subjected to bicinchoninic acid assay (Thermo Fisher; #23228, Waltham, MA, USA) in order to determine total protein concentration. 20 μg of the protein was resolved on SDS gradient 4–15% Mini-PROTEAN TGX Precast Protein gels (Bio-Rad Laboratories, Basel, Switzerland) and semi-dry transferred by Trans-Blot Turbo Transfer

System (Bio-Rad Laboratories) using manufacture's settings to PVDF membrane (Bio-Rad Laboratories; #162-0177). Primary antibodies used were anti-Smarca5 (1:1000; Bethyl Laboratories; A301-017A, Montgomery, TX, USA), anti-p21 (1:1500; SC-6246; Santa Cruz Biotechnology, Dallas, TX, USA) and anti-GAPDH (1:2500; Sigma-Aldrich; HPA040067). After overnight incubation with primary antibody, membranes were washed 3×10 min with TBST and stained 1h with peroxidase-conjugated donkey Anti-Rabbit IgG secondary antibody (1:10,000; ab20662; Abcam, Cambridge, UK) for anti-Smarca5, donkey Anti-Rabbit IgG secondary antibody (1:10,000; 711-036-152; Jackson ImmunoResearch, Ely, UK) for anti-GAPDH and donkey Anti-Mouse IgG secondary antibody (1:10,000; 715-036-150; Jackson ImmunoResearch) for anti-p21 primary antibody. Protein signal was visualized using Pierce™ ECL Western Blotting Substrate (Thermo Fisher; #PI32106) and detected and quantified with the ChemiDoc Imaging System (Bio-Rad Laboratories).

2.5. Detection of Cellular Senescence

MEFs were plated in 35-millimeter well plates and cultured as described above. The senescence detection was carried out for each studied cKO genotype between 96 h and passages 7–9 when the cells exhibited typical senescent morphology (enlarged cell size, doubled nuclei), by using the Cellular Senescence Assay Kit (Merck; KAA002, Darmstadt, Germany) which detects the pH-dependent senescence-associated β -galactosidase (SA- β -gal) activity. The resulting blue cell staining was recorded by brightfield microscopy (Primovert, Zeiss, Jena, Germany)/digital photography. The standard manufacturer's (Merck; KAA002, Darmstadt, Germany) protocol and instructions were used without any modifications.

2.6. ATAC-Sequencing and Data Analysis

The cells were harvested four days after induction with 4-OHT and ATAC was performed on 7.5×10^4 cells, in replicate for each condition, using a previously established protocol [47]. Transposase enzyme and Illumina compatible primers and barcodes for multiplexing were used as described earlier [48]. Multiplexed libraries were sequenced as 75 bp paired-end reads on the Illumina NextSeq 500 sequencer. Reads in FASTQ files were analyzed for data amount and quality using FastQC (v0.11.9) and trimmed with Trim Galore (cutadapt 0.6.4_dev, <https://github.com/FelixKrueger/TrimGalore> (accessed on 24 September 2019)), then mapped on the mouse mm10 genome using the Burrows–Wheeler Aligner (0.7.15) [49]. Duplicate reads were flagged by sambalster (v0.1.24) [50], and the aligned reads further underwent base quality score recalibration and indel realignment with the corresponding tools from GATK (v3.8) [51]. The Nextflow pipeline used is available at <https://github.com/IARCBioinfo/alignment-nf>. An average of 44 million reads was sequenced per sample. Model-based analysis of ChIP-seq (MACS2) [52] was used to call peaks within each sample, and a reproducible set of peaks between duplicates was defined with IDR [53] (irreproducible discovery rate). These sets were used as input for the DiffBind R/bioconductor package (Differential binding analysis of ChIP-Seq peak data), in which they are merged and reduced to the same size (200 bp on each side from the summit). Reads are counted in each sample for each peak of this global peak set, and this count is normalized with DESeq2 (Differential gene expression analysis based on the negative binomial distribution) native normalization method (referred to as DBA_NORMALIZATION_RLE in DiffBind).

ATAC-seq peaks were annotated according to their genomic location (500 bp, 2 kb or 10 kb upstream of transcription start site (TSS), within gene body and/or overlapping exons) based on GENECODE annotation [54], with closest gene name (from peak center to TSS), replication timing information [55] (<https://www2.replicationdomain.com/index.php>, accessed on 5 October 2021) and candidate cis-regulatory element information [56] (<https://screen.encodeproject.org/>, accessed on 3 February 2021) including histone mark and CTCF binding information. Peaks were assigned to genes as described by Iurlaro et al. [37], except only the capture Hi-C interactions [57] common to both embryonic stem cells

and fetal liver cells were used, assuming that promoter interactions common to both the pluripotent and the committed fetal cells are non-cell-of-origin specific and thus likely to be more relevant to MEFs than those exclusive to either of them. Using this approach, we assigned about 60% of the identified ATAC-peaks to genes.

2.7. Motif Analysis

Fold-change was calculated for differentially accessible ATAC peaks by dividing the average normalized count for the single or double allele knockout by the average of the normalized count for the corresponding wildtype. The MOTif aNalysis with Lisa (monaLisa) suite [58] (<https://fmicompbio.github.io/monaLisa/articles/monaLisa.html>, accessed on 14 January 2022) was used to group the genomic regions into five bins based on fold-change assigned to each region for the single and the double allele knockout individually. Motif enrichments were then calculated for each bin and stability selection-based regression approach was used to predict binding preferences of transcription factors or nucleic acid binding proteins using min.score cutoff (=10) for motif detection.

2.8. RNA-Sequencing and Data Analysis

Experiment was performed in duplicates. 1×10^6 cells were resuspended in Trizol and RNA was extracted using phenol-chloroform extraction [59]. RNA quality was assessed using Agilent TapeStation 4200 and all samples exhibited RNA Integrity Number (RIN) of 9.5 or higher. RNA libraries were prepared using KAPA Stranded RNA-seq kit with KAPA RiboErase (HMR) kit (Roche, Basel, Switzerland) to deplete rRNA. Multiplexed samples were sequenced as 75 bp paired-end reads on the Illumina NextSeq 500 sequencer. Reads were trimmed and aligned against the mm10 genome build with STAR; then the read number per gene per sample was counted with htseq-count (using the Nextflow pipeline described in <https://github.com/IARCbioinfo/RNAseq-nf>, accessed on 18 February 2020). An average of 34 million reads was sequenced per sample. The read count was normalized using the normalization method based on median of ratios, i.e., counts divided by sample-specific size factors determined by median ratio of gene counts relative to geometric mean per gene, embedded in DESeq2 R/Bioconductor package [60].

2.9. Differential Analysis of ATAC Accessibility Domains and Gene Expression

The globally normalized value matrices for both ATAC-seq and RNA-seq data were further normalized by dividing the average values of the two Smarca5-deficient replicates by the average of their respective wild-type baseline values, followed by \log_2 transformation. The gradual differential changes from the single to the double allele knockout were identified using Pavlidis Template Matching (PTM) analysis tool [61] within the TMeV suite [62,63]. PTM allows statistically significant matching of the experimentally obtained data profiles to predefined profile templates. In the used PTM settings, the wild-type for each condition was treated as baseline with a value of 0.5 (a midpoint between the minimum of 0 and maximum of 1). For ATAC-seq, the gradual changes were probed based on a template following the Smarca5 genotype (allele) increments (100% to 50% to 0%) with a p -value of 0.025, i.e., for the downregulated genes, the single allele knockout was set at 0.25 and the double allele knockout was set at 0. Following this logic, for the upregulated peaks or genes, the single allele knockout was set at 0.75 and the double allele knockout was set at 1. The differential gene expression changes were probed based on both genotype and protein levels (100%–Wild-type to 69.8%–single allele knockout to 17.4%–double allele knockout; see Figure 1C) with a template matching p -value of 0.05.

2.10. One-Way-ANOVA

A one-way ANOVA was also performed for the four replicate experimental groups (two knockout types and their corresponding wildtype samples) at p -value of 0.05 (alpha settings). The common events from PTM for the gradual upregulation based on genotype were subtracted from the resulting ANOVA-identified gene list. The same was done

for downregulated genes based on genotype to obtain an ANOVA exclusive gene list comprising of residual reproducibly modulated genes that follow patterns not overlapping with those corresponding to the gradual increase or decrease along with the shift from the single-allele to the double-allele knockout.

2.11. Pathway and Network Analysis

A union of the genotype and protein-level based differential expression gene lists obtained by PTM was created. Upregulated and downregulated genes were individually analyzed by the functional annotation tool of DAVID v6.8 [64]. Deregulated and differentially regulated genes were probed for gene ontology (GO BP, GO MF, GO CC) and functional annotations with an EASE score of 0.1. Differentially regulated genes were overlapped with custom-built lists of cancer drivers or epigenetic regulator genes (ERGs) [13]. We curated the cancer driver gene list by combining information from Cancer Gene Census [65], IntOgen database [66] and Cancer drivers as defined by Bailey et al. [67]. The derived list was converted to orthologous mouse genes using Ensembl BioMart (<https://www.ensembl.org/biomart/martview/>, accessed on 20 April 2021). Network analysis using GeneMANIA [68] was performed on the deregulated cancer drivers and ERGs using the tool's default parameters. From the available GeneMANIA network categories [68], interactions based on co-expression, physical interaction (based on protein-protein interaction data), genetic interaction and co-localization were included. In addition, when sufficient interactions were not available for these mentioned network categories, predicted interactions were included.

2.12. MTS Assay

Cells were plated in 96-well plates in triplicates and exposed to a range of doses of aristolochic acid-I (AA) for 24 h and methylnitronitrosoguanidine (MNNG) for 2 h. Metabolic activity of the cultures, as a proxy for cell viability, was measured using CellTiter 96 AQueous One Solution Cell Proliferation Assay (Promega, Fitchburg, WI, USA). Plates were incubated for 2 h at 37 °C and absorbance was measured at 492 nm. The percentage of viable cells in the carcinogen-exposed cultures was expressed relative to that of unexposed control cells, which was set to 100%.

2.13. Senescence Bypass and Immortalization

Twenty-five independent MEF cultures (T75 flasks) for each of the 4 conditions, i.e., 4-OHT induced and the corresponding un-induced wild-type cells, were cultured until the cells underwent growth arrest and cellular senescence. Cell count and viability were measured using trypan blue staining and Bio-Rad TC20 automated cell counter. This period of cellular senescence typically lasts several weeks [40]. Senescence onset and bypass were assessed by plotting growth curves for each culture, as population doublings against number of days in culture [69]. This extensive experiment was repeated and validated twice more using ten and six independent MEF cultures for each condition, respectively.

3. Results

3.1. Loss of *Smarca5* Deregulates Global Chromatin Accessibility and Gene Expression

The *Smarca5* double allele knockout has profound phenotypic effects [30]; therefore, we developed single allele knockout MEFs to allow us to inspect dosage-specific molecular and phenotypic changes associated with gradual *Smarca5* loss. Floxed *Smarca5* single ($cS5^{fl/wt}$) and double allele ($cS5^{fl/fl}$) MEFs (Figure 1A), in conjunction with conditional Cre-mediated recombination, were used to generate a *Smarca5* frame-shift null mutation [30] upon induction with 4-OHT. The same cells without the 4-OHT induction were used as corresponding wild-type controls. The *Smarca5* deletion status of the MEFs was confirmed by PCR and flow cytometry (Figure 1B,D and Supplementary Figure S1A). We assessed the *Smarca5* protein levels by immunoblotting and observed about 17% of residual protein in double allele knockout cells in the bulk culture compared to the wild-type samples 96 h

after deletion. The single allele knockout cells expressed about 70% of residual protein at the same time point (Figure 1C). Thus, the conditional knockout MEFs exhibited a gradual decrease in gene and protein dosage from wild type to single and single to double allele knockout cells. Since *Smarca5* protein levels in the double allele knockout cells are largely diminished 96 h after induction of deletion, we investigated genome-wide molecular changes four days after the knockout (Supplementary Figure S1B). At this time point, the knockout cells remain mostly viable (>90% viability).

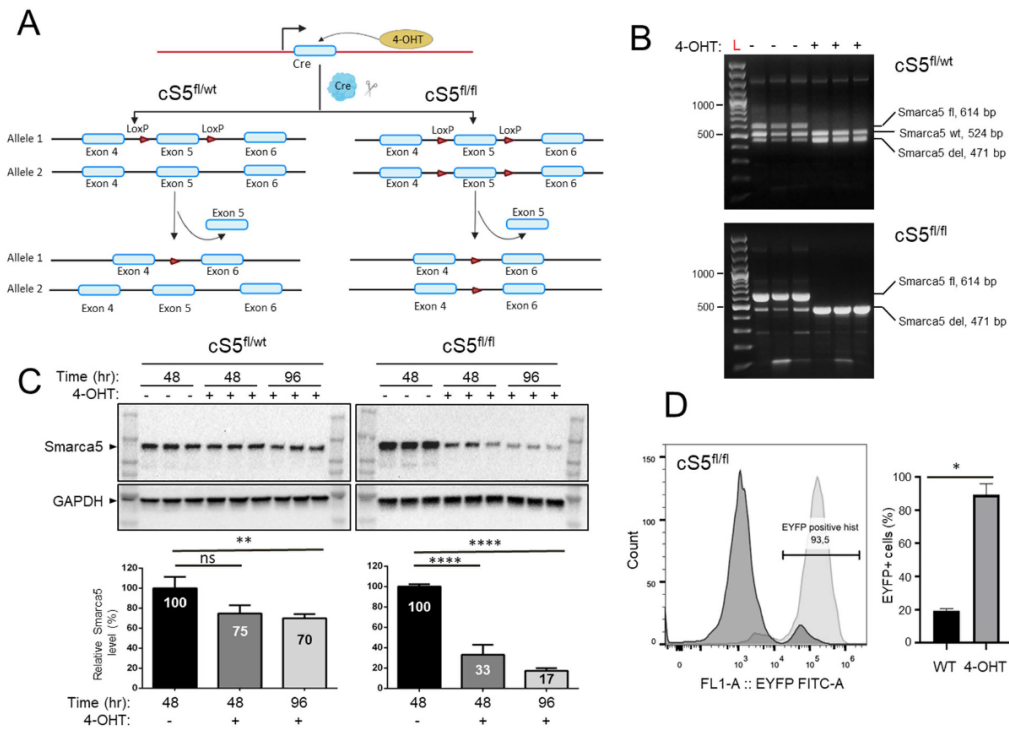


Figure 1. Characterization of the *Smarca5* deletion system. (A) Schematics of the *Smarca5* conditional knockout cassette. The cS5^{fl/fl} cells have the exon 5 of both *Smarca5* alleles floxed, while cS5^{fl/wt} MEFs have a single floxed *Smarca5* allele. The floxed allele(s) is excised upon 4-hydroxytamoxifen (4-OHT) addition. Some elements of the figure were created using BioRender.com. (B) Genotyping of the MEFs to confirm *Smarca5* deletion status using PCR. The wildtype *Smarca5* allele, the floxed allele and the allele with the exon 5 deletion differ in size and can thus be differentiated from each other, revealing the cell identity. DNA was isolated from cells 48 h after adding 4-OHT. Genotyping was done in biological triplicates, each line represents MEF cell line isolated from different embryos with CreER cS5^{fl/fl} or CreER cS5^{fl/wt} genotype. The low-representation bands below 300 bp are non-specific background amplicons. (C) Immunoblots (in the same triplicates used for genotyping) for anti-Smarca5 antibody reveal protein level depletion over time (48 h and 96 h) in the 4-OHT induced, *Smarca5* knockout MEFs compared to control without 4-OHT. A gradual protein level depletion is observed over time. (D) Confirmation of Cre-activation upon 4-OHT administration as assessed by expression of the EYFP, 96h after induction. Experiments were done in triplicates, MEF isolated from 3 embryos with CreER^{+/-} cS5^{fl/fl} EYFP^{+/+} genotype. Percent of cells expressing EYFP indicate percent of cells that are also positive for *Smarca5* knockout. Dark curve represents cells without 4-OHT and light curve represents same MEFs 96 h after 4-OHT induction, WT/4-OHT = untreated/treated with 4-OHT. ns = $p > 0.05$; * = $p \leq 0.05$; ** = $p \leq 0.01$; **** = $p \leq 0.0001$.

To study the effects of loss of chromatin remodeler Smarca5 on global chromatin accessibility, we used ATAC-seq, a technique that allows genome-wide identification of accessible

sites using a hyperactive transposase [48]. RNA-seq was used in parallel to assess gene expression changes, another key process controlled by Smarca5 [45]. We first inspected the obtained ATAC-seq and RNA-seq data for quality and reproducibility between replicates (Supplementary Figure S1C,D) and then performed differential peak calling and expression analysis on the datasets. All described analyses were carried out specifically considering the gradually decreasing Smarca5 doses between single and double knockout cells, i.e., only those differential changes in chromatin accessibility and gene expression that manifested in the same direction (up or down) in both genotypes and reflected the gradual change of Smarca5 doses (smaller differential change in single allele knockout, larger differential change in double allele knockout) were considered for interpretation. This strategy not only minimized the inclusion of changes attributable to compromised cellular fitness observed in the double allele knockout MEFs but also allowed us to focus on molecular changes that are Smarca5 dosage-dependent. For RNA-seq, the directional analysis was carried out using either genotypic (Supplementary Tables S1 and S2) or protein-based dosage determined in Figure 1C (Supplementary Tables S3 and S4) (see Section 2). A one-way ANOVA was also performed to identify all statistically meaningful differential changes, from which the above-mentioned genotypic dosage-dependent changes were subtracted. This resulted in an additional 805 differentially expressed genes that are provided in the Supplementary Materials (Supplementary Table S5). These genes, however, had a distinct and varied profile behavior and were thus not considered and biologically interpreted in association with targeted probing of Smarca5 dosage-dependent molecular programs.

ATAC-seq analysis revealed thousands of regions following a dosage-specific pattern of either increased (Figure 2A, Supplementary Table S6) or decreased chromatin accessibility (Figure 2C and Supplementary Table S7). We noticed a slightly higher number of regions that gained accessibility (higher accessibility sites: HAS) compared to those with decreased accessibility (lower accessibility sites: LAS). Motif analysis of LASs with the highest fold-change revealed enrichment of, among others, the CTCF and FOS::JUN motifs in the single allele knockout cells (Supplementary Figure S2, Bin1). This is in keeping with the established role of Smarca5 in facilitating CTCF chromatin binding [45]. Interestingly, LASs with the highest fold-change in the double allele knockout show enrichment for only FOS::JUN binding motifs (Supplementary Figure S3, Bin1), indicative of increased deregulation of cell proliferation and stress response [70,71] with stepwise loss of Smarca5. Differential gene expression analysis on the replicates also revealed more than a thousand genes exhibiting gradual deregulation (up- or downregulation) (Figure 2B,D and Supplementary Tables S1–S4). These findings indicate massive chromatin and transcriptomic remodeling following the loss of Smarca5.

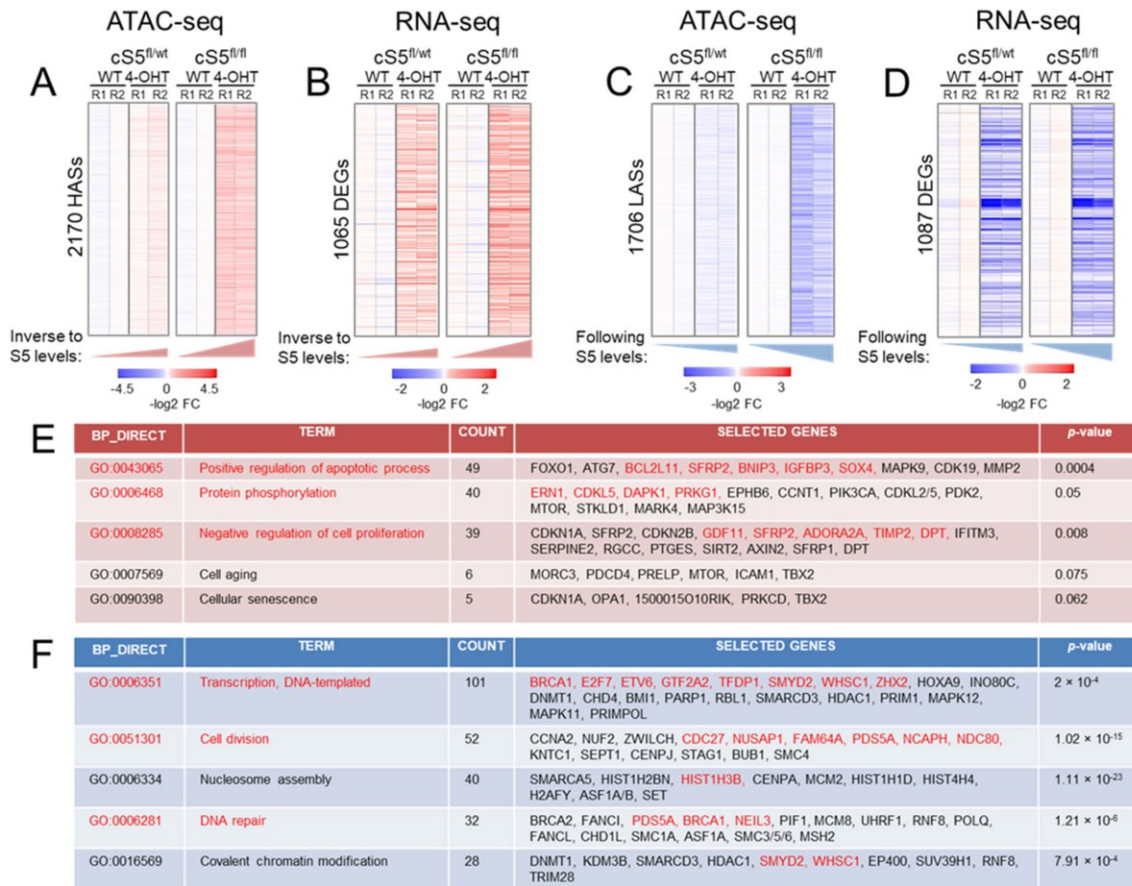


Figure 2. Epigenomic and transcriptomic remodeling upon the gradual loss of Smarca5. (A) Heatmap showing differentially accessible ATAC peaks displaying higher accessibility in the knockout cells, p -value ≥ 0.025 . Notice the gradual increase in accessibility from the single allele knockout ($cS5^{fl/wt}$, 4-OHT) to the double allele knockout ($cS5^{fl/fl}$, 4-OHT) compared to their respective wildtypes (WT), HASs = higher accessibility sites. (B) Heatmap showing gradually upregulated genes from single to double-allele knockout MEFs, p -value ≥ 0.05 . DEGs = differentially expressed genes. Notice the gradual increase in gene expression from $cS5^{fl/wt}$, 4-OHT to the $cS5^{fl/fl}$, 4-OHT compared to their respective wildtypes. (C) Heatmap showing differentially accessible ATAC peaks displaying lower accessibility in the knockout cells, p -value ≥ 0.025 . Notice the gradual decrease in accessibility from the single allele knockout to the double allele knockout. LASs = lower accessibility regions. (D) Heatmap showing the gradually downregulated genes in the knockout cells, p -value ≥ 0.05 . (E) Gene Ontology pathways (GO) in upregulated genes as interrogated by DAVID. Text in red shows events (pathways/genes) common in both chromatin accessibility and gene expression dataset as inspected by ATAC-seq and RNA-seq. (F) GO pathways in downregulated genes as interrogated by the DAVID tool (human orthologue gene symbols are shown as a default output of DAVID). Text in red font shows events (pathways/genes) common to both chromatin accessibility and gene expression datasets. WT = cells untreated with 4-OHT; \log_2 FC = \log_2 -transformed fold-change from the WT baseline condition; R1, R2 = experimental replicates 1 and 2.

3.2. Loss of Smarca5 in Primary Cells Leads to Dosage-Specific Deregulation of Pathways Involved in Cell Proliferation and Genomic Stability

To better understand the biological pathways affected by this major Smarca5 dosage-specific transcriptional reprogramming, a union of gradually deregulated genes based on the gene and protein dosage (see Section 2) was interrogated for Gene Ontology (GO)

attributions. This analysis revealed marked enrichment of gradually downregulated genes, from single to double allele knockout, involved in various aspects of cell proliferation. We also observed enrichment for genes involved in the maintenance of genomic integrity, including the major DNA damage repair pathways (nucleotide excision repair, base excision repair, double-strand break repair via homologous recombination and non-homologous end-joining (Supplementary Table S8). Similarly, genes involved in nucleosome remodeling, chromatin organization and histone modification were affected. The datasets were also probed for KEGG and BIOCARTA pathways and we observed an enrichment of similar biological pathways (data not shown). To further support our findings, we interrogated the deregulated genes using EnrichR, the results of which were largely in agreement with the observations described above (data not shown). For upregulated genes, GO annotation revealed Smarca5 dosage-dependent enrichment of processes related to cell stress and cell death including autophagy, apoptosis and negative regulation of cell proliferation (Supplementary Table S9). This is in line with the enrichment of FOS:JUN motifs in LASs in the knockout cells (Supplementary Figures S2 and S3). In addition, upregulated genes were found involved in cytokine response and a number of signaling pathways, including Wnt, MAP kinase, mTOR, p53 and Ras signaling. A total of 50 p53 targets (Supplementary Table S10) [72] were induced in the knockout cells (Figure 3A), which further validates the cellular stress response in the absence of Smarca5. We also observed enrichment of cell aging/cellular senescence, including the Trp53-Cdkn1a/p21 pathway. This is consistent with the increased levels of p21 at the mRNA and protein levels (Figure 3B), deregulation of senescence and cell cycle exit markers (Figure 3C) and increased SA- β -gal activity (Figure 3D).

We noticed that the expression of many genes involved in chromatin and epigenetic regulation was altered upon gradual Smarca5 loss. Therefore, we took advantage of a previously curated list of epigenetic regulator genes (ERGs) [13] that write, modify/revert and read epigenetic modifications in the cell to cross-reference them with the deregulated genes identified in expression analysis. Numerous ERGs were deregulated in primary MEFs upon *Smarca5* inactivation (Supplementary Table S10). Network analysis of the deregulated ERGs (Supplementary Figures S4 and S5), using GeneMANIA [68], confirmed their involvement in processes already identified by the GO analysis of all deregulated genes (e.g., DNA damage response–downregulated; cell aging–upregulated). More than 25 ERGs also exhibit differential chromatin accessibility changes upon knockout, including *Fbxo17*, *Smyd2* (Supplementary Figure S6).

Pathway analysis using genes that exhibit both differential accessibility and gene expression revealed a set of phenotypically relevant and commonly deregulated pathways between ATAC-seq and RNA-seq data (Figure 2E,F). If the analysis is extended beyond differential ATAC peaks found in gene promoters/proximal elements (Supplementary Table S11), using gene enhancer interactions based on available Hi-C data [57], as described in the methods, we find even more overlap between the two datasets. More than 180 differentially accessible chromatin regions can be linked to deregulated genes, with concerted changes in accessibility and gene expression (Supplementary Tables S12 and S13, Supplementary Figures S6 and S7). Thus, we report for the first time a catalogue of gradually deregulated genes and associated differentially accessible regulatory regions in the absence of Smarca5 that are linked to the disruption of major homeostatic pathways required for cellular fitness.

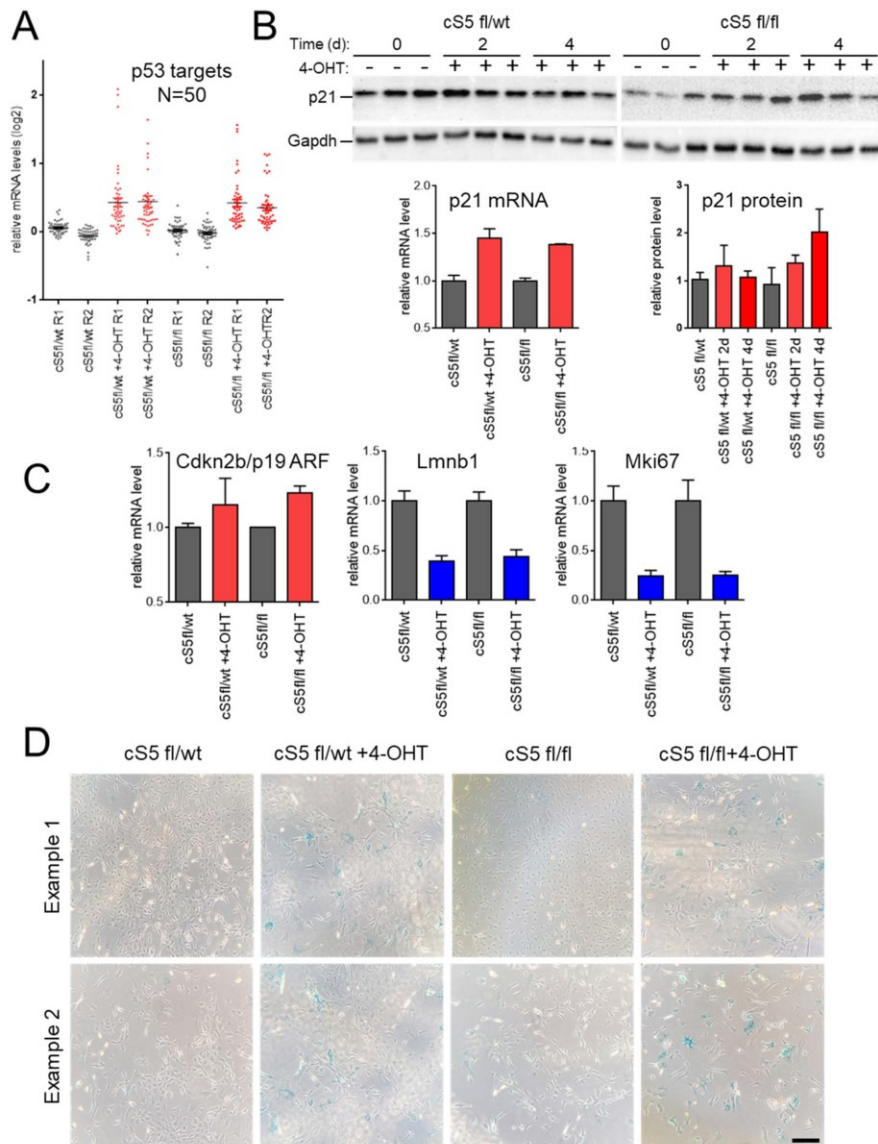


Figure 3. Effects of Smarca5 loss on senescence markers and phenotypes. (A) Induction of 50 direct p53 target genes upon treatment with 4-hydroxy-tamoxifen (4-OHT). (B) Immunoblotting and RNA-seq analyses of p21/Cdkn1a, a p53-dependent inducer of senescence. (C) RNA-seq analysis of senescence and cell-cycle exit markers. (D) Staining for senescence-associated SA-β-gal activity observed in the 4-OHT-treated cultures (already at 96 h post-treatment for *Smarca5* double-knockout (cS5^{fl/fl})). Scale bar = 100 μm.

3.3. Stepwise Allelic Knockout of Smarca5 Results in Dosage-Specific Effects on Cellular Fitness

Considering the above-described deregulated molecular programs, we characterized *Smarca5* single and double knockout primary MEFs with respect to their growth potential. For this, the cells were cultured for an extended period of 35–40 days and growth curves were generated (Figure 4A). The double knockout cells underwent growth arrest almost immediately after 4-OHT induction, entering a prolonged phase of a cellular senescence-like state (SLS), while the corresponding wild-type cells entered the SLS considerably later (Figure 4A, right panel). This SLS is characterized by an almost complete absence

of cell growth, low cell viability and SA-β-gal activity (Figures 3D and 4) and is typical for primary MEFs under stress conditions [40,73]. Analysis of the knockout cells revealed the accumulation of SA-β-gal staining in the double allele knockout already four days after *Smarca5* deletion, in morphologically still pre-senescent cells (Figure 3D), in keeping with the accelerated induction of SLS shown in Figure 4. The SLS was also characterized at the molecular level by inspecting levels of p21/Cdkn1a, a p53-dependent inducer of senescence (Figure 3B), and senescence markers like cell-cycle exit marker Mki67 and p19 ARF or lamin B1 (Figure 3C). We observed concomitant gene upregulation (Figure 3A) and increased accessibility of p53 targets like *Dapk1*, *Igfbp3* and *Bcl2l11* (Supplementary Figure S7) in the knockout cells, further validating this SLS in response to the *Smarca5* loss. The single knockout MEFs displayed growth cessation and SLS onset ten to fourteen days after 4-OHT addition (Figure 4A, left panel), i.e., later than the double allele knockout MEFs but slightly earlier than their corresponding 4-OHT un-induced, wild-type cells. These findings highlight dosage-dependent effects of *Smarca5* on cell proliferation in extended growth assays, in line with the deregulated cell cycle, senescence and apoptosis programs identified by the molecular characterization of the cells.

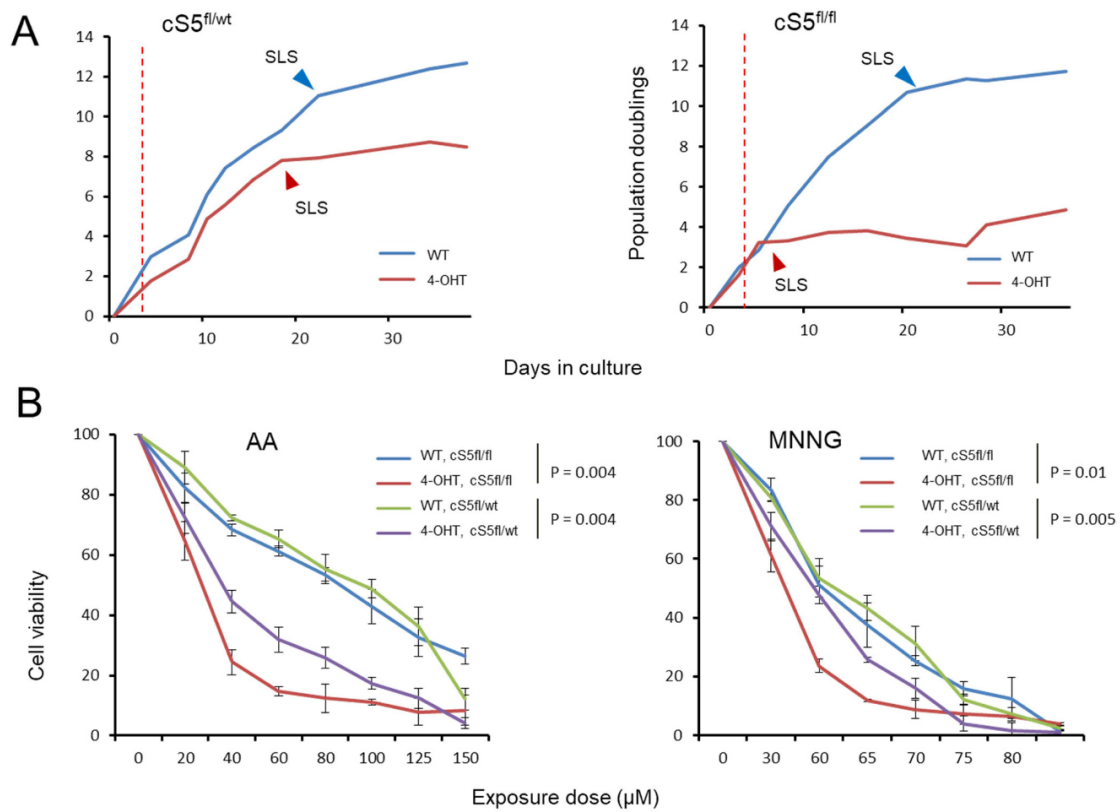


Figure 4. Impact of the stepwise *Smarca5* deletion on cell growth and cell viability upon genotoxic insults. **(A)** Growth curve for the *Smarca5* knockout MEFs when grown in culture for prolonged periods of time, **(left)**: single allele knockout, **(right)**: double allele knockout. Red dotted lines indicate the point of 4-OHT induction, arrowheads indicate the onset of senescence-like state (SLS). **(B)** Cell viability of single and double allele knockout *Smarca5* MEFs as measured by MTS assay upon exposure to different doses of AA in triplicates **(left)** and MNNG **(right)**. NOTE: *p*-values in **(B)** are based on paired *t*-test for each genotype group.

In the past, *Smarca5* loss has been linked to DNA repair defects [20,74] and has been studied in response to radiation damage [21,36,74,75]. In support of this, we found several DNA damage pathways gradually deregulated in the primary MEF knockout cells. Thus, we decided to study the impact of *Smarca5* dosage on the cells' sensitivity to genotoxic insult as a substitute functional readout for their deregulation of DNA damage repair. After deleting *Smarca5* allele(s), we exposed the cells to strong mutagens, namely AA and MNNG, a potent environmental/iatrogenic mutagen and a research mutagenic compound, respectively. AA induces ample TA to AT transversions via specific adduct formation while MNNG, an alkylating agent, causes high rates of CG to TA transitions [41]. The double knockout cells showed the highest level of sensitivity to either exposure, displaying the most prominent decrease in cell viability (Figure 4B). The single knockout cells also showed higher sensitivity to mutagen exposure than the corresponding wild-type culture, but the effect was less pronounced than in the double knockout cells (Figure 4B). To exclude the possibility that the observed differences in cell viability are the result of underlying (genotypic) differences between the single and the double allele knockout MEFs since they are derived from different crosses, we directly compared the wild-type MEFs of the two genotypes side-by-side, for all exposure doses (Supplementary Figure S8). We did not observe major differences between the two wild types (Supplementary Figure S8A,B, left panels). However, we did observe differences between the two knockout conditions (Supplementary Figure S8A,B, right panels). This suggests that the differences in cell viability between the single and the double allele knockout MEFs are likely due to changes in *Smarca5* levels rather than the baseline genetic make-up of the cells. In summary, characterization of the single and double allele knockout MEFs revealed *Smarca5* dosage-dependent effects on cell growth, SLS onset and the sensitivity of the cells to mutagen exposure.

3.4. *Smarca5* Loss Impairs the Capacity of Primary Cells to Immortalize

Since *Smarca5* is overexpressed in different human cancers [24–26,28], we next asked whether known cancer driver genes were deregulated in the obtained gene expression and chromatin accessibility data. The cancer driver genes used for this analysis were based on an in-house curated list from a set of seminal studies [65–67] as described in the methods section. More than fifty cancer driver genes showed gradually altered chromatin accessibility upon single and double-allele *Smarca5* knockout and more than 100 driver genes exhibited differential gene expression (Supplementary Table S10). Some cancer drivers displayed both decreased accessibility and decreased mRNA levels, e.g., *Brca1*, *E2f7* and *Myh11* (Supplementary Figure S6), while others displayed increased accessibility and associated mRNA upregulation, e.g., *Msi2*, *Bace2* (Supplementary Figure S7). Network analysis of these deregulated cancer drivers revealed a general trend for the downregulated genes to be involved in processes important for cellular and genetic stability, such as DNA damage repair, telomere maintenance and chromosome segregation (Supplementary Table S8 and Supplementary Figure S9). The upregulated cancer drivers, in line with the observed *Smarca5* dosage-dependent phenotypic outcomes, were principally involved in processes including apoptosis and response to cellular stress (Supplementary Table S9 and Supplementary Figure S10).

We observed the dosage-dependent deregulation of numerous cancer driver genes, as well as of expression programs involving the gradual downregulation of proliferation and upregulation of apoptosis and cellular senescence, as an immediate- or intermediate-early response to *Smarca5* knockout induction in the primary MEFs. Based on this finding, we set out to determine the long-term phenotypic impact of *Smarca5* loss on cellular fitness by taking advantage of the inherent ability of primary MEFs to bypass the prolonged SLS phase, induced by internal (e.g., oxidative/replicative) stress that can be accelerated by external stress factors (e.g., mutagen exposure), and to clonally immortalize (Figure 5A). To address this, we designed a large-scale functional experiment, involving 100 individual primary MEF cultures (Figure 5B). Twenty-five cultures each for the single and double allele

knockout MEFs and the same number of corresponding un-induced wild-type cultures were grown for several months until they either bypassed senescence or died in the process. The loss of *Smarca5* in MEFs resulted in accelerated growth arrest and senescent-like phenotype, compared to the wildtype controls (Figures 4 and 5) [76]. Notably, the inherent ability of MEF cells to overcome senescence and immortalize was strongly compromised upon loss of *Smarca5* in a dosage-dependent manner (Figure 5C). As expected, almost all wild-type cultures were immortalized. Single knockout cells overcame the SLS far less efficiently than wild-types and the double allele knockout MEFs rarely gave rise to immortalized cell lines. This experiment was repeated two more times applying the same general setup but using MEFs from different embryos and smaller numbers of individual cultures and resulted in the same findings (Supplementary Figure S11A). The *Smarca5* deletion status was confirmed by PCR and flow cytometric analysis after 4-OHT induction at the beginning of the experiment and then again by PCR in the immortalized knockout clones at the end of the experiment, to rule out the immortalization of rare wild-type cells within the *Smarca5* knockout population (data not shown). During the course of the experiment, we further noticed that the *Smarca5* knockout cultures that did overcome senescence took longer to do so than their corresponding wild-type controls (Supplementary Figure S11B). These findings, together with the reported molecular analyses, suggest an important role for *Smarca5* in maintaining regulatory programs that favor cell proliferation, senescence bypass and primary cell immortalization, thereby contributing to the early stages of primary cell transformation.

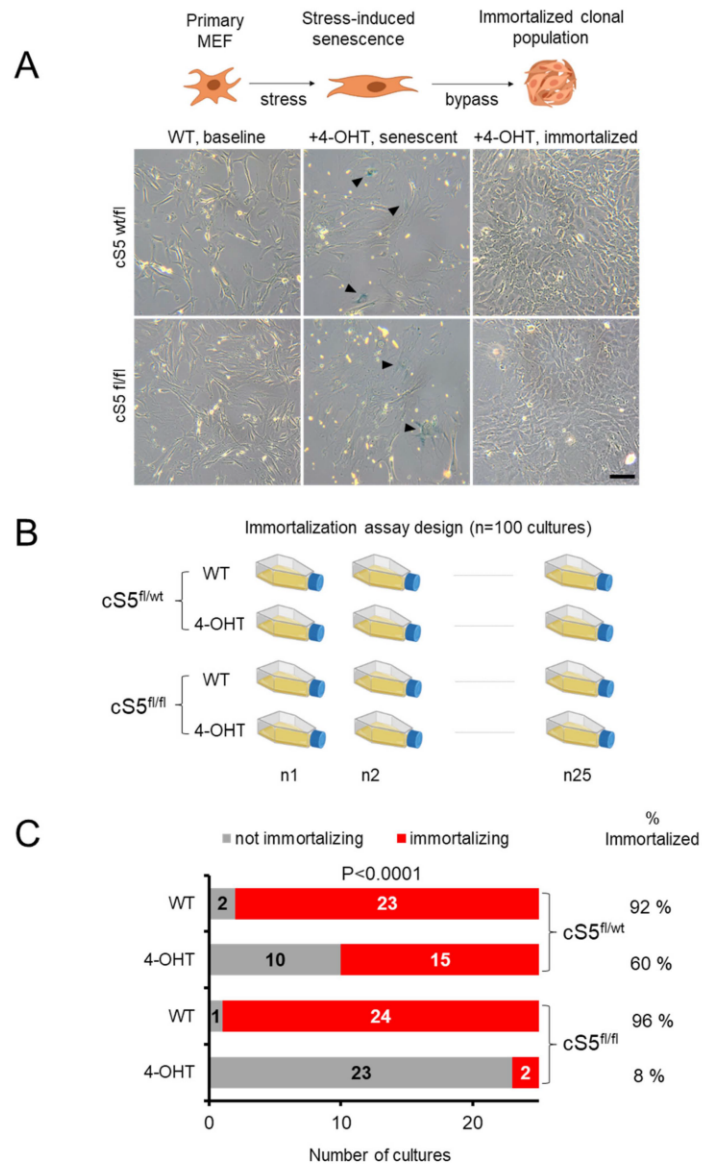


Figure 5. Large-scale analysis of the Smarca5 requirement for primary cell immortalization. (A) A schema showing senescence bypass and clonal immortalization in MEFs (top panel) and the representative cell culture images from the *Smarca5* single and double allele knockout (bottom panel). Black arrowheads in the middle panels indicate the SA-β-gal staining of cells with typical senescent morphology. Scale bar = 50 μm. (B) Immortalization setup for *Smarca5* knockout MEFs, twenty-five flasks for each condition were cultured over periods of several weeks until they bypassed senescence or died, to check the ability of the MEFs to overcome senescence and immortalize; created with BioRender.com. (C) Bar graphs show the total number of cultures out of twenty-five starting cultures that managed to immortalize when cells were grown for prolonged periods of time. NOTE: the *P*-value in (C) reflects the significance of difference between the conditions and it was calculated based on χ^2 test with the degree of freedom equal to 3.

4. Discussion

We exploit an established mammalian model of primary cell immortalization to understand the role of an essential chromatin remodeler in the early stages of cell transformation using *omics* analyses and functional phenotypic validations. The differential gene expression changes observed are in keeping with previously observed roles of Smarca5 in cell cycle progression [24,30], initiation of DNA replication at origins [77] and the finding that the absence of Smarca5 inhibits replication fork velocity [78], thus retarding cell proliferation. Likewise, upregulation of the p53 pathway [79], including its downstream effector *Cdkn1a*, has been reported upon Smarca5 loss [30]. Altogether, we observe pronounced deregulation of genes contributing to overall cellular fitness, including downregulation of genes involved in cell proliferation, genomic stability and DNA damage repair, while senescence- and apoptosis-related genes were upregulated. Based on the stepwise reduction of *Smarca5* dosage, we were able to define a comprehensive set of gene expression and chromatin accessibility changes associated with Smarca5 loss, while minimizing the contribution of secondary alterations due to effects on cell health and viability observed in homozygous knockout cells. These molecular changes are supported by functional observations in *Smarca5* knockout MEFs: (i) the gradually increased sensitivity of knockout cells to exposure with chemical mutagens (wild-type < single-allele knockout < double-allele knockout), and (ii) the *Smarca5* dosage-dependent failure of primary MEFs to escape senescence and immortalize. These findings imply, for the first time, an important role for Smarca5 in cell immortalization, one of the critical initial steps during the transformation process. Interestingly, this is in agreement with the predominantly observed upregulation of *Smarca5* in human cancer [24,27,28,80,81]. Moreover, the deregulated expression of many cancer genes in our data reinforces the link between Smarca5 and the control of important cancer-related pathways.

Suppression of Smarca5 renders human cells sensitive to X-rays [75] and other studies reported similar results for ionizing radiation [21,36]. Interestingly, we recapitulate similar results with chemical mutagens in the exposure experiments, and because we could eliminate that differences in sensitivity to mutagen exposure stem from underlying genetic differences between the crosses, we propose that the sensitivity to versus tolerance of mutagen exposure is at least partially attributable to DNA damage repair defects. These observations are in concurrence with previous studies [74,75] showing a role of Smarca5 in DNA repair, and with the presented gene expression data showing downregulation of several pathways involved in repair in primary MEFs. SMARCA5 rapidly accumulates at DNA damage sites, where it is essential for the repair of DSBs [75,82] by recruitment of RAD51 and BRCA1 [33], and we observe downregulation of *Rad51* and *Brca1* gene expression as well as HR and NHEJ pathway genes in our experimental model. Moreover, interference with cohesin function has been shown to impede DNA repair [83,84] and several genes involved in sister chromatid cohesion are downregulated in our data. Chromosomal aberrations, polyploidy [34] and cohesion defects [85], all of which are linked to genomic stability, have been reported in the absence of Smarca5. We also observed the downregulation of genes involved in telomere maintenance. Together, these findings point towards an important role of Smarca5 for genomic stability/fitness in primary MEFs.

The deregulation of ERGs in the absence of Smarca5 raises the possibility that Smarca5 is not only directly involved in chromatin-associated functions through its role as an ATPase but also by affecting the transcription of other genes involved in these processes. As the absence of Smarca5 initiates a regulatory cascade involving the misexpression of other epigenetic regulator genes, the applied experimental setup does not allow a distinction between genes regulated by Smarca5 in a direct versus indirect manner. This is due to the general unavailability of well-performing Smarca5 antibodies for chromatin-immunoprecipitation and the current lack of publicly available good-quality data for Smarca5 ChIP-seq in MEFs. Future studies aimed to better understand the role of Smarca5 will strongly depend on the development of new experimental tools to circumvent these issues.

5. Conclusions

The ability of primary cells to overcome cellular senescence and subsequent immortalized growth is a key characteristic of cancer formation. We describe the gene dosage-dependent compromised ability of Smarca5-depleted MEFs to undergo these processes, in conjunction with deregulation of corresponding gene regulatory programs, thus directly implicating this important chromatin remodeler as a key determinant for cell fate decisions associated with early stages of cell transformation and initiation of cancer development. Follow-up characterization of direct contributions of Smarca5 to the observed gene regulatory programs, as well as the roles of other chromatin remodeling factors during primary cell immortalization, is warranted to better understand the maintenance of cellular and genomic health and the possible roles of chromatin remodelers in cancerous transformation.

Supplementary Materials: The following supporting information can be downloaded at <https://www.mdpi.com/article/10.3390/cells11050808/s1>, Figures S1–S11, Tables S1–S14.

Author Contributions: S.T., J.Z. and M.K.; Generation of genetically modified mice and validation: T.T. and T.Z.; All cellular and molecular characterization: S.T.; Data processing: C.R. and V.C.; Data analysis: S.T., C.R. and J.Z.; Data interpretation: S.T., J.Z. and M.K.; Writing—original draft preparation: S.T., M.K. and J.Z.; Writing—review and editing: J.Z., M.K. and T.S.; Supervision, J.Z., M.K. and T.S.; Funding acquisition: S.T. All authors have read and agreed to the published version of the manuscript.

Funding: This research was funded by Grant Agency of the Charles University (GAUK), grant no. 1528120 to S.T.; T.S., T.T. were supported by the Grant Agency of the Ministry of Health of the Czech Republic, grant no. NU21-08-00312; T.S., S.T., T.T. and T.Z. received institutional stipend support from the Charles University (SVV260521, UNCE/MED/016, Progres Q26).

Institutional Review Board Statement: All mouse experiments were conducted in accordance with regulations and guidelines of the Czech Animal Protection Act (No. 246/1992) and with the approval of the Ethics Committee of First Faculty of Medicine of Charles University in Prague, Czech Republic (Approval Code 521/13, issued on 27 March 2013).

Informed Consent Statement: Not applicable.

Data Availability Statement: The original sequencing data is publicly available from the NCBI's Sequence Read Archive (SRA) under the accession number PRJNA746698.

Acknowledgments: We would like to acknowledge the kind help of Marie-Pierre Cros, now a retired member of the IARC EGM Branch team, for expert help with sample sequencing. We would like to thank Björn Magnus Öinert for help on the statistical analysis and we also wish to extend our gratitude to the members of the EGM Branch at IARC for the productive discussions on the project and their helpful suggestions.

Conflicts of Interest: The authors declare no conflict of interest.

Disclosure: Where authors are identified as personnel of the International Agency for Research on Cancer/World Health Organization, the authors alone are responsible for the views expressed in this article and they do not necessarily represent the decisions, policy or views of the International Agency for Research on Cancer/World Health Organization.

References

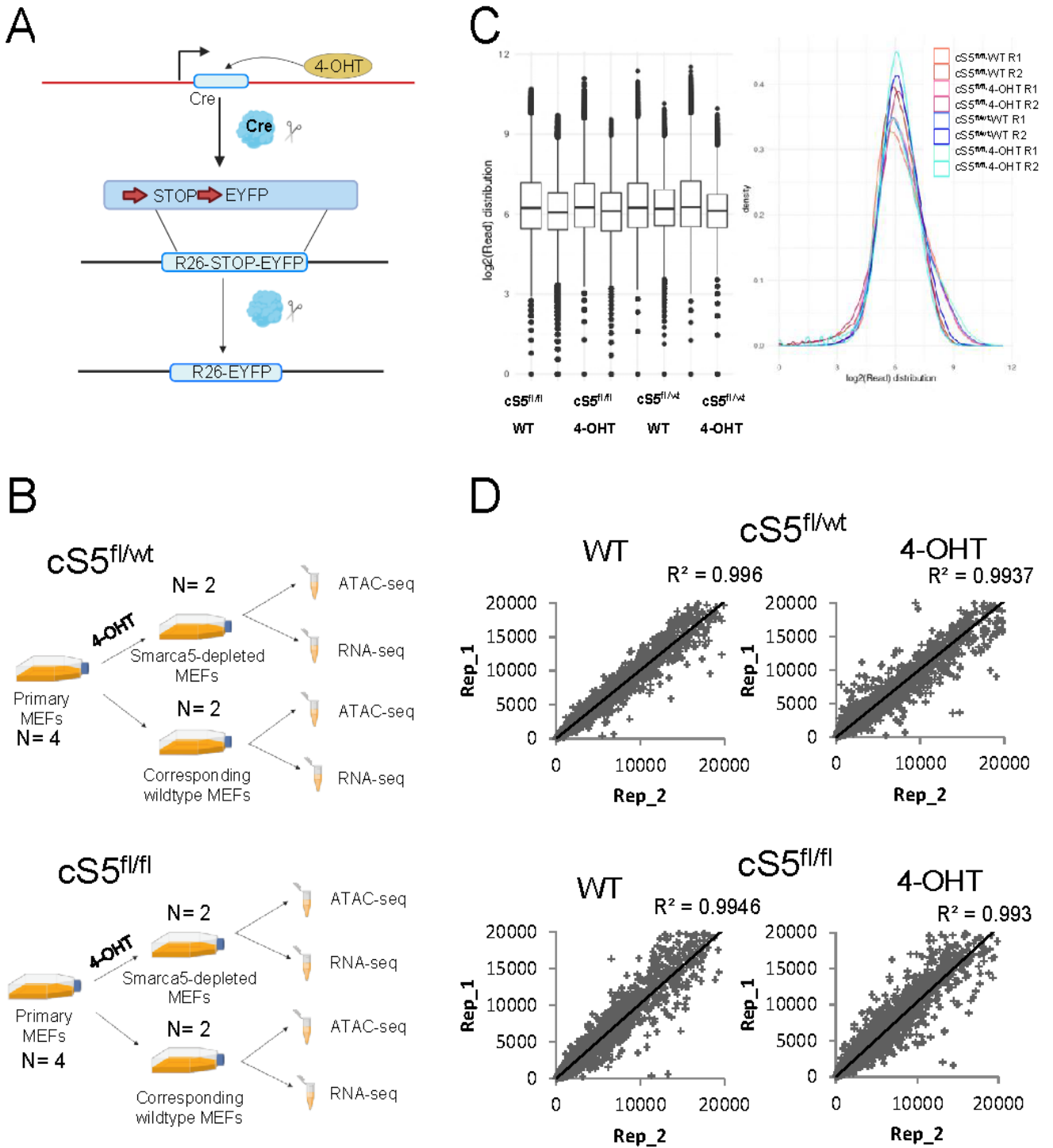
1. Felsenfeld, G.; Groudine, M. Controlling the double helix. *Nature* **2003**, *421*, 448–453. [[CrossRef](#)] [[PubMed](#)]
2. Biegel, J.A.; Busse, T.M.; Weissman, B.E. SWI/SNF chromatin remodeling complexes and cancer. *Am. J. Med. Genet C Semin. Med. Genet.* **2014**, *166*, 350–366. [[CrossRef](#)] [[PubMed](#)]
3. Wang, G.G.; Allis, C.D.; Chi, P. Chromatin remodeling and cancer, Part II: ATP-dependent chromatin remodeling. *Trends Mol. Med.* **2007**, *13*, 373–380. [[CrossRef](#)] [[PubMed](#)]
4. Lafon-Hughes, L.; Di Tomaso, M.V.; Méndez-Acuña, L.; Martínez-López, W. Chromatin-remodelling mechanisms in cancer. *Mutat. Res.* **2008**, *658*, 191–214. [[CrossRef](#)] [[PubMed](#)]
5. Bourdeaut, F.; Bièche, I. Chromatin remodeling defects and cancer: The SWI/SNF example. *Bull. Cancer* **2012**, *99*, 1133–1140. [[CrossRef](#)]
6. Wolffe, A.P. Chromatin remodeling: Why it is important in cancer. *Oncogene* **2001**, *20*, 2988–2990. [[CrossRef](#)]

7. Nair, S.S.; Kumar, R. Chromatin remodeling in cancer: A gateway to regulate gene transcription. *Mol. Oncol.* **2012**, *6*, 611–619. [[CrossRef](#)]
8. Kadoch, C.; Crabtree, G.R. Mammalian SWI/SNF chromatin remodeling complexes and cancer: Mechanistic insights gained from human genomics. *Sci. Adv.* **2015**, *1*, e1500447. [[CrossRef](#)]
9. Okawa, R.; Banno, K.; Iida, M.; Yanokura, M.; Takeda, T.; Iijima, M.; Kunitomi-Irie, H.; Nakamura, K.; Adachi, M.; Umene, K.; et al. Aberrant chromatin remodeling in gynecological cancer. *Oncol. Lett.* **2017**, *14*, 5107–5113. [[CrossRef](#)]
10. Oike, T.; Ogiwara, H.; Nakano, T.; Yokota, J.; Kohno, T. Inactivating mutations in SWI/SNF chromatin remodeling genes in human cancer. *Jpn. J. Clin. Oncol.* **2013**, *43*, 849–855. [[CrossRef](#)]
11. Shigetomi, H.; Oonogi, A.; Tsunemi, T.; Tanase, Y.; Yamada, Y.; Kajihara, H.; Yoshizawa, Y.; Furukawa, N.; Haruta, S.; Yoshida, S.; et al. The role of components of the chromatin modification machinery in carcinogenesis of clear cell carcinoma of the ovary (Review). *Oncol. Lett.* **2011**, *2*, 591–597. [[CrossRef](#)] [[PubMed](#)]
12. Gui, Y.; Guo, G.; Huang, Y.; Hu, X.; Tang, A.; Gao, S.; Wu, R.; Chen, C.; Li, X.; Zhou, L.; et al. Frequent mutations of chromatin remodeling genes in transitional cell carcinoma of the bladder. *Nat. Genet.* **2011**, *43*, 875–878. [[CrossRef](#)]
13. Halaburkova, A.; Cahais, V.; Novoloaca, A.; Araujo, M.; Khoueiry, R.; Ghantous, A.; Herceg, Z. Pan-cancer multi-omics analysis and orthogonal experimental assessment of epigenetic driver genes. *Genome Res.* **2020**, *30*, 1517–1532. [[CrossRef](#)] [[PubMed](#)]
14. Cairns, B.R. Chromatin remodeling: Insights and intrigue from single-molecule studies. *Nat. Struct. Mol. Biol.* **2007**, *14*, 989–996. [[CrossRef](#)] [[PubMed](#)]
15. Côté, J.; Quinn, J.; Workman, J.L.; Peterson, C.L. Stimulation of GAL4 derivative binding to nucleosomal DNA by the yeast SWI/SNF complex. *Science* **1994**, *265*, 53–60. [[CrossRef](#)] [[PubMed](#)]
16. Khorasanizadeh, S. The nucleosome: From genomic organization to genomic regulation. *Cell* **2004**, *116*, 259–272. [[CrossRef](#)]
17. Clapier, C.R.; Cairns, B.R. The biology of chromatin remodeling complexes. *Annu. Rev. Biochem.* **2009**, *78*, 273–304. [[CrossRef](#)]
18. Corona, D.F.; Tamkun, J.W. Multiple roles for ISWI in transcription, chromosome organization and DNA replication. *Biochim. Biophys. Acta* **2004**, *1677*, 113–119. [[CrossRef](#)]
19. Collins, N.; Poot, R.A.; Kukimoto, I.; García-Jiménez, C.; Delleire, G.; Varga-Weisz, P.D. An ACF1–ISWI chromatin-remodeling complex is required for DNA replication through heterochromatin. *Nat. Genet.* **2002**, *32*, 627–632. [[CrossRef](#)]
20. Atsumi, Y.; Minakawa, Y.; Ono, M.; Dobashi, S.; Shinohe, K.; Shinohara, A.; Takeda, S.; Takagi, M.; Takamatsu, N.; Nakagama, H.; et al. ATM and SIRT6/SNF2H Mediate Transient H2AX Stabilization When DSBs Form by Blocking HUWE1 to Allow Efficient γ H2AX Foci Formation. *Cell Rep.* **2015**, *13*, 2728–2740. [[CrossRef](#)]
21. Aydin, Ö.Z.; Vermeulen, W.; Lans, H. ISWI chromatin remodeling complexes in the DNA damage response. *Cell Cycle* **2014**, *13*, 3016–3025. [[CrossRef](#)]
22. Helfricht, A.; Wiegant, W.W.; Thijssen, P.E.; Vertegaal, A.C.; Luijsterburg, M.S.; van Attikum, H. Remodeling and spacing factor 1 (RSF1) deposits centromere proteins at DNA double-strand breaks to promote non-homologous end-joining. *Cell Cycle* **2013**, *12*, 3070–3082. [[CrossRef](#)]
23. Erdel, F.; Rippe, K. Chromatin remodelling in mammalian cells by ISWI-type complexes—Where, when and why? *FEBS J.* **2011**, *278*, 3608–3618. [[CrossRef](#)]
24. Zhao, X.C.; An, P.; Wu, X.Y.; Zhang, L.M.; Long, B.; Tian, Y.; Chi, X.Y.; Tong, D.Y. Overexpression of hSNF2H in glioma promotes cell proliferation, invasion, and chemoresistance through its interaction with Rsf-1. *Tumor Biol.* **2016**, *37*, 7203–7212. [[CrossRef](#)] [[PubMed](#)]
25. Stopka, T.; Zakova, D.; Fuchs, O.; Kubrova, O.; Blafkova, J.; Jelinek, J.; Necas, E.; Zivny, J. Chromatin remodeling gene SMARCA5 is dysregulated in primitive hematopoietic cells of acute leukemia. *Leukemia* **2000**, *14*, 1247–1252. [[CrossRef](#)] [[PubMed](#)]
26. Tommasi, S.; Pinto, R.; Danza, K.; Pilato, B.; Palumbo, O.; Micale, L.; De Summa, S. miR-151-5p, targeting chromatin remodeler SMARCA5, as a marker for the BRCAness phenotype. *Oncotarget* **2016**, *7*, 80363–80372. [[CrossRef](#)] [[PubMed](#)]
27. Jin, Q.; Mao, X.; Li, B.; Guan, S.; Yao, F.; Jin, F. Overexpression of SMARCA5 correlates with cell proliferation and migration in breast cancer. *Tumor Biol.* **2015**, *36*, 1895–1902. [[CrossRef](#)] [[PubMed](#)]
28. Gigeq, C.O.; Lisboa, L.C.; Leal, M.F.; Silva, P.N.; Lima, E.M.; Khayat, A.S.; Assumpção, P.P.; Burbano, R.R.; Smith Mde, A. SMARCA5 methylation and expression in gastric cancer. *Cancer Investig.* **2011**, *29*, 162–166. [[CrossRef](#)] [[PubMed](#)]
29. Sánchez-Molina, S.; Mortusewicz, O.; Bieber, B.; Auer, S.; Eckey, M.; Leonhardt, H.; Friedl, A.A.; Becker, P.B. Role for hACF1 in the G2/M damage checkpoint. *Nucleic Acids Res.* **2011**, *39*, 8445–8456. [[CrossRef](#)]
30. Kokavec, J.; Zikmund, T.; Savvulidi, F.; Kulvait, V.; Edelmann, W.; Skoultchi, A.I.; Stopka, T. The ISWI ATPase Smarca5 (Snf2h) Is Required for Proliferation and Differentiation of Hematopoietic Stem and Progenitor Cells. *Stem Cells* **2017**, *35*, 1614–1623. [[CrossRef](#)]
31. Zhang, C.; Chen, Z.; Yin, Q.; Fu, X.; Li, Y.; Stopka, T.; Skoultchi, A.I.; Zhang, Y. The chromatin remodeler Snf2h is essential for oocyte meiotic cell cycle progression. *Genes Dev.* **2020**, *34*, 166–178. [[CrossRef](#)] [[PubMed](#)]
32. Stopka, T.; Skoultchi, A.I. The ISWI ATPase Snf2h is required for early mouse development. *Proc. Natl. Acad. Sci. USA* **2003**, *100*, 14097–14102. [[CrossRef](#)] [[PubMed](#)]
33. Nakamura, K.; Kato, A.; Kobayashi, J.; Yanagihara, H.; Sakamoto, S.; Oliveira, D.V.; Shimada, M.; Tauchi, H.; Suzuki, H.; Tashiro, S.; et al. Regulation of homologous recombination by RNF20-dependent H2B ubiquitination. *Mol. Cell* **2011**, *41*, 515–528. [[CrossRef](#)] [[PubMed](#)]

34. Zikmund, T.; Paszekova, H.; Kokavec, J.; Kerbs, P.; Thakur, S.; Turkova, T.; Tauchmanova, P.; Greif, P.A.; Stopka, T. Loss of ISWI ATPase SMARCA5 (SNF2H) in Acute Myeloid Leukemia Cells Inhibits Proliferation and Chromatid Cohesion. *Int. J. Mol. Sci.* **2020**, *21*, 2073. [[CrossRef](#)] [[PubMed](#)]
35. Hanahan, D.; Weinberg, R.A. Hallmarks of cancer: The next generation. *Cell* **2011**, *144*, 646–674. [[CrossRef](#)] [[PubMed](#)]
36. Smeenk, G.; Wiegant, W.W.; Marteijn, J.A.; Luijsterburg, M.S.; Sroczynski, N.; Costelloe, T.; Romeijn, R.J.; Pastink, A.; Mailand, N.; Vermeulen, W.; et al. Poly(ADP-ribosyl)ation links the chromatin remodeler SMARCA5/SNF2H to RNF168-dependent DNA damage signaling. *J. Cell Sci.* **2013**, *126*, 889–903. [[CrossRef](#)] [[PubMed](#)]
37. Iurlaro, M.; Stadler, M.B.; Masoni, F.; Jagani, Z.; Galli, G.G.; Schübeler, D. Mammalian SWI/SNF continuously restores local accessibility to chromatin. *Nat. Genet.* **2021**, *53*, 279–287. [[CrossRef](#)]
38. Barisic, D.; Stadler, M.B.; Iurlaro, M.; Schübeler, D. Mammalian ISWI and SWI/SNF selectively mediate binding of distinct transcription factors. *Nature* **2019**, *569*, 136–140. [[CrossRef](#)]
39. Hahn, W.C.; Weinberg, R.A. Modelling the molecular circuitry of cancer. *Nat. Rev. Cancer* **2002**, *2*, 331–341. [[CrossRef](#)]
40. Odell, A.; Askham, J.; Whibley, C.; Hollstein, M. How to become immortal: Let MEFs count the ways. *Aging* **2010**, *2*, 160–165. [[CrossRef](#)]
41. Olivier, M.; Weninger, A.; Ardin, M.; Huskova, H.; Castells, X.; Vallée, M.P.; McKay, J.; Nedelko, T.; Muehlbauer, K.-R.; Marusawa, H.; et al. Modelling mutational landscapes of human cancers in vitro. *Sci. Rep.* **2014**, *4*, 4482. [[CrossRef](#)] [[PubMed](#)]
42. Korenjak, M.; Zavadil, J. Experimental identification of cancer driver alterations in the era of pan-cancer genomics. *Cancer Sci.* **2019**, *110*, 3622–3629. [[CrossRef](#)] [[PubMed](#)]
43. Huskova, H.; Ardin, M.; Weninger, A.; Vargova, K.; Barrin, S.; Villar, S.; Olivier, M.; Stopka, T.; Herceg, Z.; Hollstein, M.; et al. Modeling cancer driver events in vitro using barrier bypass-clonal expansion assays and massively parallel sequencing. *Oncogene* **2017**, *36*, 6041–6048. [[CrossRef](#)]
44. Dluhosova, M.; Curik, N.; Vargova, J.; Jonasova, A.; Zikmund, T.; Stopka, T. Epigenetic control of SPI1 gene by CTCF and ISWI ATPase SMARCA5. *PLoS ONE* **2014**, *9*, e87448. [[CrossRef](#)] [[PubMed](#)]
45. Wiechens, N.; Singh, V.; Gkikopoulos, T.; Schofield, P.; Rocha, S.; Owen-Hughes, T. The Chromatin Remodelling Enzymes SNF2H and SNF2L Position Nucleosomes adjacent to CTCF and Other Transcription Factors. *PLoS Genet.* **2016**, *12*, e1005940. [[CrossRef](#)]
46. Hayashi, S.; McMahon, A.P. Efficient recombination in diverse tissues by a tamoxifen-inducible form of Cre: A tool for temporally regulated gene activation/inactivation in the mouse. *Dev. Biol.* **2002**, *244*, 305–318. [[CrossRef](#)] [[PubMed](#)]
47. Corces, M.R.; Trevino, A.E.; Hamilton, E.G.; Greenside, P.G.; Sinnott-Armstrong, N.A.; Vesuna, S.; Satpathy, A.T.; Rubin, A.J.; Montine, K.S.; Wu, B.; et al. An improved ATAC-seq protocol reduces background and enables interrogation of frozen tissues. *Nat. Methods* **2017**, *14*, 959–962. [[CrossRef](#)]
48. Buenrostro, J.D.; Wu, B.; Chang, H.Y.; Greenleaf, W.J. ATAC-seq: A Method for Assaying Chromatin Accessibility Genome-Wide. *Curr. Protoc. Mol. Biol.* **2015**, *109*, 21.29.21–21.29.29. [[CrossRef](#)]
49. Li, H.; Durbin, R. Fast and accurate short read alignment with Burrows-Wheeler transform. *Bioinformatics* **2009**, *25*, 1754–1760. [[CrossRef](#)]
50. Faust, G.G.; Hall, I.M. SAMBLASTER: Fast duplicate marking and structural variant read extraction. *Bioinformatics* **2014**, *30*, 2503–2505. [[CrossRef](#)]
51. McKenna, A.; Hanna, M.; Banks, E.; Sivachenko, A.; Cibulskis, K.; Kernytzky, A.; Garimella, K.; Altshuler, D.; Gabriel, S.; Daly, M.; et al. The Genome Analysis Toolkit: A MapReduce framework for analyzing next-generation DNA sequencing data. *Genome Res.* **2010**, *20*, 1297–1303. [[CrossRef](#)] [[PubMed](#)]
52. Zhang, Y.; Liu, T.; Meyer, C.A.; Eeckhoute, J.; Johnson, D.S.; Bernstein, B.E.; Nusbaum, C.; Myers, R.M.; Brown, M.; Li, W.; et al. Model-based Analysis of ChIP-Seq (MACS). *Genome Biol.* **2008**, *9*, R137. [[CrossRef](#)] [[PubMed](#)]
53. Qunhua, L.; James, B.B.; Haiyan, H.; Peter, J.B. Measuring reproducibility of high-throughput experiments. *Ann. Appl. Stat.* **2011**, *5*, 1752–1779. [[CrossRef](#)]
54. Frankish, A.; Diekhans, M.; Ferreira, A.-M.; Johnson, R.; Jungreis, I.; Loveland, J.; Mudge, J.M.; Sisu, C.; Wright, J.; Armstrong, J.; et al. GENCODE reference annotation for the human and mouse genomes. *Nucleic Acids Res.* **2019**, *47*, D766–D773. [[CrossRef](#)] [[PubMed](#)]
55. Weddington, N.; Stuy, A.; Hiratani, I.; Ryba, T.; Yokochi, T.; Gilbert, D.M. ReplicationDomain: A visualization tool and comparative database for genome-wide replication timing data. *BMC Bioinform.* **2008**, *9*, 530. [[CrossRef](#)]
56. Moore, J.E.; Purcaro, M.J.; Pratt, H.E.; Epstein, C.B.; Shores, N.; Adrian, J.; Kawli, T.; Davis, C.A.; Dobin, A.; Kaul, R.; et al. Expanded encyclopaedias of DNA elements in the human and mouse genomes. *Nature* **2020**, *583*, 699–710. [[CrossRef](#)]
57. Schoenfelder, S.; Furlan-Magaril, M.; Mifsud, B.; Tavares-Cadete, F.; Sugar, R.; Javierre, B.M.; Nagano, T.; Katsman, Y.; Sakthidevi, M.; Wingett, S.W.; et al. The pluripotent regulatory circuitry connecting promoters to their long-range interacting elements. *Genome Res.* **2015**, *25*, 582–597. [[CrossRef](#)]
58. Machlab, D.; Burger, L.; Sonesson, C.; Rijli, F.M.; Schübeler, D.; Stadler, M.B. monaLisa: An R/Bioconductor package for identifying regulatory motifs. *bioRxiv* **2021**. [[CrossRef](#)]
59. Rio, D.C.; Ares, M., Jr.; Hannon, G.J.; Nilsen, T.W. Purification of RNA using TRIzol (TRI reagent). *Cold Spring Harb. Protoc.* **2010**, *2010*, pdb.prot5439. [[CrossRef](#)]
60. Love, M.I.; Huber, W.; Anders, S. Moderated estimation of fold change and dispersion for RNA-seq data with DESeq2. *Genome Biol.* **2014**, *15*, 550. [[CrossRef](#)]

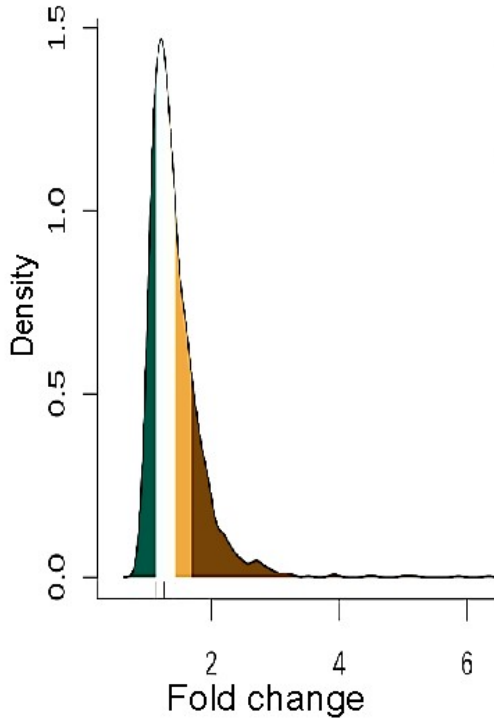
61. Pavlidis, P.; Noble, W.S. Analysis of strain and regional variation in gene expression in mouse brain. *Genome Biol.* **2001**, *2*, research0042. [[CrossRef](#)] [[PubMed](#)]
62. Saeed, A.I.; Sharov, V.; White, J.; Li, J.; Liang, W.; Bhagabati, N.; Braisted, J.; Klapa, M.; Currier, T.; Thiagarajan, M.; et al. TM4: A free, open-source system for microarray data management and analysis. *Biotechniques* **2003**, *34*, 374–378. [[CrossRef](#)] [[PubMed](#)]
63. Howe, E.; Holton, K.; Nair, S.; Schlauch, D.; Sinha, R.; Quackenbush, J. MeV: MultiExperiment Viewer. In *Biomedical Informatics for Cancer Research*; Ochs, M.F., Casagrande, J.T., Davuluri, R.V., Eds.; Springer: Boston, MA, USA, 2010; pp. 267–277.
64. Huang, W.; Sherman, B.T.; Lempicki, R.A. Bioinformatics enrichment tools: Paths toward the comprehensive functional analysis of large gene lists. *Nucleic Acids Res.* **2009**, *37*, e16. [[CrossRef](#)] [[PubMed](#)]
65. Sondka, Z.; Bamford, S.; Cole, C.G.; Ward, S.A.; Dunham, I.; Forbes, S.A. The COSMIC Cancer Gene Census: Describing genetic dysfunction across all human cancers. *Nat. Rev. Cancer* **2018**, *18*, 696–705. [[CrossRef](#)] [[PubMed](#)]
66. Martínez-Jiménez, F.; Muiños, F.; Sentís, I.; Deu-Pons, J.; Reyes-Salazar, I.; Arnedo-Pac, C.; Mularoni, L.; Pich, O.; Bonet, J.; Kranas, H.; et al. A compendium of mutational cancer driver genes. *Nat. Rev. Cancer* **2020**, *20*, 555–572. [[CrossRef](#)] [[PubMed](#)]
67. Bailey, M.H.; Tokheim, C.; Porta-Pardo, E.; Sengupta, S.; Bertrand, D.; Weerasinghe, A.; Colaprico, A.; Wendl, M.C.; Kim, J.; Reardon, B.; et al. Comprehensive Characterization of Cancer Driver Genes and Mutations. *Cell* **2018**, *173*, 371–385.e18. [[CrossRef](#)]
68. Warde-Farley, D.; Donaldson, S.L.; Comes, O.; Zuberi, K.; Badrawi, R.; Chao, P.; Franz, M.; Grouios, C.; Kazi, F.; Lopes, C.T.; et al. The GeneMANIA prediction server: Biological network integration for gene prioritization and predicting gene function. *Nucleic Acids Res.* **2010**, *38*, W214–W220. [[CrossRef](#)]
69. Celis, J.E.; Carter, N.; Simons, K.; Small, J.V.; Hunter, T.; Shotton, D. *Cell Biology: A Laboratory Handbook*; Elsevier: Amsterdam, The Netherlands, 2005.
70. Mehic, D.; Bakiri, L.; Ghannadan, M.; Wagner, E.F.; Tschachler, E. Fos and jun proteins are specifically expressed during differentiation of human keratinocytes. *J. Investig. Derm.* **2005**, *124*, 212–220. [[CrossRef](#)]
71. Angel, P.; Karin, M. The role of Jun, Fos and the AP-1 complex in cell-proliferation and transformation. *Biochim. Biophys. Acta* **1991**, *1072*, 129–157. [[CrossRef](#)]
72. Fischer, M. Census and evaluation of p53 target genes. *Oncogene* **2017**, *36*, 3943–3956. [[CrossRef](#)]
73. Whibley, C.; Odell, A.; Nedelko, T.; Balaburski, G.; Murphy, M.; Liu, Z.; Stevens, L.; Walker, J.; Routledge, M.; Hollstein, M. Wild-type and Hupki (human p53 knock-in) murine embryonic fibroblasts: p53/ARF pathway disruption in spontaneous escape from senescence. *J. Biol. Chem.* **2010**, *285*, 11326–11335. [[CrossRef](#)] [[PubMed](#)]
74. Toiber, D.; Erdel, F.; Bouazoune, K.; Silberman, D.M.; Zhong, L.; Mulligan, P.; Sebastian, C.; Cosentino, C.; Martinez-Pastor, B.; Giacosa, S.; et al. SIRT6 Recruits SNF2H to DNA Break Sites, Preventing Genomic Instability through Chromatin Remodeling. *Mol. Cell* **2013**, *51*, 454–468. [[CrossRef](#)] [[PubMed](#)]
75. Lan, L.; Ui, A.; Nakajima, S.; Hatakeyama, K.; Hoshi, M.; Watanabe, R.; Janicki, S.M.; Ogiwara, H.; Kohno, T.; Kanno, S.; et al. The ACF1 complex is required for DNA double-strand break repair in human cells. *Mol. Cell* **2010**, *40*, 976–987. [[CrossRef](#)]
76. Parrinello, S.; Samper, E.; Krtolica, A.; Goldstein, J.; Melov, S.; Campisi, J. Oxygen sensitivity severely limits the replicative lifespan of murine fibroblasts. *Nat. Cell Biol.* **2003**, *5*, 741–747. [[CrossRef](#)] [[PubMed](#)]
77. Sugimoto, N.; Yugawa, T.; Iizuka, M.; Kiyono, T.; Fujita, M. Chromatin remodeler sucrose nonfermenting 2 homolog (SNF2H) is recruited onto DNA replication origins through interaction with Cdc10 protein-dependent transcript 1 (Cdt1) and promotes pre-replication complex formation. *J. Biol. Chem.* **2011**, *286*, 39200–39210. [[CrossRef](#)] [[PubMed](#)]
78. Bhaskara, S.; Jacques, V.; Rusche, J.R.; Olson, E.N.; Cairns, B.R.; Chandrasekharan, M.B. Histone deacetylases 1 and 2 maintain S-phase chromatin and DNA replication fork progression. *Epigenetics Chromatin* **2013**, *6*, 27. [[CrossRef](#)]
79. Ding, Y.; Wang, W.; Ma, D.; Liang, G.; Kang, Z.; Xue, Y.; Zhang, Y.; Wang, L.; Heng, J.; Zhang, Y.; et al. Smarca5-mediated epigenetic programming facilitates fetal HSPC development in vertebrates. *Blood* **2021**, *137*, 190–202. [[CrossRef](#)]
80. Shibayama, Y.; Takahashi, K.; Yamaguchi, H.; Yasuda, J.; Yamazaki, D.; Rahman, A.; Fujimori, T.; Fujisawa, Y.; Takai, S.; Furukawa, T.; et al. Aberrant (pro)renin receptor expression induces genomic instability in pancreatic ductal adenocarcinoma through upregulation of SMARCA5/SNF2H. *Commun. Biol.* **2020**, *3*, 724. [[CrossRef](#)]
81. Tan, Y.; Zhang, T.; Liang, C. Circular RNA SMARCA5 is overexpressed and promotes cell proliferation, migration as well as invasion while inhibits cell apoptosis in bladder cancer. *Transl. Cancer Res.* **2019**, *8*, 1663–1671. [[CrossRef](#)]
82. Erdel, F.; Schubert, T.; Marth, C.; Längst, G.; Rippe, K. Human ISWI chromatin-remodeling complexes sample nucleosomes via transient binding reactions and become immobilized at active sites. *Proc. Natl. Acad. Sci. USA* **2010**, *107*, 19873–19878. [[CrossRef](#)]
83. Ström, L.; Lindroos, H.B.; Shirahige, K.; Sjögren, C. Postreplicative Recruitment of Cohesin to Double-Strand Breaks Is Required for DNA Repair. *Mol. Cell* **2004**, *16*, 1003–1015. [[CrossRef](#)] [[PubMed](#)]
84. Nasmyth, K.; Haering, C.H. Cohesin: Its roles and mechanisms. *Annu. Rev. Genet.* **2009**, *43*, 525–558. [[CrossRef](#)] [[PubMed](#)]
85. Hakim, M.A.; Bochar, D.A.; Schmiesing, J.A.; Dong, Y.; Barak, O.G.; Speicher, D.W.; Yokomori, K.; Shiekhattar, R. A chromatin remodelling complex that loads cohesin onto human chromosomes. *Nature* **2002**, *418*, 994–998. [[CrossRef](#)] [[PubMed](#)]

Suppl. Figure S1

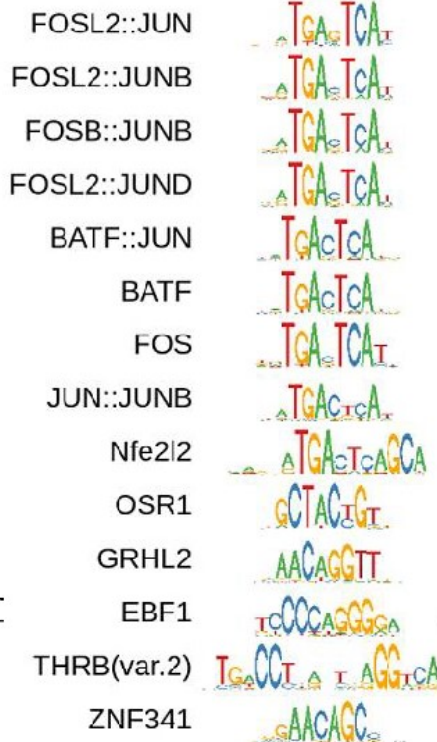


Supplementary Figure S1. A) Schematics of the conditionally expressed EYFP cassette. The *lox-P* flanked STOP sequence is excised upon 4-OHT induction and the EYFP is expressed in *Cre*-expressing cells of the double mutant MEFs. Image created with BioRender.com **B)** Study design for assessing chromatin accessibility and gene expression changes upon *Smarca5* deletion in single allele (top) and double allele knockout (bottom) MEFs. The readouts are taken four days (96 hours) after the knockout. **C)** Box plot displaying \log_2 transformed normalized read distribution for ATAC-seq samples (left) and line plot displaying density of read distribution for the same samples (right). **D)** RNA-seq correlation plots for read counts between replicates.

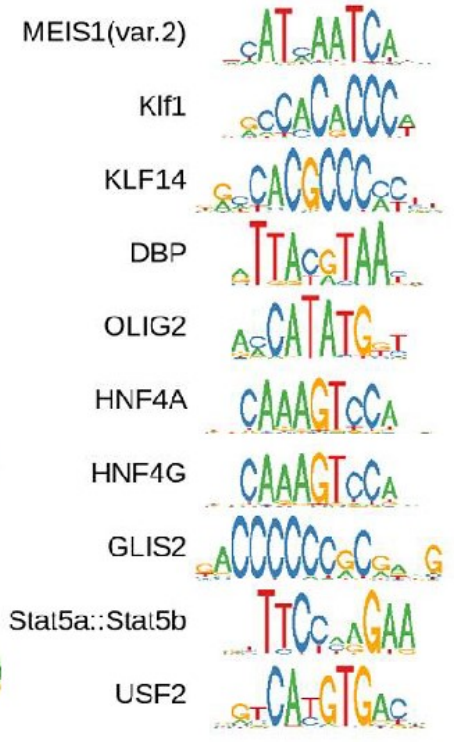
Suppl. Figure S2



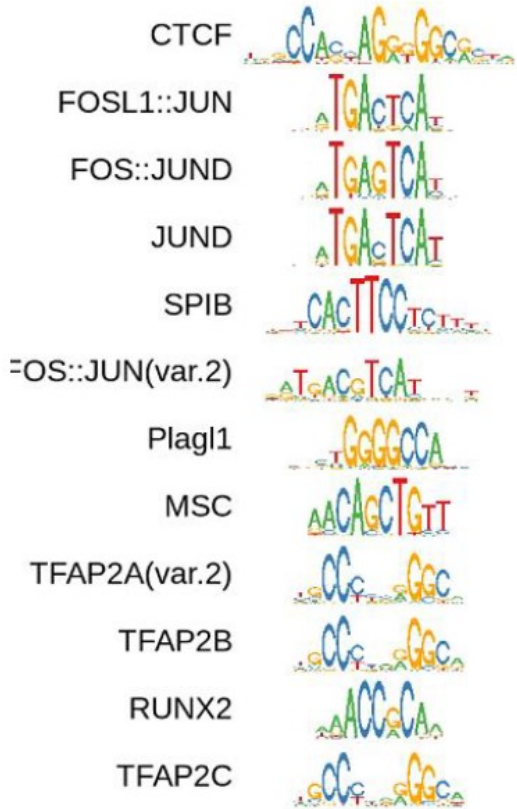
Bin 2



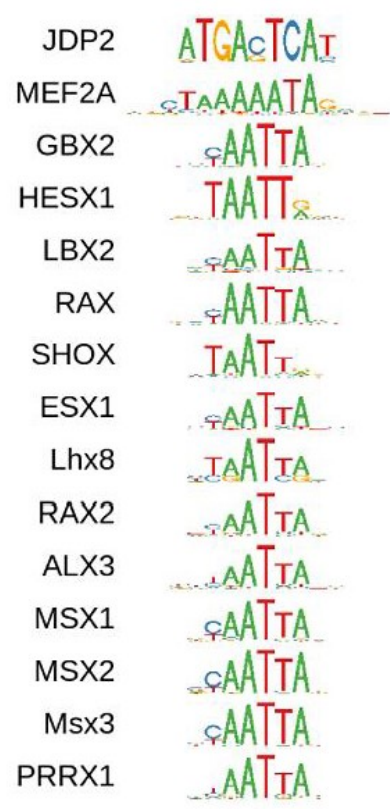
Bin 4



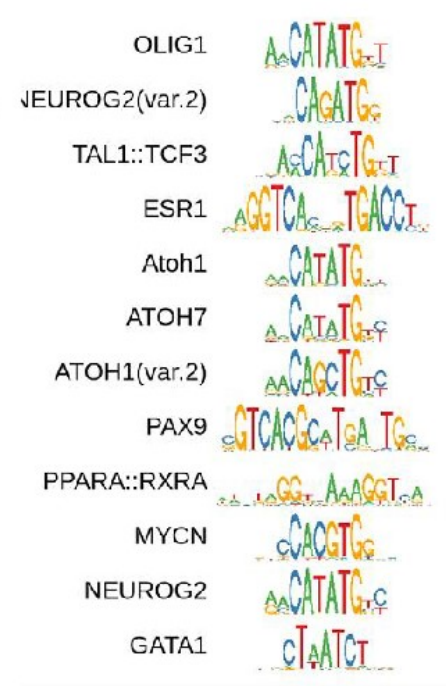
Bin 1



Bin 3

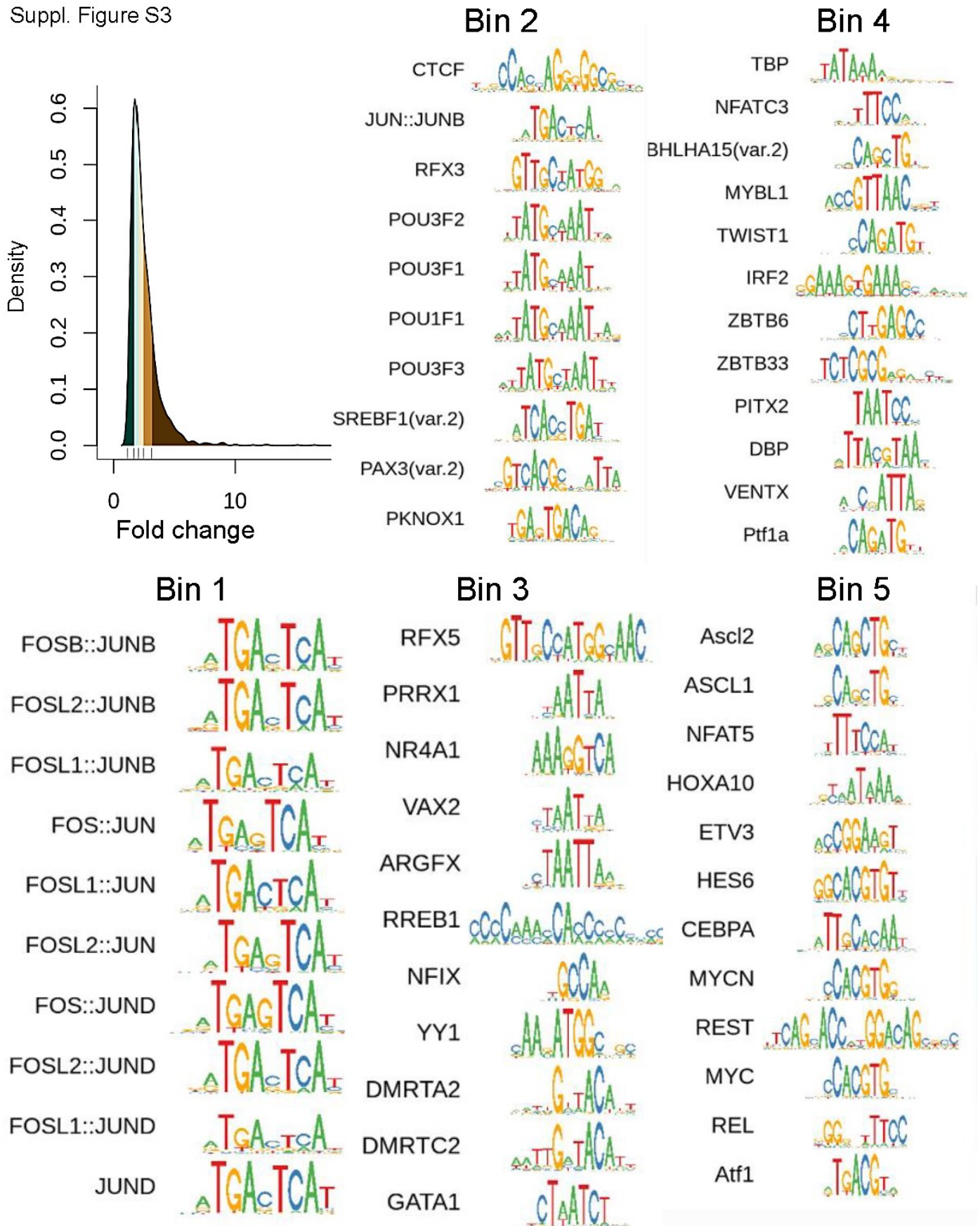


Bin 5



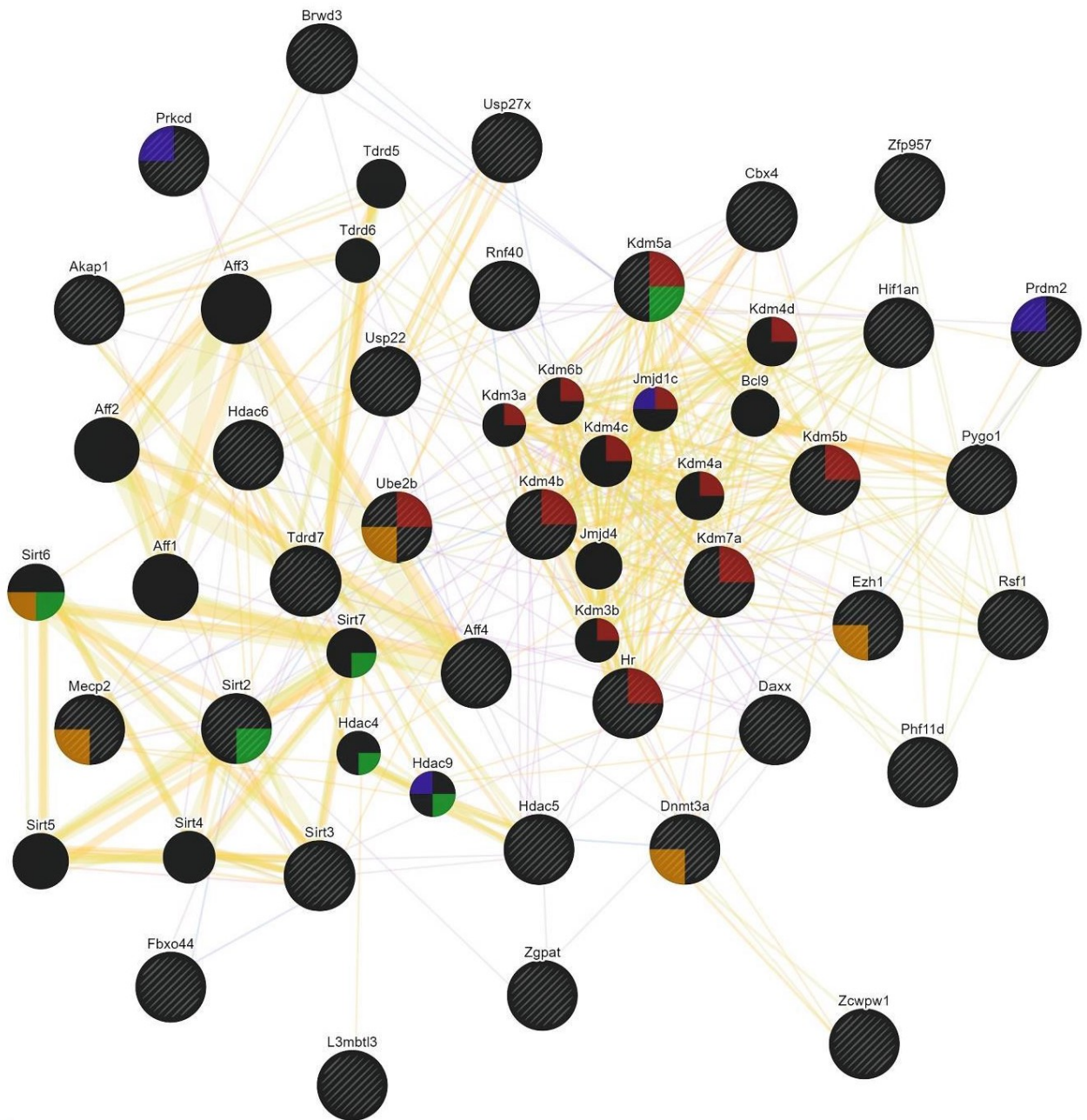
Supplementary Figure S2. Motif analysis of LASs in Smarca5 single-allele knockout MEFs as assessed by ATAC-seq. Motif analysis using HASs didn't result in significant enrichment of motifs in any bin.

Suppl. Figure S3



Supplementary Figure S3. Motif analysis of LASs in Smarca5 double allele knockout MEFs as assessed by ATAC-seq. Motif analysis using HASs didn't result in significant enrichment of motifs in any bin.

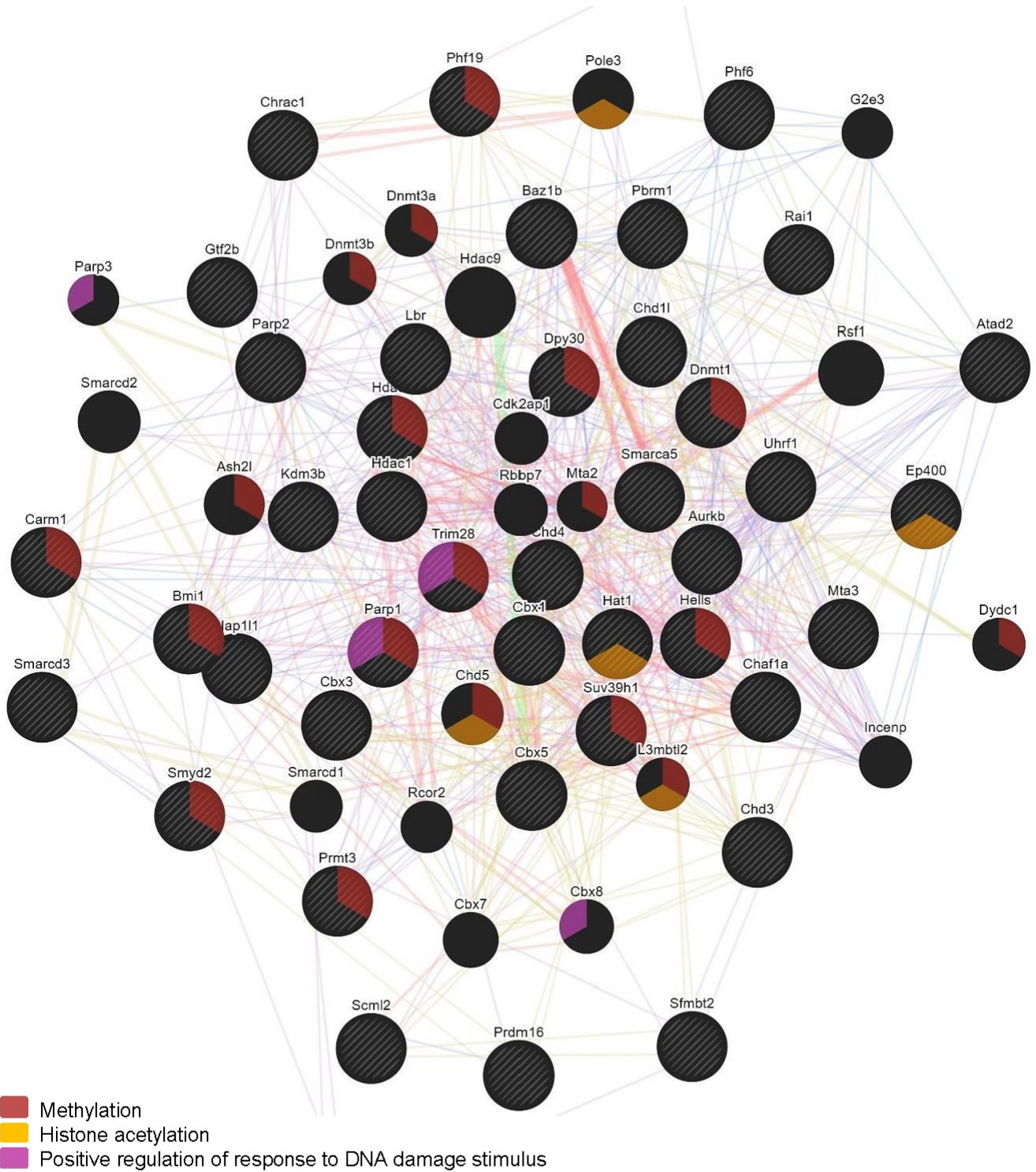
Suppl. Figure S4



- Histone demethylation
- Histone deacetylation
- Chromatin organization involved in negative regulation of transcription
- Aging

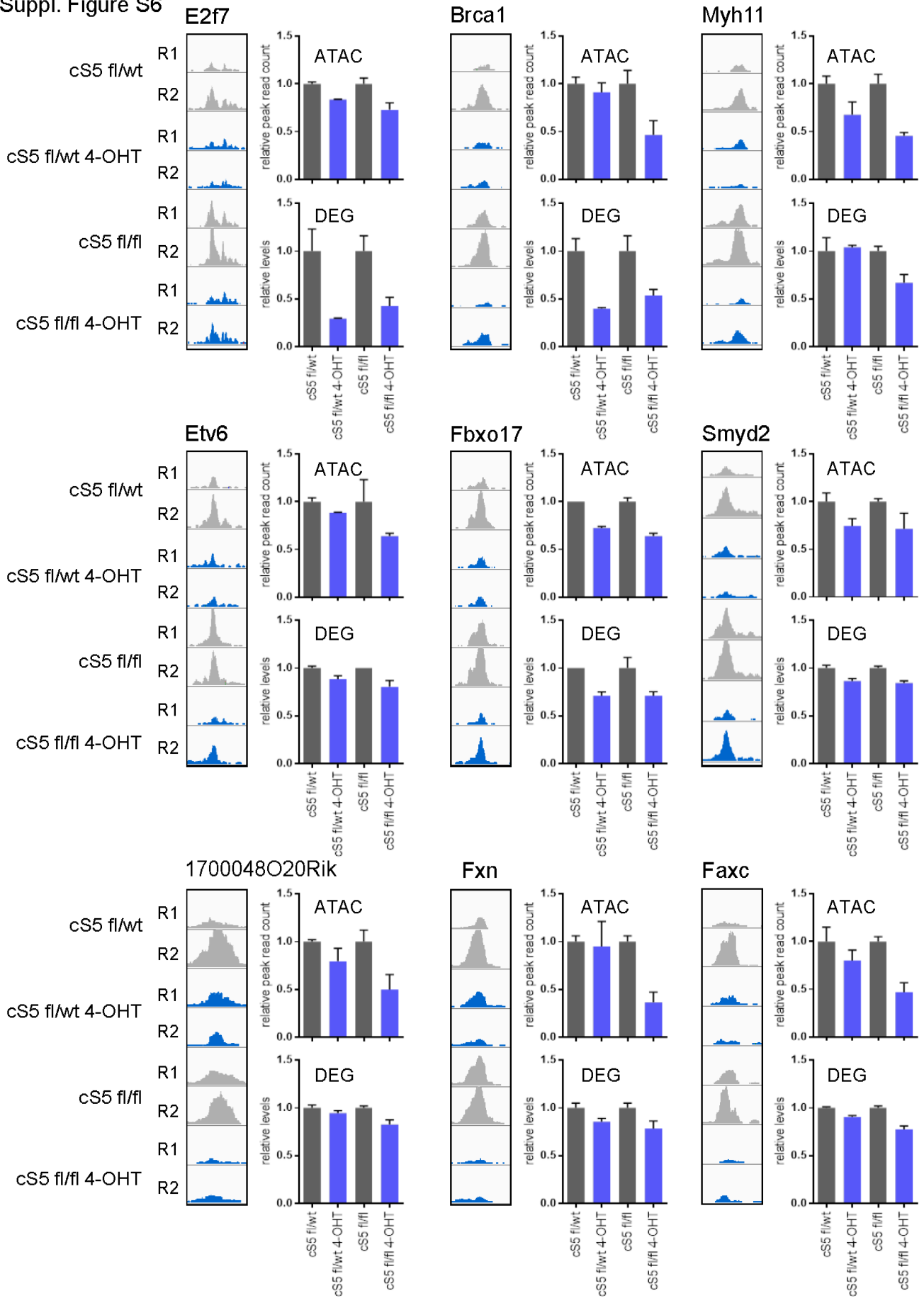
Supplementary Figure S4. GeneMANIA network map of gradually upregulated ERGs in Smarca5 knockout MEFs. Network lines represent GeneMANIA network categories – yellow: predicted, purple: co-expression, pink: physical interactions, blue: co-localization, green: genetic-interactions.

Suppl. Figure S5



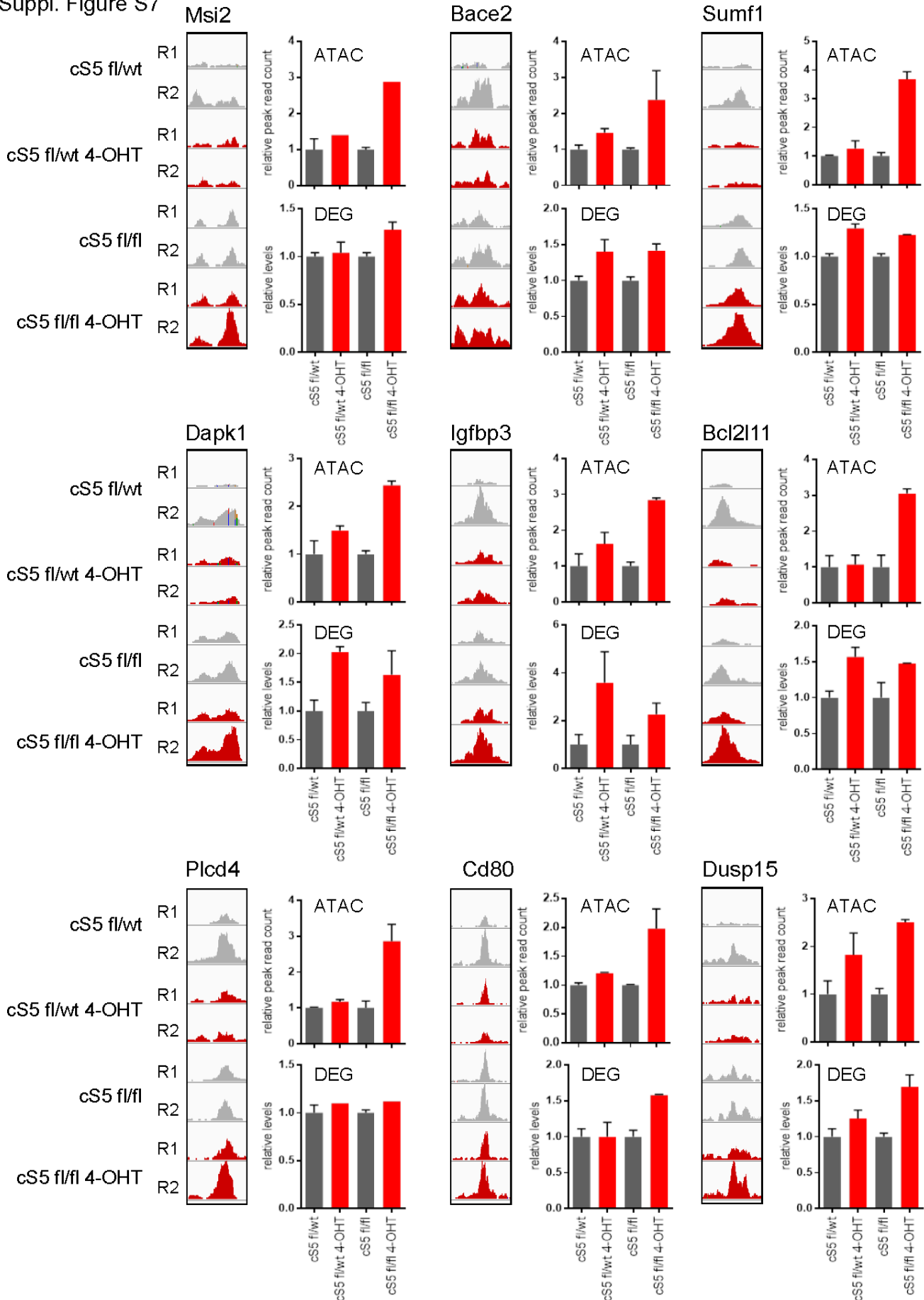
Supplementary Figure S5. GeneMANIA network map of gradually downregulated ERGs in Smarca5 knockout MEFs. Network lines represent GeneMANIA network categories – yellow: predicted, purple: co-expression, pink: physical interactions, blue: co-localization, green: genetic-interactions.

Suppl. Figure S6



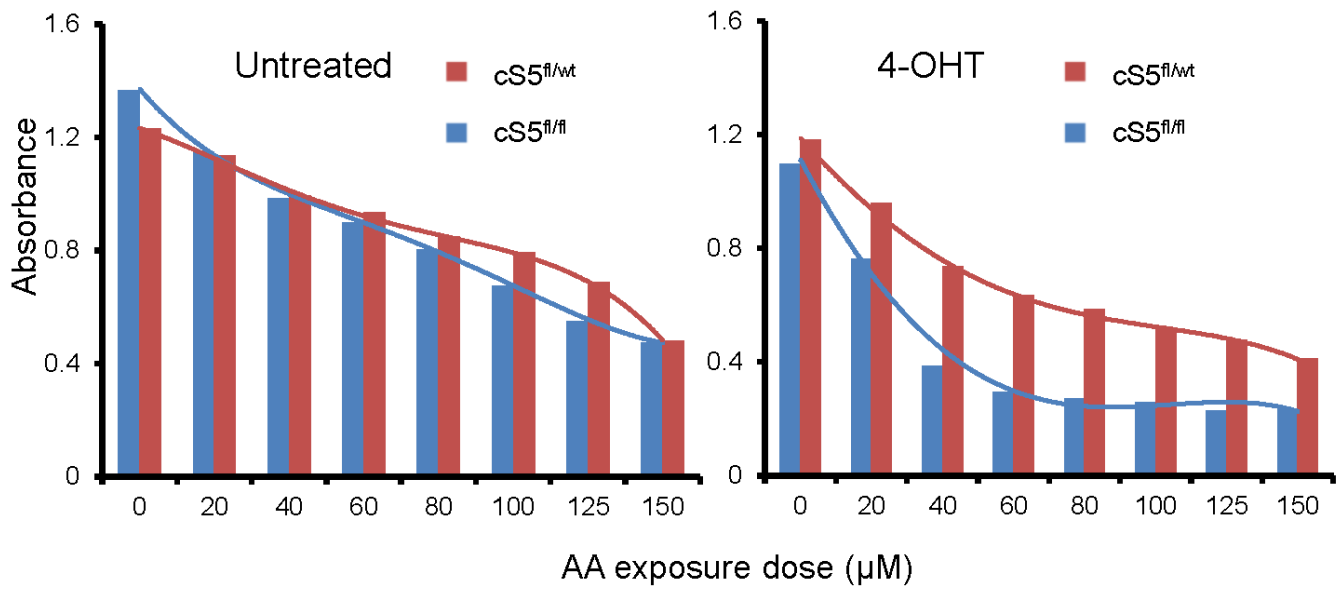
Supplementary Figure S6. Concordance of ATAC-seq and RNA-seq MEF cell data for decreased accessibility of select regulatory regions (low accessibility sites, LASs) and corresponding genes (DEGs) down-modulated upon stepwise knock-out of Smarca5. Vertical histograms display the ATAC-seq peaks for replicate (R1, R2) experiment across the studied genotypes (note that peaks represent *raw data, before across-experiment normalization* shown in Suppl. Fig. S1C). The adjacent bar graphs show normalized relative peak read counts for ATAC-seq (top graph) and the normalized relative mRNA levels (bottom graph) for a given gene. The top two rows show six enhancers and their regulated genes, the bottom row shows 3 proximal promoters and their genes. cS5 – conditional Smarca5 KO; fl/wt and fl/fl – single- and double allele knock-out, respectively; 4-OHT – treatment with 4-hydroxy-tamoxifen.

Suppl. Figure S7

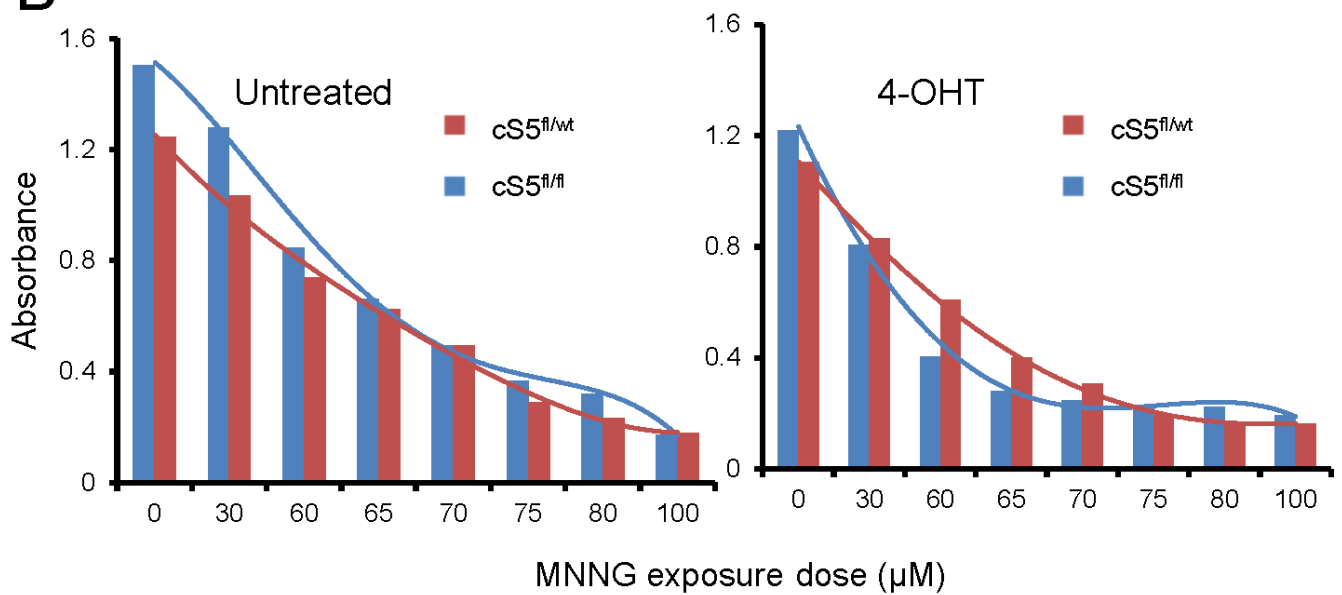


Supplementary Figure S7. Concordance of ATAC-seq and RNA-seq MEF cell data for increased accessibility of select regulatory regions (high accessibility sites, HASs) and corresponding genes (DEGs) up-modulated upon stepwise knock-out of Smarca5. Vertical histograms display the ATAC-seq peaks for replicate (R1, R2) experiment across the studied genotypes (note that peaks represent *raw data, before across-experiment normalization* shown in Suppl. Fig. S1C). The adjacent bar graphs show normalized relative peak read counts for ATAC-seq (top graph) and the normalized relative mRNA levels (bottom graph) for a given gene. The top two rows show six enhancers and their regulated genes, the bottom row shows 3 proximal promoters and their genes. cS5 – conditional Smarca5 KO; fl/wt and fl/fl – single- and double allele knock-out, respectively; 4-OHT – treatment with 4-hydroxy-tamoxifen.

A

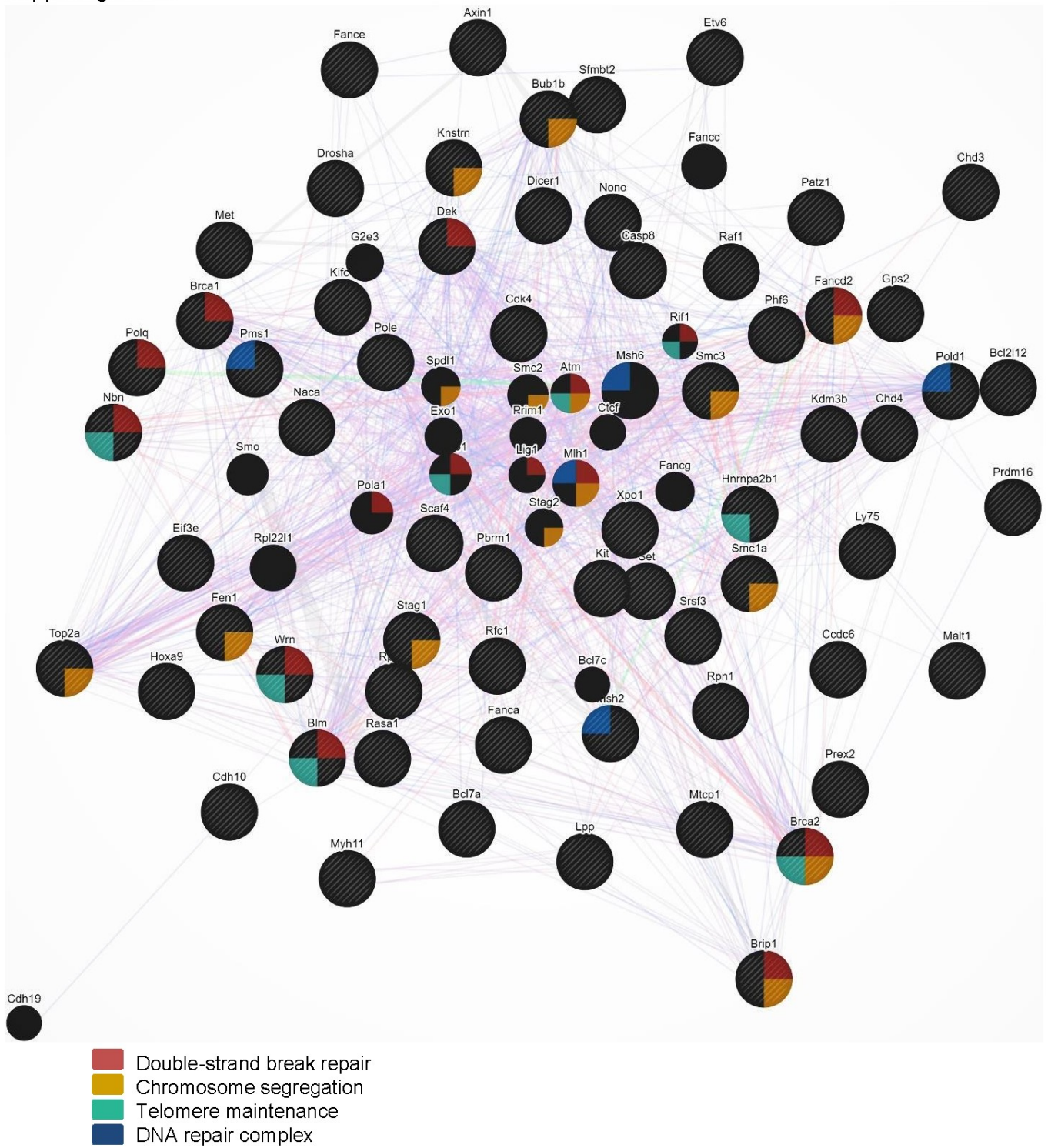


B



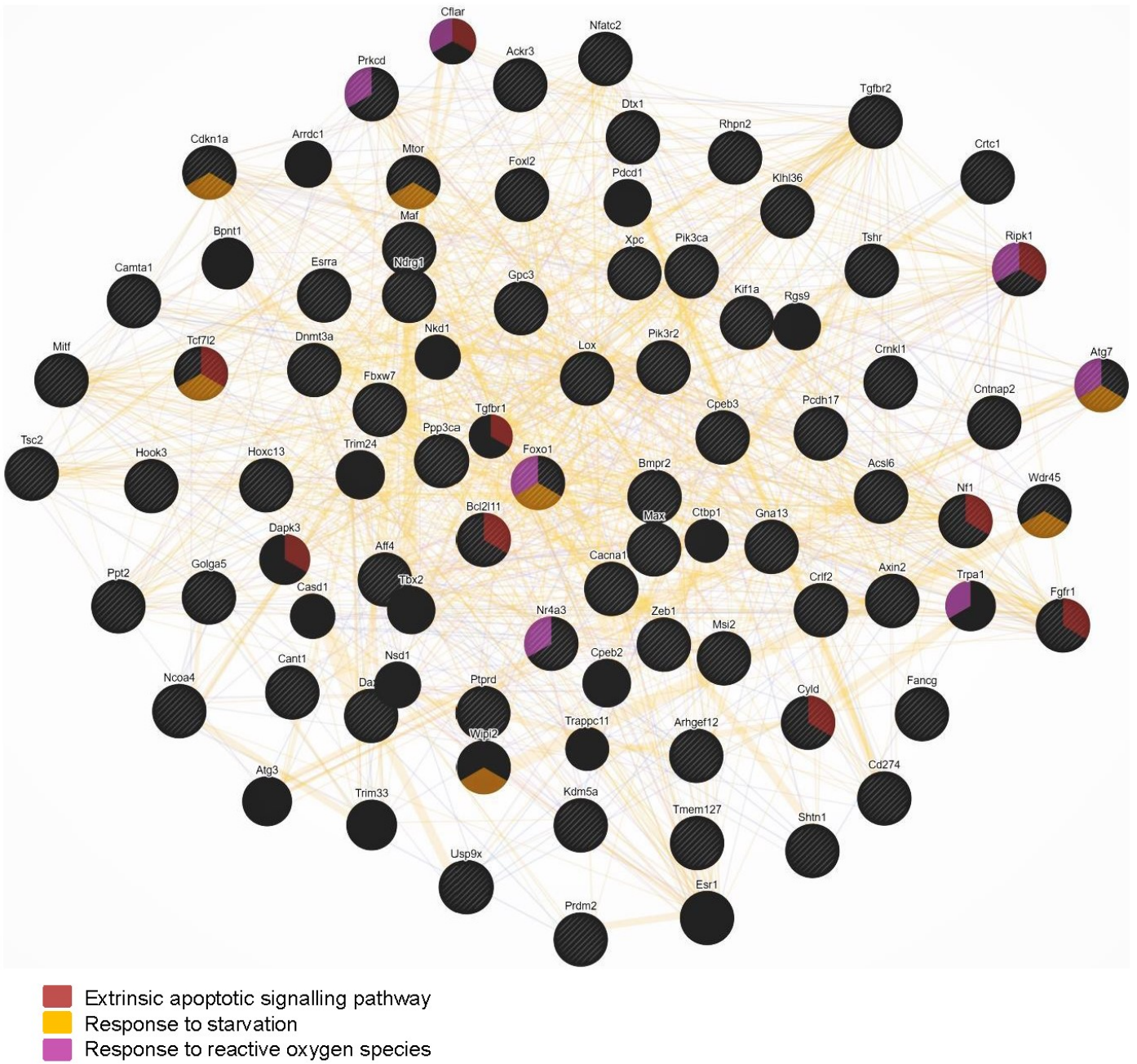
Supplementary Figure S8: A) Comparison of the proliferative differences as assessed by absolute absorbance measure via MTS assay of single and double allele knockout (right) and their respective wildtypes (left) side-by-side upon exposure to various doses of aristolochic acid-I (AA). **B)** Comparison of the proliferative differences as assessed by absolute absorbance measure via MTS assay of single and double allele knockout (left) and their respective wildtypes (right) side-by-side upon exposure to various doses of methylnitronitrosoguanidine (MNNG).

Suppl. Figure S9

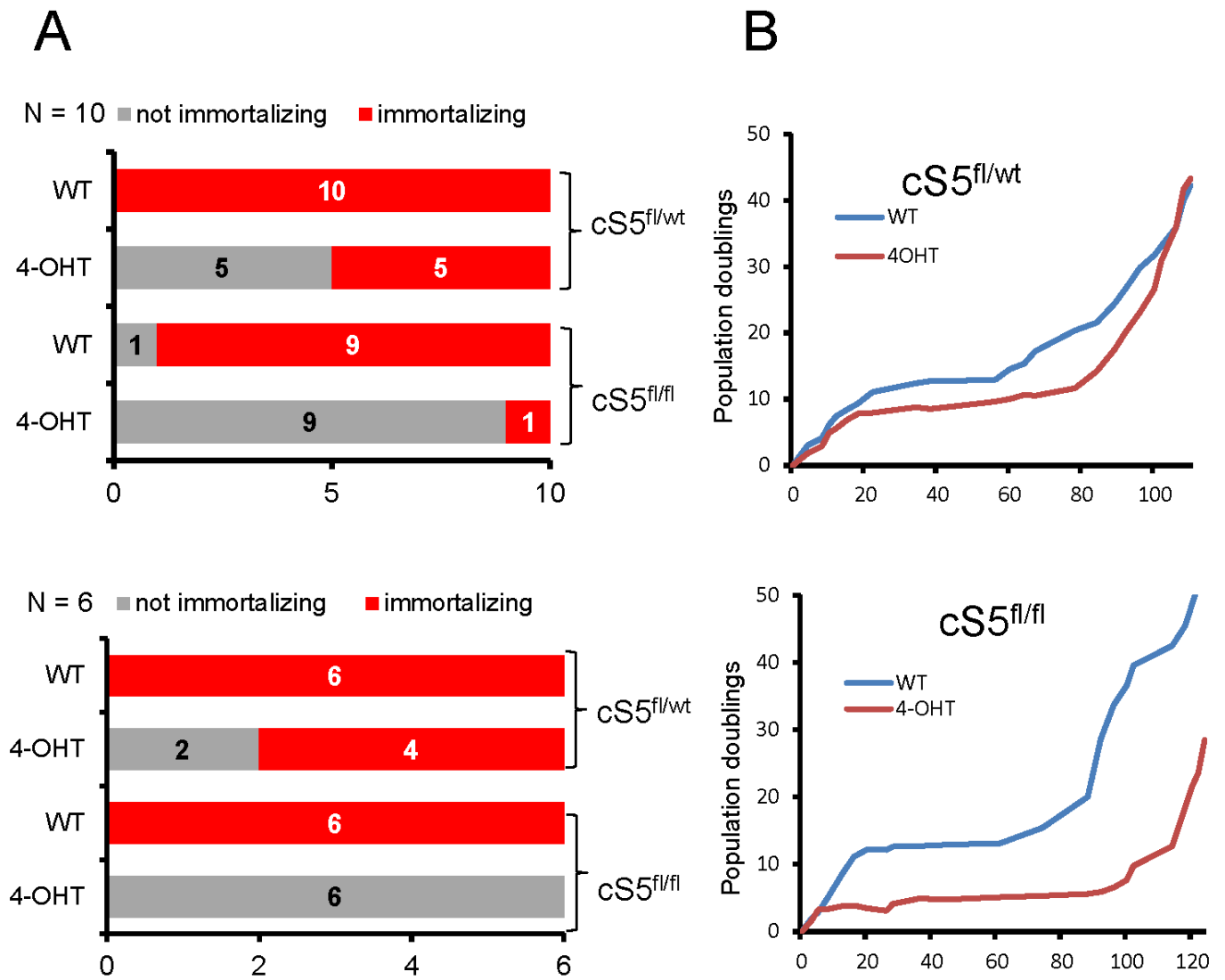


Supplementary Figure S9. The interaction network map of gradually downregulated cancer driver genes in *Smarca5* knockout MEFs. Network lines represent GeneMANIA network categories – purple: co-expression, pink: physical interactions, blue: co-localization, green: genetic-interactions.

Suppl. Figure S10



Supplementary Figure S10. GeneMANIA network map of gradually upregulated cancer driver genes in *Smrca5* knockout MEFs. Network lines represent GeneMANIA network categories – yellow: predicted, purple : co-expression, pink : physical interactions, blue : co-localization, green : genetic-interactions.



Supplementary Figure S11. A) Bar graphs show the total number of cultures out of ten (top) and six (bottom) starting cultures that managed to immortalize when cells were grown for prolonged periods of time, WT = untreated with 4-OHT. **B)** Growth curves of the single allele (top) and double allele (bottom) knockout MEFs with their corresponding wildtypes that bypassed senescence and immortalized.

5 Diskuse

ISWI ATPáza SMARCA5 je esenciální protein hrající roli v mnoha pro buňku velmi důležitých procesech, jako je transkripce a replikace genů či oprava DNA. Protein SMARCA5 je aktivní v komplexech s dalšími proteiny, zejména s BAZ proteiny, kde v důsledku své ATPázové aktivity plní funkci katalytické podjednotky, zatímco BAZ proteiny představují protein-protein interagující kofaktory rozpoznávající modifikace histonů a DNA. V předchozích studiích provedených v naší laboratoři bylo prokázáno, že *Smarca5* je esenciální pro brzký embryonální vývoj, konkrétně v období stadia blastocysty s poruchou gastrulace, jak dokázal myší model s delecí tohoto genu (Stopka and Skoultschi 2003). Model navazoval na objev významu *Smarca5* v myší krvetvorbě (a také klonování první myší sekvence *Smarca5*) a práci o *Smarca5* ve stresové erythropoéze. Dále také na odhalení role *Smarca5* v obnovení diferenciace po dosažení kompletní remise u akutní myeloidní leukemie (Stopka, Zakova et al. 2000). Dalším krokem ve studiu *Smarca5* bylo vytvoření modelu kondicionální delecce toho genu v krvetvorných kmenových buňkách (Vav1Cre model), jež umožnil odhalení nezastupitelné role *Smarca5* při časném vývoji hematopoetických kmenových buněk a jejich progenitorů (Kokavec, Zikmund et al. 2017). Oba výše zmíněné myší modely jsou letální (z důvodu těžké anemie ve fetálním období u Vav1 modelu a v případě klasického delecčního modelu během časného embryonálního vývoje), což bohužel neposkytlo možnost zkoumat pozdější stadia krvetvorby a také neumožnilo studovat, jak konkrétně se *Smarca5* na vývoji kmenových buněk a progenitorů podílí. Zatímco přítomnost erythropoézy je kritickým faktorem přežití myšího modelu, lymfocyty jsou v myši postradatelné, díky tomu model delecce *Smarca5* v lymfocytech není letální. Z toho důvodu, ale také i vzhledem k možné účasti SMARCA5 na opravě dvouvláknových zlomů DNA (Lan, Ui et al. 2010), (Toiber, Erdel et al. 2013) (v našich předchozích datech *in vivo* modelech prozatím neprokázané), jsme se rozhodli zkoumat dopad delecce *Smarca5* na vývojový proces lymfopoézy, během níž k řízeným dvouvláknovým zlomům na DNA přirozeně dochází (během V(D)J rekombinace).

Pro studium lymfoidního vývoje a zjištění role *Smarca5* v těchto procesech jsme využili myší model s kondicionální delecí *Smarca5* v buňkách exprimujících povrchový marker CD2 (hCD2iCre model), což v myši zahrnuje vedle T lymfocytů i B lymfocyty a dále také některé typy NK buněk. Ukázalo se, že *Smarca5* je nezbytný i pro vývoj těchto zmíněných buněčných typů, jelikož jedinci s delecí *Smarca5* neměly téměř žádné maturované T a B lymfocyty v periferní krvi. Další analýzou vývoje těchto buněčných linií v thymu a kostní dřeni, jsme

zjistili, že u T-lymfocytů docházelo k bloku při přechodu ze stadia DN3 do DN4 (odlišené na základě exprese povrchových markerů CD25 a CD44) a u B-lymfocytů při přechodu z pro-B do pre-B stádia jejich diferenciaci. Podrobnější studium však nepotvrdilo, že by delece *Smarca5* vedla k poruše rekombinace T buněčného receptoru (TCR). Zkřížení modelu s kondicionální delecí *Smarca5* v CD2⁺ buňkách s OT-II transgenním myším modelem exprimujícím αβ-TCR specifický pro ovalbumin, u kterého během diferenciaci neprobíhá rekombinace TCR receptoru, nevedlo k překonání vývojového bloku v DN3 stádiu diferenciaci T-lymfocytů. Dále data ze sekvenace transkriptomu ukázala, že expresní vzorec konstantních (*Trbc*) a variabilních (*Trbv*) genových segmentů, a tedy jejich relativní využití při přestavbě TCRβ, v DP T-lymfocytech není delecí *Smarca5* ovlivněno (Zikmund, Kokavec et al. 2019).

Vývojový blok při přechodu z DN3 do DN4 stádia T-lymfocytů a pro-B do pre-B přechodu B-lymfocytů byl také popsán u myšího modelu s neomorfni alelou *Pole3*, který se nachází s proteinem SMARCA5 v komplexu CHRAC, což naznačuje klíčovou úlohu tohoto komplexu v lymfoidním vývoji (Siamishi, Iwanami et al. 2020). U dalších delečních modelů vazebných partnerů *Smarca5* však nebyly defekty v krvetvorbě pozorovány. Například delece *Acf1* (tvoří se *Smarca5* komplex ACF) vede k defektům ve spermatogenezi, ale poruchy krvetvorby nebyly pozorovány (Dowdle, Mehta et al. 2013). Delece genů pro další vazebné partnery *Smarca5* *Rsf1* a *Bptf* jsou embryonálně letální a nebylo u nich tedy možné studovat krvetvorbu (Koscielny, Yaikhom et al. 2014), (Landry, Sharov et al. 2008). U myších modelů s delecí genů pro *Baz2a*, *Chrac1*, *Baz2b*, *Cecr2* (všechny vytváří komplexy s proteinem SMARCA5), nebyly také popsány žádné defekty v krvetvorbě (Koscielny, Yaikhom et al. 2014), (Dicipulo, Norton et al. 2021).

Výzkum delečních modelů pro gen *Smarca5* prokázal esenciální význam této ISWI ATPázy pro proliferující a diferencující buňky, ať už se jedná o embryonální kmenové buňky (Stopka and Skoultchi 2003), hematopoetické progenitory (Kokavec, Zikmund et al. 2017), (Zikmund, Kokavec et al. 2019), myší embryonální fibroblasty, které po delecí *Smarca5* přestávají proliferovat a ztrácí schopnost imortalizace (Thakur, Cahais et al. 2022), tak i různé leukemické linie derivované z pacientů s akutní myeloidní leukemií (Zikmund, Paszekova et al. 2020). Vzhledem k tomu, že delece *Smarca5* vedla ve výše zmíněných modelech k zástavě proliferace a diferenciaci, případně vstupu do senescence a následné apoptózy, tyto modely neumožnily detailnější studium vlivu *Smarca5* na diferenciaci buněk. Z toho důvodu jsme se rozhodli vytvořit myší model exprimující transgenní SMARCA5 protein. Původně jsme se domnívali, že pokud budeme exprimovat *Smarca5* v transgenním systému, povede to k nadprodukci proteinu, nicméně, jak jsme ukázali, vzhledem k prozatím nejasnému

mechanismu, který nadprodukcí na proteinové úrovni brání, dosáhli jsme pouze zanedbatelného navýšení exprese. Následně jsme zjistili, že exprese transgenního SMARCA5 proteinu je oproti endogennímu naopak výrazně nižší, zvláště při přítomnosti pouze jedné alely transgenů. Z toho důvodu jsme se rozhodli použít tento myší model s transgenní expresí cDNA lidského *SMARCA5*, který jsme dále následně zkřížili s delečními modely kondiční inaktivace *Smarca5*, což nám umožnilo studovat vliv různých hladin SMARCA5 proteinu na hematopoézu (množství produkované z jedné či dvou alel transgenů s využitím delečního modelu ve srovnání s kontrolou). Transgenní model byl vytvořen vložením cDNA pro lidský *SMARCA5* gen do lokusu *Rosa26*, kde je exprimován z endogenního promotoru. Dále také obsahuje proteinovou značku FLAG na C-konci proteinu, která umožňuje identifikaci transgenního proteinového produktu od endogenního myšího proteinu, jež je prakticky identický kromě několika nekonzerovaných aminokyselin, nacházejících se zejména na nestrukturovaném N-koci proteinu (homologie přes 97 %). Využití lidské cDNA umožnilo odlišení na úrovni RNA od myší endogenní RNA a srovnání exprese transgenů i na této úrovni. *SMARCA5* transgen je exprimován kondičně a jeho expresi je možné spustit tkáňově-specificky využitím transgenů Cre-rekombinázy exprimované pod příslušným promotorem. Bez aktivace Cre rekombinázou, je z transgenního konstruktů exprimován fluorescenční protein tdTOMATO, který slouží jako pozitivní kontrola přítomnosti sekvence transgenů a je obklopen LoxP místy. Po expresi Cre rekombinázy dochází k jeho vyštěpení a expresi *SMARCA5* RNA a proteinu.

Abychom ověřili, zda je námi vytvořený transgenní *SMARCA5* konstrukt funkční a je schopný nahradit funkce endogenní *Smarca5*, zkřížili jsme transgenní model s hCD2iCre kondičně *Smarca5* delečním modelem. Jak jsme ukázali dříve, delece *Smarca5* v CD2⁺ buňkách vede k bloku diferenciaci a zmenšení thymu, což vede ke ztrátě T buněk (a také B buněk, jelikož u myši je CD2 aktivní i v tomto podtypu lymfocytů) (Zikmund, Kokavec et al. 2019). V přítomnosti transgenů, tj. exprese zhruba 85 % množství endogenního proteinu z jedné alely transgenů, jsme pozorovali téměř úplnou záchranu fenotypu hCD2iCre delečního *Smarca5* modelu, tedy odstranění vývojového bloku v přechodu z DN3 do DN4 stádia u T lymfocytů a pro-B do pre-B stádia B lymfocytů. Nicméně, jisté změny fenotypu byly stále zřetelné, což nám umožnilo se zabývat tím, jak silně jsou jednotlivé krvetvorné podtypy závislé na dávce SMARCA5 proteinu. Ukázali jsme, že právě lymfoidní linie byla na pokles hladiny SMARCA5 nejcitlivější.

Pro účely studia vlivu snížené hladiny SMARCA5 na celý proces krvetvorby jsme nově vytvořený transgenní model zkřížili s Vav1iCre kondičně *Smarca5* delečním modelem, který exprimuje Cre rekombinázu pod promotorem Vav1, tedy ve většině stádií krvetvorby

počínaje hematopoetickou kmenovou buňkou. Exprese SMARCA5 transgenů vedla k záchraně embryonální letality tohoto modelu, ke které u něj dochází v 18. dni fetálního vývoje na podkladě těžké anemie a poruchy vývoje krvetvorného orgánu fetálních jater (Kokavec, Zikmund et al. 2017). U transgenních zvířat exprimujících *Vav1iCre* a současně *SMARCA5* transgen na pozadí delece tohoto genu byly pozorovány defekty v krvetvorbě, obzvláště pokud měly jen jednu alelu transgenů (*S5tg*), kdy byl protein SMARCA5 exprimován jen na úrovni asi 10 % množství endogenního proteinu v kostní dřeni a asi 27 % v thymu. Konkrétně byla v periferní krvi pozorována výrazná lymfopenie a jen zcela mírná anémie. Myelocytární parametry byly srovnatelné s kontrolními vzorky, což ukazuje, že myelopoéza není závislá na vysoké expresi SMARCA5 proteinu. Tento fenotyp byl spojený s výrazně nižší expresí SMARCA5 proteinu, na úrovni RNA však tento defekt pozorován nebyl a množství *Smarca5* RNA bylo srovnatelné u transgenních zvířat i jejich kontrol. Dle naší hypotézy dochází k regulaci SMARCA5 na proteinové úrovni během hematopoézy, tomuto fenoménu se v naší laboratoři dále věnujeme a rádi bychom ho objasnili.

Při studiu časnějších vývojových stádií progenitorů, jež vycházejí z pluripotentní hematopoetické kmenové buňky, v kostní dřeni jsme pozorovali, že dochází k akumulaci multipotentních hematopoetických progenitorů (MPP) – konkrétně zejména frakce MPP3 a také MPP2. Zajímavé je, že u MPP4 progenitorů, které diferencují do lymfoidní linie, jsme změnu zastoupení a počtu nepozorovali. Při analýze kostní dřene transgenních zvířat pomocí průtokové cytometrie jsme pozorovali, že se u nich nachází zvláštní populace buněk připomínající MPP2 a MPP3 progenitory, avšak neexprimující CD34 molekulu typickou pro toto stádium. Tato aberantní (tj. normálně se nevyskytující) populace pravděpodobně pochází z populací MPP2 a MPP3 progenitorů, které nebyly schopné dále diferencovat a je dalším projevem defektu krvetvorby u transgenních zvířat. Dále bylo pozorováno snížené zastoupení jak myeloidních, tak lymfoidních progenitorů. Na rozdíl od periferní krve byly v kostní dřeni pozorovány defekty pouze u jedinců s jednou alelou transgenů *S5tg*, zatímco jedinci s dvěma alelami *S5tg* měli fenotyp srovnatelný s kontrolami. Konzistentně s *hCD2iCre* modelem bylo pozorováno, že snížená hladina proteinu SMARCA5 má největší vliv na vývoj lymfocytů, a to především B-lymfocytů. Také u *Vav1iCre* modelu bylo pozorováno, že k bloku ve vývoji dochází při přechodu z DN3 do DN4 stádia u T-lymfocytů a ze stádia pro-B do pre-B u B-lymfocytů. Defekty ve vývoji v nepřítomnosti *Smarca5* byly však u *Vav1iCre* modelu výrazně závažnější, což dokazuje, že hladina SMARCA5 proteinu je důležitá nejen v pozdějších lymfoidních stádiích ale zejména pro jejich liniově specifické hematopoetické progenitory.

Dále jsme se zabývali tím, zda dochází k změnám v množství proteinu SMARCA5 během diferenciace krvetvorných progenitorů. Pomocí analýzy metodou kvantitativní cílené proteomiky jsme zjistili, že pozorovaný blok ve vývoji progenitorů koresponduje právě se změnou mírou exprese proteinu SMARCA5. U kontrolních zvířat bylo pozorováno, že dochází k výraznému navýšení množství tohoto proteinu při přechodu z LSK (Lineage negativní, Sca1 pozitivní, c-kit pozitivní) do LS⁻K (Lineage negativní, Sca1 negativní, c-kit pozitivní) stádia. Transgenní zvířata s dvěma alelami transgenu měla celkově nižší hladinu SMARCA5 proteinu a docházelo u nich pouze malému navýšení množství při přechodu z LSK do LS⁻K stádia. Zatímco u zvířat s pouze jednou alelou transgenu docházelo dokonce k mírnému snížení množství SMARCA5 proteinu u LS⁻K stádia proti LSK. Toto pozorování odpovídá dříve zmíněnému vývojovému bloku, protože akumulované MPP patří do LSK stádia a myeloidní (CMP) a lymfoidní (CLP) progenitory, u nichž byl pozorován úbytek, patří do LS⁻K stádia. Výsledky získané z modelu se dvěma kopiemi transgenu ukazují, že *Smarca5* je během hematopoézy regulován nezávisle na promotoru, ze kterého dochází k jeho expresi, jelikož k této regulaci dochází jak u endogenního, tak u transgenního proteinu, který je exprimován z *Rosa26* promotoru. Předchozí výzkum ukázal, že SMARCA5 může být degradován cestami závislými na culinu a proteazomu (Emanuele, Elia et al. 2011), což představuje zajímavý a nový koncept, který je zjevně důležitý pro diferenciaci krvetvorby. V současné době pracujeme na jeho objasnění a, jak bylo zmíněno výše, regulací SMARCA5 v hematopoéze na proteinové úrovni se dále zabýváme. Můžeme však potvrdit, že minimálně v našich myších modelech dochází k této regulaci jak u lidského, tak u myšího SMARCA5 proteinu. Tudiž zjištěný fenotyp nesouvisí s liniíovou specificitou transgenu. V našich projektech máme také k dispozici model s myší transgenní *Smarca5 cDNA*, jehož konstrukt byl u tohoto modelu také vložen do *Rosa26* lokusu a je exprimován ve všech buňkách ze silného arteficiálního CAG promotoru. I u tohoto modelu byla však pozorována snížená exprese SMARCA5 proteinu v kostní dřeni, snížená produkce transgenní SMARCA5 tedy není dána přítomností lidské cDNA pro tento protein.

Abychom prokázali, že se u studovaných Vav1Cre transgenních myší s *S5tg* jedná opravdu o defekt na úrovni hematopoetických progenitorů a že hematopoetická „niche“ (tedy oblast přežívání a zrání kmenové buňky v krvetvorném orgánu) jako taková není poškozena, provedli jsme sérii transplantačních experimentů. Nejdříve jsme transplantovali kostní dřev z kontrolních myší divokého typu do *S5tg* transgenních zvířat a kontrol. Příjemci kostní dřevě byli ozářeni různými dávkami záření (0-6 Gy), iradiace je zapotřebí pro uvolnění „niche“ původními progenitory. Bylo pozorováno, že zdravá kostní dřev z kontrolních dárců je schopná

plně nahradit krvetvorbu transgenních jedinců, kteří exprimují pouze jednu alelu transgenu *S5tg*, a to bez nutnosti jakékoli předchozí iradiace, tudíž příjemci s *S5tg* genotypem mají významně permissivní „niche“ pro transplantaci. U zvířat se dvěma alelami transgenu *S5tg* docházelo také k velmi dobrému přihojení dárcovských buněk a k nahrazení krvetvorby dárcovskou docházelo už při nižších dávkách iradiace než u kontrolních zvířat. Toto pozorování dokazuje, že hematopoetická nika transgenních zvířat je schopna akceptovat transplantát a obnovit celou krvetvorbu na úroveň srovnatelnou s kontrolními zvířaty. V následném kompetitivním transplantačním experimentu jsme transplantovali transgenní kostní dřev smíchanou v poměru 3:1 s kostní dřev divokého typu do subletálně iradiovaných kontrolních zvířat. Kostní dřev se dvěma alelami transgenu *S5tg* byla schopná částečně nahradit produkci myelocytů, ale ne lymfocytů a kostní dřev s pouze jednou alelou *S5tg* transgenu nebyla schopná kompetovat s kontrolní kostní dřev v produkci všech buněčných podtypů. Tento experiment dále potvrdil, že defekt u *S5tg* myši je opravdu na úrovni transgenních hematopoetických progenitorů a opět jsme největší defekt pozorovali především u lymfocytů, a to zejména u B-lymfocytů. Velmi podobných výsledků bylo dosaženo ve studii, kde byla kompetitivně (poměr 1:1) transplantována kostní dřev s neomorfní alelou *Pole3* (vazebný partner *Smarca5*). V této studii byl pozorován defekt v repopulaci lymfoidní řady, ale myeloidní řada byla repopulována bez problémů (Siamishi, Iwanami et al. 2020). Co se týče jiných chromatin remodelačních komplexů, byl podobný experiment proveden u knock-out myšního modelu ARID1A (SWI/SNF rodina), delece zde vedla k defektům ve všech řadách hematopoetických buněk a akumulaci hematopoetických progenitorů, které nebyly schopny repopulovat hematopoézu v kompetitivním transplantačním experimentu (Han, Madan et al. 2019).

Dále jsme chtěli zjistit, jestli je možné pomocí SMARCA5 transgenního modelu zachránit embryonální letalitu celotělového *Smarca5* delečního modelu a vytvořit tak model, který by exprimoval pouze transgenní SMARCA5. Dokázali jsme, že to je možné pouze při přítomnosti dvou alel transgenu a embrya s tímto genotypem jsou výrazně méně životaschopná než kontroly. Pozorovali jsme výrazně sníženou četnost narození genotypu s pouze transgenní SMARCA5 – pouze 1 % oproti 25 % očekávané Mendelovské pravděpodobnosti. Embrya závislá na jedné alele transgenu *S5tg* umírala během různých stádií vývoje od časných až do vývojových stádií těsně před porodem. Jedinci, kteří se narodili, v některých případech zemřeli hned v prvních dnech života vzhledem k jejich snížené hmotnosti a vitalitě. Ti jedinci, kteří se však dožili odstavu (věk 4 týdnů), vykazovali fenotyp shodný s *Vav1* transgenním modelem – lymfopenii postihující zejména B-lymfocyty. Myšší model s produkcí *S5tg* transgenu ve všech tkáních těla na pozadí endogenní exprese *Smarca5* jsme dále také využili pro potvrzení

schopnosti transgenní lidské SMARCA5 vytvářet komplexy s myšimi vazebnými partnery. Bylo potvrzeno, že transgenní protein vytváří všechny komplexy dle očekávání a potvrdili jsme tedy, že může nahradit endogenní protein. Tento *S5tg* model nám umožnil studovat složení ISWI komplexů tkáňově specifickým způsobem. Ačkoli našim výsledkům dominují kanonické komplexy s proteiny BAZ (jak bylo aktualizováno v (Oppikofer, Bai et al. 2017)), rozhodně nelze vyloučit, že mohou existovat i jiné interakce, které nejsou snadno detekovatelné metodikou hmotnostní spektrometrie, kterou jsme použili. Tyto nekanonické komplexy mohou být závislé na kontextu a obtížně detekovatelné ve směsi buněčných populací. Nicméně naše data také ukazují na zapojení CTCF do komplexu ISWI v některých tkáních, zejména ve fetální hematopoéze, jak bylo popsáno dříve (Barisic, Stadler et al. 2019).

Pozorování podobná výše zmíněným byla učiněna i u delečních myších modelů ostatních chromatin remodelujících faktorů z SWI/SNF super-rodiny. Například u modelu s mutovaným *Baf57* (podjednotka BAF komplexu remodelujícího chromatin), kde došlo k narušení jeho vazby na DNA, došlo k blokaci vývoje CD8 pozitivních T-lymfocytů, a to i při mutaci pouze jedné alely. Podobný blok diferenciací byl pozorován u myši s heterozygotní delecí *Brg1*, podjednotky chromatin remodelačního komplexu BAF (Chi, Wan et al. 2002). Ale na rozdíl od *Smarca5* delečního modelu vede delece *Brg1* k bloku diferenciací v přechodu z DN4 do DP fáze vývoje T-lymfocytů, tedy později. Dochází k snížení exprese c-kit u *Brg1* deficitních thymocytů a pravděpodobně i narušení Wnt signalizace, která expresi c-kit reguluje. Dále také byly pozorovány defekty ve pre-TCR signální dráze, která je zásadní právě pro přechod z DN3 do DN4 stádia (Chi, Wan et al. 2003). Dalším chromatin remodelačním faktorem s významnou úlohou v hematopoéze je Mi-2 β (rodina Mi-2, komplex NuRD), který je také nezbytný pro přechod z DN4 do DP fáze vývoje T-lymfocytů a zejména pro vývoj CD4 pozitivních T-lymfocytů. Ukázalo se, že Mi-2 β hraje roli při expresi CD4 a jeho delece způsobuje defekt ve vývoji této linie, zatímco vývoj CD8⁺ je delecí Mi-2 β ovlivněn pouze minimálně (Williams, Naito et al. 2004).

Jedním z hlavních důvodů, proč jsme se zaměřili na studium rolí *Smarca5* v kmenových buňkách, bylo to, že v kmenových buňkách dochází k rozličným dějům, jež mají vztah k cytopeniím, imunodeficitům, autoimunitám až po stavy vedoucí k maligním transformacím krvetvorné kmenové buňky. Není tedy náhodou, že SMARCA5 byl zvažován jako onkogen, který je prokazatelně nadměrně exprimován jak u leukemií, tak u solidních nádorů (Li, Gong et al. 2021), (Stopka, Zakova et al. 2000). Na druhou stranu se zdá, že jeho blízký homolog SMARCA1 může mít naopak spíše tumor supresorickou úlohu. SMARCA5 byl nalezen v komplexu s fúzním transgenem NUP98-NSD1 u dětské akutní leukémie (Jevtic, Matafora et al.

2022). To naznačuje, že složení komplexů SMARCA5 hraje významnou roli v jeho proonkogenním účinku. Například exprese jeho interakčního partnera *Rsf1* (komplex RSF) byla spojena s horším přežitím u nádorových onemocnění (Cai, Yang et al. 2021). Výsledky získané z SMARCA5 transgenního modelu také ukazují, že ačkoli exprese mRNA z alely transgenu byla srovnatelná s endogenní alelou, její exprese na úrovni proteinu byla výrazně nižší. To naznačuje, že regulace stability proteinu SMARCA5 by mohla hrát důležitou roli při prevenci nadměrné produkce SMARCA5 v kmenových buňkách. Zásadní je určit roli SMARCA5 v lymfopoéze a jeho zapojení do lymfoidních patologií, z našich výsledků vyplývá, že pro tento buněčný typ je hladina SMARCA5 nejdůležitější. Existují již důkazy (přehled v (Li, Gong et al. 2021)) o významu SMARCA5 a jeho vazebných partnerů u lymfomu z pláštěových buněk (BPTF) a nehodgkinských lymfomů (RBBP4, BPTF). Přesný mechanismus působení SMARCA5 a jeho zapojení do dalších patologií, například agresivních lymfomů, však dosud nebyl odhalen. Naše práce je však dokladem toho, že výzkum souvislostí mezi expresí *Smarca5*, s tím související vytvářením konkrétních epigenetických komplexů, a regulací genové exprese v kmenových buňkách je zapotřebí k pochopení vzniku některých patologických stavů.

6 Závěr a grantová podpora

- SMARCA5 je esenciální pro proliferující a diferencující buňky včetně hematopoetických kmenových buněk.
- Delece *Smarca5* vede k zastavení proliferace, akumulaci progenitorů a apoptóze.
- Myší model se sníženou transgenní expresí SMARCA5 proteinu je schopný zachránit letalitu *Smarca5* delečních modelů (Vav1iCre, celotělový knock-out).
- Transgenní SMARCA5 se váže ve všech očekávaných komplexech se svými partnery a jeho exprese je nižší než exprese endogenního proteinu.
- Snížená exprese *Smarca5* vede k akumulaci hematopoetických progenitorů, vedoucí k těžké lymfopenii a lehké anémii. Nejvíce jsou zasaženy B-lymfocyty.
- Hematopoetické kmenové buňky exprimující pouze transgenní SMARCA5 protein nejsou schopné repopulovat hematopoézu v transplantačních experimentech. Opět jsou nejvýrazněji ovlivněny lymfocytární linie, hlavně B-lymfocyty.
- Regulace hladiny SMARCA5 proteinu je nezbytnou součástí procesu hematopoézy.

Disertační práce byla vytvořena za podpory následujících grantů:

Ministerstvo zdravotnictví České republiky: NU22-05-00374, NU21-08-00312

Grantová agentura České republiky: 24-10435S, 24-10353S

Ministerstvo školství, mládeže a tělovýchovy České republiky: SVV 260637,

UNCE/MED/016, COOPERATIO, Programme EXCELES (LX22NPO5102)

7 Seznam použité literatury

- Alenghat, T., J. Yu and M. A. Lazar (2006). "The N-CoR complex enables chromatin remodeler SNF2H to enhance repression by thyroid hormone receptor." *EMBO J* **25**(17): 3966-3974.
- Alvarez-Saavedra, M., Y. De Repentigny, P. S. Lagali, E. V. Raghu Ram, K. Yan, E. Hashem, D. Ivanochko, M. S. Huh, D. Yang, A. J. Mears, M. A. Todd, C. P. Corcoran, E. A. Bassett, N. J. Tokarew, J. Kokavec, R. Majumder, I. Ioshikhes, V. A. Wallace, R. Kothary, E. Meshorer, T. Stopka, A. I. Skoultchi and D. J. Picketts (2014). "Snf2h-mediated chromatin organization and histone H1 dynamics govern cerebellar morphogenesis and neural maturation." *Nat Commun* **5**: 4181.
- Aydin, O. Z., J. A. Marteiijn, C. Ribeiro-Silva, A. Rodriguez Lopez, N. Wijgers, G. Smeenk, H. van Attikum, R. A. Poot, W. Vermeulen and H. Lans (2014). "Human ISWI complexes are targeted by SMARCA5 ATPase and SLIDE domains to help resolve lesion-stalled transcription." *Nucleic Acids Res* **42**(13): 8473-8485.
- Barisic, D., M. B. Stadler, M. Iurlaro and D. Schubeler (2019). "Mammalian ISWI and SWI/SNF selectively mediate binding of distinct transcription factors." *Nature* **569**(7754): 136-140.
- Becker, P. B. (2002). "Nucleosome sliding: facts and fiction." *EMBO J* **21**(18): 4749-4753.
- Bowman, G. D. (2010). "Mechanisms of ATP-dependent nucleosome sliding." *Curr Opin Struct Biol* **20**(1): 73-81.
- Boyer, L. A., M. R. Langer, K. A. Crowley, S. Tan, J. M. Denu and C. L. Peterson (2002). "Essential role for the SANT domain in the functioning of multiple chromatin remodeling enzymes." *Mol Cell* **10**(4): 935-942.
- Boyer, L. A., R. R. Latek and C. L. Peterson (2004). "The SANT domain: a unique histone-tail-binding module?" *Nat Rev Mol Cell Biol* **5**(2): 158-163.
- Cai, G., Q. Yang and W. Sun (2021). "RSF1 in cancer: interactions and functions." *Cancer Cell Int* **21**(1): 315.
- Cavellan, E., P. Asp, P. Percipalle and A. K. Farrants (2006). "The WSTF-SNF2h chromatin remodeling complex interacts with several nuclear proteins in transcription." *J Biol Chem* **281**(24): 16264-16271.
- Collins, N., R. A. Poot, I. Kukimoto, C. Garcia-Jimenez, G. Dellaire and P. D. Varga-Weisz (2002). "An ACF1-ISWI chromatin-remodeling complex is required for DNA replication through heterochromatin." *Nat Genet* **32**(4): 627-632.
- Corona, D. F., A. Eberharter, A. Budde, R. Deuring, S. Ferrari, P. Varga-Weisz, M. Wilm, J. Tamkun and P. B. Becker (2000). "Two histone fold proteins, CHRAC-14 and CHRAC-16, are developmentally regulated subunits of chromatin accessibility complex (CHRAC)." *EMBO J* **19**(12): 3049-3059.
- Daxinger, L., S. K. Harten, H. Oey, T. Epp, L. Isbel, E. Huang, N. Whitelaw, A. Apedaile, A. Sorolla, J. Yong, V. Bharti, J. Sutton, A. Ashe, Z. Pang, N. Wallace, D. J. Gerhardt, M. E. Blewitt, J. A. Jeddloh and E. Whitelaw (2013). "An ENU mutagenesis screen identifies novel and known genes involved in epigenetic processes in the mouse." *Genome Biol* **14**(9): R96.
- Deindl, S., W. L. Hwang, S. K. Hota, T. R. Blosser, P. Prasad, B. Bartholomew and X. Zhuang (2013). "ISWI remodelers slide nucleosomes with coordinated multi-base-pair entry steps and single-base-pair exit steps." *Cell* **152**(3): 442-452.
- Dicipulo, R., K. A. Norton, N. A. Fairbridge, Y. Kibalnyk, S. C. Fox, L. K. Hornberger and H. E. McDermid (2021). "Cecr2 mutant mice as a model for human cat eye syndrome." *Sci Rep* **11**(1): 3111.

Dluhosova, M., N. Curik, J. Vargova, A. Jonasova, T. Zikmund and T. Stopka (2014). "Epigenetic control of SPI1 gene by CTCF and ISWI ATPase SMARCA5." *PLoS One* **9**(2): e87448.

Dowdle, J. A., M. Mehta, E. M. Kass, B. Q. Vuong, A. Inagaki, D. Egli, M. Jasin and S. Keeney (2013). "Mouse BAZ1A (ACF1) is dispensable for double-strand break repair but is essential for averting improper gene expression during spermatogenesis." *PLoS Genet* **9**(11): e1003945.

Eckey, M., S. Kuphal, T. Straub, P. Rummele, E. Kremmer, A. K. Bosserhoff and P. B. Becker (2012). "Nucleosome remodeler SNF2L suppresses cell proliferation and migration and attenuates Wnt signaling." *Mol Cell Biol* **32**(13): 2359-2371.

Emanuele, M. J., A. E. Elia, Q. Xu, C. R. Thoma, L. Izhar, Y. Leng, A. Guo, Y. N. Chen, J. Rush, P. W. Hsu, H. C. Yen and S. J. Elledge (2011). "Global identification of modular cullin-RING ligase substrates." *Cell* **147**(2): 459-474.

Erdel, F. and K. Rippe (2011). "Chromatin remodelling in mammalian cells by ISWI-type complexes--where, when and why?" *FEBS J* **278**(19): 3608-3618.

Erdel, F., T. Schubert, C. Marth, G. Langst and K. Rippe (2010). "Human ISWI chromatin-remodeling complexes sample nucleosomes via transient binding reactions and become immobilized at active sites." *Proc Natl Acad Sci U S A* **107**(46): 19873-19878.

Ewing, A. K., M. Attner and D. Chakravarti (2007). "Novel regulatory role for human Acf1 in transcriptional repression of vitamin D3 receptor-regulated genes." *Mol Endocrinol* **21**(8): 1791-1806.

Fairman-Williams, M. E., U. P. Guenther and E. Jankowsky (2010). "SF1 and SF2 helicases: family matters." *Curr Opin Struct Biol* **20**(3): 313-324.

Fyodorov, D. V., M. D. Blower, G. H. Karpen and J. T. Kadonaga (2004). "Acf1 confers unique activities to ACF/CHRAC and promotes the formation rather than disruption of chromatin in vivo." *Genes Dev* **18**(2): 170-183.

Goodwin, L. R. and D. J. Picketts (2018). "The role of ISWI chromatin remodeling complexes in brain development and neurodevelopmental disorders." *Mol Cell Neurosci* **87**: 55-64.

Grune, T., J. Brzeski, A. Eberharter, C. R. Clapier, D. F. Corona, P. B. Becker and C. W. Muller (2003). "Crystal structure and functional analysis of a nucleosome recognition module of the remodeling factor ISWI." *Mol Cell* **12**(2): 449-460.

Guertg, C., P. Lienemann, V. Sirri, I. Grummt, D. Hernandez-Verdun, M. O. Hottiger, M. Fussenegger and R. Santoro (2010). "The NoRC complex mediates the heterochromatin formation and stability of silent rRNA genes and centromeric repeats." *EMBO J* **29**(13): 2135-2146.

Hakimi, M. A., D. A. Bochar, J. A. Schmiesing, Y. Dong, O. G. Barak, D. W. Speicher, K. Yokomori and R. Shiekhattar (2002). "A chromatin remodelling complex that loads cohesin onto human chromosomes." *Nature* **418**(6901): 994-998.

Han, L., V. Madan, A. Mayakonda, P. Dakle, T. W. Woon, P. Shyamsunder, H. B. M. Nordin, Z. Cao, J. Sundaresan, I. Lei, Z. Wang and H. P. Koeffler (2019). "Chromatin remodeling mediated by ARID1A is indispensable for normal hematopoiesis in mice." *Leukemia* **33**(9): 2291-2305.

He, S., S. Limi, R. S. McGreal, Q. Xie, L. A. Brennan, W. L. Kantorow, J. Kokavec, R. Majumdar, H. Hou, Jr., W. Edelmann, W. Liu, R. Ashery-Padan, J. Zavadil, M. Kantorow, A. I. Skoultchi, T. Stopka and A. Cvekl (2016). "Chromatin remodeling enzyme Snf2h regulates embryonic lens differentiation and denucleation." *Development* **143**(11): 1937-1947.

Helfricht, A., W. W. Wiegant, P. E. Thijssen, A. C. Vertegaal, M. S. Luijsterburg and H. van Attikum (2013). "Remodeling and spacing factor 1 (RSF1) deposits centromere proteins at DNA double-strand breaks to promote non-homologous end-joining." *Cell Cycle* **12**(18): 3070-3082.

Chang, E. Y., H. Ferreira, J. Somers, D. A. Nusinow, T. Owen-Hughes and G. J. Narlikar (2008). "MacroH2A allows ATP-dependent chromatin remodeling by SWI/SNF and ACF complexes but specifically reduces recruitment of SWI/SNF." *Biochemistry* **47**(51): 13726-13732.

Chi, T. H., M. Wan, P. P. Lee, K. Akashi, D. Metzger, P. Chambon, C. B. Wilson and G. R. Crabtree (2003). "Sequential roles of Brg, the ATPase subunit of BAF chromatin remodeling complexes, in thymocyte development." *Immunity* **19**(2): 169-182.

Chi, T. H., M. Wan, K. Zhao, I. Taniuchi, L. Chen, D. R. Littman and G. R. Crabtree (2002). "Reciprocal regulation of CD4/CD8 expression by SWI/SNF-like BAF complexes." *Nature* **418**(6894): 195-199.

Chong, S., N. Vickaryous, A. Ashe, N. Zamudio, N. Youngson, S. Hemley, T. Stopka, A. Skoultchi, J. Matthews, H. S. Scott, D. de Kretser, M. O'Bryan, M. Blewitt and E. Whitelaw (2007). "Modifiers of epigenetic reprogramming show paternal effects in the mouse." *Nat Genet* **39**(5): 614-622.

Ito, T., M. Bulger, M. J. Pazin, R. Kobayashi and J. T. Kadonaga (1997). "ACF, an ISWI-containing and ATP-utilizing chromatin assembly and remodeling factor." *Cell* **90**(1): 145-155.

Ito, T., M. E. Levenstein, D. V. Fyodorov, A. K. Kutach, R. Kobayashi and J. T. Kadonaga (1999). "ACF consists of two subunits, Acf1 and ISWI, that function cooperatively in the ATP-dependent catalysis of chromatin assembly." *Genes Dev* **13**(12): 1529-1539.

Jevtic, Z., V. Matafora, F. Casagrande, F. Santoro, S. Minucci, M. Garre, M. Rasouli, O. Heidenreich, G. Musco, J. Schwaller and A. Bachi (2022). "SMARCA5 interacts with NUP98-NSD1 oncofusion protein and sustains hematopoietic cells transformation." *J Exp Clin Cancer Res* **41**(1): 34.

Jin, Q., X. Mao, B. Li, S. Guan, F. Yao and F. Jin (2015). "Overexpression of SMARCA5 correlates with cell proliferation and migration in breast cancer." *Tumour Biol* **36**(3): 1895-1902.

Kato, A. and K. Komatsu (2015). "RNF20-SNF2H Pathway of Chromatin Relaxation in DNA Double-Strand Break Repair." *Genes (Basel)* **6**(3): 592-606.

Klement, K., M. S. Luijsterburg, J. B. Pinder, C. S. Cena, V. Del Nero, C. M. Wintersinger, G. Dellaire, H. van Attikum and A. A. Goodarzi (2014). "Opposing ISWI- and CHD-class chromatin remodeling activities orchestrate heterochromatic DNA repair." *J Cell Biol* **207**(6): 717-733.

Kokavec, J., T. Zikmund, F. Savvulidi, V. Kulvait, W. Edlmann, A. I. Skoultchi and T. Stopka (2017). "The ISWI ATPase Smarca5 (Snf2h) Is Required for Proliferation and Differentiation of Hematopoietic Stem and Progenitor Cells." *Stem Cells* **35**(6): 1614-1623.

Koscielny, G., G. Yaikhom, V. Iyer, T. F. Meehan, H. Morgan, J. Atienza-Herrero, A. Blake, C. K. Chen, R. Easty, A. Di Fenza, T. Fiegel, M. Griffiths, A. Horne, N. A. Karp, N. Kurbatova, J. C. Mason, P. Matthews, D. J. Oakley, A. Qazi, J. Regnart, A. Retha, L. A. Santos, D. J. Sneddon, J. Warren, H. Westerberg, R. J. Wilson, D. G. Melvin, D. Smedley, S. D. Brown, P. Flicek, W. C. Skarnes, A. M. Mallon and H. Parkinson (2014). "The International Mouse Phenotyping Consortium Web Portal, a unified point of access for knockout mice and related phenotyping data." *Nucleic Acids Res* **42**(Database issue): D802-809.

Kuzelova, A., N. Dupacova, B. Antosova, S. S. Sunny, Z. Kozmik, Jr., J. Paces, A. I. Skoultchi, T. Stopka and Z. Kozmik (2023). "Chromatin Remodeling Enzyme Snf2h Is Essential for Retinal Cell Proliferation and Photoreceptor Maintenance." *Cells* **12**(7).

Lan, L., A. Ui, S. Nakajima, K. Hatakeyama, M. Hoshi, R. Watanabe, S. M. Janicki, H. Ogiwara, T. Kohno, S. Kanno and A. Yasui (2010). "The ACF1 complex is required for DNA double-strand break repair in human cells." *Mol Cell* **40**(6): 976-987.

Landry, J., A. A. Sharov, Y. Piao, L. V. Sharova, H. Xiao, E. Southon, J. Matta, L. Tessarollo, Y. E. Zhang, M. S. Ko, M. R. Kuehn, T. P. Yamaguchi and C. Wu (2008). "Essential role of chromatin remodeling protein Bptf in early mouse embryos and embryonic stem cells." PLoS Genet **4**(10): e1000241.

Lazzaro, M. A. and D. J. Picketts (2001). "Cloning and characterization of the murine Imitation Switch (ISWI) genes: differential expression patterns suggest distinct developmental roles for Snf2h and Snf2l." J Neurochem **77**(4): 1145-1156.

LeRoy, G., A. Loyola, W. S. Lane and D. Reinberg (2000). "Purification and characterization of a human factor that assembles and remodels chromatin." J Biol Chem **275**(20): 14787-14790.

Li, J., G. Langst and I. Grummt (2006). "NoRC-dependent nucleosome positioning silences rRNA genes." EMBO J **25**(24): 5735-5741.

Li, Y., H. Gong, P. Wang, Y. Zhu, H. Peng, Y. Cui, H. Li, J. Liu and Z. Wang (2021). "The emerging role of ISWI chromatin remodeling complexes in cancer." J Exp Clin Cancer Res **40**(1): 346.

Loyola, A., G. LeRoy, Y. H. Wang and D. Reinberg (2001). "Reconstitution of recombinant chromatin establishes a requirement for histone-tail modifications during chromatin assembly and transcription." Genes Dev **15**(21): 2837-2851.

Martens, M. (2013). "Developmental and cognitive troubles in Williams syndrome." Handb Clin Neurol **111**: 291-293.

Meng, J., X. T. Zhang, X. L. Liu, L. Fan, C. Li, Y. Sun, X. H. Liang, J. B. Wang, Q. B. Mei, F. Zhang and T. Zhang (2016). "WSTF promotes proliferation and invasion of lung cancer cells by inducing EMT via PI3K/Akt and IL-6/STAT3 signaling pathways." Cell Signal **28**(11): 1673-1682.

Mueller-Planitz, F., H. Klinker and P. B. Becker (2013). "Nucleosome sliding mechanisms: new twists in a looped history." Nat Struct Mol Biol **20**(9): 1026-1032.

Oppikofer, M., T. Bai, Y. Gan, B. Haley, P. Liu, W. Sandoval, C. Ciferri and A. G. Cochran (2017). "Expansion of the ISWI chromatin remodeler family with new active complexes." EMBO Rep **18**(10): 1697-1706.

Percipalle, P., N. Fomproix, E. Cavellan, R. Voit, G. Reimer, T. Kruger, J. Thyberg, U. Scheer, I. Grummt and A. K. Farrants (2006). "The chromatin remodelling complex WSTF-SNF2h interacts with nuclear myosin 1 and has a role in RNA polymerase I transcription." EMBO Rep **7**(5): 525-530.

Perpelescu, M., N. Nozaki, C. Obuse, H. Yang and K. Yoda (2009). "Active establishment of centromeric CENP-A chromatin by RSF complex." J Cell Biol **185**(3): 397-407.

Poot, R. A., L. Bozhenok, D. L. van den Berg, S. Steffensen, F. Ferreira, M. Grimaldi, N. Gilbert, J. Ferreira and P. D. Varga-Weisz (2004). "The Williams syndrome transcription factor interacts with PCNA to target chromatin remodelling by ISWI to replication foci." Nat Cell Biol **6**(12): 1236-1244.

Poot, R. A., G. Dellaire, B. B. Hulsmann, M. A. Grimaldi, D. F. Corona, P. B. Becker, W. A. Bickmore and P. D. Varga-Weisz (2000). "HuCHRAC, a human ISWI chromatin remodelling complex contains hACF1 and two novel histone-fold proteins." EMBO J **19**(13): 3377-3387.

Postepska-Igielska, A., D. Kronic, N. Schmitt, K. M. Greulich-Bode, P. Boukamp and I. Grummt (2013). "The chromatin remodelling complex NoRC safeguards genome stability by heterochromatin formation at telomeres and centromeres." EMBO Rep **14**(8): 704-710.

Prasad, P., A. Lennartsson and K. Ekwall (2015). "The roles of SNF2/SWI2 nucleosome remodeling enzymes in blood cell differentiation and leukemia." Biomed Res Int **2015**: 347571.

Ribeyre, C., R. Zellweger, M. Chauvin, N. Bec, C. Larroque, M. Lopes and A. Constantinou (2016). "Nascent DNA Proteomics Reveals a Chromatin Remodeler Required for Topoisomerase I Loading at Replication Forks." *Cell Rep* **15**(2): 300-309.

Sadeghifar, F., S. Bohm, A. Vintermist and A. K. Ostlund Farrants (2015). "The B-WICH chromatin-remodelling complex regulates RNA polymerase III transcription by promoting Max-dependent c-Myc binding." *Nucleic Acids Res* **43**(9): 4477-4490.

Sanchez-Molina, S., O. Mortusewicz, B. Bieber, S. Auer, M. Eckey, H. Leonhardt, A. A. Friedl and P. B. Becker (2011). "Role for hACF1 in the G2/M damage checkpoint." *Nucleic Acids Res* **39**(19): 8445-8456.

Santoro, R., J. Li and I. Grummt (2002). "The nucleolar remodeling complex NoRC mediates heterochromatin formation and silencing of ribosomal gene transcription." *Nat Genet* **32**(3): 393-396.

Sheu, J. J., B. Guan, J. H. Choi, A. Lin, C. H. Lee, Y. T. Hsiao, T. L. Wang, F. J. Tsai and M. Shih Ie (2010). "Rsf-1, a chromatin remodeling protein, induces DNA damage and promotes genomic instability." *J Biol Chem* **285**(49): 38260-38269.

Sheu, J. J., J. H. Choi, I. Yildiz, F. J. Tsai, Y. Shaul, T. L. Wang and M. Shih Ie (2008). "The roles of human sucrose nonfermenting protein 2 homologue in the tumor-promoting functions of Rsf-1." *Cancer Res* **68**(11): 4050-4057.

Shih Ie, M., J. J. Sheu, A. Santillan, K. Nakayama, M. J. Yen, R. E. Bristow, R. Vang, G. Parmigiani, R. J. Kurman, C. G. Trope, B. Davidson and T. L. Wang (2005). "Amplification of a chromatin remodeling gene, Rsf-1/HBXAP, in ovarian carcinoma." *Proc Natl Acad Sci U S A* **102**(39): 14004-14009.

Siamishi, I., N. Iwanami, T. Clapes, E. Trompouki, C. P. O'Meara and T. Boehm (2020). "Lymphocyte-Specific Function of the DNA Polymerase Epsilon Subunit Pole3 Revealed by Neomorphic Alleles." *Cell Rep* **31**(11): 107756.

Stopka, T. and A. I. Skoultschi (2003). "The ISWI ATPase Snf2h is required for early mouse development." *Proc Natl Acad Sci U S A* **100**(24): 14097-14102.

Stopka, T., D. Zakova, O. Fuchs, O. Kubrova, J. Blafkova, J. Jelinek, E. Necas and J. Zivny (2000). "Chromatin remodeling gene SMARCA5 is dysregulated in primitive hematopoietic cells of acute leukemia." *Leukemia* **14**(7): 1247-1252.

Strohner, R., A. Nemeth, P. Jansa, U. Hofmann-Rohrer, R. Santoro, G. Langst and I. Grummt (2001). "NoRC--a novel member of mammalian ISWI-containing chromatin remodeling machines." *EMBO J* **20**(17): 4892-4900.

Takehima, H., T. Niwa, T. Takahashi, M. Wakabayashi, S. Yamashita, T. Ando, Y. Inagawa, H. Taniguchi, H. Katai, T. Sugiyama, T. Kiyono and T. Ushijima (2015). "Frequent involvement of chromatin remodeler alterations in gastric field cancerization." *Cancer Lett* **357**(1): 328-338.

Thakur, S., V. Cahais, T. Turkova, T. Zikmund, C. Renard, T. Stopka, M. Korenjak and J. Zavadil (2022). "Chromatin Remodeler Smarca5 Is Required for Cancer-Related Processes of Primary Cell Fitness and Immortalization." *Cells* **11**(5).

Thompson, P. J., K. A. Norton, F. H. Niri, C. E. Dawe and H. E. McDermid (2012). "CECR2 is involved in spermatogenesis and forms a complex with SNF2H in the testis." *J Mol Biol* **415**(5): 793-806.

Toiber, D., F. Erdel, K. Bouazoune, D. M. Silberman, L. Zhong, P. Mulligan, C. Sebastian, C. Cosentino, B. Martinez-Pastor, S. Giacosa, A. D'Urso, A. M. Naar, R. Kingston, K. Rippe and R. Mostoslavsky (2013). "SIRT6 recruits SNF2H to DNA break sites, preventing genomic instability through chromatin remodeling." *Mol Cell* **51**(4): 454-468.

Wang, Y., J. Qin, Q. Liu, X. Hong, T. Li, Y. Zhu, L. He, B. Zheng and M. Li (2016). "SNF2H promotes hepatocellular carcinoma proliferation by activating the Wnt/beta-catenin signaling pathway." *Oncol Lett* **12**(2): 1329-1336.

Williams, C. J., T. Naito, P. G. Arco, J. R. Seavitt, S. M. Cashman, B. De Souza, X. Qi, P. Keables, U. H. Von Andrian and K. Georgopoulos (2004). "The chromatin remodeler Mi-2beta is required for CD4 expression and T cell development." *Immunity* **20**(6): 719-733.

Xiao, A., H. Li, D. Shechter, S. H. Ahn, L. A. Fabrizio, H. Erdjument-Bromage, S. Ishibe-Murakami, B. Wang, P. Tempst, K. Hofmann, D. J. Patel, S. J. Elledge and C. D. Allis (2009). "WSTF regulates the H2A.X DNA damage response via a novel tyrosine kinase activity." *Nature* **457**(7225): 57-62.

Yang, Y. I., J. H. Ahn, K. T. Lee, M. Shih Ie and J. H. Choi (2014). "RSF1 is a positive regulator of NF-kappaB-induced gene expression required for ovarian cancer chemoresistance." *Cancer Res* **74**(8): 2258-2269.

Zhang, X., L. Fu, D. Xue, X. Zhang, F. Hao, L. Xie, J. He, J. Gai, Y. Liu, H. Xu, Q. Li and E. Wang (2017). "Overexpression of Rsf-1 correlates with poor survival and promotes invasion in non-small cell lung cancer." *Virchows Arch* **470**(5): 553-560.

Zhao, X. C., P. An, X. Y. Wu, L. M. Zhang, B. Long, Y. Tian, X. Y. Chi and D. Y. Tong (2016). "Overexpression of hSNF2H in glioma promotes cell proliferation, invasion, and chemoresistance through its interaction with Rsf-1." *Tumour Biol* **37**(6): 7203-7212.

Zhou, Y. and I. Grummt (2005). "The PHD finger/bromodomain of NoRC interacts with acetylated histone H4K16 and is sufficient for rDNA silencing." *Curr Biol* **15**(15): 1434-1438.

Zhou, Y., R. Santoro and I. Grummt (2002). "The chromatin remodeling complex NoRC targets HDAC1 to the ribosomal gene promoter and represses RNA polymerase I transcription." *EMBO J* **21**(17): 4632-4640.

Zikmund, T., J. Kokavec, T. Turkova, F. Savvulidi, H. Paszekova, S. Vodenkova, R. Sedlacek, A. I. Skoultchi and T. Stopka (2019). "ISWI ATPase Smarca5 Regulates Differentiation of Thymocytes Undergoing beta-Selection." *J Immunol* **202**(12): 3434-3446.

Zikmund, T., H. Paszekova, J. Kokavec, P. Kerbs, S. Thakur, T. Turkova, P. Tauchmanova, P. A. Greif and T. Stopka (2020). "Loss of ISWI ATPase SMARCA5 (SNF2H) in Acute Myeloid Leukemia Cells Inhibits Proliferation and Chromatid Cohesion." *Int J Mol Sci* **21**(6).